Rab35-regulated lipid turnover by myotubularins represses mTORC1 activity and controls myelin growth

Inaugural-Dissertation

to obtain the academic degree

Doctor rerum naturalium (Dr. rer. nat.)

submitted to the Department of Biology, Chemistry and Pharmacy

of the Freie Universität Berlin

by

Linda Sawade

from Berlin, Germany

2019

Period of doctorate studies:	November 2013 to August 2019
Supervisor:	Prof. Dr. Volker Haucke
Institute:	Leibniz-Forschungsinstitut für Molekulare Pharmakologie (FMP), Berlin

1st Reviewer: Prof. Dr. Volker Haucke

2nd Reviewer: Prof. Dr. Stephan Sigrist

Date of defense: 29.10.2019

Affidavit

I declare that my PhD thesis at hand has been written independently and with no other sources and aids than quoted.

Berlin, August the 13th, 2019

Acknowledgements

First of all, I would like to express my deep gratitude to my supervisor, Prof. Dr. Volker Haucke, for his guidance, support and constant motivation throughout my PhD studies, which were crucial for the success of this project.

I owe special thanks to our collaboration partners Prof. Dr. Alessandra Bolino (INSPE, Milan, Italy), and her team Federica Grandi, Marianna Mignanelli, and Roberta Di Guardo who performed great work with the Schwann cell-specific *Rab35* knockout mice and provided us the MTMR2 shRNA. I am also very grateful to Prof. Dr. Arnaud Echard (Pasteur-Institut, Paris, France) who provided us with the GFP-Rab35^{endo} KI HeLa cells, and especially the *Rab35*$^{Fl/Fl}$ mice for conditional gene knockout. Many thanks also to his team, Dr. Kerstin Klinkert and Dr. Francina Langa Vives, as well as to Prof. Dr. Stephen Shaw (formerly: NIH, Bethesda, USA) and Dr. Genaro Patiño-López (formerly: NIH; now: Hospital Infantil de México, Ciudad de México, México), who generated these animals. Furthermore, I would like to thank Prof. Dr. Cesare Montecucco and his team (University of Padova, Italy), especially Dr. Samuele Negro, for the training in preparation of sciatic nerves and Schwann cell cultures *in vitro*. Special thanks also to Dr. Eberhard Krause, the former head of the mass spectrometry facility at the FMP-Berlin (Germany), and his team, especially Heike Stephanowitz, for the BioID-mass spectrometry. Many thanks to Dr. Dmytro Puchkov, the head of the electron microscopy facility, and his team for the ultrastructural analysis of the conditional Rab35 knockout neurons in culture. I would also like to thank Dr. Burkhard Wiesner, Jenny Eichhorst and Dr. Martin Lehmann from the Imaging facility (FMP Berlin), who provided us with terrific microscopes, technical knowledge and support. I am also very grateful for financial funding by the Grant SFB 958 (Deutsche Forschungsgemeinschaft).

I would like to thank the secretary office, Heidemarie Petschick and Alexandra Chylla, who were always helpful and supportive, as well as to the FMP-IT, especially Alexander Heyne. Special thanks to Prof. Dr. Tanja Maritzen for the management and supervision of animal experimental administration, and to the animal house facility, Dr. Natali Wisbrun and her team Eva Lojek, Sina Scholz and Jeanette Unasch.

Furthermore, I would like to thank the technicians of the Haucke lab: Delia Löwe, especially for the management of the common cell and neuron culture. Uwe Fink for his skills and advices regarding protein purifications. Claudia Schmidt for providing help whenever required. Silke Zillmann for the ordering management and genotypings, as well as Sophia Griese. Many thanks to Sabine Hahn, for the support with astrocytic culture preparations, and

especially for the time when I joined the lab as an unexperienced undergraduate student. And special thanks to Maria Mühlbauer for the technical assistance and her great support in this project.

I owe special thanks to Dr. Natalie Kaempf and Dr. Domenico Azarnia Tehran for fruitful discussions, advices and especially their kind support in many ways. I thank Dr. Natalia Kononenko, who supervised me as an undergraduate and during my first year as a PhD, and Dr. Tania Lopez Hernandez and Dennis Vollweiter for introducing me into the wonderful world of astrocytes and "R", respectively. Thanks to Dr. Wen-Ting Lo for his advices regarding affinity purifications. Thanks also to our former lab member Katarina Ketel, who worked on MTM1, and thus, already obtained the basic constructs which made the work with this protein family a bit easier. And thanks to all other past and present members of the Haucke lab I've got to know over the years and who contributed to a joyful atmosphere in the lab: Jelena Bacetic, Marietta Bergmann, Svenja Bolz, Caroline Bruns, Gabrielle Capin, Gala Claßen, Katrin Diesenberg, Michael Ebner, Marielle Eichhorn-Grünig, Fabian Feutlinske, Paula Samsó Ferre, Niclas Gimber, Marine Gil, Hannes Gonschoir, Claudia Gras, Manuel Hessenberger, Lennart Hoffmann, Burkhard Jakob, Wonyul Jang, Maria Jäpel, Christina Kath, Philipp Koch, Gaga Kochlamazashvili, Seong Joo Koo, Michael Krauß, Marijn Kuijpers, André Lampe, Gregor Lichtner, Guan-Ting Liu, Fabian Lukas, Albert Mackintosh, Marta Maglione, Charles Malek, Andrea Marat, Kristine Oevel, Christoph Ott, Filiz Sila Rizalar, Giulia Russo, Hannah Schachtner, Christopher Schmied, Jan Schmoranzer, Irene Schütz, Kyungyuen Song, Tolga Soykan, Wiebke Stahlschmidt, Anela Vukoja, Alexander Wallroth, Alexander Walter, Haibin Wang, Anna Wawrzyniak and Mirjana Weimershaus.

Finally, and most important, I owe my deepest gratitude to my family for all their support throughout my life, and to Thomas Lenz who especially backed me up over the last years.

I Table of content

II Summary

Myelination has been evolved in the vertebrate system as an essential mechanism to facilitate axonal signal transduction and provide trophic support for neurons. Formation and maintenance of myelin sheaths are tightly regulated throughout the development by diverse cell metabolic pathways. Consequently, the impairment of myelin homeostasis, for instance by an altered metabolism of myelinating glial cells, can lead to severe axonal degeneration. Inherited peripheral neuropathies such as the most commonly inherited Charcot-Marie-Tooth (CMT) diseases are a heterogeneous group of disorders, caused by mutations in more than 80 different genes. The demyelinating CMT-type 4B results from loss-of-function or missense mutations in myotubularin-related protein 2 (MTMR2), MTMR5 or MTMR13. These proteins belong to the family of MTMR phosphatidylinositol (PI) phosphatases that specifically hydrolyze the endomembrane signaling lipids PI(3)P and PI(3,5)P_2 at the D-3 position. How dysregulated PI(3)-phosphate conversion in myelinating Schwann cells can lead to such a severely affected myelin homeostasis, as observed in the absence of CMT-associated MTMRs, is still elusive.

Here, we show that the small GTPase Rab35, a critical regulator of endomembrane trafficking, interacts with CMT-associated MTMR lipid phosphatases. Rab35 binds and recruits the pseudophosphatases MTMR13 and MTMR5, and via these, also the active phosphatase MTMR2. In agreement with the critical involvement of these proteins in the myelin homeostasis of the peripheral nervous system (PNS), Schwann cell-specific Rab35 ablation results in severe peripheral demyelination in mice. Sciatic nerves of these animals are characterized by aberrantly myelinated fibers with Tomacula and myelin outfoldings. This progressive focal hypermyelination is accompanied by abnormally elevated activity of mTORC1, a central cell signaling hub that needs to be crucially balanced for proper myelination. Inhibiting mTORC1 activity by pharmaceutical treatment of these mice using Rapamycin leads to a partial amelioration of the nerve morphology. Moreover, reduced myelin segment formation and myelin abnormalities in Rab35-depleted Schwann cells *ex vivo*, in Schwann cell and dorsal root ganglion neuron co-cultures, are rescued by Rapamycin application. These findings strongly indicate that mTORC1 hyperactivity contributes to the observed impairment of myelin homeostasis in conditional *Rab35* knockout (KO) animals.

Furthermore, the absence of Rab35 or the active phosphatase MTMR2, or both, result in elevated mTORC1 activity in different cultured cell types, including primary cells of the nervous system. This hyperactivity is displayed independently of receptor tyrosine kinase (RTK) and AKT activation. Notably, physiological mTORC1 activity can be restored in

Rab35-depleted cells by overexpression of MTMR2, suggesting a sequential function of the small GTPase and active MTMR complexes in repressing mTORC1. In accordance with the lipid phosphatase activity of MTMR2, we further show that dysregulated PI(3)-phosphate levels in the absence of Rab35 are causative for the observed mTORC1 hyperactivation, and likely result from an impaired recruitment of MTMR complexes. Rab35-depleted cells display an accumulation of PI(3)P and likely its product, $PI(3,5)P_2$. Importantly, pharmacological interference with VPS34-mediated PI(3)P synthesis restores physiological levels of mTORC1 activity. We observe this mechanism in non-myelinating cells as well as in Schwann cells. Elevated mTORC1 activity and PI(3)P accumulation are accompanied by increased levels of the myelin protein P0 in differentiated *Rab35* KO Schwann cells in culture. Importantly, P0-protein levels are reduced and comparable to WT levels upon pharmacological inhibition of mTORC1, VPS34, and especially the $PI(3,5)P_2$-synthesizing enzyme PIKfyve. This suggests that $PI(3,5)P_2$ is the critical lipid for mTORC1 activation in PNS myelinating glial cells and thus, provides a possible explanation for the crucial effect of the loss of MTMR proteins on myelin homeostasis. Moreover, our data indicate a similar role for Rab35 in myelinating glial cells of the central nervous system (CNS).

Taken together, we could identify Rab35 as a novel critical regulator of both, myelin homeostasis and mTORC1 activity. We propose a mechanism in which Rab35 represses mTORC1 activity by the recruitment of PI(3)-phosphate-hydrolyzing MTMR complexes to lysosomal sites. These findings may have implications for a potential therapeutic treatment of CMT4B-patients by pharmaceutical mTORC1-inhibition, for instance with Rapamycin.

III Zusammenfassung

Myelinisierung ist ein essenzieller Mechanismus innerhalb der evolutionären Entwicklung der Wirbeltiere, für die Beschleunigung der axonalen Signaltransduktion sowie die trophische Unterstützung von Neuronen. Formation und lebenslanger Erhalt der Myelinscheiden sind durch zahlreiche Zell-metabolische Stoffwechselwege streng reguliert. Beeinträchtigungen der Myelin Homöostase, die beispielsweise aus Abweichungen im Metabolismus von myelinisierenden Gliazellen resultieren, können somit zur schwerwiegenden Degeneration von Axonen führen. Vererbbare Neuropathien im peripheren Nervensystem (PNS), wie die am häufigsten vererbte Charcot-Marie-Tooth (CMT) Krankheit, sind eine heterogene Gruppe von Erkrankungen, die durch Mutationen in mehr als 80 verschiedenen Genen verursacht werden können. Der demyelinisierende CMT-Krankheitstyp 4B wird durch Genmutationen ausgelöst, die zum Verlust oder der Fehlfunktion von myotubularin-related protein 2 (MTMR2), MTMR5 oder MTMR13 führen. Diese Proteine gehören zur Gruppe der MTMR Phosphatidylinositol (PI) Phosphatasen, die spezifisch die endomembranen Signallipide PI(3)P und PI(3,5)P_2 an der 3‘-Phosphatgruppe hydrolysieren. Unklar ist jedoch, wie sich eine Deregulation der Umsetzung der Lipide in myelinisierenden Schwann-Zellen in der Abwesenheit dieser MTMR Phosphatasen so schwerwiegend auf die Myelin Homöostase auswirken kann.

In dieser Arbeit zeigen wir, dass Rab35, eine kleine GTPase, die in der Regulation des intrazellulären Membrantransports involviert ist, mit diesen CMT-assoziierten MTMR Lipidphosphatasen interagiert. Rab35 bindet und rekrutiert die Pseudophosphatasen MTMR13 und MTMR5, und dadurch auch die mit ihnen im Komplex gebundene aktive Phosphatase MTMR2. Entsprechend der kritischen Rolle dieser Proteine in der Regulation der Myelin Homöostase im PNS, führt die Schwann-Zell-spezifische Ablation von Rab35 *in vivo* zu einer schweren Demyelinisierung des Ischias-Nervs in Mäusen. Die Tiere weisen aberrant-myelinisierte periphere Nervenfasern mit Tomacula und Myelinscheidenausfaltungen auf. Diese voranschreitende fokale Hypermyelinisierung ist begleitet von einer abnormal erhöhten Aktivität einer der zentralen Signalverschaltungskomplexe für die Regulation der Myelinscheidenformation, mTORC1, im Nervengewebe. Ein Entgegenwirken der mTORC1-Hyperaktivität durch die pharmakologische Inhibierung mit Rapamyzin führt zu einer partiellen Verbesserung der Nervenmorphologie. Die chronische Applikation von Rapamyzin in Rab35-depletierten Schwann-Zellen *ex vivo* behebt zudem die reduzierte Formation von Myelinsegmenten und -abberrationen in Co-Kulturen von Schwann-Zellen und dorsal root ganglion (DRG)-Neuronen. Dies lässt darauf schließen, dass die abnormal erhöhte mTORC1-

Aktivität in Schwann-Zellen zu der beeinträchtigten Myelin Homöostase in den konditionellen *Rab35* knockout (KO) Tieren beiträgt.

Des Weiteren führt die Depletion von Rab35, der aktiven Phosphatase MTMR2, oder beider Proteine zu erhöhter mTORC1-Aktivität in verschiedenen kultivierten Zelltypen, unter anderem auch in Primärzellen des Nervensystems. Dieser Effekt ist unabhängig von der Stimulation der mTORC1-aktivierenden Rezeptortyrosinkinasen sowie der daraus resultierenden AKT-Aktivierung. Interessanterweise kann eine physiologische mTORC1-Aktivität durch Überexpression von MTMR2 in Rab35-depletierten Zellen wiederhergestellt werden. Dies lässt auf einen sequenziellen Ablauf der mTORC1-Repression durch die kleine GTPase und aktiven MTMR Komplexen schließen. Damit übereinstimmend haben wir festgestellt, dass eine fehlende Regulierung von PI(3)-Phosphaten in der Abwesenheit von Rab35 ursächlich für die beobachtete mTORC1-Hyperaktivität ist und vermutlich aus einer beeinträchtigten Rekrutierung von MTMR Komplexen resultiert. Kultivierte Zellen in denen die Expression von Rab35 gänzlich oder größtenteils unterdrückt wird, weisen eine Akkumulation von PI(3)P und möglicherweise auch von $PI(3,5)P_2$ Lipiden auf. In diesen Zellen kann durch pharmakologische Unterbindung der PI(3)P Synthese durch Inhibierung von VPS34 die mTORC1-Aktivität wieder auf physiologische Level reduziert werden. Diesen Mechanismus sehen wir sowohl in nicht-myelinisierenden als auch in Schwann-Zellen. Neben der mTORC1-Hyperaktivität und der Akkumulation von PI(3)P Lipiden weisen differenzierte *Rab35* KO Schwann-Zellen in Kultur erhöhte Myelin Protein P0-Level auf. Diese können bemerkenswerterweise durch die chronische Applikation der Kulturen mit Inhibitoren gegen mTORC1, VPS34, und insbesondere gegen das $PI(3,5)P_2$-synthetisierende Enzym, PIKfyve, wieder reduziert werden. Dies legt den Schluss nahe, dass $PI(3,5)P_2$ das entscheidende mTORC1-aktivierende Lipid in den myelinisierenden Gliazellen des PNS‘ ist, und bietet somit eine mögliche Erklärung für die Auswirkung des Verlustes von MTMR Proteinen auf die Myelin Homöostase. Unsere Daten weisen zudem darauf hin, dass Rab35 eine ähnliche Funktion in Oligodendrozyten, den myelinisierenden Zellen des zentralen Nervensystems übernimmt.

Zusammenfassend identifizieren unsere Ergebnisse Rab35 als bisher unentdeckten Regulator der Myelinscheidenformation im PNS, sowie als Repressor von mTORC1. Wir vermuten, dass Rab35 die Aktivität von mTORC1 durch die Rekrutierung von MTMR Phosphatasen zu Lysosomen unterdrückt. Diese Ergebnisse deuten darauf hin, dass die therapeutische Behandlung mit mTORC1-inhibierenden Pharmaka wie Rapamyzin zu einer Verbesserung des Krankheitsverlaufs von CMT4B Patienten führen könnte.

1. Introduction

1.1 Myelination of the vertebrate nervous system

The electrical insulation of neuronal axons by compacted glial membrane wrapping appeared for the first time in evolution approximately 425 Mio years ago in placoderms. Myelination is one of the crucial acquisitions that underly the potential of higher organisms to develop large and complex nervous systems by enabling rapid and efficient nerve conduction in small diameter axons (Zalc, 2008; 2016). “Myelin” originates from the greek term of marrow (“myelos”) and was first coined by Rudolf Virchow (Virchow, 1854). The vertebrate nervous system is composed of the central nervous system (CNS), including spinal cord and brain, and the peripheral nervous system (PNS) with its nerves that connect the CNS with organs and limbs. The CNS is further subdivided into the grey and white matter, whereas the latter contains almost exclusively myelinated fibers with a dry weight myelin proportion of 50 - 60 % (Morell and Norton, 1980). In contrast, peripheral nerves contain bundles of small diameter, non-myelinated and large, myelinated axons in a ratio of 4 to 1 (Voyvodic *et al.*, 1989; Griffin and Thompson, 2008). The axonal diameter is a key determinant for and directly proportional to the signal conduction velocity (Rushton, 1951; Waxman, 1980). In invertebrates, long fibers require a large diameter to transmit signals with a sufficient speed (Young, 1938). Myelination of vertebrate axons circumvents the requirement of large fiber surfaces by preventing the loss of charge, reducing membrane capacitance during signal propagation, and providing trophic support for axonal integrity (Nave, 2010). The extent of myelination is tightly regulated and adapted to the axonal diameter, represented by a constant g-ratio. It is defined as the axon diameter divided by the total fiber diameter, and between 0.6 - 0.7 for myelinated fibers in PNS and CNS. The g-ratio increases slightly with age whereas significant deviations indicate pathological conditions (Rushton, 1951; Berthold *et al.*, 1983; Friede and Beuche, 1985; Kidd *et al.*, 2013).

1.2 Myelinating glial cells

Oligodendrocytes (OLs) and Schwann cells (SCs) myelinate axons of the CNS and PNS, respectively. They are presumed to be evolutionarily developed from a common progenitor that might descendant from the invertebrate ensheathing glial cells (Zalc *et al.*, 2008; 2016). Nevertheless, their cell morphology is quite distinct, especially in the mature myelinating stage (Fig. 1-1). Multibranching OLs produce up to 40 myelin segments on multiple axons by the sequential extension of axon-contacting filopodia, followed by lamellopodial wrapping (Pfeiffer *et al.*, 1993; Asou *et al.*, 1995). In contrast, SCs form a single segment by deformation

of their whole cell body (Kidd *et al.*, 2013). In addition, SCs origin from neural crest cells, whereas OLs are derived from neuroepithelial cells (Jessen *et al.*, 1994; Rowitch, 2004). Proliferating oligodendrocyte precursor cells (OPCs) migrate to their destined localization into future white matter tracts of the CNS with regulatory contributions of extrinsic signals from neurons and other glial cells of the developing brain (Rowitch, 2004). In peripheral nerves, SC precursors co-migrate with growing axons and their survival and differentiation depend on axonal signals (Jessen & Mirsky, 2005; Nave and Salzer, 2006).

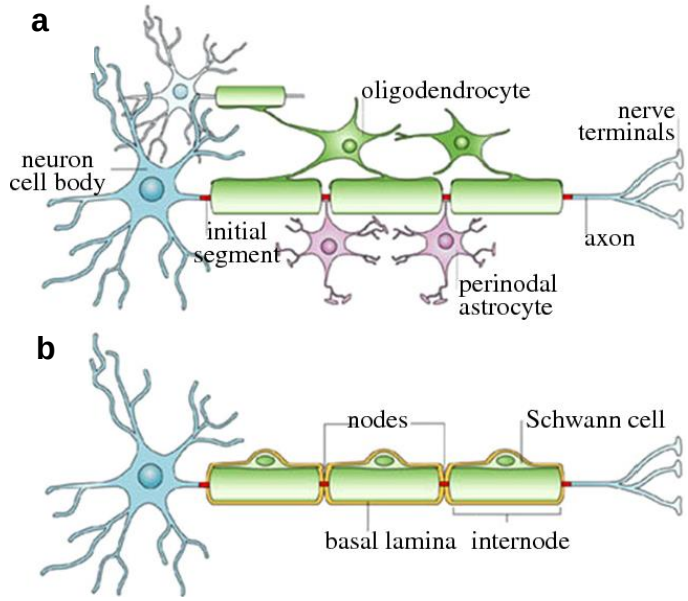

Figure 1-1: Myelin segment formation in the CNS and PNS. (a) Oligodendrocytes in the CNS form internodes on different axons by several filopodial extensions. Perinodal astrocytes with so far unknown function contact the axon in nodal regions. **(b)** Schwann cells in the PNS form each one segment only and a surrounding basal lamina. Taken from (Poliak and Peles, 2003).

In the human brain most myelin sheaths are formed during the first year, but their development is not completed before the age of 20 (Fields, 2008). Bipolar OPCs are already observed at embryonic day (E) 9.5 in the mouse telencephalon, shortly after neuronal specification (Timsit *et al.*, 1995; Poncet *et al.*, 1996; Perez-Villegas *et al.*, 1999). SC precursors are generated in rodent nerves at E12-15. Immature SCs start to segregate axon bundles at E13-17. Postnatally, immature SCs perform axonal sorting, and eventually differentiate into mature pro- and thus myelinating SCs or non-myelinating Remak bundle forming cells (Jessen *et al.*, 1994; Dong *et al.*, 1995; Jessen and Mirsky, 2005). Similar to post-mitotic mature OLs, differentiated SCs exit from the cell cycle. However, upon nerve injury SCs can re-enter the cell cycle by dedifferentiation of mature into immature SCs (Jessen and Mirsky, 2005). Maturation and differentiation within both lineages require complex morphogenetic changes and thus, a tight regulation of the gene expression pattern.

OPCs are characterized by expression of the receptor tyrosine kinase PDGFRα (Platelet derived growth factor receptor) and the chondroitin sulphate proteoglycan NG2 (neural glial antigen 2), regulated by the transcription factors Olig-1 and Olig-2 (Stallcup and Beasley, 1987;

Pringle *et al.*, 1992; Wegner, 2008). Upon differentiation into late progenitors and pro-myelinating OLs, O4-reactive glycoproteins and galactocerebrosides (GalC) are upregulated, whereas NG2- and PDGFRα-expression is lost (Bansal *et al.* 1992; Barateiro and Fernandes 2014). Myelination induction in mature OLs is supposed to be controlled by the transcription factor MyRF (myelin regulatory factor) that binds to myelin protein and lipid synthesis genes (Bujalka *et al.*, 2013). During the transition to myelinating OLs, major myelin components such as the myelin-associated glycoprotein (MAG), 2′,3′-cyclic nucleotide 3′-phosphodiesterase (CNPase), as well as myelin basic protein (MBP) and proteolipid protein (PLP) are upregulated (Fig. 1-2a) (McMorris, 1984; Verity and Campagnoni 1988; Miron and Kuhlmann, 2011). A distinct proportion of OPCs with around 5 to 8 % of all glial cells remain in the adult brain as precursors for myelin remodeling (Dawson *et al.*, 2000; Young *et al.*, 2013).

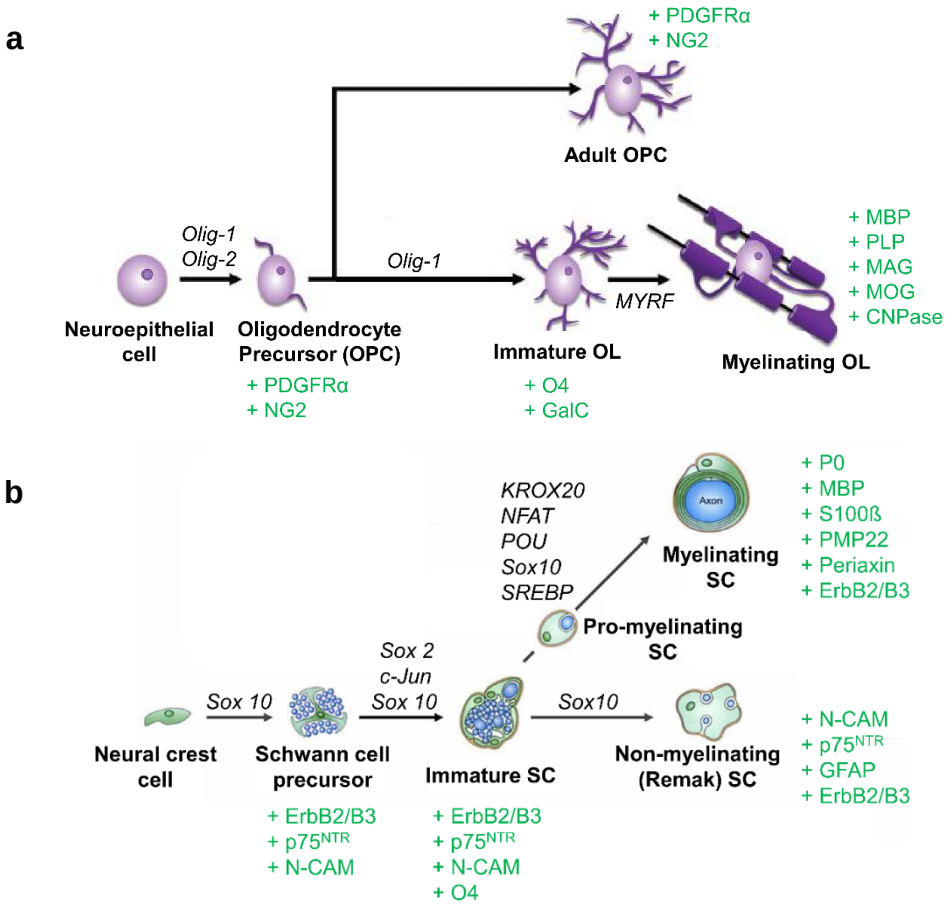

Figure 1-2: Lineage progression of myelinating glial cells. (a) PDGFRα/NG2$^+$ OPCs are derived from neuroepithelial cells and differentiate into O4/GalC$^+$ immature and eventually myelinating oligodendrocytes (OL) that express major myelin components. Modified from (Armada-Moreira *et al.*, 2015). **(b)** Schwann cell precursors assemble with axons via nerve CAM (N-CAM) and ErbB2/B3 paracrine signaling and differentiate into immature O4$^+$ SCs. The pro-myelin stage is marked by upregulation of transcription factors for myelin protein- and lipid-synthesis, and downregulation of cell adhesion molecules (N-CAM). Modified from (Jessen and Mirsky, 2019). green – selected set of proteins expressed in each stage; italic – selected transcription factors that regulate the respective stage transition.

Proteins mainly expressed in immature SCs and downregulated upon differentiation, include the low-affinity neurotrophin receptor $p75^{NTR}$, and the transcription factors c-Jun and Sry box protein (Sox)-2, regulated by cAMP-signaling (Scherer *et al.*, 1994; Parkinson *et al.*, 2004; 2008). The EGF-like receptors, ErbB2 and -B3, and Sox10 are expressed throughout all lineage stages, and are required for proliferation, differentiation and myelination (Kim *et al.*, 1997). Cell cycle exit is mediated by the cyclin-dependent kinase inhibitor p27(Kip1), which is upregulated by the master transcription factor for differentiation into myelinating SCs, the zinc finger protein KROX20/Egr2 (Zorick *et al.*, 1999; Parkinson *et al.*, 2004). KROX20 is repressed in immature SCs by Sox-2 and transcriptionally upregulated in the pro-myelinating stage by POU domain transcription factors, Sox10 and NFAT (nuclear factor of activated T cells) (Topilko *et al.*, 1994; Jaegle *et al*, 2003; Le *et al.*, 2005; Ghislain and Charnay, 2006; Kao *et al.*, 2009; Jang *et al.*, 2010). Following differentiation initiation, myelin-associated proteins such as the scaffolding protein periaxin, the nuclear factor-κB, and the myelin compaction proteins, myelin protein 0 (P0) and MBP are expressed (Lemke and Chao, 1988; Morgan *et al.*, 1991; Parkinson *et al.*, 2003; Patzig *et al.*, 2011; Yoon *et al.*, 2008). Lipid synthesis is induced by upregulation of the sterol regulatory element-binding protein (SREBP) transcription factors (Camargo *et al.*, 2009). In contrast, the expression of cell adhesion molecules (CAM) is downregulated upon differentiation into myelinating but not in non-myelinating mature SCs (Jessen *et al.*, 1987) (Fig. 1-2b).

1.3 The function of myelination

The concentrical wrapping and subsequent compaction of several layers of glial membrane around axons fulfills essential functions in the facilitation of nerve conductance. Myelin segments cover around 99 % of the axonal surface. These internodes are regularly spaced and separated by small gaps of around 1 µm, the nodes of Ranvier (Ranvier, 1871; Salzer *et al.*, 2015). The axon is electrically insulated in internode regions and almost devoid of ion channels, whereas voltage-gated sodium channels ($Na_{v1.6}$ and $Na_{v1.3}$) are concentrated in the nodes (Kordeli *et al.*, 1990; Rasband *et al.*, 1999a). Voltage-gated potassium channels ($K_{v1.1}$ and $K_{v1.3}$) are clustered in a region between node and paranode, the juxtaparanode, and thereby electrically separated from Na_v-channels (Chiu and Ritchie, 1984; Rasband *et al.*, 1999b). The sodium channel density is around six times higher in the nodes of myelinated fibers than on surfaces of non-myelinated axons (Pellegrino *et al.*, 1984; Black *et al.*, 1990). Thus, action potentials that are propagated continuously along the latter, are generated in the nodal regions of myelinated axons only. This saltatory conduction (latin: saltare – jump) allows for fast signal

propagation with up to 150 m/s compared to a maximum of 10 m/s in unmyelinated axons (; Ritchie, 1982; Purves *et al.*, 2001). As concluded from theoretical models, the internode length is adapted to an optimal conduction velocity and correlates almost linearly with the axonal diameter (Waxman, 1980; Murray and Blakemore, 1980; Hildebrand *et al.*, 1993; Simpson *et al.* 2013). In addition, the lamellae number of internodes, which corresponds to the myelin thickness, is strongly correlated to the axonal diameter as well (Hildebrand and Hahn, 1978). Notably, saltatory conduction requires less energy than continuous AP generation (Harris and Atwell, 2012; Waxman *et al.*, 2006).

The axon length is not only critical for signal transduction speed but also for the energy-requiring axonal transport of vesicular cargo and molecules, which maintain axonal and synaptic integrity (Roy *et al.*, 2005). In agreement, the loss of myelin compaction proteins results in early defects in the anterograde and retrograde axonal transport *in vivo* (Lappe-Siefke *et al.*, 2003; Edgar *et al.*, 2004). In the CNS, monocarboxylate transporters that transfer pyruvate and lactate are located in myelin sheaths (MCT1) and the underlying axolemma (MCT2) (Rinholm *et al.*, 2011). Downregulation of MCT1 expression results in a severe progressive neurodegeneration in the brain, but also in peripheral motor neurons, which is rescued by the addition of free lactate (Lee *et al.*, 2012). Trophic support of axons is presumably also enabled by the physical protection of ensheathed axon from activated autoreactive T cells (Neumann *et al.*, 2002), the secretion of stress-protective proteins (Krämer-Albers *et al.*, 2007) and by the production of neurotrophic factors such as the glial cell-derived neurotrophic factor (GDNF) (Wilkins *et al.*, 2003). In addition, SCs transfer mRNA and ribosomes to axons (Court *et al.* 2008; 2011a; Sotelo *et al.* 2013). Moreover, in contrast to CNS axons, peripheral nerve fibers are capable to regenerate after axon injury, greatly supported by SCs. Dedifferentiated SCs perform myelin breakdown to clear the injury sites and support axonal regeneration and neuronal survival before eventual remyelination (Allen and Barres, 2009; Arthur-Farraj *et al.*, 2012).

1.4 Myelin structure

In peripheral nerves, all axons are ensheathed by SCs and arranged within fascicles prior to myelination. This process of radial sorting is performed by pro-myelinating SCs that already attach to axons as precursor cells. They radially form bundles with subsequent separation and association in a 1:1 ratio with large-diameter axons for subsequent myelination. Alternatively, several small diameter, mainly sensory axons are segregated and ensheathed as ‘Remak bundles’ (Webster *et al.*, 1973; Sherman and Brophy, 2005). Axons with a diameter of more

than 1 µm in the PNS, and minimal 0.2 µm to 0.8 µm in the CNS become myelinated (Rushton, 1951; Waxman and Bennett, 1972; Remahl and Hildebrand, 1982; Peters *et al.*, 1991). The ultrastructure and qualitative lipid composition of CNS and PNS myelin sheaths is similar (Werner and Nave, 2005; Chrast *et al.*, 2011). In accordance, fibers that span through the CNS and PNS throughout their development get sequentially myelinated by both cell types (Zalc *et al.*, 2016). Nevertheless, the protein composition of CNS and PNS myelin partially differs. Myelin basic protein (MBP) is one of the most abundant proteins with 8 % in both, CNS and PNS myelin, whereas the most abundant compaction proteins are proteolipid protein (PLP) or myelin protein 0 (P0), respectively, making up around 20 % of total myelin protein (Jahn *et al.*, 2009; Patzig *et al.*, 2011). Interestingly, P0 is the major PNS and CNS myelin protein in fish, implicating that P0 was replaced by PLP in the CNS just with the amphibian evolution (Patzig *et al.*, 2016; Zalc *et al.*, 2016).

Compacted myelin membrane layers comprise a high lipid content of at least 70 % of dry weight, enriched in galactosphingolipids, saturated long-chain fatty acids and especially cholesterol with more than 25 % of total lipid (Norton and Poduslo, 1973; Baumann and Pham-Dinh, 2001; Saher and Simons, 2010). During radial myelin growth, the innermost myelin layer spirally expands around the axon underneath the previously formed membrane layers with simultaneous longitudinal extension to the future node of Ranvier (Bunge *et al.*, 1989; Asou *et al.*, 1995). Conversely, the compaction of the sheaths starts at the outermost layer of already deposited myelin. This process includes tight apposition of membrane layers and extrusion of the cytoplasmic content. The bilipid layers of compact myelin are interconnected by mainly low molecular weight proteins, characterized by a slow turn-over rate (Toyama *et al.*, 2013). For instance, MBP connects the cytoplasmic leaflets of two opposing membranes by oligomerization into a cohesive protein meshwork (Readhead *et al.*, 1987; Uschkureit *et al.*, 2000; Kidd *et al.*, 2013). Compaction at extracellular leaflets is performed by the membrane residing PLP and its splice isoform DM20 or P0 protein and peripheral myelin protein 22 (PMP22), in the CNS and PNS, respectively, through interactions between their extracellular domains (Stoffel *et al.*, 1984; Filbin *et al.*, 1990; Martini *et al.*, 1995; Shapiro *et al.*, 1996; Möbius *et al.*, 2008). This process includes expression downregulation and extrusion of large, negatively charged glycoproteins from these membrane areas (Aggarwal *et al.*, 2011; Bakhti *et al.*, 2013). The directionality of compaction is mediated by compaction antagonists such as the CNPase, which maintains the separation of single membrane layers (Gravel *et al.*, 1996; Yin *et al.*, 1997; Snaidero *et al.*, 2014). A function of CNPase-mediated cyclic adenosine monophosphate (cAMP) conversion is so far not linked to this process. These non-compacted

regions are required for ongoing myelin growth. Additional myelin-associated proteins such as MAG, MOG or PMP2, as well as Claudin-11, the depolymerization of F-actin and the membrane lipid composition presumably contribute to compaction and stability maintenance of myelin membranes (Chow *et al.*, 2005; Majava *et al.*, 2010; Aggarwal *et al.*, 2011; 2013; Zalc *et al.*, 2016). Interestingly, myelin proteins are distinctively synthesized and delivered to the nascent myelin sheath. MBP mRNA is transported and locally translated at glial-axonal contact sites. The synthesized protein subsequently diffuses back and starts to compact the outer myelin layers (Wake *et al.*, 2011; Kidd *et al.*, 2013). In contrast, PLP and the non-compaction protein MAG are synthesized in the endoplasmatic reticulum. After initial transport and incorporation into the OL cell body membrane, both proteins are internalized by endocytosis and targeted to late endosomes/lysosomes for subsequent delivery into the myelin sheaths (Simmons and Trajkovic, 2006; Winterstein *et al.*, 2008; Mironova *et al.*, 2016).

The myelinated fiber is dual polarized, in radially and longitudinally distinct compartments (Fig. 1-3). Radial polarity spans from the abaxonal to the adaxonal membrane via the compacted myelin sheath. In Schwann cell-myelinated fibers, the abaxonal compartment is surrounded by a basal lamina and contains the nucleus. It is interrupted by periodic appositions, enriched in a periaxin-dystroglycan complex which connects cellular cytoskeleton and extracellular matrix (ECM) proteins (Sherman *et al.*, 2012a). They delineate the cajal bands, cytoplasmic channels that contain ß1-integrins, and cytoskeletal proteins for interaction with the basal lamina (Court *et al.*, 2004; 2011b). The compacted myelin region is interspaced by Schmidt-Lantermann-incisures (SLI) that retain cytoplasm and are coupled by gap junctions for intrasheath transport. Interconnected cytoplasmic pockets with active diffusion are also observed in CNS myelin (Velumian *et al.* 2011). The myelinic channel network provides a path for the helical transport of membrane, proteins and RNA, from the glia cytoplasm to the leading edge of myelin growth at the inner tongue and the lateral expansions. Most channels partially and gradually disappear when myelination is terminated. The lateral edges and SLIs remain open, presumably for postnatal myelin remodeling, trophic support of neurons and cross-signaling with the axon (Berthold and Nilsson, 2002; Snaidero *et al.*, 2014). The innermost, non-compacted myelin layer is connected to the axolemma through the periaxonal space by glial and axonal adhesion molecules such as CADM1-4 (Maurel *et al.*, 2007; Spiegel *et al.*, 2007). In addition, glial receptors and their cognate axonal ligands interact through this space.

The adaxonal site is longitudinally subdivided into nodal, paranodal, juxtaparanodal and internodal regions. Nodes of Ranvier are maintained by a meshwork of axonal and glial adhesion molecules (CAMs), extracellular matrix (ECM) and cytoskeletal proteins. Clusters of

voltage-gated channels are anchored to the axonal cytoskeleton by $Ankyrin_G$ and ß-IV spectrins (Kordeli *et al.*, 1995; Davis *et al.*, 1996; Berghs *et al.*, 2000; Eshed *et al.*, 2005), presumably promoted by perinodal astrocytes or SC microvilli which flank CNS and PNS nodal regions, respectively (Saito *et al.*, 2003).The paranodal regions are composed of closely apposed glial membrane loops which retain cytoplasm and represent the lateral growth edges of each myelin layer. Each loop contacts the axon by autotypic junctional complexes of adherens, tight and gap junctions (Rosenbluth, 2009; Snaidero *et al.*, 2014), and electrically separate the juxta-paranodal region with its axonal K_{v1}^{+}-channel clusters (Chiu and Ritchie, 1984; Rasband *et al.*, 1999b). Formation and maintenance of these compartments is actin- and myosin-dependent (Trapp *et al.*, 1989; Fernandez-Valle *et al.* 1997; Wang *et al.* 2008).

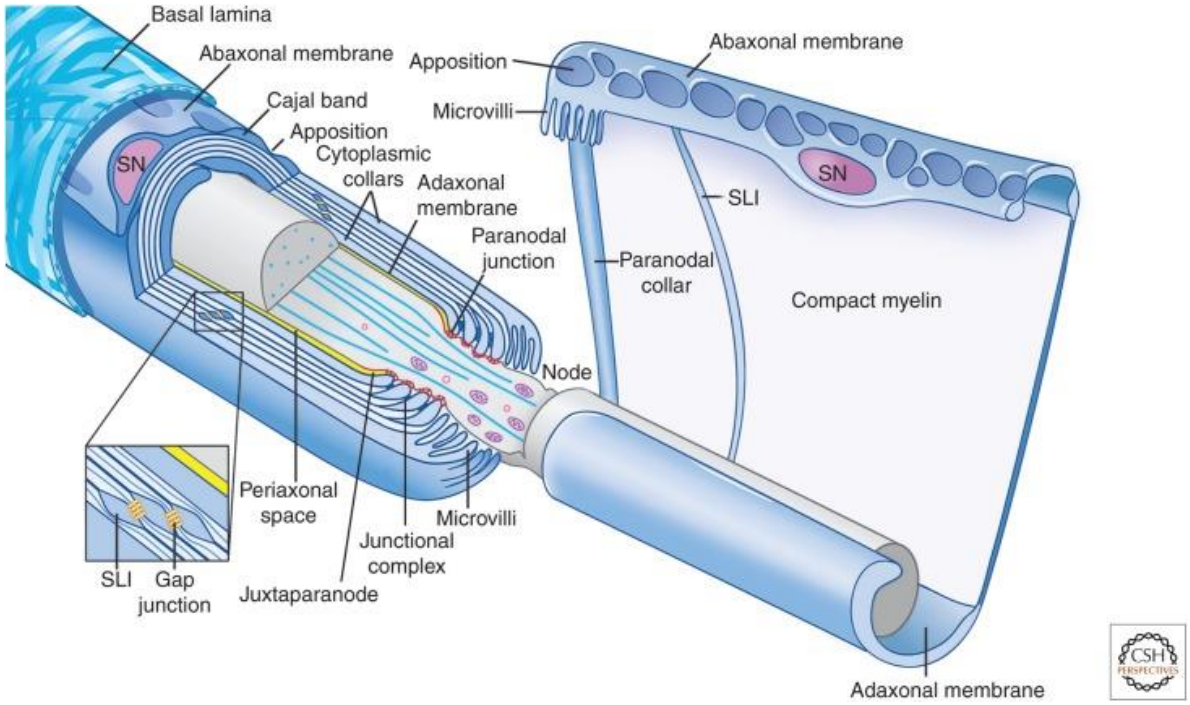

Figure 1-3: Ultrastructure of a myelinated PNS fiber. Radial polarization: adaxonal membrane, compacted sheath, abaxonal membrane; Longitudinal polarization: Node, SC microvilli, paranodal loops, juxtaparanode region, internode (myelin segment); (SN) - Schwann cell nucleus; (SLI) - Schmidt-Lantermann-Inscisure. Taken from (Salzer, 2015).

1.5 Cell signaling pathways in myelination

Several extrinsic and intrinsic factors are transduced by canonical cell signaling pathways in myelinating glial cells. These are partially distinct in the different lineage stages and regulate the transcriptional machinery during proliferation, migration and maturation, as well as myelination induction, maintenance and remodeling. The basal lamina is crucial for SC cell polarity establishment and abaxonal membrane organization (Bunge *et al.*, 1982; 1986; Court *et al.*, 2011b). Autocrine signaling between laminins or collagens with their cognate

receptors at the abaxonal membrane such as ß-integrins, activate cAMP-PKA (Protein kinase A) and class I phosphoinositide-3 kinase (PI3K) signaling. These pathways regulate the transcription of several proteins via POU-domain transcription factors and KROX20 (Howe and McCarthy 2000; Chernousov *et al.* 2008; Monk *et al.*, 2009; Glenn and Talbot, 2013a; Petersen *et al.*, 2015). In addition, downstream, the cytoskeleton-regulating proteins Rac1 and CDC42 are essential for axonal sorting and ensheathment (Bacon *et al.*, 2007; Benninger *et al.*, 2007; Nodari *et al.*, 2007; Chernousov *et al.* 2008). The formation of the basal lamina starts already in the pro-myelinating stage, and is likely guided by axonal signals (Bunge *et al.* 1982) In turn, axonal regeneration after injury is supported by upregulation of integrins (Salzer, 2015; Chang *et al.*, 2018). In contrast to the great loss of OLs upon axonal injury, SCs ensure their survival by activating autocrine circuits, involving PDGF, insulin growth factor (IGF)-1 and neurotrophin (NT)-3 signaling (Ludwin, 1990; Jessen and Mirsky, 1999).

Proper myelination depends to a large extent on the synergistic relationship between neurons and myelinating glial cells (Rushton, 1951; Matthews, 1968; Murray and Blakemore, 1980; Waxmann, 1997). Already the maturation and proliferation of SC precursors and immature SCs is promoted by axonally-anchored neural cell recognition molecule-activated Notch1 and TGFß (transforming growth factor ß)-activated JNK (c-Jun N-terminal kinase) signaling with its terminal component, the transcription factor c-Jun (Hu *et al.*, 2003; Parkinson *et al.*, 2004). Both pathways are downregulated by KROX20 during myelination induction. A key juxtacrine signaling pathway is the activation of the adaxonal residing ErbB2/B3 homo- or heterodimer receptor tyrosine kinases (RTK) by the axonal transmembrane ligand NRG1-typeIII (Brinkmann *et al.*, 2008; Newbern and Birchmeier, 2010). In the PNS, NRG1-III represents the master growth factor for SC proliferation, axonal ensheathment, and myelin thickness (Chen *et al.*, 1994; Morrissey *et al.*, 1995; Michailov *et al.*, 2004; Ogata *et al.*, 2004; Taveggia *et al.*, 2005). This multifunctional outcome is supposed to be achieved by cAMP-mediated modulation of ErbB2/B3 signaling. Both, NRG1-III and cAMP, but not NRG1-III alone, are required to induce myelination in *in vitro* SC mono-cultures (Arthur-Farraj *et al.* 2011). Axonal NRG1-III expression levels positively correlate with the myelin thickness and might even define the axonal fate for non- or myelinating ensheathment: Overexpression of NRG1-III leads to excessive myelination of large diameter axons, and even de novo myelination of the usually just ensheathed sympathetic axons (Michailov *et al.*, 2004; Taveggia *et al.*, 2005). Its genetic inactivation results in reduced myelin thickness and thus, hypomyelination of the PNS (Michailov *et al.* 2004; Brinkmann *et al.*, 2008). In oligodendrocytes, expression of the major RTK that controls OPC proliferation PDGFRα is lost during maturation and thus, myelin

induction is regulated by a set of different growth factors (Raff *et al.*, 1988; Pringle *et al.*, 1989; Fruttiger *et al.*, 2000; Hu *et al.*, 2012). For instance, Fibroblast Growth Factor (FGF) signaling plays a major role in mature OLs and promotes myelination (Carson *et al.*, 1993; Furusho *et al.*, 2012). In some CNS areas, NRG-overexpression results in an increased myelin thickness (hypermyelination) as well. Unlike the PNS, depleting NRG1 protein levels has not an overall CNS hypomyelination effect (Brinkmann *et al.*, 2008; Taveggia *et al.*, 2008).

Transmembrane NRG1 proteins are cleaved by metalloproteases (Falls, 2003). Its cleavage by the α -secretase ADAM17/TACE results in inactivation whereas cleavage by the ß-secretase BACE1 reveals the RTK-ligand EGF (epidermal growth factor)-like domain. Thus, inactivation of either enzyme in mice results in PNS hyper- or hypomyelination, respectively (Hu *et al.*, 2006; Willem *et al.*, 2006; La Marca *et al.*, 2011). NRG1 typeI and -typeII are released from the membrane by BACE1-cleavage and act as paracrine signals. In contrast, the major PNS-neuronally expressed -typeIII remains tethered to the axonal surface and activates ErbB2/B3 as a juxtacrine signal (Meyer *et al.*, 1997; Taveggia *et al.*, 2005). FGF receptors, PDGFRα and ErbB2/B3 are RTKs and activate PI3K/AKT, MAPK (mitogen-activated protein kinases MEK and ERK) and PLCy (phospholipase C) pathways, which are involved in the regulation of myelination in PNS and/ or CNS (Figure 1-4). In SCs, PLCy-mediated activation of cytosolic NFAT proteins by calcineurin induces gene transcription for axonal sorting and ensheathment and promotes myelination by KROX20 activation (Kao *et al.*, 2009). PI3K/AKT and MEK/ERK signaling display crosstalk, for instance on the activation of mTORC1, and defects in either pathway lead to profound myelin impairments *in vivo*, reminiscent of common pathological features (Newbern *et al.*, 2011; Norrmén and Suter, 2013; Furusho *et al.*, 2017).

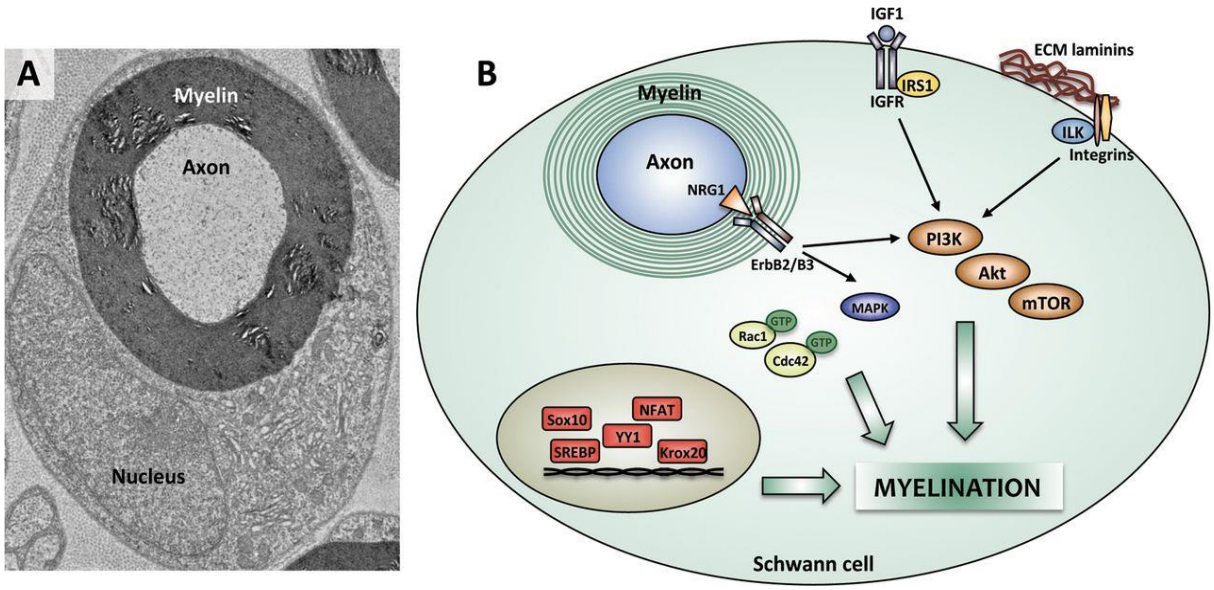

Figure 1-4: Signaling pathways that control myelination in Schwann cells. (a) Electron micrograph of a myelinated axon in the mouse peripheral sciatic nerve, surrounded by compacted myelin sheath and Schwann

cell cytoplasm. **(b)** Schwann cell myelination is regulated by different canonical pathways. It is activated upon (juxta-) paracrine signaling, either from the basal lamina or from axonal Neuregulin (NRG1) via glial receptor tyrosine kinases ErbB2/B3. Downstream, activation of PI3K/AKT or MAPK/ERK translates myelin promoting cues into the transcriptional activation of myelin synthesis. Rac1 and CDC42 regulate cytoskeletal adaptions. Taken from (Norrmén and Suter, 2013).

1.5.1 mTORC1 is a central regulator of myelination

Cells must adapt to different environmental conditions in order to ensure their survival by a tightly regulated metabolism. The serine/ threonine kinase mTOR (mechanistic target of rapamycin) is a key regulator in this process. External stimuli, such as mitogens, growth factors and amino acids are translated by different signaling cascades from the cell environment and converge at the mTOR complex 1 (mTORC1). In nutrient-rich environments mTORC1 is activated and promotes the synthesis of proteins, lipids and nucleotides and thereby cell growth. Under conditions of constrained nutrients, low oxygen or reduced energy levels, mTORC1 is inactivated and the minimal requirements for cell survival are achieved by upregulation of (macro-)autophagy, by which molecules from the cell interior are recycled. This pathway is conserved from yeast to human (Tatebe and Shiozaki, 2017). Higher eukaryotes contain one highly conserved gene for the kinase, which is present in two complexes, mTORC1 and mTORC2 (Sabatini *et al.*, 1994). Raptor and the rapamycin-sensitive peptidyl-prolyl-isomerase FKBP12 are mTORC1 core components (Sabatini *et al.*, 1994; Kim *et al.*, 2002a; 2003a). mTORC2 includes Rictor and mSin1 (Sarbassov *et al.*, 2004; Yang *et al.*, 2006). mLST8 is a component of both complexes. In addition, PRAS40 and DEPTOR are mTORC-associated proteins (Sancak *et al.*, 2007; Peterson *et al.*, 2009).

1.5.1.1 Canonical pathways that regulate mTORC1 activity

Mitogens and growth factors, such as EGF, PDGF or IGF are sensed by RTKs at the plasma membrane (PM). Dimerization and autophosphorylation of the transmembrane receptors upon ligand binding, recruits phosphatidylinositol 3'-kinase class I (PI3K) which phosphorylates phosphatidylinositol-4,5-bisphosphate [$PI(4,5)P_2$] at the D-3 position. The corresponding synthesis of PI-3,4,5-trisphosphate [$PI(3,4,5)P_3$] leads to PM-recruitment of PDK1 (3-phosphoinositide-dependent kinase 1) and the AGC serine/threonine kinase AKT1 (Ak strain transforming 1) (Stephens *et al.*, 1998; Liu *et al.*, 2015a). In addition, the PM-residing mTORC2 complex is activated (Ebner *et al.*, 2017). PDK1 and mTORC2 activate AKT through phosphorylation at Threonin-308 and Serine-478, respectively (Sarbassov *et al.*, 2005). Simultaneously, the dual protein and lipid phosphatase and tensin homolog on chromosome 10 (PTEN) is recruited, which terminates AKT activation by dephosphorylation of $PI(3,4,5)P_3$ to

$PI(4,5)P_2$ (Shenoy *et al.*, 2012). Activated AKT phosphorylates, among several proteins involved in cellular pathways, the heterotrimeric tuberous sclerosis complex (TSC) component TSC2. It is associated in a complex with TSC1 and TBC1D7 and functions as a GAP (GTPase activating protein) for the small GTPase Rheb (Inoki *et al.*, 2002). Phosphorylated TSCs subsequently dissociate from lysosomes and allow for Rheb-mediated facilitation of mTORC1 activity (Sancak *et al.*, 2010; Demetriades *et al.*, 2014; Menon *et al.*, 2014). In addition, RTK-activation results in phosphorylation of the MAPK/ERK kinase (MEK) by the Raf kinase (Avruch *et al.*, 2001; Zarich *et al.*, 2006). Thereby activated ERK (extracellular signal-regulated kinase) inactivates TSC2 and Raptor by phosphorylation (Nishida and Gotoh, 1993; Ma *et al.*, 2005; Carriere *et al.*, 2010). In contrast, AMP-activated protein kinase (AMPK) is activated by glucose deprivation or phosphorylation by LKB1 (liver kinase B1) during hypoxia or upon energy stress. The latter also activates REDD1 (regulated in DNA damage and development 1), and both, AMPK and REDD1 inhibit mTORC1 through activation of the TSC complex (Schneider *et al.*, 2008; Mihaylova and Shaw, 2011; Han *et al.*, 2015a).

Amino acid (aa) stimulation is crucial for the recruitment of mTORC1 to late endosomol/ lysosomal (LE/ Lys) membranes through the heterodimer of four Ras-related GTPases (Rag) A to D (Sancak *et al.*, 2010). GTP-bound RagA or -B form active complexes with GDP-bound RagC or –D, that directly bind the mTORC1-component Raptor (Sancak *et al.*, 2008). Rags are activated by the lysosomal residing pentameric Ragulator complex that functions as a GEF (guanine nucleotide exchange factor) for RagA/B, and inhibited by the GAP complex GATOR1 (Sancak *et al.*, 2008; 2010; Bar-Peled *et al.*, 2012;). The availability of aa is translated to mTORC1 by cytosolic sensors (Sestrin2, Castor1 and Samtor) which inhibit the Rag-GAP complex GATOR1 at the lysosomal compartment directly or indirectly, and thereby enable the activation of the Rag pentamer (Bar-Peled *et al.*, 2013; Wolfson *et al.*, 2015; 2017; Chantranupong *et al.*, 2016; Gu *et al.*, 2017). These sensors are activated upon aa-import by membrane residing aa-transporters or lysosomal aa-export upon protein degradation (Taylor *et al.*, 2013). In addition, the lysosomal residing amino acid exporter SLC38A9 displays a conformational change upon arginine sensing that results in a weaker interaction with Ragulator and thus, increases the GEF-activity of the latter (Zoncu *et al.*, 2011; Bar-Peled *et al.*, 2012; Wang *et al.*, 2015; Rebsamen *et al.*, 2015).

1.5.1.2 Regulation of mTORC1 activity by PI(3)-phosphates

The major PI(3)P synthesizing enzyme class III PI3 Kinase VPS34 (vacuolar protein sorting complex 34), which produces around 65 % of cellular PI(3)P (Volinia *et al.*, 1995;

Devereaux *et al.*, 2013) is strongly implicated in mTORC1 activation. Overexpression or siRNA-mediated depletion of VPS34 results in TSC-independent increased or reduced mTORC1 activity, respectively. In turn, increased VPS34 activity was observed upon amino acid stimulation or glucose-mediated inhibition of AMPK (Byfield *et al.*, 2005; Nobukuni *et al.*, 2005). In mouse fibroblasts (MEF) from VPS34 knockout (KO) animals, aa-stimulated mTORC1 activity is markedly decreased (Jaber *et al.*, 2012). This mechanism might be mediated by the PI3P-dependent lysosomal translocation and activation of Phoshpolipase D (PLD) (Yoon *et al.*, 2011). PLD hydrolizes phosphatidylcholine (PC) to phosphatic acid (PA). This is presumed to facilitate the recruitment of mTORC1 through binding of FKBP12 to PA (Fang *et al.*, 2001; 2003; Xu *et al.*, 2011; Yoon *et al.*, 2011). In addition, the intracellular leucyl-tRNA synthetase (LRS), which activates mTORC1 through its GAP activity towards RagC/D, directly binds to and activates VPS34 (Han *et al.*, 2012; Yoon *et al.*, 2016). VPS34 is only functional as a heterodimer with its myristorylated regulatory subunit p150 (VPS15), a threonine/serine kinase that modulates the activity of VPS34 (Panaretou *et al.*, 1997). This dimer forms the core of two complexes: Autophagic VPS34 complex I (VPS34, VPS15, Beclin1/ATG6 , ATG14L and NRBF2) and endosomal VPS34-complex II (VPS34, VPS15, Beclin1 and UVRAG) (Cao *et al.*, 2014). Under low energy conditions or upon glucose starvation when mTORC1 is downregulated, AMPK-mediated phosphorylation inhibits the endosomal VPS34-complex II as well (Kim *et al.*, 2013a). Lysosomal PI(3)P is also reported as a recruitment factor for the Kinesin-1-, Protrudin- and FYCO1-machinery which mediates lysosomal positioning. In this process lysosomes are translocated to the cell periphery upon amino acid stimulation (Wullschleger *et al.*, 2006; Korolchuk *et al.*, 2011; Raiborg *et al.*, 2015; Hong *et al.*, 2017). PI(3,5)P_2, the product of PI(3)P phosphorylation at the D-5 position by PI(3)-phosphate 5-kinase type III PIKfyve (Fab1 in yeast), is directly linked to mTORC1 activation as well (Sbrissa *et al.*, 1999; Zolov *et al.*, 2012; Bridges *et al.*, 2012). PIKfyve-depleted adipocytes display decreased mTORC1 activity upon amino acid and insulin stimulation, but independent of AKT activation. In addition, elevated mTORC1 activity was observed when cells were directly supplemented with PI(3,5)P_2. As causative, the authors identified PI(3,5)P_2-mediated recruitment of Raptor (Bridges *et al.*, 2012). This finding was later confirmed in yeast for the Raptor-homologue Kog1 (Jin *et al.*, 2014). PIKfyve is associated in a complex with the PI(3,5)P_2 D-5-phosphatase Fig4 (Vac7 in yeast), scaffolded by Vac14 (Jin *et al.*, 2008; McCartney *et al.*, 2014). Disruption of the complex by removing either of the components results in decreased cellular PI(3,5)P_2 levels (Mironova *et al.*, 2016). This approach caused hypersensitivity of yeast cells towards rapamycin, a compound that selectively inhibits

mTORC1. In addition, the authors reported a PI(3,5)P_2-dependent recruitment of the mTORC1 target Sch9, the yeast homologue of the serine/threonine protein kinase p70 S6 Kinase 1 (S6K) (Jin *et al.*, 2014). Conversely, PI(3,4)P_2, synthesized by the late endosomal/ lysosomal class II PI3-kinase type C2ß has been shown to locally repress mTORC1 activity in response to growth factor starvation (Marat *et al*., 2017).

1.5.1.3 mTORC1 controls the metabolic switch of cells

The activation status of mTORC1 represents the main switch between anabolism and catabolism of the cell (Fig. 1-5). Upon activation, mTORC1 phosphorylates the eukaryotic translation initiating factor (eIF) 4E-binding protein 1 (4E-BP1) and S6K (Threonine-389). The complex thereby activates global mRNA translation, and especially translation of the highly eIF4E-sensitive transcripts, which encode for proliferation- and cell survival-regulatory proteins (Gingras *et al.*, 1999; Holz *et al.*, 2005; Csibi *et al.*, 2014; Nandagopal and Roux, 2015). The translation of 5'-terminal oligopyrimidine (TOP) mRNAs is specifically dependent in an all-or-none fashion on mTORC1 activity. These mRNAs encode ribosomal proteins, elongation factors and polypyrimidines (Jefferies *et al.*, 1994; Avni *et al.*, 1997; Meyuhas, 2000). In addition, S6K phosphorylates the 40s ribosomal protein S6 (S6), which is especially involved in the translation of cell size-regulating genes (Fumagalli and Thomas, 2000; Ruvinsky *et al.*, 2005). SREBPs are important transcription factors for lipid, fatty acid and cholesterol synthesis, and activated by mTORC1-dependent phosphorylation of S6K and lipin1 (Porstmann *et al.*, 2008; Düvel *et al.*, 2010; Li *et al.*, 2010; Peterson *et al.*, 2011). mTORC1 also promotes trafficking and maturation of SREBPs by phosphorylation of the SREBP-inhibitor CRTC2 (Han *et al.*, 2015b). Simultaneously, mTORC1 inhibits autophagy by phosphorylation of the autophagy-initiation complex ULK1/Atg13/FIP200 (Hosokawa *et al.*, 2009; Jung *et al.*, 2009). Moreover, the phosphorylation of TFEB (transcription factor EB), a master regulator of gene expression for lysosomal and autophagosomal proteins, prevents its translocation to the nucleus (Settembre *et al.*, 2011; Martina *et al.*, 2012).

Finally, mTORC1 elicits negative feedback loops that ensure its transient activation. S6K directly inhibits the mTORC2 components Rictor and mSin1 by phosphorylation (Julien *et al.*, 2010; Liu *et al.*, 2013). S6K and growth factor receptor bound protein 10 (Grb10) inhibit the interaction of insulin receptor substrate 1 (IRS1) with the insulin receptor (IR) upstream of mTORC1 (Harrington *et al.*, 2004; Hsu *et al.*, 2011). In contrast, S6K promotes mTORC1 activity by phosphorylation at Serin-2448 in a positive feedback loop (Chiang and Abraham, 2005; Copp *et al.*, 2009; Rosner *et al.*, 2010).

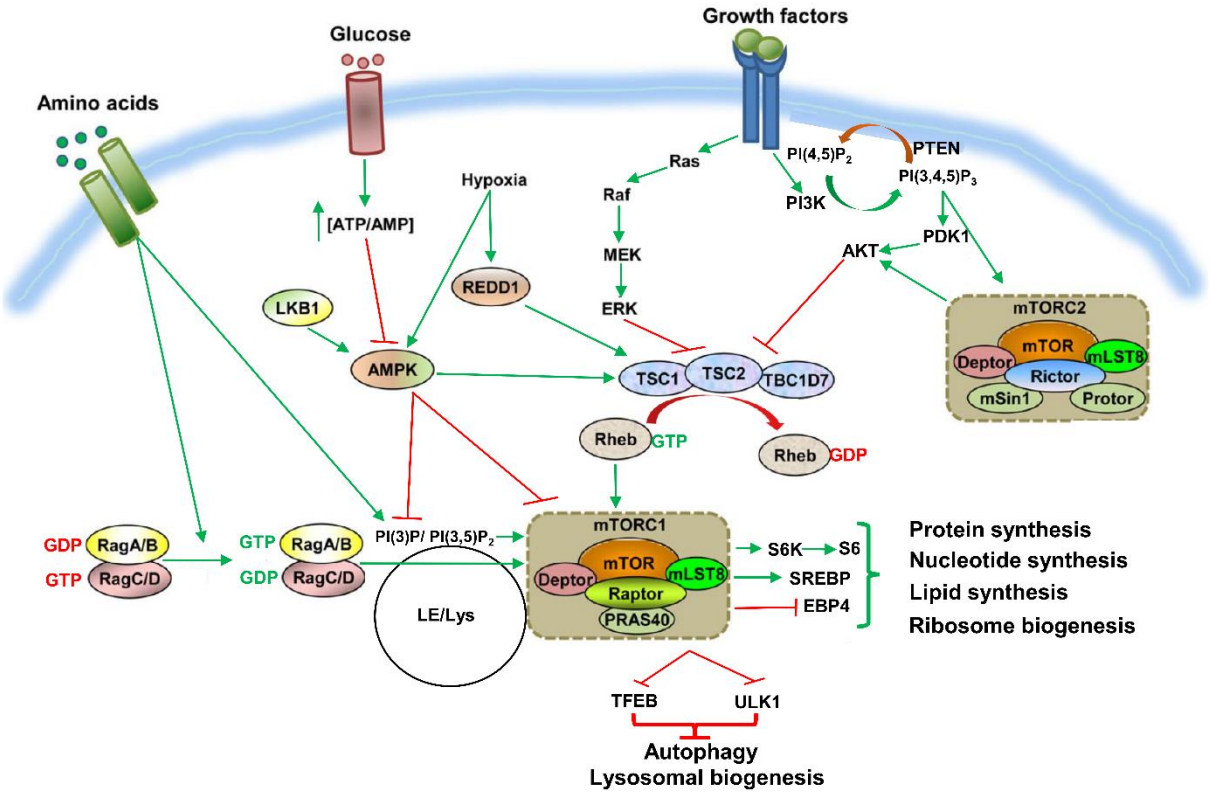

Figure 1-5: Regulation of mTORC1 activity. mTORC1 is recruited to lysosomes upon amino acid stimulation by Rag-complexes. Its activity is facilitated by growth factor stimulation via PI3K/AKT or MAPK/ERK. The complex promotes synthesis of lipids and proteins and thus cell growth. Under conditions of growth factor or amino acid deprivation, mTORC1 activity is downregulated by TSC complexes. During hypoxia or energy depletion, AMPK and REDD1 mediate mTORC1 inhibition and thus promote autophagy and lysosomal biogenesis. LE/Lys – late endosomal/ lysosomal compartment. Modified from (Kim *et al.*, 2013b).

1.5.1.4 Altered mTORC1 activity leads to impaired myelin homeostasis

The first indications for an essential regulation of the myelin homeostasis by mTORC1 were just reported around one decade ago. Overactivation of PI3K/AKT in OLs by expression of constitutively active AKT(CA) or depletion of PTEN *in vivo*, results in radial hypermyelination, thus an increase in the myelin sheath thickness in the CNS (Flores *et al.*, 2008; Goebbels *et al.*, 2010). In the transgenic AKT(CA) mice, this phenotype, accompanied by an increase in myelin protein levels, was traced back to elevated mTORC1 activity as the only altered AKT-target in these mutants, and was ameliorated by Rapamycin-mediated mTORC1 inhibition (Narayanan *et al.*, 2009). In turn, application of rapamycin or knockdown of mTOR in OL cultures leads to reduced myelination *in vitro* (Tyler *et al.*, 2009). *In vivo*, Rapamycin treatment results in an altered expression of a cohort of transcripts, including transcription factors for differentiation, myelin lipid synthesis enzymes and major myelin proteins (Tyler *et al.*, 2011). Moreover, the activity of mTORC1, detected by the S6K

phosphorylation site S-2448, positively correlates with the extent of CNS myelination *in vivo* (Tyler *et al.*, 2009). In the PNS, mTORC1 activation is mainly observed downstream to adaxonal NRG1-ErbB2/B3 signaling (Heller *et al.*, 2014). In contrast to the CNS, the first studies that investigated knockout of PTEN in SCs *in vivo* reported radial hypermyelination for small diameter (< 2 µm) fibers only (Goebbels *et al.*, 2010; 2012). In addition, and more pronounced than in the CNS, aberrantly myelinated nerve fibers were observed. These fibers were characterized by focal sausage-like thickening of the myelin sheath ('tomacula') and myelin outfoldings at paranodal regions. These features, referred to as focal hypermyelination, could be rescued by rapamycin treatment as well (Goebbels *et al.*, 2012). The authors claimed striking similarities of the myelin morphology to two forms of human neuropathies with focal hypermyelination, Charcot-Marie-Tooth (CMT) disease type 4B and Hereditary Neuropathy with liability to pressure palsies (HNPP). In turn, the depletion of mTOR *in vivo* causes hypomyelination in the CNS as well as in the PNS (Sherman *et al.*, 2012b; Wahl *et al.*, 2014). In three independent following studies, the crucial involvement of mTORC1 in myelination, with only minor contribution of mTORC2, was revealed by the specific ablation of Rictor or Raptor *in vivo* (Bercury *et al.*, 2014; Lebrun-Julien *et al.*, 2014; Norrmén *et al.*, 2014). Transgenic mice depleted of Raptor display severe hypomyelination in CNS and PNS. Furthermore, lower levels of SREBPs and their targets, the fatty acid synthase, stearolyl-CoA desaturase-1, 3-hydroxy-3-methylglutaryl-CoA reductase (HMGCR) and isopentenyldiphosphate delta isomerase 1(IDI1) were observed. In addition, Raptor depletion results in reduced levels of cholestorol, nonessential fatty acids, phosphatidylcholine, ceramide, sphingomyelin, glycosylceramide, phosphatidylethanolamine and phosphatidylinositol, in the spinal cord and sciatic nerves (Lebrun-Julien *et al.*, 2014; Norrmén *et al.*, 2014). These findings revealed mTORC1 as crucially implicated in the regulation of the myelin lipid production in both, the CNS and PNS (Lebrun-Julien *et al.*, 2014; Norrmén *et al.*, 2014). Furthermore, the expression of major myelin proteins is markedly downregulated in these mice. Raptor depletion in the CNS results in a reduction of mRNA and protein levels of MAG, MOG, PLP and CNP (Bercury *et al.*, 2014; Lebrun-Julien *et al.*, 2014). For MBP, mainly protein levels are reduced, suggesting a distinct effect on MBP translation. In the PNS, reduced MBP and P0 protein but not MAG protein levels were reported (Norrmén *et al.*, 2014).

Most recent studies indicate a more complex function of mTORC1 in the PNS than promoting myelinogenesis only. Hyperactivation of mTORC1 is observed to have dosage- and time-dependent effects (Beirowski *et al.*, 2017; Figlia *et al.*, 2017; Jiang *et al.*, 2018). In the PNS, strong hyperactivation of mTORC1 in *TSC2* KO^{SC} mice results in hypo- instead of

hypermyelination. In contrast, *TSC1* KO^{SC} mice display an initial delay in the myelination onset, followed by focal hypermyelination of PNS fibers (Beirowski *et al.*, 2017). mTORC1 activity is more modestly increased upon TSC1 depletion, due to destabilized but not abolished TSC2 GAP activity (Zeng *et al.*, 2011). Thus, this contrasting outcome was interpreted as a dosage-dependent effect, resulting from the promoting function of mTORC1 in the proliferation of precursor and immature Schwann cells. The complex inhibits the cell cycle exit in different cell types by the indirect repression of the cyclin dependent kinase (CdK)-inhibitor p27kip1 (Hong *et al.*, 2008; Ji *et al.*, 2012; Ke *et al.*, 2016; Beirowski *et al.*, 2017). In agreement with a thus presumed time-dependent effect of mTORC1 elevation, the early ablation of *TSC1* KO^{SC} using a Desert hedge hoc (Dhh)-controlled Cre recombinase (Jiang *et al.*, 2018) instead of a P0-controlled one (Beirowski *et al.*, 2017), expressed at E12 and E13.5, respectively, leads to sustained hypomyelination similar to *TSC2* KO^{SC} nerves. The authors also observed an upregulation of the polo-like kinase (PLK) that promotes the G2/M transition during cell cycle progression (Jiang *et al.*, 2018). In addition, mTORC1 was reported to indirectly inhibit KROX20 through S6K and thereby the onset of myelination, thus mTORC1 activity needs to be repressed in promyelinating Schwann cells to allow for proper myelination (Figlia *et al.*, 2017). In turn, the SC-specific conditional ablation of PTEN or TSC1 in adult mice using tamoxifen induction, causes not only focal but also radial hypermyelination (Figlia *et al.*, 2017; Jiang *et al.*, 2018), reminiscent of the myelin promoting function of mTORC1 observed in the CNS. Why elevated mTORC1 activity leads to focal hypermyelination is equally unknown as the underlying molecular mechanisms of the formation of these aberrant myelin features. mTORC1-independent targets downstream to PTEN and AKT, such as PI(3,4,5)P_3 or Rac1, respectively, are suggested to contribute to radial hypermyelination (Goebbels *et al.*, 2012; Snaidero *et al.*, 2014; Domenech-Estevez *et al.*, 2016). In the CNS, mTORC1 activation mediated by MAPK/ERK signaling downstream of fibroblast growth factor receptor 2 (FGFR2), was recently postulated to increase myelin thickness independent of the PI3K/AKT pathway (Ishii *et al.*, 2013; Furusho *et al.*, 2017). In the PNS, ERK overactivation results not only in mTORC1 hyperactivation and focal hypermyelination but also radial hypermyelination, which was partially assigned to mTORC1 independent targets of ERK (Sheean *et al.*, 2014).

1.6 Myelin in pathological conditions

Impaired myelin homeostasis in the CNS leads to common neurodegenerative diseases such as Multiple Sclerosis and leukodystrophies, but also to psychiatric disorders as Schizophrenia or depressions (Raymond, 2017; Gibson *et al.*, 2018). In the PNS, a plethora of

proteins are associated with the heterogeneous group of inherited neuropathies including Charcot-Marie tooth disease (CMT) (Berger *et al.*, 2006a; Pareyson *et al.*, 2017). CMT diseases result from mutations in more than 80 different genes known to date, and represent the most commonly inherited neuropathy with a current estimation of 10 to 28 affected individuals per 100.000 (Skre, 1974; Saporta *et al.*, 2014; Pareyson *et al.*, 2017). These neuropathies mostly result in neuronal degeneration and are characterized by progressive muscle weakness and atrophy of the distal extremities, often accompanied by a sensory loss (Berger *et al.*, 2006a; Saporta *et al.*, 2014). According to the classical system, CMT disease types are categorized depending on the primarily affected cell type into demyelinating (type I; CMT1-like) or axonal (type II; CMT2-like) neuropathies, with nerve conduction velocity (NCVs) below or above 38 m/s, respectively (Reilly *et al.*, 2011). Autosomal dominant demyelinating CMT1 subtypes result from gene duplications of the myelin protein PMP22 (CMT1A), or mutations in the myelin compaction protein P0 (CMT1B), the transcription factor KROX20 (CMT1D) or the X-linked gap junction beta-1 gene/Connexin32 (GJB1; CMTX1) (Warner *et al.*, 1998; Pareyson *et al.*, 2017). The CMT4 subgroup comprises demyelinating neuropathies that are inherited in an autosomal recessive fashion and characterized by an early onset during childhood (Baets *et al.*, 2011). These types are caused by mutations in the scaffolding protein Periaxin (CMT4F), the adaptor protein SH3TC2 (SH3 Domain And Tetratricopeptide Repeats 2; CMT4C), the CDC42-GEF Frabin/FDG4 (CMT4H) or MTMR proteins (CMT4B) (Harding and Thomas, 1980; Baets *et al.*, 2011; El-Abassi *et al.*, 2014). Myelin outfoldings are a hallmark of CMT4B, but can also be observed in CMT4F and CMT4H, as well as in HNPP, caused by haplo-insufficiency of PMP22 (Adlkofer *et al*, 1997; Guilbot *et al.*, 2001; Azzedine *et al.*, 2003; Senderek *et al.*, 2003; Nave *et al.*, 2007; Stendel *et al.*, 2007; Nakhro *et al.* 2013). The appearance of myelin outfoldings is also reported from young animals as part of the developing sheath formation in CNS and PNS, but the underlying molecular mechanism remains elusive (Berthold and Nilsson, 2002; Bolino *et al.*, 2004; Goebbels *et al.*, 2012). Interestingly, different CMT-disease subtypes are caused by mutations in genes that are associated with PIs, the major signaling lipids of endomembrane trafficking. Mutations in the lipid-binding PH (pleckstrin homology) domain of the fission GTPase Dynamin-2 underly dominant intermediate CMT (DI-CMT), and the CMT4H-related GEF Frabin also harbors PH- and FYVE-lipid binding domains (McNiven, 2005; Zuchner *et al.*, 2005; Delague *et al.*, 2007; Stendel *et al.*, 2007). Intriguingly, CMT4B and CMT4J are caused by mutations in enzymes that are directly implicated in PI(3)-phosphate lipid conversion, suggesting a significant role of the signaling lipids PI(3)P, PI(3,5)P2 and presumably also PI(5)P in myelination and axonal maintenance (Fig. 1-6) (Suter,

2007; Vaccari *et al.*, 2011; Mironova *et al.*, 2016). Loss of function mutations in the PI(3,5)P_2 5-phosphatase Fig4/Sac3 results primarily in axonal degeneration in both, PNS and CNS, but is accompanied by thinly myelinated fibers (Chow *et al.*, 2007; Sbrissa *et al.*, 2007). CMT4B comprises three disorder subtypes that are caused by mutations in myotubularin-related PI phosphatase (MTMR)-proteins, that specifically hydrolyze PI(3)P and PI(3,5)P_2 at the D-3 position (Senderek *et al.*, 2003; Nakhro *et al.*, 2013; Bolino *et al.*, 2014).

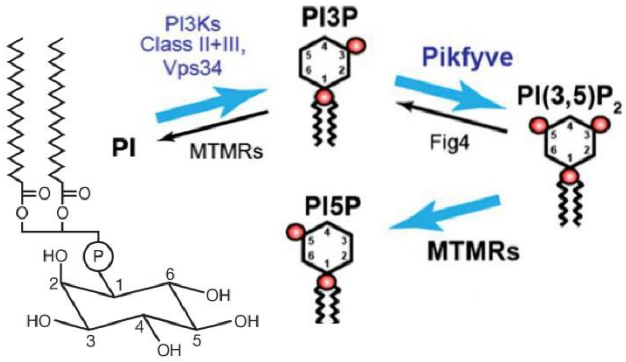

Figure 1-6: Interconversion of PI(3)P, PI(3,5)P_2 and PI(5)P. PI(3)P is synthesized from PI by class II and III PI-3 Kinases. It serves as the only known precursor for PI(3,5)P_2 production by PIKfyve, which is associated in a complex with the 5'-phosphatase Fig4. MTMR proteins are 3'-phosphatases with a preference for PI(3)P and PI(3,5)P_2. PI – phosphatidylinositol. Modified from (Di Paolo and De Camilli, 2006; Zolov *et al.*, 2012).

1.6.1 Myotubularins are crucially involved in myelination

1.6.1.1 The family of myotubularin-related lipid phosphatases

Myotubularin-related lipid phosphatases (MTMRs) are a conserved family of multi-domain proteins that dephosphorylate the phosphatidylinositol ring of PI-phosphates at the D-3 position with a specificity towards PI(3)P and PI(3,5)P_2 *in vitro* (Blondeau *et al.*, 2000; Taylor *et al.*, 2000; Schaletzky *et al.*, 2003; Tronchére *et al.*, 2004). In human, the family includes fifteen members: myotubularin 1 (MTM1) and MTMR1 to MTMR14. Nine of these, MTM1, MTMR1 to -R4 and MTMR6 to -R8 as well as MTMR14/JUMPY, contain a catalytically active protein tyrosine phosphatase (PTP) domain, characterized by an invariant PTP active site motif $C(X)_5R$ (Alonso *et al.*, 2004). MTMR5(Sbf1), -R9 and -R10 to -R13(Sbf2) are pseudophosphatases that contain an inactive PTP domain with substitutions of the conserved cysteine and arginine residues in its catalytic site (Robinson and Dixon, 2006).

Except for MTMR14, all family members contain a PH -glucosyltransferase, Rab-like GTPase activator and myotubularin (PH-GRAM) domain and a coiled-coil (CC) region, N-terminal and C-terminal to the PTP-domain, respectively (Figure 1-7). The PH-GRAM domain mediates binding to PI(3,5)P_2 and PI(5)P *in vitro* (Berger *et al.*, 2003; Schaletzky *et al.*, 2003; Tsujita *et al.*, 2004), while the CC region is required for homo- and hetero-oligomerization (Berger *et al.*, 2006b; Zou *et al.*, 2009; 2012). Additional domains are found in closely related MTMRs, such as a C-terminal PDZ (protein-binding PSD95, Dlg-1, Zo-1)-domain in MTM1,

-R1 and –R2, a FYVE (Fab1, YO1B, Vac and EEA1) in MTMR3 and -R4, or PH and DENN (differentially expressed in neoplastic versus normal cells) domains in MTMR5 and -R13 (Isakoff *et al.*, 1998; Lorenzo *et al.*, 2005; Berger *et al.*, 2006b). MTMR pseudophosphatases have a main function in the recruitment and activity modulation of active MTMR phosphatases. The complex formation between an inactive and an active MTMR is mediated by the CC region (Berger *et al.*, 2006b), and results in increased catalytic activity, elevated substrate specificity and altered localization of the latter. This is reported for MTMR6, –R7, and –R8, each forming a complex with MTMR9 (Mochizuki and Majerus, 2003; Zou *et al.*, 2009, 2012), MTM1 that oligomerizes with MTMR12 (Caldwell *et al.*, 1991), and MTMR2 which associates with MTMR5 or MTMR13 (Kim *et al.*, 2003b; Berger *et al.*, 2006b).

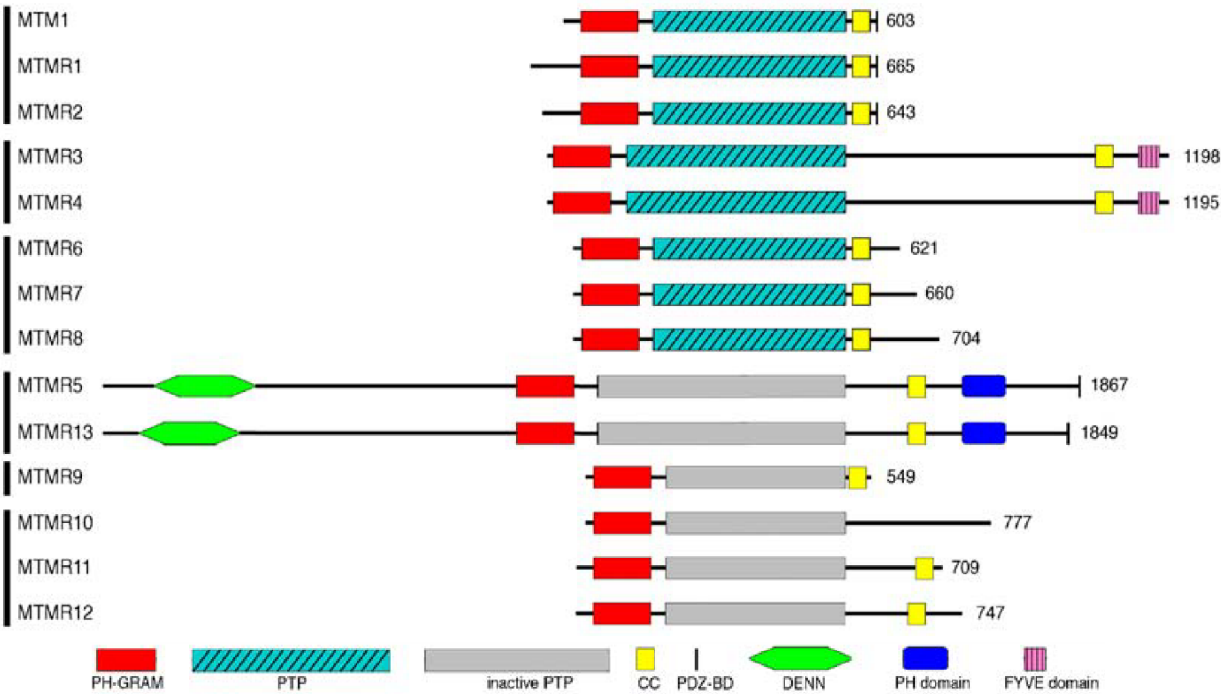

Figure 1-7: Myotubularin-related (MTMR) protein domain structures. PH – pleckstrin homology; GRAM - glycosyltransferase, Rab-like GTPase activator and myotubularin; PTP – protein tyrosine phosphatase; CC – coiled-coil region; PDZ-BD - PSD-95/Dlg-1/ZO1-binding domain; DENN - differentially expressed in neoplastic versus normal cells; FYVE - Fab1, YOTB, Vac1, EEA1 domain. Taken from (Bolis *et al.*, 2007).

As regulators of the signaling PI lipids which serve as hallmarks of intracellular membrane identities, MTMR proteins are mainly involved in endomembrane trafficking. Despite of their common substrate specificity towards PI(3)P and PI(3,5)P_2, some members are reported to regulate the lipid pool on distinct compartments (Fig. 1-8). PI(3)P and PI(3,5)P_2 are sequential key players of the endo-lysosomal pathway. PI(3)P, mainly generated by VPS34 with contributions of class II PI3K, is the major lipid at early or recycling endosomal membranes,

where endocytosed cargo is sorted, either for recycling back to the plasma membrane or into the lysosomal pathway for degradation (Mayinger, 2012). PI(3)P-dependent formation of and cargo sorting into intraluminal vesicles (ILV), as well as the partial conversion of PI(3)P into $PI(3,5)P_2$ mediated by PIKfyve, is required for the maturation of endosomes into late endosomal multi-vesicular bodies (MVBs) and their eventual fusion with lysosomes (Raiborg *et al.*, 2013; Sbrissa *et al.*, 1999; Zolov *et al.*, 2012). In addition, PI(3)P is synthesized on autophagosomal membranes and crucial for their maturation and eventual fusion with lysosomes (Taguchi-Atarashi *et al.*, 2010; Cebollero *et al.*, 2012; Wu *et al.*, 2014).

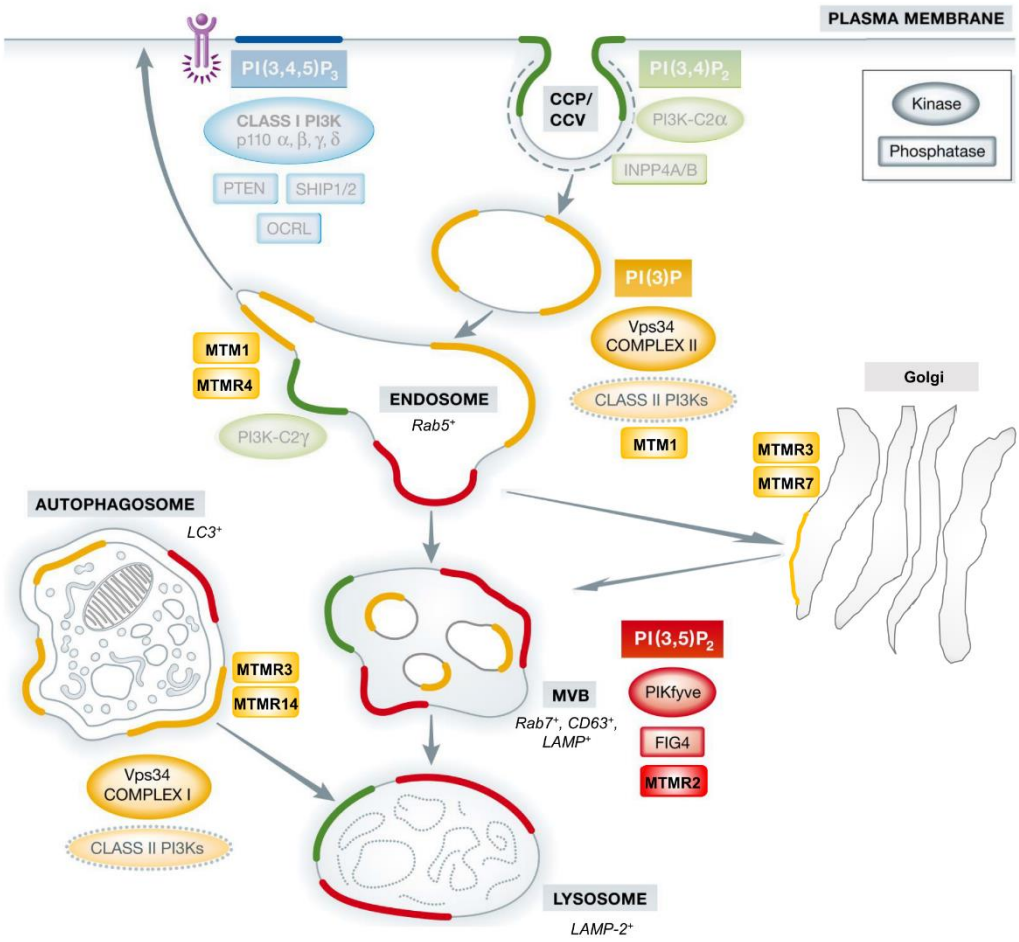

Figure 1-8: PI(3)-phosphates and metabolizing enzymes in endomembrane trafficking. Schematic overview of the localization of PI(3)-phosphates (rectangle) and their converting phosphatases (oval) and kinases (rounded rectangle). $PI(3,4,5)P_3$ is produced upon RTK-activation at the plasma membrane. Receptors or other cargo are internalized in endocytic compartments whose maturation and fusion with endosomes requires the conversion from plasma membranous $PI(3,4)P_2$ into PI(3)P. Upon endosomal sorting, receptors are either recycled back to the PM after ligand dissociation, as the transferrin receptor (TfR), or directed into the lysosomal degradation pathway, as the EGF receptor (EGFR). PI(3)P is partially converted into $PI(3,5)P_2$ by PIKfyve during the maturation of early into late endosomal MVBs and their eventual fusion with lysosomes. PI(3)P production is also required for the formation and maturation of autophagosomes, which eventually fuse with lysosomes, and trafficking from and to the trans-golgi network. MVB – multi vesicular body; CCV/ CCP – Clathrin-coated vesicle/ pit. Modified from (Marat and Haucke, 2016) according to (Hnia *et al.*, 2012).

MTM1 and MTMR4 are observed on early and recycling endosomes (Lorenzo *et al.*, 2006; Cao *et al.*, 2007; Naughtin *et al.*, 2010; Ketel *et al.*, 2017), MTMR2 and -R5 on late endosomes (Berger *et al.*, 2003; Kim *et al.*, 2003b). MTMR14 and MTMR3 localize to autophagosomal structures (Vergne *et al.*, 2009; Taguchi-Atarashi *et al.*, 2010) and MTMR7 partially to golgi-like granules (Mochizuki and Majerus, 2003). The complex MTMR6/-R9 acts in negative regulation of apoptosis by controlling $PI(3,5)P_2$ levels, while the MTMR8/-R9 complex is a negative regulator of autophagy by dephosphorylation of PI(3)P (Zou *et al.*, 2009; 2012). MTM1 and MTMR2 are observed to act sequentially in the endolysosomal system. MTM1 hydrolizes PI(3)P at early endosomes (Rab5-positive), MTMR2 at late endosomes (Rab7-positive) (Cao *et al.*, 2007, 2008). Finally, though MTMRs are ubiquitously expressed (Laporte *et al.*, 1998), a distinct tissue enrichment is observed for some family members. A 2.4 kbp *MTM1* transcript is found in muscle tissue and testis only, and its loss results in the severe muscle disease X-linked centronuclear myopathy (XLCNM) (Laporte *et al.*, 1996; 1998; Tosch *et al.*, 2006). MTMR2 enrichment in neurons and Schwann cells was reported, and its mutations result in the severe neuropathy CMT4B1 (Berger *et al.*, 2002; Bolino *et al.*, 2002; 2004).

1.6.1.2 CMT-associated MTMRs

Mutations in MTMR2 or its alternating complex partners MTMR13 and MTMR5 cause CMT4B1, -B2 or –B3, respectively. The common pathology in human patients is a severe demyelinating peripheral neuropathy with an early onset during childhood. It is caused by defects in the Schwann cell myelin homeostasis and characterized by focally folded myelin sheaths at paranodal regions (Senderek *et al.*, 2003, Bolino *et al.*, 2004; Nakhro *et al.*, 2013). Death can occur already in the fourth to fifth decade mainly due to respiratory failure (Quattrone *et al.*, 1996). In addition, azoospermia is found in CMT4B3 patients and one -B1 case, as well as in the corresponding mouse models (Firestein *et al.*, 2002; Laporte *et al.*, 2003; Bolino *et al.*, 2004; Bohlega *et al.*, 2011), and glaucoma in 50 % of all CMT4B2 and -B3 cases (Bird, 1998; Hirano *et al.*, 2004). In CMT4B3 patients, impairments of the CNS, such as cerebellar or brain atrophies, cognitive defects or intellectual disabilities are reported. Finally, MTMR5 mutations can also lead to axonal neuropathy and the fork and bracket syndrome, characterized by degenerated fiber bundles in facial and oculomotoric nerves (Alazami *et al.*, 2014; Romani *et al.*, 2016; Manole *et al.*, 2017).

MTMR proteins are highly conserved. Human and mice homologues confer sequence identities greater than 90 %. In accordance, *MTMR2* and *MTMR13* KO mice display a demyelinating neuropathy, though in a milder form than humans, with a late axonal loss (Bolino

et al., 2004; Tersar *et al.*, 2007; Ng *et al.*, 2013). *MTMR5* KO mice are characterized by azoospermia only (Firestein *et al.*, 2002). MTMR2 is the closest related to the active phosphatases MTMR1 and MTM1, with a sequence identity of 69.7 % and 63.4 %, respectively. MTMR13 and MTMR5 are most closely related with 59 % sequence identity. Similar to MTM1 in XLCNM, MTMR2 disease-related truncation or missense mutations are mainly located in evolutionary highly conserved residues in the PTP- and PH-GRAM domain, thus abolishing specifically the phosphatase activity and the presumed ability to bind to lipids (Laporte *et al.*, 1997; 1998; Taylor *et al.*, 2000; Berger *et al.*, 2002; Tsujita *et al.*, 2004; Goryunov *et al.*, 2008). In accordance, disrupting the complex Fig4-Vac14-PIKfyve, which leads to reduced levels of $PI(3,5)P_2$, can ameliorate the phenotype of MTMR2 loss. *Fig4* heterozygosity rescues myelin outfoldings in *MTMR2* KO mouse *in vivo*, and PIKfyve depletion rescues myelin outfoldings *in vitro* (Vaccari *et al.*, 2011). Reports about the endogeneous localization of MTMRs are rare due to the limited availability of functional antibodies. MTMR2 was detected in the cytosol of neurons, axons and in Schwann cell cytoplasm, such as the SC perinuclear region, paranodes and SLIs. Here, it is partially localized to punctate, presumably endo-/ lysosomal structures (Previtali *et al.*, 2003; 2007; Ng *et al.*, 2013). Despite of the general lipid binding ability of MTMR2 by its PH-GRAM domain, its recruitment to endomembranes is rather not constitutive but regulated, for instance by complex formation. Upon overexpression, MTMR2 is diffusively localized in the cytoplasm, with partial enrichment in the perinuclear region. The latter is more frequently observed upon co-expression with MTMR5 or MTMR13 (Laporte *et al.*, 2002; Berger *et al.*, 2003; Kim *et al.*, 2002b; 2003b; Robinson and Dixon, 2006). Despite both pseudophosphatases contain the additional lipid-binding PH-domain at the C-terminus, it was shown to be dispensable for the membrane association of MTMR5 (Kim *et al.*, 2003b). Instead, in membrane fractionation experiments the inactive PTP domain was sufficient to associate MTMR13 with membrane fractions (Robinson and Dixon, 2006). In addition, delocalization of MTMR2 from the cytoplasm towards vacuolar membranes was observed upon hypoosmotic shock in COS7 cells, a condition in which $PI(3,5)P_2$ levels are increased (Berger *et al.*, 2003). However, MTMR2 is also reported to regulate a late endosomal PI(3)P pool (Cao *et al.*, 2008). *In vitro* experiments showed that complex formation with MTMR2 results in a 4.6-fold increase of its specificity towards PI(3)P and 3.4-fold towards PI(3,5)P2 when MTMR5 is bound (Kim *et al.*, 2003b), or a 10-fold increase to PI(3)P and 25-fold to $PI(3,5)P_2$ when MTMR13 is bound (Berger *et al.*, 2006b). Furthermore, a strong interdependence between MTMR2 and MTMR13 is observed *in vivo*, in form of reduced protein levels in the absence of each other (Robinson and Dixon, 2006; Zou *et*

al., 2009; 2012; Gupta *et al.*, 2013; Ng *et al.*, 2013). A functional interaction of the complex partners was recently demonstrated in *D. melanogaster*. Sbf, the fly homologue of MTMR5 and MTMR13, recruits mtm, the single homologue of mammalian MTM1, MTMR1 and -R2, to regulate a class II PI-3 Kinase (PI3KC2)-dependent PI(3)P pool during endosomal trafficking and macrophage protrusion formation (Velichkova *et al.*, 2010; Jean *et al.*, 2012). The latter process also implies Rab21 recruitment and activation by Sbf via its N-terminal DENN domain (Jean *et al.*, 2012). This interaction, as demonstrated later by the same group also in human cells, mediates autophagosome to lysosome fusion (Jean *et al.*, 2015). In a screen for potential Rab-protein interactors in *D. melanogaster*, Sbf was detected in association with another small GTPase, Rab35 (Gillingham *et al.*, 2014).

In neuronal postsynapses, MTMR2 was reported to interact with PSD95 via its PDZ domain and represses endocytosis of the AMPA-receptor subunit GluA2 (Lee *et al.*, 2010). In axons, MTMR2 interacts with the axonal neurofilament light chain (NF-L), a protein that causes the axonal neuropathy CMT2E (Previtali *et al.*, 2003). Though no changes in NF-L protein levels could be observed in CMT4B patients, this interaction might contribute to the severe axonal loss in humans (Previtali *et al.*, 2003). Electron microscopic analysis of *MTMR2* and *MTMR13* KO mice nerve fibers reveal intact adherens junctions at paranodal loops as well as functional axo-glial junctions between neuronal axolemma and Schwann cell membrane (Bolino *et al.*, 2004; Robinson *et al.*, 2008). MTMR2-mediated repression of membrane addition through its interaction with the scaffolding protein Dlg-1 (discs large homolog 1) was recently proposed to underly the CMT4B phenotype (Bolis *et al.*, 2005; 2009). Dlg-1 belongs to the MAGUK family (membrane-associated guanylate kinase-like) and links transmembrane proteins with the intracellular cytoskeleton. It is located at paranodal loops and SLIs in Schwann cells (Bolino *et al.*, 2004; Bolis *et al.*, 2005; 2009). Interestingly, Dlg-1 also activates PTEN in SCs, which represses PI3K/AKT activity and thereby excessive myelin growth (Cotter *et al.*, 2010). In contrast to this indirect connection to PTEN, overexpression of MTMR2 was recently reported to lead to sustained AKT or ERK activation (Berger *et al.*, 2011; Franklin *et al*., 2011). Nevertheless, *MTMR2* or *MTMR13* KO mice do not display altered levels of either phosphorylated AKT or ERK (Ng *et al.*, 2013; Bolino *et al.*, 2016). Despite of that, myelin outfoldings in the absence of MTMR2 could be ameliorated *in vitro* and *in vivo* by downregulation of Nrg1-III/ErbB receptor signaling through facilitation of the inactivating α-secretase TACE (Bolino *et al.*, 2016). However, the underlying molecular mechanism is not elucidated so far.

1.7 The small GTPase Rab35 is implicated in myelination

Rab (Ras-related protein in brain; Touchot *et al.* 1987) GTPases (GTP hydrolases) make up the largest branch of small monomeric GTPases of the Ras superfamily, besides the Ras, Rho, Arf and Ran subfamilies, with 11 different proteins identified in yeast and more than 60 Rabs that are encoded in the human genome (Klöpper *et al.*, 2012). Similar to PIs, they represent essential molecular switches in intracellular membrane trafficking and vesicular transport by serving as a platform for effector proteins involved in membrane tethering, fusion, fission and cell signaling (Zerial and McBride; 2001; Rink *et al.*, 2005; Grosshans *et al.*, 2006). Rab GTPases are characterized by a prenylated C-terminal amphipathic helix, which is inserted into the bilipid layers of membranes upon activation (Ghomashchi *et al.*, 1995). Inactive, guanosine nucleotide diphosphate (GDP)-bound Rab proteins are kept soluble in the cytosol by Rab-GDP dissociation inhibitors (Rab-GDIs). Their recruitment to the respective membrane compartment is mediated by Guanine nucleotide exchange factors (GEFs). These enzymes facilitate the replacement of GDP for guanosine triphosphate (GTP) in the Ras-typical globular domain, which induces a conformational change. Thereby, the disordered switch I and II regions become stabilized and highly organized, and thus, allow for interaction and recruitment of effector proteins (Barr and Lambright, 2010; Blümer *et al.*, 2013). Eventually, GTPase activating proteins (GAPs) promote the Rab-catalytic activity to hydrolyze GTP, which results in Rab protein inactivation and is followed by its GDI-mediated membrane dissociation (Fig. 1-9) (Milburn *et al.*, 1990; Sasaki *et al.*, 1990; Pylypenko *et al.*, 2006; Wu *et al.*, 2007; Wittinghofer and Vetter, 2011). Rab GAPs and GEFs are characterized by TBC (Tre2/Bub2/Cdc16) and DENN-domains, respectively (Barr and Lambright, 2010; Yoshimura *et al.*, 2010).

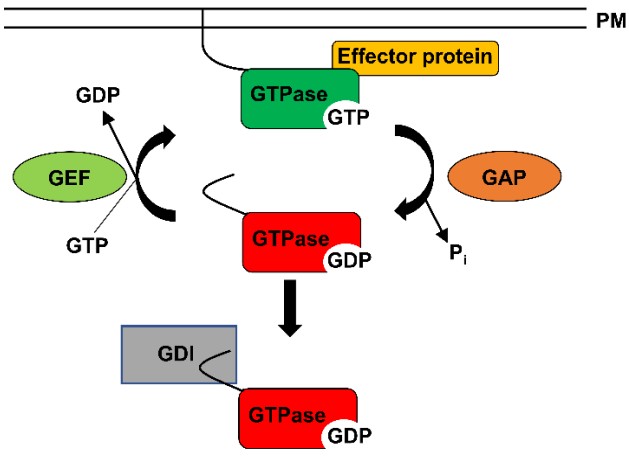

Figure 1-9: Activity cycle of small GTPases. Small GTPases as Rab proteins cycle between an active, GTP-bound and an inactive, GDP-bound form. GAPs facilitate the GTPase activity whereas GEFs mediate the dissociation of GDP and its exchange for GTP. Inactive GTPases are sequestered in the cytosol by GDIs. Active GTPases can insert their amphipathic C-terminus into bilipid layers of membranes, and recruit and activate effector proteins at these sites.

Rab35, or Rab1C due to its highest sequence homology to Rab1A and B, is phylogenetically highly conserved throughout metazoans (Pereira *et al.*, 2001; Klöpper *et al.*,

2012). It is reported to localize mainly at the plasma membrane, endocytic vesicles and endosomal membranes, but has also been detected recently on late endosomal/ lysosomal compartments (Hsu *et al.*, 2010; Wheeler *et al.*, 2015). Rab35 has an established role in the endosomal recycling of different receptors and cell surface proteins to the plasma membrane, such as cadherins, MHC (major histocompatibility complex class I and II), transferrin or T-cell receptors, the Ca^{2+}-activated potassium channel $KCa_{2.3}$ or the glucose transporter GLUT4 in adipocytes (Patino-Lopez *et al.*, 2008; Walseng *et al.*, 2008; Gao *et al.*, 2010; Allaire *et al.*, 2010; Davey *et al.*, 2012). In addition, depletion of Rab35 alters the endosomal trafficking of CI-Mannose-6-Phosphate receptors and Shiga-toxin to the TGN (Fuchs *et al.*, 2007; Cauvin *et al.*, 2016). The GEFs DENND1A-C (or Connecdenn 1,2,3) and Folliculin, and the GAPs TBC1D10A-C (EPI64A-C) and TBC1D13 (Chaineau *et al.*, 2013) are upstream regulators of Rab35. The set of direct Rab35 effector proteins identified so far, include the $PI(4,5)P_2$ 5'-phosphatase OCRL, the oxidoreductase MICAL1, the actin-bundling protein Fascin, the apical determinant Podocalyxin, and the ARF-6 GAP ACAP-2 (Zhang *et al.*, 2009Dambournet *et al.*, 2011; Klinkert *et al.*, 2016; Fremont *et al.*, 2017). By direct interaction with these proteins Rab35 is implicated in a variety of cell physiological processes, such as cytokinesis, cell polarity, phagocytosis, cell adhesion and migration, apoptosis and cytoskeleton remodeling (Kouranti *et al.*, 2006; Zhang *et al.*, 2009; Dambournet *et al.*, 2011; Marat *et al.*, 2012; Chaineau *et al.*, 2013; Allaire *et al.*, 2013). In addition, Rab35 is strongly associated with cancer progression. A couple of recent reports implicate the small GTPase in PI3K/AKT signaling, though with partially contrasting results. Due to a proposed suppression of EGFR recycling or facilitation of EGFR degradation by Rab35, enhanced AKT activation in the absence of Rab35 was observed in different cancer cell lines (Allaire *et al.*, 2013; Zheng *et al.*, 2017). In contrast, in somatic cancer or HEK293E cells, overexpression of the consecutive active mutant Rab35Q67L results in sustained AKT activation, presumably by promoting class I PI3K activity downstream to PDGFR internalization. Thus, the depletion of Rab35 reduced AKT activation in these cells (Wheeler *et al.*, 2015).

Consistent with its ubiquitous abundance (Zhu *et al.*, 1994), Rab35 is also expressed in the nervous system (Jeong *et al.*, 2018) and, at least for CNS cells, a couple of processes are reported to depend on Rab35 regulation. Among these, Rab35 is implicated in neurite outgrowth, but also axon elongation and even in neurodegenerative diseases associated with alpha-synuclein stabilization and exocytosis (Chevallier *et al.*, 2009; Kobayashi *et al.*, 2014a; b; Chiu *et al.*, 2016; Villarroel-Campos *et al.*, 2016; Steger *et al.*, 2016; 2017; Bae *et al.*, 2018). In addition, Rab35 is reported to function in the recycling of synaptic vesicles (SVs) in

neuromuscular junctions (NMJs) of *D. melanogaster* (Fig. 1-10) (Uytterhoeven *et al.*, 2011). Fly mutants with a loss of function mutation in Skywalker, a putative Rab35 GAP, display elevated endosomal recycling of synaptic vesicles. This phenotype is accompanied by a larger pool of readily releasable vesicles, increased neurotransmission and more efficient degradation of ubiquitinated SV proteins. An amelioration of increased neurotransmission and reduced endosomal SV recycling was observed by overexpression of inactive Rab35 or by the heterozygous deletion of *Rab35* in Skywalker mutants. The authors proposed a mechanism in which the small GTPase promotes recycling of SVs via endosomes, which facilitates the degradation of dysfunctional SV proteins via the lysosomal pathway. In consequence, newly synthesized SV proteins would be formed with functional SV proteins only, leading to a more efficient neurotransmission than direct recycling. However, TBC1D24, the mammalian homologue of Skywalker that underlies the human DOORS (deafness, onychdystrophy, osteodystrophy, mental retardation, and seizures) syndrome (Campeau *et al.*, 2014), was so far only identified as a GAP for ARF-6 (Falace *et al.*, 2014; 2016) and not Rab35.

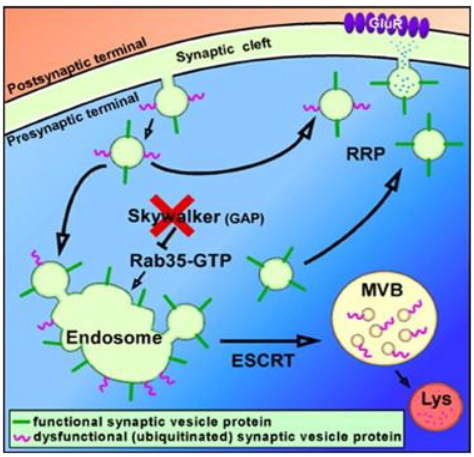

Figure 1-10: Model of Rab35 function in SV recycling in *D. melanogaster*. In the absence of its putative GAP Skywalker, increased activation of Rab35 (-GTP) directs endocytosed synaptic vesicles to recycle via endosomal compartments. Dysfunctional SV proteins are sorted into the lysosomal pathway for degradation. SVs with functional proteins only are reformed, and replenish the readily releasable pool of vesicles (RRP) for exocytosis. MVB – multi vesicular body; Lys – lysosome; ESCRT – endosomal sorting complex required for transport. Taken from (Uytterhoeven *et al.*, 2011).

In addition to its function in neurons, Rab35 has also been recently implicated in the myelin homeostasis of oligodendrocytes. Knockdown of the small GTPase or its GAPs TBC1D10A-C resulted in impaired exosome secretion in oligodendrocytic lineage cells (Oli-neu). Exosomes are extracellular vesicles with 30-150 nm in diameter that contain mRNA, proteins and lipids and mediate intercellular communication (Kalra *et al.*, 2016). They are released from late endosomal MVBs (LAMP-/ CD63- /TSG101-positive compartments). Regulated by a so far unknown mechanism, these late endosomes do not enter the degradational lysosomal pathway, but instead fuse with the plasma membrane and release their ILV content (Trajkovic *et al.*, 2006; Frühbeis *et al.*, 2013). OL-derived exosomes might function in the trophic support for neurons but also influence myelin formation (Krämer-Albers *et al.*, 2007).

The exosomal release of mRNA has been implicated in both, stimulating and inhibiting myelin formation (Bakhti *et al.*, 2010; Pusic *et al.*, 2016). In Oli-neu cells, the absence of Rab35 resulted in an intracellular accumulation of PLP in lysosomal-associated protein 1 (LAMP-1)-positive late endosomal/lysosomal compartments (Hsu *et al.*, 2010). The authors proposed a function of Rab35 in the docking of these compartments to the PM for subsequent release of myelin proteins. However, the consequences on myelin formation was not investigated in that context. Current literature suggests that MAG and PLP delivery to LE/Lys is crucial for OL differentiation and myelin sheath formation (Simmons and Trajkovic, 2006; Winterstein *et al.*, 2008; Mironova *et al.*, 2016). In contrast, another study reported a gain of OL differentiation and myelin segment formation *in vitro,* in the oligodendroglial cell line FBD-102b and primary OPCs depleted of Rab35 by siRNA or shRNA-mediated knockdown, respectively (Miyamoto *et al.*, 2014). The authors proposed a function of Rab35 in the repression of OL differentiation and myelination, mediated by the recruitment of ACAP2 and subsequent inactivation of ARF6. How active ARF-6 in turn promotes OL differentiation and myelination is not revealed yet.

1.8 Aims

Impairments of the myelin homeostasis can lead to severe axonal degeneration and underly a wide range of common neurodegenerative diseases of the central and peripheral nervous system (PNS). Recent investigations, especially of inherited demyelinating disorders such as Charcot-Marie-Tooth (CMT) neuropathies, revealed a cohort of proteins crucially involved in the regulation of myelin formation. Despite of that, the molecular mechanisms by which these proteins contribute to a proper myelin homeostasis are incompletely resolved. The small GTPase Rab35 is linked to myelin formation in oligodendrocytes by two independent recent studies. However, the reported findings are slightly contrasting regarding the regulatory function of Rab35 in the formation and maintenance of myelin.

We aimed to investigate how acute loss of Rab35 would affect oligodendrocytic myelin formation and thus, made use of a novel conditional Rab35 knockout (KO) mouse. Moreover, in order to reveal proteins which could mediate the function of Rab35 in this process, we performed an interactor screen. Thereby identified Rab35-effector proteins directed us to investigate PNS myelination upon acute Rab35 loss in Schwann cells by ultrastructural analysis, cell biological and biochemical approaches.

2. Material and Methods

2.1 Material

2.1.1 Chemicals and consumables

If not otherwise indicated in the corresponding section, chemicals and consumables were obtained from Thermo Fisher, Sigma, Roth, Sarstedt, GE Healthcare or Merck (table 2-18).

2.1.2 Solutions, media and buffers

Solutions and buffers were prepared using millipore-filtered water and pH-adjusted with HCl or NaOH.

Table 2-1: Solutions for molecular biology methods.

Solution	Composition	Solvent
10x TBE (TRIS-Borate-EDTA)	890 mM Boric Acid 20 mM EDTA	890 mM TRIS
50x TAE (TRIS-Acetate-EDTA)	100 mM glacial acetic acid 50 mM EDTA → adjusted to pH 8.2 – 8.4	200 mM TRIS
10x OrangeG loading dye	2 mg/mL OrangeG (Sigma, O-1625)	70 % (v/v) glycerin
Antibiotic stock solutions (sterile filtered)	100 mg/mL Ampicillin 50 mg/mL Kanamycin 34 mg/mL Chloramphenicol	H_2O
LB (Lysogeny broth) medium	1.0 % (w/v) yeast extract 0.5 % (w/v) tryptone 0.5 % (w/v) NaCl → adjusted to pH 7.4	H_2O
LB plates	15 g/L LB Agar powder (Roth; X965)	LB medium
2 x YT () medium	1.0 % (w/v) yeast extract 1.6 % (w/v) tryptone 0.5 % (w/v) NaCl → adjusted to pH 7.4	H_2O
BLB (Biopsy lysis buffer)	200 mM NaCl 5 mM EDTA 0.2 % (w/v) SDS → adjusted to pH 8.5	100 mM TRIS
TLB (Tail lysis buffer)	25 mM NaOH 0.2 mM EDTA → pH 12	H_2O
TNB (Tail neutralization buffer)	40 mM TRIS-HCl → pH 5	H_2O

Table 2-2: Solutions and media for preparation and culturing of mammalian (primary) cells. The reagent supplier and corresponding ordering number is specified where necessary.

Solution/ medium	Composition	Source
mCCM (mammalian cell culturing medium)	10 % (v/v) FBS (heat-inactivated for primary cells) 1% (v/v) P/S:100 U/mL Penicillin; 100 µg/mL Streptomycin in DMEM (Dulbecco's modified Eagle medium; high glucose (4.5 g/L), + 2 mM L-glutamine)	Biochrom, S-0115 Thermo Fisher, 15140122 Thermo Fisher, 11965062
Neuronal basic medium	27.8 mM D-(+)-Glucose 2.4 mM $NaHCO_3$ 1.3 µM Transferrin Holo, Bovine Plasma in MEM (Minimum Esssential Medium)	Roth, HN06 Merck Millipore, 616420 Thermo Fisher, 51200-046
Neuronal digestion solution	137 mM NaCl 5 mM KCl 7 mM Na_2HPO_4 in 25 mM HEPES → adjusted to pH 7.2	
Neuronal dissociation solution	12 mM $MgSO_4$ x $7H_2O$ in HBSS (-Mg^{2+}/Ca^{2+})	 Thermo Fisher, 14175-053
Neuronal plating medium	10 % (v/v) FBS (heat-inactivated) 2 mM L-glutamine 25 µg/mL Insulin (in 10 mM HCl) 1 % (v/v) P/S in Neuron basic medium	Biochrom, S-0115 Sigma, 91077C Thermo Fisher, 15140122
Neuronal growth medium	5 % (v/v) FBS (heat-inactivated) 0.5 mM L-glutamine 1x B-27 Supplement 1 % (v/v) P/S in Neuron basic medium	Biochrom, S-0115 Thermo Fisher, 25030081 Thermo Fisher, 17504044 Thermo Fisher, 15140122
10x EBSS (Earle's Balanced Salt solution) stock solution	1.16 M NaCl 54 mM KCl 10 mM NaH2PO4xH20 1 % (w/v) D-(+)-Glucose 0.005% phenol-red in H_2O	 Roth, HN06
OPC dissociation (Papain) buffer	1x EBSS-stock 1mM MgSO4 0.46 % (w/v) D-(+)-Glucose 2 mM EGTA 26 mM NaHCO3 in H_2O	 Roth, HN06
10x LOS (low-ovomucoid solution)	20 mg/mL BSA (bovine serum albumin) 20 mg/mL Trypsin Inhibitor (Ovomucoid) 0.005% phenol-red in D-PBS (Dulbecco's Phosphate-Buffered Saline; +Ca^{2+}/Mg^{2+}) --> adjust to pH7.4	Sigma, 8806 Worthington, LS003086 Thermo Fisher, 14287-080

6x HOS (high-ovomucoid solution)	30 mg/mL BSA 30 mg/mL Trypsin Inhibitor (Ovomucoid) 0.005% phenol-red in D-PBS (+Ca^{2+}/Mg^{2+}) --> adjust to pH7.4	Sigma, 8806 Worthington, LS003086 Thermo Fisher, 14287-080
Immunopanning buffer	0.02% BSA 500 µg/mL insulin in D-PBS (+Ca^{2+}/Mg^{2+})	Sigma, A4161 Sigma, I6634 Thermo Fisher, 14287-080
Sato-supplement 100x	150 mM BSA 130 mM apo-Transferrin bovine 10 mM Putrescine 20 µM Progesterone 23 µM Sodium Selenite in DMEM (4.5 g/L glucose)	Sigma, A4161 Sigma, T1147 Sigma, P8783 Sigma, S5261 Thermo Fisher, 11960044
DSM (DMEM-Sato based growth medium)	1x Sato-supplement 2 mM L-glutamine 5 µg/mL Insulin (in 10 mM HCl) 5 µg/mL N-Acetyl-cysteine 10 ng/mL d-Biotin 1x Trace Elements B 1x B-27 Supplement 1 % (v/v) P/S in DMEM (4.5 g/L glucose)	 Thermo Fisher, 25030081 Sigma, I6634 Sigma, A8199 Sigma, B4639 Thermo Fisher, 25-022-CI Thermo Fisher, 17504044 Thermo Fisher, 15140122 Thermo Fisher, 11960044
Growth factor stock solutions (sterile filtered; -20 °C storage)	10 µg/mL PDGF-AA (platelet-derived growth factor AA) in sterile 0.2% BSA in D-PBS (+Ca^{2+}/Mg^{2+})	PreproTech, #100-13A
	10 µg/mL NT-3 (neurotrophin-3) in sterile 0.2% BSA in D-PBS (+Ca^{2+}/Mg^{2+})	PreproTech, #450-03
	10 µg/mL CNTF (ciliary neurotrophic factor) in sterile 0.2% BSA in D-PBS (+Ca^{2+}/Mg^{2+})	PreproTech, #450-13
	10 mM Forskoline in DMSO	Sigma, F6886
	4 µg/mL T3 (thyroid hormone triiodothyronine) in D-PBS (+Ca^{2+}/Mg^{2+})	Sigma, T6397
	10 µg/mL NRG1 (Neuregulin1) in sterile water	Sigma, H7660
	5 mg/mL ascorbic acid in sterile water	Sigma, A4544
OPC proliferation medium	10 ng/mL NT-3 10 ng/mL PDGF-AA 10 ng/mL CNTF 10 µM Forskolin in DSM	
OPC differentiation medium	10 ng/mL CNTF 10 µM Forskolin 40 ng/mL T3 in DSM	
SC dissociation medium	0.25 % (w/v) Trypsin 0.1 % (w/v) Collagenase A in Leibovitz's L-15 medium (L-15)	Thermo Fisher, 27250018 Sigma, 10103586001 Thermo Fisher, 11415049

SC pre-differentiation medium	5 % (v/v) heat-inactivated horse serum (HS) 1 % (v/v) P/S in DMEM (4.5 g/l glucose, +GlutaMAX, +Pyruvate)	Thermo Fisher, 26050088 Thermo Fisher, 15140122 Thermo Fisher, 31966021
SC differentiation medium	1 µM Forskolin 20 ng/mL NRG1 40 ng/mL T3 50 µg/mL ascorbic acid in DSM	
2x HBS (HEPES buffered saline) buffer	280 mM NaCl 10 mM KCl 1.5 mM $Na_2 HPO_4$ 12 mM dextrose in 50 mM HEPES → adjusted to pH 7.05	
0.1x TE (TRIS-EDTA) buffer	0.1 mM EDTA in 1 mM TRIS → adjusted to pH 8.0	

Table 2-3: Buffers used for live-cell imaging and immunocytochemistry assays.

Buffer	Composition	Solvent
10x Imaging basic-buffer	35 mM KCl 1.2 M NaCl 4 mM KH_2PO_4 50 mM $NaHCO_3$ 50 mM D-(+)-glucose water free (Roth, HN06) 12 mM Na_2SO_4 → adjusted to pH 7.4	200 mM TES
1x Imaging buffer	50 mM NaCl 1.3 mM $CaCl_2$ 1.2 mM $MgCl_2$ 50 µM APV (Sigma, A5282) 10 µM CNQX (Sigma. C-239) → osmolarity-adjusted to neuron cell culture medium with D-(+)-Mannitol (Sigma, M4125)	1x Imaging basic buffer
High-potassium imaging buffer	80 mM KCl 1.2 mM MgCl 2 1.3 mM CaCl 2 → osmolarity-adjusted to neuronal culturing medium with D-(+)-Mannitol (Sigma, M4125)	1x Imaging basic buffer
10x PBS (Phosphate buffered saline)	100 mM Na_2HPO_4* $2H_2O$ 26.8 mM KCl 1.37 M NaCl 17.6 mM KH_2PO_4 → adjusted to pH 6.8	H_2O
PFA fixative (4 %)	4 % (w/v) paraformaldehyde (PFA) 4 % (w/v) sucrose → adjusted to pH 7.4	1x PBS

Immunocytochemistry (ICC) blocking solution	0.3 % (v/v) Triton X-100 10 % (v/v) NGS/NDS	1x PBS
ICC antibody solution	0.3 % (v/v) Triton X-100 5 % (v/v) NGS/NDS	1x PBS
PFA fixative (2 %)	2 % (w/v) paraformaldehyde (PFA) 2 % (w/v) sucrose → adjusted to pH 7.4	1x PBS
PIB (PIPES-based buffer)	137 mM NaCl 2.7 mM KCl → adjusted to pH 6.8	20mM PIPES
Lipid-ICC permeabilization solution	20 µM Digitonin (Thermo Fisher Scientific, bn2006)	PIB
Lipid-ICC blocking solution	5 % (v/v) NGS (normal goat serum) 50 mM ammonium chloride	PIB
Lipid-ICC antibody solution	5 % (v/v) NGS	PIB

Table 2-4: Solutions and buffers used for biochemical assays.

Solution/Buffer	Composition	Solvent
5x Lysis buffer stock	500 mM KCl 10 mM $MgCl_2$ 5 % (v/v) Triton X-100 (Sigma, 11332481001) → adjusted to pH 7.4	100 mM HEPES
1x Lysis buffer working solution	1x lysis buffer 0.3 % (w/v) PIC (mammalian inhibitor cocktail; Sigma, P8340) 1 mM PMSF (Roth, 6367) 1 % (w/v) phosphatase inhibitor cocktail 2 (Sigma. P5726) 1 % (w/v) phosphatase inhibitor cocktail 3 (Sigma, P0044)	H_2O
2x Bradford solution	150 µM Brilliant Blue G250 17 % (v/v) ortho-Phosphorsäure 10 % (v/v) Ethanol	H_2O
6x SDS-PAGE sample buffer	12 % (w/v) SDS 60 % (v/v) glycerin 30% (v/v) 2-mercaptoethanol 0.3 % (w/v) bromophenol blue → adjusted to pH 6.8	375 mM TRIS
4x Separating gel buffer	0.4 % (w/v) SDS → adjusted to pH 8.8	1.5 M TRIS
4x Stacking gel buffer	0.4 % (w/v) SDS → adjusted to pH 6.8	0.5 M TRIS
1x SDS running buffer	192 mM Glycine 0.1 % (w/v) SDS → adjusted to pH 8.3	25 mM TRIS
Coomassie staining solution	1 g/L Coomassie brillian blue G250 10 % (v/v) acetic acid 25 % (v/v) methanol	H_2O

Coomassie destain solution	10 % (v/v) acetic acid 25 % (v/v) methanol	H_2O
1x Transfer Buffer	192 mM Glycine 10 % (v/v) Methanol	25 mM TRIS
Ponceau S staining solution	0.3 % (w/v) Ponceau S 3 % (v/v) glacial acetic acid	H_2O
Ponceau destain solution	1 % (v/v) glacial acetic acid	H_2O
PBS-T	0.05 % (v/v) TWEEN-20 (Roth, 9127)	1x PBS
Immunoblot blocking buffer (HRP-detection)	5 % (w/v) milk (Roth, T145)	1x PBS
Immunoblot blocking buffer (Fluorescence-detection)	Odyssey® Blocking Buffer-PBS (LI-COR, LI 927)	-
Immunoblot primary antibody solution	3 % (w/v) BSA 0.02 % (w/v) NaN_3	1x PBS-T
BioID (proximity-dependent biotin identification) - wash buffer 1	2 % (w/v) SDS	H_2O
BioID- wash buffer 2	0.1 % (w/v) sodium deoxycholate 1 % (v/v) Triton X-100 500 mM NaCl 1 mM EDTA → adjusted to pH 6.8	50 mM HEPES
BioID- wash buffer 3	250 mM Lithium chloride 0.5 % (v/v) NP-40 0.5 % (w/v) sodium deoxycholate 1 mM EDTA → adjusted to pH 8.1	10 mM TRIS-base
BioID- wash buffer 4	50 mM NaCl → adjusted to pH 7.4	50 mM TRIS-base

2.1.3 Enzymes

Enzymes for molecular biological methods were stored at -20 °C and used in concentrations as indicated in the respective method part. FastDigest restriction enzymes (not listed) were purchased from Thermo Fisher. Enzymes used for cell biological assays are specified in each method section.

Table 2-5: Enzymes used for molecular biological applications.

Label	Producer	Order number
FastAP – alkaline phosphatase	Thermo Fisher	EF0654
Phusion high fidelity DNA Polymerase		F-530L
T4 DNA ligase		ELL0016
Taq DNA Polymerase	Bio&SELL	BS91.711.0500
Proteinase K	NEB	P8102

2.1.4 Kits

Kits were stored and used according to Manufacturer's instructions.

Table 2-6: Kits, the corresponding manufacturer's and methods they were used for.

Type	Producer	Application
NucleoBond®Xtra Plasmid Midi-EF	Macherey-Nagel	Preparation of plasmid DNA
NucleoBond® PC 20 Plasmid Mini		
NucleoSpin® Gel and PCR Clean-up		Purification of DNA
Pierce BCA Protein Assay Kit	Thermo Fisher	Determination of protein concentration
Profection Mammalian Transfection System-Calcium Phosphate E1200	Promega	Transfection of neuronal cell cultures

2.1.5 Standards for gel electrophoresis

For gel-electrophoresis, 5 µL or 0.5 µg of the DNA- or the Protein Markers were used, respectively.

Table 2-7: Standards used as markers in gel electrophoresis.

Marker	Producer	Order number
GeneRuler^{TM} 1 kb DNA Ladder	Thermo Fisher	SM0311
GeneRuler^{TM} 100 bp DNA Ladder		SM0241
PageRuler Prestained Protein Ladder		26616/ -19
Triple Color Protein Standard II	Serva	39257

2.1.6 DNA oligonucleotides

DNA oligonucleotides used as primers for polymerase chain reactions (PCR), were obtained from BioTeZ as lyophilized powder, dissolved in nuclease-free water (Roth, T143) to 100 µM and stored at -20 °C.

Table 2-8: Primers used in analytical PCR reactions for genotyping of mouse genomic DNA. fw - forward; rev - reverse.

Primer	Sequence [5'-3']	Target
TM63_ EllaCre_fw	CCGGGCTGCCACGACCAA	CAG-*Cre*
TM64_EllaCre_rev	GGCGCGGCAACACCATTTTT	
P0-Cre_fw	CCACCACCTCTCCATTGCAC	P_0-*Cre*
P0-Cre_rev	GCTGGCCCAAATGTTGCTGG	
Lox5F_fw	ACTGGGATACACTGTGCTTG	*Rab35* WT/ *Rab35*$^{Fl/-}$/ *Rab35*$^{Fl/Fl}$
Lox5R_rev	GCTCCCAAGAATTCCAACTC	*Rab35* WT
PL452-LoxP-Sc1R_rev	GAGGGACCTAATAACTTCGT	*Rab35*$^{Fl/-}$/ *Rab35*$^{Fl/Fl}$

Table 2-9: Primers used in preparative PCR reactions for cloning. Overlapping regions are highlighted in capital letters, restriction sites in bold. fw - forward; rev – reverse; PTP- protein tyrosine phosphatase; CC – coiled-coil region; PH- pleckstrin homology domain

Primer	Sequence [5'-3']
GST-Rab35_EcoR1_fw	atat**gaattc**ATGGCCCGGGACTACGACCACCTCTTCAA
GST-Rab35_Not1_rev	atat**gcggccgc**TTAGCAGCAGCGTTTCTTTCG
GST-Rab35ΔC_Not1_rev	atat**gcggccgc**ttaCTGCTGTTTCGCCAAGTTGTC
BirA*-Rab35_ EcoRV _fw	aagt**gatatc**cATGGCCCGG
BirA*-Rab35_Hindlll_rev	cctt**aagctt**TTAGCAGCAGC
mCherry_Rab35_EcoRI_fw	atat**gaattc**ATGGCCCGGGACTACGACCACCTCTTCAA
mCherry_Rab35_XbaI_rev	ccgc**tctaga**TTAGCAGCAGCGTTTCTTTCG
mCherry_Rab35Q67L_fw	TGGGACACGGCAGGGttaGAGCGCTTCCGC
mCherry_Rab35Q67L_rev	GCGGAAGCGCTCtaaCCCTGCCGTGTCCCA
mCherry_MTMR5_AgeI_fw	atat**accggt**ATGGTGAGCAAGGGCGAGGAGGATAACAT
mCherry_MTMR5_Hindlll_rev	ccgc**aagctt**atCTTGTACAGCTCGTCCATGCC
mCherry_MTMR13_KpnI_fw	atat**ggtacc**ATGGTGAGCAAGGGCGAGGAGGATAACAT
mCherry_MTMR13_EcoRV_rev	ccgc**gatatc**ccCTTGTACAGCTCGTCCATG
mCherry_MTMR13-DENN_BamHI_fw	atat**ggatcc**GCCCGGCTGGCTGACTACTTCATCGTGGTAG
mCherry_MTMR13-DENN_NotI_rev	cagt**gcggccgc**TCAATGAGGATTTGGATTCTC
mCherry_MTMR13-PH-GRAM_EcoRV_fw	cgta**gatatc**TCAGAGAATACTGACATTGCC
mCherry_MTMR13-PH-GRAM_NotI_rev	cagt**gcggccgc**TCAATGAGGATTTGGATTCTC
mCherry_MTMR13-PTP_BamHI _fw	atat**ggatcc**GCCTCCGAGAAGTCTACAATGGAACAG
mCherry_MTMR13-PTP_NotI_rev	cagt**gcggccgc**TCAGCCTGTGGACAGGGTCTCTTCTATG
mCherry_MTMR13-PTP+CC_BamHI_fw	atat**ggatcc**GCCTCCGAGAAGTCTACAATGGAACAG
mCherry_MTMR13-PTP+CC_NotI_rev	cagt**gcggccgc**TCAGGAAGGTAGGTTGGTAGACAC
mCherry_MTMR13-PH_BamHI_fw	atat**ggatcc**AACAGGTCCTTTGAGGGAACAC
mCherry_MTMR13-PH_NotI_rev	cagt**gcggccgc**TCAGGCATCAGAGATACAACTCTGG

2.1.7 RNA oligonucleotides

2.1.7.1 siRNAs

For RNA interference, small interfering RNA oligonucleotides (siRNA) were (re-)ordered as lyophilized powder from Sigma and dissolved to a concentration of 100 µM in nuclease-free water (Roth, T143).

Table 2-10: siRNA sequences and references.

siRNA	Target organism	Sequence [5' - 3']	Source
MTMR2	human	GAAAAUGGGUGGAAGCUAU	Dharmacon (L-050609) / Sigma (custom)
Rab35	human	AGAAGAUGCCUACAAAUUUtt	Ambion (s95004) / Sigma (custom)
MISSION® Universal Negative Control #1 (scrambled)	-	-	Sigma (SIC001)

2.1.7.2 shRNAs

pLKO.1-plasmid encoded small hairpin RNA oligonucleotides (shRNA), expressed under the control of a U6-promoter, were used to interfere with gene expression in primary cells by lentiviral transduction. The non-targeting scrambled shRNA-containing construct with parallel eGFP-expression (RHS6848), and the mouse (ms)MTMR2-targeting shRNA-containing construct (TRCN0000030098), were obtained from Dharmacon. Glycerol stocks of transformed *E. coli* TOP10 were prepared, from which the plasmids were purified and dissolved in nuclease-free water to a concentration of 1 µg/mL for the virus production in HEK293T cells.

Table 2-11: shRNA sequences and references.

shRNA	Target organism	Sequence [5' - 3']	Source
msMTMR2	mouse	AAAGGACATGATTGGAGTAGC	Dharmacon
TRC Lentiviral negative Control (scrambled)	-	ACCGGACACTCGAGCACTTTTTGAATTC	

2.1.8 DNA-plasmids and expression vectors

Expression constructs were either received from elsewhere or obtained by cloning, as specified in table 2-12. Vectors used as backbones for the recombinant protein expression were chosen regarding the desired cell type. For mammalian cell lines, pcDNA3.1-based vectors (Invitrogen) were routinely used that drive strong and constitutive expression of inserted genes under control of the cytomegalovirus (CMV) promoter (Xia *et al*., 2006). pCMV6, pEGFPC2, pcEGFP_MK or pcmCherry_MK plasmids are pcDNA3.1-derived vectors with fluorescent tags for N-terminal fusion on the inserted protein (MK - generated by Michael Krauss, FMP, Berlin). For neuron-specific expression of synaptotagmin1-pHluorin in primary neuronal cultures, a modified pcDNA3-based plasmid that contains a human synapsin1 gene promoter was used (Wienisch and Klingauf, 2006). pGEX-4T vectors were used as backbones for the recombinant expression of proteins in bacteria, based on the T7-expressionsystem (Studier und Moffatt, 1986).

Plasmid DNA was stored in nuclease- and endotoxin-free (EF) water (NucleoBond®Xtra Plasmid Midi-EF kit) at -20 °C or 4 °C for long-term or short-term, respectively.

Table 2-12: Constructs for recombinant protein expression. *Plasmids were used as templates for cloning only. ms – mouse; hu - human

Construct	Insert species	Vector backbone	Reference
FLAG-MTMR13*	hu	pcDNA3.1	gift from Gilbert Di Paolo
FLAG-MTMR13	hu	pc(HA)_MK	this study
eGFP-MTMR2	hu	pcEGFP_MK	cloned by Katharina Ketel
eGFP-MTM1	hu	pcEGFP_MK	cloned by Katharina Ketel
eGFP-MTMR1	ms	pcEGFP_MK	cloned by Katharina Ketel
eGFP-MTMR5	hu	pEGFPC2	gift from Michael Clague
GST-Rab35	ms	pGEX4T-1	this study
GST-Rab35ΔC (aa1-180)	ms	pGEX4T-1	this study
GST-Rab1A	ms	pGEX4T-1	gift from Mitsunori Fukuda (Tohoku University, Sendai, Japan)
GST-Rab5	hu	pGEX4T-1	
GST-Rab7	hu	pGEX4T-1	
GST-Rab11	hu	pGEX4T-1	
mCherry-MTMR5	hu	pEGFPC2	this study
mCherry-MTMR13 (FL_aa1-1849)	hu	pcmCherry_MK	this study
mCherry-MTMR13-DD (aa1-471)	hu	pcmCherry_MK	this study
mCherry-MTMR13-PH-GRAM (aa806-1018)	hu	pcmCherry_MK	this study
mCherry-MTMR13-PTP (aa1100-1591)	hu	pcmCherry_MK	this study
mCherry-MTMR13-PTP+CC (aa1100-1697)	hu	pcmCherry_MK	this study
mCherry-MTMR13-PH (aa1743-1849)	hu	pcmCherry_MK	this study
mCherry-Rab35	ms	pcmCherry_MK	this study
mCherry-Rab35Q67L	ms	pcmCherry_MK	this study
mycBirA*	*E. coli*	pcDNA3.1	Roux *et al*., 2012 (‚mycBioID') (addgene #35700)
mycBirA*-Rab35	ms	pcDNA3.1_mycBirA*	this study
myc-MTMR2	ms	pCMV6	origene #MR215223
Syt1-pHluorin	ms	pcDNA3.1_ Synapsin promoter	gift from Markus Wienisch (Wienisch and Klingauf, 2006)
YFP-Rab35mouse*	ms	pUAST	Zhang *et al*., 2007 (addgene # 46014)

2.1.9 Antibodies and probes

2.1.9.1 Primary antibodies

Antibodies used for immunoblotting, -cytochemistry or -histochemistry were usually dissolved in water to a concentration of 1 mg/mL. Most antibodies, if not explicitly advised against by the corresponding manufacturer, were additionally diluted one to one in 90 % Glycerin in 1x PBS for storage at -20 °C, in order to avoid repetitive freezing and thawing. The depicted working dilutions listed in table 2-13 refer to the glycerol-diluted stock concentrations.

Table 2-13: Primary antibodies listed by the corresponding antigen. ICC – immunocytochemistry; IHC – immunohistochemistry; IB – immunoblotting.; rb - rabbit, ms – mouse, gp – guinea pig, ch – chicken, gt – goat; hu – human; AF –Alexa Fluor

Antigen	Host species	Dilution		Source	Catalogue number
		ICC or [IHC]	IB		
α-tubulin	ms		1:1,000	Sigma	T5168
ß-actin	ms		1:5,000	Sigma	A5441
AKT	rb		1:1,000	Cell signaling	4691
AKT (p-S473)	rb		1:1,000	Cell signaling	4060
BrdU	rat	1:200		Abcam	ab6326
Caspase-3 active	rb	1:200		R&D technologies	AF835
CD63-AF647	ms	1:100		BD Bioscience	561983
CNPase	ms	1:200		Sigma	C5922
EEA1	rb	1:50		Cell signaling	2411
ERK	rb		1:1,000	Cell signaling	9102
ERK (p-T202/Y204)	rb		1: 800	Cell signaling	9101
FLAG	ms	1:200	1: 1,000	Sigma	F3165
GFP	ch	1:2,000		Abcam	ab13970
GFP	rb	1:500	1:5,000	Abcam	ab6556
HSC70	ms		1:1,000	Thermo Fisher	MA3006
LAMP-1 (ms)	rat	1:250		BD Biosciences	553792
LAMP-1 (hu)	ms	1:200		BD pharmingen	555798
LAMP-2	rb	1:200		Abcam	ab18528
LC3	rb		1:500	Novus Biologicals	NB600-1384
LC3	ms	1:100		MBL international	M152-3
MBP	rb	1:400		Synaptic Systems	295 003
MBP	rat	[1:50]		kindly provided by Dr. Virginia Lee	
MTMR2	ms		1:500	BioRad	MCA3595Z
mTOR	rb		1:1,000	Cell signaling	2983
mTOR (p-S2448)	rb		1:1,000	Cell signaling	5536
Myc	rb		1:5,000	Abcam	ab9106
NF-M	ch	[1:500]		Covance	PCK-593P
NG2	rb	1:200		Millipore	AB5320
P0 (MPZ)	rb	1:200		Abcam	ab31851
PI(4)P (IgM)	ms	1:200		Echelon	z-p004

PLP	rb	1:200		Abcam	ab28486
Rab7	rb	1:50		Cell signaling	9367
Rab35	rb		1:500	Proteintech Group	11329-2-AP
RFP	rb		1:1,000	MBL international	PM005
S6	ms	1:25	1:1,000	Cell signaling	2317
S6– (p-S235/236)	rb	1:200		Cell signaling	2211
	rb		1:1,000	Cell signaling	4858
p70 S6K (p-T389)	rb		1:500	Cell signaling	9234
S6K	rb		1:1,000	Cell signaling	9202
Synapsin1	gp	1:200		Synaptic systems	106004
Synaptophysin	ms	1:500		Synaptic systems	101011
Synaptophysin luminal domain	rb	1:400		kind gift from Reinhard Jahn ("G96")	
Synaptotagmin1	ms	1:100		Synaptic systems	105011
Synaptotagmin1 luminal domain	rb	1:100		Synaptic systems	105103
Tubulin	ms		1:2,000	Sigma	T4026
Vinculin	ms		1:10,000	Millipore	05-386

2.1.9.2 Secondary antibodies

Secondary antibodies for immunocytochemistry were Alexa Fluor (AF)-conjugated. Secondary antibodies used for immunoblotting were either horse radish peroxidase- (HRP) conjugated or coupled to a near-infrared fluorescent dye for fluorescence detection using the LI-COR system.

Table 2-14: Secondary antibodies, their conjugation and reference. * highly x-adsorbed; ICC – immunocytochemistry; IHC – immunohistochemistry; IB – immunoblots.; rb - rabbit, ms – mouse, gp – guinea pig, ch – chicken, gt – goat; dk - donkey; AF –Alexa Fluor; HRP – horse radish peroxidase; TRITC – Tetramethylrhodamine; FITC - Fluorescein isothiocyanate

Antigen	Fluorophore /Conjugate	Host species	Dilution		Source	Catalogue number
			ICC [IHC]	IB		
ms IgG*	AF488	gt	1:400		Thermo Fisher	A11029
ms IgG*	AF568	gt	1:400			A11031
ms IgG*	AF647	gt	1:400			A21236
rb IgG*	AF488	gt	1:400			A11034
rb IgG*	AF568	gt	1:400			A11036
rb IgG	AF647	gt	1:400			A21244
gp IgG*	AF647	gt	1:400			A21450
rat IgG*	AF647	dk	1:400			A21247
ms IgM	AF568	gt	1:400			A21043
ch IgY	AF488	gt	1:400		Abcam	ab150169
rat IgG*	AF647	dk	1:400		Jackson Immuno Research Labs	712-605-153
rat IgG	TRITC	dk	[1:100]			712-025-150
ch IgGY^{++} (IgG)	FITC	dk	[1:100]			703-095-155
rb IgG	HRP	gt		1:5,000		111-035-003
ms IgG	HRP	gt		1:5,000		115-035-003
ms IgG	HRP	rb		1:5,000	Dako	P 0260

rb IgG	HRP	gt	1:10,000		P 0448
rb IgG	IRDye 680RD	gt	1:10,000	LI-COR Biosciences	926 -68071
rb IgG	IRDye 800CW	gt	1:10,000		926 -32211
ms IgG	IRDye 680RD	gt	1:10,000		925 -68070
ms IgG	IRDye 800CW	gt	1:10,000		926 -32210
ms IgG	IRDye 680LT	gt	1:5,000		926-68020

2.1.9.3 Probes

Phalloidin probes were used equivalent to secondary antibodies in immunocytochemistry. DAPI was diluted to a stock concentration of 5 mg/mL and stored at 4 °C. For application in immunocytochemistry assays the stock was further diluted to 1 µg/mL in mounting medium. A eGFP-tagged tandem version of the PI(3)P binding domain of Hrs (eGFP-2xFYVE (Hrs)) was recombinantly expressed in *E. coli*, purified and stored in 50 % glycerol at -80 °C (Uwe Fink, FMP, Berlin).

Table 2-15: Probes used for fluorescence detection.

Probe	Conjugate	Target	Dilution		Source	Catalogue number
			ICC	IB		
Phalloidin	AF568	F-actin	1:50		Thermo Fisher	A12380
Phalloidin	AF647		1:50			A22287
Streptavidin	HRP	biotin		1:5,000		SA10001
DAPI	-	DNA	1:5,000		Sigma	D9542
eGFP-2x FYVE (Hrs)	-	PI(3)P	0.025 µg/µL		Gillooly *et al.*, 2003	

2.1.10 Inhibitors

Compounds used to pharmacological inhibit enzymes were dissolved in DMSO to indicated concentrations as stock solutions and stored at room temperature (RT) or -20 °C.

Table 2-16: Compounds used for enzyme inhibition.

Inhibitor	Target protein	Stock solution	Storage temperature	Source
Apilimod	PIKFyve	25 mM	RT	BioVision, B1129
Compound-19	VPS34	10 mM	RT	Selleckchem, S8456
Rapamycin	mTORC1-component FKBP12	2 mM	-20	Santa Cruz, sc3504
SAR405	VPS34	10 mM	RT	kind gift from Sprint Bioscience, Huddinge, Sweden
VPS34-IN1	VPS34	10 mM	RT	provided by Dr. James Hastie (MRC PPU Reagents, Dundee)

2.1.11 Mammalian cell lines

Human embryonic kidney cells 293T (HEK) were used for biochemical experiments due to their high replication rate, transfection efficiency and protein expression (Wurm, 2004). In addition, this HEK293-derived cell line (T) expresses a temperature-sensitive mutant version of the SV40 large T antigen that makes it especially suitable for the production of retrovirus (Pear *et al.*, 1993). The epithelial cervical cancer cell line HeLa was used for immunocytochemistry due to its higher adherence properties compared to HEK cells (Potthoff *et al*., 2012). HEK and HeLa cell lines were obtained from ATCC. The TALEN-edited HeLa knock in (KI) cell line, that expresses endogeneous Rab35 N-terminally tagged with eGFP (eGFP-Rab35^{endo} HeLa cells), was a kind gift of the lab of Prof. Dr. Arnaud Echard (Cauvin *et al*., 2016). Stonin-2 WT immortalized mouse embryonic fibroblasts (MEF) cells were kindly provided by Prof. Dr. T. Maritzen (FMP, Berlin). All mammalian cell lines were cultured in DMEM with 4.5 g/L glucose (Thermo Fisher) containing 10 % heat-inactivated FBS (Gibco) and 100 U/mL penicillin and 100 µg/mL streptomycin (Gibco) (mCCM) during experimental procedures and were routinely tested for mycoplasma contamination.

2.1.12 Bacteria strains

For the amplification and storage of plasmid DNA, chemically competent *E. coli* from the TOP10 strain (Invitrogen; Hanahan, 1983) were used. To express recombinant proteins, IPTG-induced in bacteria, the *E. coli* strain BL21-CodonPlus (DE3)-RP (Stratagene) was routinely used. For GST-Rab protein chimera, a significantly higher amount of stable proteins was purified upon expression in *E. coli* Rosetta (DE3) (Novagen), which display improved expression yield and a better purity of proteins due to additional eukaryotic tRNA-codons that are rarely used in *E. coli*. (Tegel *et al*., 2010).

2.1.13 Mouse strains

Rab35$^{Fl/Fl}$ mice in a C57BL/6 WT mice background, with insertions of loxP sites flanking exon 2 and 3 for Cre-mediated recombination, were a kind gift of and generated by Dr. Genaro Patiño López (formerly: NIH, Bethesda, USA), Prof. Dr. Stephen Shaw (NIH, Bethesda, USA) and Prof. Dr. Arnaud Echard (Institut Pasteur, Paris, France). The Cre recombination system, based on the Cre recombinase and the 34 bp loxP recognition sites that consist of two 13 bp inverted repeats separated by a spacer region of 8 bp, originates from the P1 phage (Sternberg & Hamilton, 1981). Cre-mediated recombination in these mice leads to

the excision of exons 2 and 3 from the Rab35 gene as a circular DNA molecule, and thereby to an early transcription termination.

To obtain a conditional Rab35 gene knockout, *Rab35*$^{Fl/Fl}$ mice were interbred with a *Cre-ER*^{TM} (*Cre*^{ER}) mouse line in a C57BL/6 WT background (B6.Cg-Tg (*CAG-Cre*/Esr1*)5Amc/J) that was obtained from the Jackson Laboratory. This mouse line ubiquitously expresses a chimera of Cre recombinase and a mutated version of the ligand-binding domain of the estrogen receptor, with an increased affinity for tamoxifen (TMX), under control of the CAG-promoter, and thus allows for tamoxifen-inducible Cre recombination (Danielian *et al*.1998; Hayashi and McMahon, 2002). The resulting heterozygeous *Rab35*$^{Fl/+}$ x CAG-*Cre*^{ER} mice were crossed with homozygeous *Rab35*$^{Fl/Fl}$ animals to obtain homozygeous *Rab35*$^{Fl/Fl}$ with (icKO) or without *Cre*^{Er} (WT). Breeding and experiments with animals for *in vitro* recombined *Rab35* knockout were conducted according to the guidelines of the "Landesamt für Gesundheit und Soziales" (LAGeSo) and with their permission.

For the Schwann cell-specific *Rab35* gene knockout *in vivo*, *Rab35*$^{Fl/Fl}$ mice were interbred with a P0-*Cre* line (B6N.FVB-Tg(Mpz-cre)26Mes/J), which starts to express the Cre recombinase under control of the Schwann cell-specific P0-promoter on embryonic day (E)13.5 (Feltri *et al*., 1999). This work was performed in the lab of Prof. Dr. A. Bolino (INSPE, Milan, Italy), conducted according to the Italian national regulations and covered by experimental protocols reviewed by local Institutional Animal Care and Use Committees.

2.1.14 Software

Table 2-17: Software products, databases and internet tools.

Software	Source	Application
OligoCalc	http://biotools.nubic.northwestern.edu/OligoCalc.htmL	Melting point calculation of PCR-Primer
Adobe Illustrator CS6	Adobe Systems Incorporated	Preparation of figures
ApE plasmid editor	http://jorgensen.biology.utah.edu/wayned/ape/	DNA analysis incl. theoretical cloning preparation and primer design
GraphPad Prism 5.0	GraphPad	Statistical analysis and calculations, graph preparations
Image J	https://imagej.nih.gov/ij/	Evaluation of microscopy images
Intas GDS	INTAS Science Imaging Instruments GmbH, Goettingen, Germany	Agarose gel documentation
Image Lab	Bio-Rad	Semi-quantitative (HRP) immunoblot documentation and evaluation

LI-COR	LI-COR	Quantitative (fluorescent) immunoblot documentation and evaluation
MARS Data Analysis Software	BMG LABTECH	Analysis of microplate reader data (protein concentration)
MaxQuant	https://maxquant.net/	Identification and quantification of proteins from peptides detected in mass spectrometry
Micromanager v1.4.14	https://micro-manager.org/	Image acquisition on an epifluorescence microcope
Microsoft Office	Microsoft	Figure preparation, documentations
NCBI/Blast	http://blast.ncbi.nlm.nih.gov/	Homology determination of siRNA-targets
PyRAT (Python Based Relational Animal Tracking)	Scionics Computer Innovation GmbH	Animal facility software, managing of breedings and mouse strains
R	https://www.r-project.org/foundation/	Statistical analysis
Scaffold (Proteome Software)	http://www.proteomesoftware.com/products/scaffold/	Identification and quantification of proteins from peptides detected in mass spectrometry
Genesys	Syngene	DNA gel electrophoresis documentation
Uniprot	https://www.uniprot.org/	Gene and protein research; homology determination of proteins
ZEN	Zeiss	Image acquisition on confocal laser-scanning microscope (LSM)

2.1.15 Suppliers

Table 2-18: Suppliers for chemicals, consumables, devices and reagents.

Abbreviation	Company
Abcam	Abcam PLC, Cambridge, USA
Ambion	→ Thermo Fisher
ATCC	ATCC, Manassas, USA
BD Biosciences	BD Biosciences, San Jose, USA
Beckman	Beckman-Coulter, Krefeld, Germany
Bio&SELL	Bio&SELL, Feucht, Germany
Bio-Rad	Bio-Rad LABORATORIES Inc., Hercules, USA
BioTeZ	BioTeZ Berlin Buch GmbH, Berlin, Germany
BMG LABTECH	BMG LABTECH GmbH, Ortenberg, Germany
Cell signaling	Cell signaling technologies (CST), Boston, USA
Covance	Covance Inc., Princeton, USA
Dako	Agilent Technologies, Santa Clara, USA
Dharmacon	Dharmacon Inc., Lafayette, USA
Echelon	Echelon Biosciences Inc., Salt Lake City, USA
Eppendorf	Eppendorf, Hamburg, Germany
GE Healthcare	GE Healthcare, Chicago, USA

Harvard Apparatus	Harvard Apparatus, Holliston, USA
Invitrogen	→ Thermo Fisher
Jackson ImmunoResearch labs	Jackson ImmunoResearch Europe Ltd., Newmarket, United Kingdom
Jackson Laboratory	The Jackson Laboratory, Bar Harbor, USA
LGC genomics	LGC genomics GmbH, Berlin, Germany
LI-COR	LI-COR Biosciences, Lincoln, USA
Macherey-Nagel	Macherey-Nagel GmbH & Co. KG, Düren, Germany
Merck	Merck, Darmstadt, Germany
MBL International	MBL International Corporation, Woburn, USA
Millipore	Merck Millipore, Billerica, USA
NEB	New England Bio Labs, Ipswich, USA
Nikon	Nikon Corporation, Tokyo, Japan
Novus Biologicals	Novus Biologicals LLC, Centennial, USA
Okolab	Okolab Inc., San Bruno, USA
Preprotech	PeproTech EC, Ltd, London, United Kingdom
Promega	Promega GmbH, Mannheim, Germany
Proteintech	Proteintech Group, Manchester. United Kingdom
Roth	Carl Roth GmbH + Co. KG, Karlsruhe, Germany
R&D technologies	R&D Technologies Inc., North Kingstown, UK
Sarstedt	Sarstedt AG & Co. KG, Nümbrecht, Germany
Semrock	IDEX Health & Science, Rochester, USA
Serva	SERVA Electrophoresis GmbH, Heidelberg, Germany
Sigma	Sigma-Aldrich Chemie GmbH, Schnelldorf, Germany
Stratagene	Stratagene, La Jolla, USA
Synaptic systems	Synaptic Systems GmbH, Goettingen, Germany
Thermo Fisher	Thermo Fisher Scientific Inc., Waltham, USA
VWR	VWR International, Radnor, USA
Zeiss	Carl Zeiss GmBH, Jena, Germany

2.2 Methods

2.2.1 Molecular Biology Methods

2.2.1.1 Preparative and analytical Polymerase chain reaction (PCR)

The polymerase chain reaction (PCR) is used to amplify specific DNA sequences from DNA templates with thermostable DNA-polymerases, by repetitive thermo- and duration-controlled incubation cycles. The template DNA is first denaturated from double stranded (ds) into single-stranded (ss)DNA by high temperature. Following this, specific DNA-oligonucleotides can anneal to the ssDNA and serve as primers for the following DNA-sequence synthesis. After elongation, the newly synthesized DNA strands are utilized as additional templates in the next cycles. This results in an exponential DNA amplification (Saiki *et al*., 1988).

DNA fragments were amplified from plasmid or genomic DNA in a Thermocycler

peqSTAR 2X (VWR). For preparative purpose, when the desired fragment or gene was further used for cloning, Phusion high fidelity DNA Polymerase was used. It possesses 3'- to 5' –end exonuclease proofreading activity and therefore a low error rate. For analytical purpose the less precise Taq Polymerase was used to verify successful plasmid transformation of bacterial clones in colony PCRs, for instance. This polymerase was also used in genotyping PCRs of genomic DNA isolated from mouse biopsies (2.2.1.2).

Primers were designed using the ApE-plasmid editor and the online tool Oligo Calc, with the following criteria to ensure efficient and specific annealing: The overlap with the DNA-template was 21 bp to 30 bp. The salt-adjusted melting temperature (Tm) was between 50 °C and 65 °C with less than 5 °C difference between the two primers. In addition, the guanine-cytosine (GC) content was between 40 % and 50 %. The last nucleobase pair in the overlapping region was always a GC, as these nucleobases have a stronger bonding efficiency (three hydrogen bonds) than adenine- thymine. In the case of preparative PCR, restriction sites for subsequent ligation with the target DNA, and a random overhang of 4 bp for proper restriction enzyme reaction, were introduced at the 5'- end of each primer sequence. In order to screen clones in colony PCRs, one of the two primers was chosen to anneal at the vector backbone, and the other at the insert region.

Deoxy nucleotide triphosphates (dNTPs; Thermo Fisher, R0181) were mixed in a stock solution with a concentration of each at 5 mM, serving as free nucleotides for DNA elongation. Polymerase buffer and $MgCl_2$ solutions were supplied by the corresponding polymerase manufacturer. PCR samples were prepared in a usual volume of 20 µL. A loading dye, 1x OrangeG, was added for detection of DNA migration in the following agarose gel electrophoresis. The PCR sample composition is specified in Table 2-19. A positive and negative control for PCR performance, containing DNA with or without the desired fragment, respectively, as well as a sample containing water instead of DNA, were always carried along.

The corresponding performance protocols are specified in tables 2-20 to 2-21. All PCRs were started cold. The annealing temperature (T_a) was calculated from the melting temperature of the least stable primer pair ($T_{m\ primer}$) and the PCR product ($T_{m\ product}$) according to Rychlik and colleagues (1990):

(I) $$T_a = 0.3 * T_{m\ Primer} + 0.7 * T_{m\ Product} - 14.9$$

The elongation temperature and duration corresponded to the optimal working temperature of the used Polymerase and its elongation speed, respectively.

Table 2-19: PCR mixtures used for preparative or analytical DNA amplification.

Component	Final concentration	
	preparative PCR	**analytical/ colony PCR**
Template	plasmid DNA 20 ng/µL	*E. coli* culture 1/100 µL
Forward primer	0.5 µM	
Reverse primer	0.5 µM	
Polymerase buffer	1x	
$MgCl_2$	-	2 mM
dNTPs	0.2 mM each	
DNA Polymerase	0.05 U/µL	0.1 U/µL
10x OrangeG dye	1x	
H_2O	ad 20 µL	

Table 2-20: PCR performance protocol for preparative PCR.

Process		Temperature [°C]	Duration
Start		98	2 min
30x	Denaturation	98	10 s
	Annealing	formula (I)	30 s
	Elongation	72	30 s/ kbp
End		72	10 min

Table 2-21: PCR performance protocol for analytical (colony) PCR.

Process		Temperature [°C]	Duration
Start		95	2 min
30x	Denaturation	95	30 s
	Annealing	formula (I)	30 s
	Elongation	72	1 min/ kbp
End		72	10 min

In order to analyze the PCR products, the whole volume or 50 % of preparative or analytical PCR samples, respectively, were loaded onto 1 % to 2 % (w/v) agarose gels.

2.2.1.2 Genotyping of transgenic mice

Genomic DNA, isolated from biopsies of transgenic mice (2.2.1.13), was analyzed for the presence of the respective transgene by analytical PCR followed by agarose gel electrophoresis. The *Rab35* locus was analyzed regarding the homogeneous insertion of a loxP sequence in the intron 1 region in front of exon number 2. Therefor three primers in two different combinations and PCRs were used: Lox5F as the forward primer that anneals in the

intron 1 region. Lox5R as a reverse primer, annealing in the intron 1 region in *Rab35* WT locus only (product: 573 bp). And PL452-Loxp-Sc1R as a reverse primer that anneals within the inserted loxP site (product: 647 bp) in DNA from hemizygously or homozygously loxP-positive *Rab35*$^{(Fl)}$ mice. Homozygous *Rab35*$^{Fl/Fl}$ mice were thus identified by the lack of a WT-PCR product. For quality reasons, WT and "Fl" PCRs were performed separately (Table 2-22 and table 2-23).

The presence of the CAG-*CRE-ER*^{TM} transgene was verified using the primer pair "TM63_EllaCre" and "TM64_EllaCre" that amplified a 445 bp product (Table 2-22 and table 2-24).

Table 2-22: PCR mixtures used for analytical amplification from mouse genomic DNA.

Component	***Rab35* WT/"Fl"**	**CAG-*Cre***
genomic DNA	1 µL	
Forward primer	0.5 µM	0.375 µM
Reverse primer	0.5 µM	0.375 µM
Taq Polymerase buffer	1x	
$MgCl_2$	2 mM	
dNTPs	0.2 mM each	0.15 mM each
Taq DNA polymerase	0.1 U/µL	
10x OrangeG dye	1x	
H_2O	ad 20 µL	

Table 2-23: PCR performance protocol for amplification of genomic *Rab35* WT- and *Rab35*^{Fl}-fragments.

Process		**Temperature [°C]**	**Duration**
Start		95	2 min
35x	Denaturation	95	30 s
	Annealing	58	50 s
	Elongation	72	40 s
End		72	10 min

Table 2-24: PCR performance protocol for amplification of the genomic *Cre*-fragment.

Process		**Temperature [°C]**	**Duration**
Start		95	2 min
30x	Denaturation	95	30 s
	Annealing	55	30 s
	Elongation	72	30 s
End		72	10 min

2.2.1.3 Agarose gel electrophoresis

DNA fragments or plasmids were separated according to their size using agarose gel electrophoresis Compact chambers from Biometra. Depending on the size of the analyzed DNA fragments or plasmids, 0.7 % to 2 % (w/v) agarose (Bio&Sell, BS10.35.10) were dissolved in 1x TBE or 1x TAE buffer by heating in a microwave. The UV absorbance-possessing DNA interchelator ethidium bromide (0.3 µg/mL; Roth, 2218) was subsequently added for UV-mediated detection of DNA. Gels were casted and chilled at RT until gelatinization. Except for ready-to-use PCR or DNA-restriction samples, lx OrangeG loading dye was added before loading onto the gel. As a reference 5µL 100 bp or 1 kb DNA-Ladders (Thermo Fisher) were used. Electrophoresis was performed in TBE or TAE buffer at 10 V/cm electrode distance for 20 min to 30 min until the 50 bps OrangeG-migration frontline reached the lower edge of the gel. DNA was visualized due to ethidium bromide incorporation by 302 nm UV light using the Gel documentation GBOX/F3 system and controlled by the corresponding software GeneSys from Syngene. For preparative agarose gelelectrophoresis DNA fragments were excised from the gel on a UV transillumination table (UVT-28 LV from Herolab) with a low and short UV exposure to prevent point mutations.

2.2.1.4 Purification of DNA from agarose gels

Amplificated PCR-fragments or restricted DNA fragments and plasmids were purified from excised agarose gel pieces using the NucleoSpin® Gel and PCR Clean-up kit (Macherey-Nagel) according to the manufacturer's instructions. In brief, excised agarose gel pieces were dissolved in high-salt buffer, the DNA solution was loaded and purified on a silica membrane. Pure DNA-fragments were diluted in 15 µL, DNA-plasmids in 30 µL TE-buffer.

2.2.1.5 DNA-restriction digest

Each 10 µL of purified PCR-DNA fragments or 2 µg of target-DNA vectors were restricted in a 20 µL reaction volume. The samples were supplemented with 1 µL of each FastDigest restriction endonucleases (Fermentas) and 1x FastDigest Green buffer, allowing for subsequent loading on agarose gels. In order to prevent subsequent re-ligation of the restricted, linearized DNA-vectors, 1 U of FastAP thermosensitive alkaline phosphatase (Thermo Fisher, EF0654) was added to dephosphorylate the 5'-ends. The restriction reaction was performed at 37 °C for 20 min, followed by 5 min incubation at 80 °C to inactivate all enzymes. A DNA vector sample without restriction enzymes was carried along and served as a

negative control. The samples were loaded on agarose gel for subsequent separation and purification of the restricted DNA.

2.2.1.6 Ligation

T4-DNA ligase (Thermo Fisher, ELL0016) was used to insert the fragment into vector DNA after restriction. It catalyzes the re-formation of phosphodiester bounds between the DNA 3'- and 5'-ends. First, the DNA-concentration of the purified restriction products was determined. In 20 µL reaction volume, 1 Weiss Unit of ligase, 1x ligase buffer and 50 ng to 100 ng of target vector were used, supplemented with a three- to six-fold molar excess of the insert. To control for undesired plasmid re-ligation, a vector sample without fragment DNA was used. Ligation samples were incubated for 1 h at RT and stored at -20 °C or were subsequently used for transformation.

2.2.1.7 Transformation of chemically competent *E. coli*

For transformation, 50 µL glycerol stocks of chemically competent *E. coli* Top10 or BL21DE3 in 0.1 M $CaCl_2$ were thawed on ice and supplemented with 10 ng plasmid DNA or 10 µL ligation products. The samples were gently mixed and incubated for 30 min at 4 °C. The uptake of plasmid DNA was triggered by a heat-shock for 90 s at 42 °C. This leads to perforation of the bacterial plasma membrane, enabled by calcium ions that counteract the electrostatic repulsion between membrane and DNA. After 5 min chilling on ice, the bacteria were directly plated on prewarmed LB agar plates with 100 µg/mL ampicillin when the transformed plasmid contained the resistance marker gene for the bacteriostatic antibiotic ampicillin. If kanamycin resistance was encoded in the transformed plasmid, bacteria were supplemented with 400 µL LB medium without antibiotics and cultured first for 1 h at 37 °C and 180 rpm, allowing for expression of the kanamycin resistance protein before exposure to the bacteriocidal antibiotic kanamycin. The bacteria were then pelleted from the antibiotic-free suspension at 700 x g for 1 min. After removal of $4/5^{th}$ of supernatant volume, the cells were recollected in the remaining LB-medium supernatant and plated onto prewarmed LB agar plates containing 50 µg/mL kanamycin.

The plates were incubated overnight at 37 °C. Newly transformed clones, picked from LB agar plates with sterile plastic tips, were transferred into 200 µL LB-medium (with corresponding antibiotics) per well of a 96 well plate and cultured for 2 h at 37 °C on a Heidolph Titramax 1000 plate shaker at 350 rpm. 2 µL of the suspension was directly used to perform colony PCR for the verification of positive clones.

2.2.1.8 Preparation of bacterial glycerol stocks

Glycerol stocks were prepared for long term storage of transformed bacteria, by inoculating 2 mL LB medium, containing 100 µg/mL ampicillin or 50 µg/mL kanamycin, with the clone suspension and grown overnight at 37 °C and 180 rpm in a bacteria incubator shaker. The bacterial suspension was then concentrated to 750 µL by centrifugation at 4,000 x g for 5 min at 4 °C, diluted one to one in sterile 50 % (v/v) glycerol and stored in cryotubes at -80°C.

2.2.1.9 Cultivation of transformed bacteria

Transformed *E. coli* Top10 were picked from cryopreserved cultures or LB-Agar plates with a sterile pipette tip and were used for inoculation of 2 mL LB-Medium with 100 µg/mL ampicillin or 50 µg/mL kanamycin. This preculture was incubated for 8 h at 37 °C and 180 rpm in a bacteria incubator shaker (New Brunswick Scientific, Innova 42). For a higher yield of plasmid DNA, 100 mL LB-Medium with antibiotics were then inoculated with 0.1 % (v/v) (100 µL) of this preculture and incubated over night at 37 °C and 180 rpm. The next day, the bacteria were sedimented by centrifugation at 4,000 x g for 15 min at 4 °C. Bacterial pellets were either stored at -20 °C or immediately resuspended for isolation of plasmid DNA.

2.2.1.10 Isolation of plasmid DNA

Plasmid DNA was isolated from precultures of transformed *E. coli* TOP10 using the Plasmid Mini-Kit NucleoBond® PC20 from Macherey-Nagel. The procedure is based on a modified sodiumdodecylsulfate (SDS)-alkaline lysis of cells (Birnboim and Doly, 1979). In brief, bacterial pellets were resuspended in a TRIS-based physiological buffer containing EDTA, to chelate divalent metal cations. This destabilizes the cell wall and impairs the function of DNases. Glucose supplementation ensures iso-osmolarity of the buffer in order to prevent the cells from bursting, whereas RNA is hydrolyzed by supplementation of RNase. During subsequent lysis, the detergent SDS disrupts the cell membrane, which enables NaOH permeability for subsequent dsDNA-denaturation into single strands. By neutralization with a potassium acetate buffer, hydrogen bonds are re-established in smaller DNA fragments and thus, plasmid DNA is re-naturated and dissolved, while the genomic DNA precipitates together with SDS, cellular proteins and cell debris through hydrophobic interactions. Lysates were cleared from these precipitates by centrifugation and were applied to a silica column. The bound plasmid DNA was washed and finally eluted in nuclease-free water (Roth, T143).

Plasmid Midi DNA preparation was performed when higher amounts of plasmid DNA were required using the Macherey-Nagel NucleoBond®Xtra Midi-EF kit. Here, additional washing steps of the silica-bound DNA were performed that ensure an efficient removal of the bacterial endotoxins for the subsequent usage of plasmids in cell transfections. In addition, plasmid DNA was eluted from the column with an alkaline buffer, precipitated with 2-Propanol, pelleted and dissolved in millipore-filtered, endotoxin-free (EF) water (Machery-Nagel). The DNA-concentration and purity were determined with a BioPhotomer Plus from Eppendorf at a wavelength of 260 nm and adjusted to 1 µg/µL.

2.2.1.11 Spectrophotometric determination of DNA concentration

The DNA-concentration in solutions was determined in UV-transparent cuvettes using a BioPhotometer plus (Eppendorf). The absorption was measured at a wavelength of 260 nm and the concentration calculated using the Lambert-Beer law:

(II) $$c_{dsDNA} = \frac{A_{260\,nm}}{b * \varepsilon_{dsDNA}} * d$$

c_{dsDNA}- concentration of dsDNA; A_{260nm} – absorption at a wavelength of 260 nm; b – pathlength: 1 cm; ε_{dsDNA} – molar extinction coefficient for dsDNA at 260 nm (50 mL µg^{-1} cm^{-1}); d - dilution

DNA solutions were considered as sufficiently pure, if a ratio of absorbances at 260 nm and 280 nm, the absorbance maximum of proteins, between 1.7 to 2 was achieved.

2.2.1.12 Sequencing of DNA

DNA samples were sequenced by LGC genomics (Germany) using the Sanger method, based on the incorporation of chain-terminating 2'-3'-dideoxynucleotides by DNA-polymerases during *in vitro* replication (Sanger and Coulson, 1975).

2.2.1.13 Isolation of genomic DNA

Genomic DNA was isolated from earbiopsies of adult mice with the Proteinase K method according to Wang & Storm (2006). Here, the tissue was digested, and cells were simultaneously disrupted in 350 µL/mm^2 biopsy lysis buffer (BLB) containing high salt concentrations, SDS-detergent and EDTA. The buffer was freshly supplemented with 1 % (v/v) Proteinase K, to prevent the degradation of genomic DNA during lysis by digesting nucleases. After 30 min to 2 h incubation at 55°C and 900 rpm in a Thermomixer (Eppendorf, 5437,), the tissue was lysed and cell remnants were removed by centrifugation for 5 min at 17,000 x g in a tabletop centrifuge. The DNA-containing supernatant was transferred into a

new tube and an equal volume of 2-Propanol was applied. The tube was gently inverted until genomic DNA visibly precipitated. The precipitates were subsequently sedimented by centrifugation at 17,000 x g for 5 min, washed in 70 (v/v) % ethanol and pelleted again. The DNA-pellet was dried for 5 min at 60 °C and dissolved in 50 µL millipore-filtered water.

Genomic DNA from small tail biopsies of mouse pups was isolated with the HotSHOT method according to Warman and colleagues (Truett *et al*., 2000). It is based on the use of alkaline lysis, similar to the method of Birnboim and Doly (1979) (see 2.2.1.10) but omitting SDS or potassium acetate and thus, without DNA precipitation. The neutralization solution is replaced by 40 mM TRIS-HCl at pH 5 (TNB). The tissue pieces were digested for 1 h at 95 °C in 50 µL/ 2 mm tail lysis buffer (TLB) and then chilled to RT. TNB was applied in a volume ratio of 1:1. For analysis by genotyping PCR, 1 µL of the DNA solutions were used.

2.2.2 Cell biology methods

2.2.2.1 Cultivation and passaging of mammalian cell lines

Human embryonic kidney 293T (HEK), HeLa and eGFP-Rab35^{endo} knock-in (KI) HeLa cell cultures were cultivated in Dulbecco's Modified Eagle Medium (DMEM) with high glucose (4.5 g/L) and 2 mM L-glutamine, supplemented with 10 % (v/v) fetal bovine serum (FBS), 100 U/mL Penicillin and 100 µg/mL Streptomycin (1% (v/v) P/S) (mammalian cell culturing medium, mCCM) at 37 °C under humidified conditions of 5 % CO_2 in a CO_2-incubator (New Brunswick Scientific, Galaxy 170S). The cultivation of cell cultures was performed under sterile conditions. All solutions, buffers and reagents were filtered sterile, water was autoclaved before usage. Media and washing buffers were incubated in a waterbath to warm up to 37 °C before application.

Confluent cells were passaged every two to five days. Therefor medium was aspirated and the cells were rinsed one time with Dulbecco's Phosphate-Buffered Saline (D-PBS -Ca^{2+}/Mg^{2+}; Thermo Fisher, 14190169) to remove remaining FBS, which would interfere with trypsinization. Cells were then dissociated from dishes by incubation in the synthetic trypsin substitute TrypLE Express Enzyme solution (TrypLE; Thermo Fisher, 12605036), used in appropriate volumes according to the manufacturer's instructions. After 5 min at 37 °C, dissociation was stopped by collecting the detached cells in mCCM. The cells were seeded in appropriate dilutions for desired confluency. Cells were cultivated and used for experiments until reaching a passaging number of 35.

For immunocytochemistry (ICC), HeLa and eGFP-Rab35^{endo} KI HeLa cells were seeded on glass coverslips, coated with an extracellular matrix protein solution to ensure a proper attachment to the glass surface. Therefor the coverslip surface was covered with a thin layer of 5 % (v/v) Matrigel (Corning, 356231) in serum-reduced Opti-MEM^{TM} (Thermo Fisher, 51985-042). After incubation for 1 h at RT, the solution was removed by rinsing one time with D-PBS -Ca^{2+}/Mg^{2+}, and cells were seeded.

For long-term storage, dissociated cultures from 10 cm dishes were collected in 3 mL mCCM, supplemented with additional 30 % (v/v) FBS to a final concentration of 40 % (v/v), and 10 % (v/v) DMSO. Each 1 mL was transferred into a cryotube. The stocks were frozen stepwise by incubation for 2 h at -20 °C followed by 12 h incubation at -80 °C before transfer to and long-term storage in liquid-nitrogen tanks at -196 °C. In order to cultivate cells from DMSO-stocks, the cells were thawed slowly on ice, supplied with an excess of mCCM and pelleted at 300 x g for 5 min to remove DMSO completely, before seeding in fresh mCCM.

2.2.2.2 Transfection of mammalian cell lines using JetPrime

JetPrime (VWR, 114-75) was used to transfect HeLa cells with DNA plasmids for ICC, or HeLa and HEK cells with siRNA for RNAi-mediated gene knockdown. Neither the molecular structure nor the constitution of this reagent is published. However, the transfection mechanism is equivalent to another commonly used “proton-sponge” reagent polyethylenimin (PEI; Dateki *et al*., 2016; Sandbichler *et al*., 2013). These cationic polymer-based reagents interact with negatively charged siRNA or DNA to form complexes, in which the nucleic acids are protected from nucleases. In addition, the excess of cationic charge of these complexes allow for binding to the negatively charged cell membrane, more specifically, to surface residing heparan sulfate proteoglycans. Thereby, the complex is internalized by endocytosis and delivered to early endosomes (Boussif *et al*., 1995). The high pH-buffering capacity of the amino nitrogen facilitates luminal accumulation of protons and thereby chloride ions within these endosomes. This results in osmotic swelling and eventually vesicle lysis of the endosomal membrane with subsequent release of the nucleic acids (Medina-Kauwe *et al*., 2005).

Cells with a confluency of 60 % to 80 % were transfected according to the manufacturer’s instructions, by mixing 2 µg DNA or 100 pmol siRNA per 6-well with 200 µL 1x JetPrime buffer. JetPrime reagent was then added in a ratio of 2:1 (v/w) with the nucleic acids. After incubation of 10 min at RT, the transfection solution was applied to the cells. For co-transfections with more than one plasmid, a 1:1 amount of substance ratio was used with a

total amount of 2 µg. After 4 h incubation, cells were rinsed with phosphate buffered saline (PBS) and supplied with new mCCM. The cells were fixed 24 h post-transfection. For reverse transfection with siRNA, the transfection solution was applied to the diluted cell suspension during passaging prior to the seeding onto 6-well plates. After 12 h, when cells were settled, wells were rinsed with PBS and fresh mCCM was applied. For biochemical analysis, siRNA-transfected HEK cells were harvested 96 h post-transfection. For rescue experiments, plasmid DNA encoding the siRNA-resistant gene was introduced 48 h post-transfection using calcium phosphate. siRNA-transfected HeLa cells were passaged to coverslips for ICC after 48 h and fixed 96 h post-transfection.

2.2.2.3 Transfection of mammalian cell lines using calcium phosphate

To introduce DNA-plasmids into eGFP-Rab35^{endo} KI HeLa or HEK cells for affinity purifications of proteins or lentiviral production, calcium phosphate transfection was performed. Its effect is based on the spontaneous precipitation of calcium ions together with phosphates, in which DNA and siRNA is incorporated if present during precipitate formation. The precipitate adheres to cell surfaces and thereby facilitates the endocytic uptake of DNA and siRNA into the cells (Graham and van der Eb, 1973).

For affinity purifications assays, cells with a confluency of 60 % to 80 % were transfected 12 h to 24 h after passaging. Appropriate amounts of DNA, depending on the culture size as specified in table 2-25, were incubated for 5 min at RT in 0.24 M $CaCl_2$ in 0.1x TE. This solution was added dropwise to 2x HBS buffer in a volume ratio of 1:1, under gentle vortexing. After 20 min incubation at RT, the precipitate solution was added to the cells and incubated overnight. The cells were then rinsed and supplied with fresh mCCM. Experiments were performed 24 h to 48 h post-transfection.

Table 2-25: Calcium phosphate transfection mixture for different cell culture dishes.

Cell culture dishes [cm]	Plasmid DNA [µg]	2x HBS [µL]	0.24 M $CaCl_2$ in 0.1x TE [µL]
6	6	250	250
10	15	500	500
15	30	1,250	1,250

2.2.2.4 Production of lentiviral particles

The production of lentiviral particles and transduction of mammalian cells was done in accordance with the S2 guidelines (LAGESO). In primary cell cultures, siRNA-transfection

usually result in a low transfection rate. Thus, lentiviral particles are produced in order to deliver shRNA with a high efficiency by transduction. The lentivirus is a modified HI virus, able to introduce RNA and DNA into non-dividing cells but unable to replicate (Naldini *et al*., 1996). For virus production, a 2nd generation lentiviral packaging system from Dharmacon was used. Here, HEK cells are transfected with three plasmids, of which each contains a component of the virus and thus, start to generate the virus upon co-expression only. The lentiviral packaging plasmid psPAX2 (addgene, #12260) contains the pol, gag, rev and tat viral genes and the rev-response element (RRE). The envelope plasmid pMD2.G (addgene, #12259) encodes the G protein of the Vesicular Stomatitis Virus (VSV-G) envelope for a broad host infectivity. The transfer plasmid contains the transgene, here, shRNAs under control of a U6 promoter for transcription by the RNA Polymerase III. The shRNA is encoded between the Long Terminal Repeats (LTRs). The plasmid also contains the psi packaging sequence as a recognition site for packaging of the shRNA into viral particles. As transfer plasmids, pLKO.1 vectors were used, encoding either for mouse (ms)MTMR2 targeting shRNA (Dharmacon, TRCN0000030098), or non-targeting shRNA (scrambled) as a control (pLKO.1_scrambled shRNA; Dharmacon, RHS6848). The latter additionally encoded eGFP under control of a CMV promoter.

For lentiviral production, 15 cm dishes of HEK cells were transfected using calcium phosphate, 12 h after seeding and with a high confluency of 80 % to 90 %, in order to compensate for decreased cell proliferation and increased cell death during virus production. Cells, cultivated in 15 cm dishes, were co-transfected overnight with 30 µg of shRNA-encoding plasmids, 21 µg of pMD2.G and 9 µg psPAX2, thus, in a ratio of 1.5 : 1.05: 0.45 and in a total volume of 2.5 mL transfection solution. The cells were treated as S2 cultures from that point on. The next morning, the cells were washed once with D-PBS. Fresh mCCM was applied in a reduced volume of 60 % to increase the virus titer. Two consecutive rounds of virus harvest were performed after 24 h and 48 h. The virus-containing medium was collected and HEK cells were supplied with fresh mCCM. Mammalian cell debris was subsequently removed from the collected medium by centrifugation at 200 x g for 5 min at RT. The viral particle-containing supernatant was stored at 4 °C. Supernatants from both harvest rounds were pooled and filtered using a 0.45 µm falcon filter in order to remove remaining cell debris. The viral particles were then concentrated 100 x to high-titer viral supernatants by centrifugation in an Amicon Ultra-15 100 kDa filter column (Merck, Z740210) at 5,000 x g and 4 °C for 15 min per 15 mL supernatant. Aliquots with each 20 %

of concentrated viral supernatant from a 15 cm dish were stored at -80 °C. Thawed aliquots for transduction were stored up to two weeks at 4 °C if not emptied at once.

For calculation of the achieved infection units per mL, the virus titer, HEK cells were seeded in defined cell numbers in 24-well plates and transduced with different titrations of the concentrated viral supernatant, from 10 % to 0.001 % (v/v) volume per well. After three days, cells were trypsinized and the proportion of eGFP-positive cells was determined using a Neubauer cell counting chamber. The titer was then calculated as follows:

(III) $titer\ [\frac{U}{mL}] = \frac{\mathrm{n}_{\mathrm{cells}}t_0 * \frac{\%\ GFP^+}{100}}{\text{viral supernatant [mL]}}$

$\mathrm{n}_{\mathrm{cells}}t_0$ - seeded cell number; % eGFP$^+$ - proportion of eGFP-positive = transduced cells

The usual titer of concentrated viral supernatant was around $1*10^8$ to $1*10^9$ U/mL. For pLKO.1_msMTMR2 shRNA-plasmids, which did not contain an eGFP-encoding gene, the production of lentiviral particles was done side by side with the control plasmid to achieve a comparable titer.

2.2.2.5 Preparation of primary cell cultures from mice

All primary cell cultures were obtained from postnatal mice after decapitation according to the guidelines of the Landesamt für Gesundheit und Soziales (LAGeSo) Berlin. For isolation of the different cell types, mice of distinct age (postnatal day; p) were used according to the literature and published protocols to achieve a maximum in cell number and culture quality. The isolation of the respective brain regions or nerves was done in a semi-sterile hood, all following steps under a sterile hood. All solutions, buffers and reagents for preparation and cultivation of primary cell cultures were filtered sterile. Millipore-filtered water was autoclaved before usage. If not otherwise indicated, cells were cultivated in cell culture dishes or on coverslips in well plates in CO_2 incubators (New Brunswick Scientific, Galaxy 170S) at 5 % CO_2 and 37 °C under humidified conditions. Cell media were equilibrated in CO_2 incubators, washing buffers were warmed up to 37 °C by water bath incubation before application. For cell counting, samples of cell suspensions were diluted 1:1 with Trypan blue. This dye enters the cytoplasm of dead cells through their porous cell membrane. Thus, only alive cells were counted, under non-sterile conditions, using a Neubauer chamber and an Olympus CKX-31 phase contrast microscope.

In order to improve the polypeptide coating and thereby the cell adhesion to the glass surface, all coverslips used for the seeding of neuronal, oligodendrocytic or Schwann cell

cultures were cleaned before usage. Cleaning was performed in 1 N HCl for 24 h, with subsequent washes in Aceton and 70 % Ethanol, each for 24 h. The coverslips were then stored in 96 % Ethanol. On the day of preparation, coverslips were first dried under sterile conditions, transferred to well plates and then coated as specified in the corresponding preparation sections.

2.2.2.5.1 Primary neuronal cultures

Primary neuronal cultures for life cell imaging or ICC were prepared by isolating hippocampi from mice at postnatal days one to four (P1 to P4). After decapitation of the mice, brains were transferred into a 3.5 cm cell culture dish containing ice-cold Hanks' balanced salt solution (HBSS -Mg^{2+}/Ca^{2+}; Thermo Fisher, 14175-053) supplemented with 20 % (v/v) FBS and 1 % (v/v) P/S. Under a binocular stereo microscope, the hemispheres were first isolated from the middle brain and the brainstem, the meninges then removed from the cortex surface and finally hippocampi were separated from the entorhinal cortex. After removal of remaining blood vessels, isolated hippocampi from up to six animals were pooled in HBSS with 20 % (v/v) FBS and 1% (v/v) P/S in a new dish and cut into equally sized pieces of around 1 mm^3 to 2 mm^3. The tissue pieces were transferred into a 15 mL falcon tube containing 5 mL of HBSS with 20 % FBS and 1% (v/v) P/S. When cells were settled down, the supernatant was aspirated. After two additional washing steps with 5 mL of the same solution, the tissue was rinsed twice with 5 mL HBSS with P/S only, in order to remove the serum before digestion. Following this, 2 mL neuronal digestion solution with 5 mg/mL Trypsin (Sigma, T1005) and 375 U/mL DNase I (Sigma, D5025), in order to prevent tissue clumping by free-floating DNA fragments, were applied for 15 min at 37 °C. The digestion was stopped by rinsing twice with 5 mL FBS-supplemented, and twice with FBS-omitted HBSS. The tissue was mechanically dissociated in 2 mL neuronal dissociation solution with 375 U/mL Units DNase I, using a siliconized glass Pasteur pipette with a fire-induced narrow opening at the tip. The tissue solution was triturated up to eight times until a homogeneous cell solution was obtained. 2 mL FBS-supplemented HBSS were added and the cells were sedimented by centrifugation for 8 min at 400 x g and 4 °C. The cell pellet was resuspended in a small volume of neuronal plating medium (50 µL/ hippocampus), cells were counted, and the solution was adjusted to a cell concentration of 1,600 cells/µL before seeding. To ensure cell attachment, coverslips were first coated with Poly-L-lysine hydrobromide in water (PLL; Biochrom, L7240) for 2 h at RT, rinsed twice with water and were finally dried, before a drop of cell solution with a

defined number of cells (2-26) was applied. After 1 hr incubation at 37 °C and 5 % CO_2, when cells were attached to the coverslips, equilibrated neuronal plating medium was added.

Table 2-26: Numbers of seeded neurons and corresponding medium volumes for differently sized coverslips.

Coverslip diameter [mm]	PLL volume [µL]	Cell number [x 10^3]	Medium volume [mL]
24	200	80	2
18	120	50	1.5
12	80	30	1

The cultures were fed on the first day *in vitro* (DIV1) by replacing 50 % of the culturing medium with neuronal growth medium, supplemented with 2 µM Cytosine β-D-arabinofuranoside hydrochloride (Ara-C; Sigma, C6645). In addition, the cells were supplemented with 0.4 µM Tamoxifen (TMX; Sigma, T5648, (Z)-4-hydroxytamoxifen) dissolved in Ethanol, to induce expression of the CRE recombinase and thereby the gene knockout in *Rab35* icKO cells. On DIV2 another half of culture medium was exchanged for neuronal growth medium containing TMX and 4 µM Ara-C. Thus, from DIV2 on, the cultures were kept in the presence of 3 µM Ara-C, a nucleoside analogue which inhibits proliferation and thereby allows to restrict the number of glial cells, mainly astrocytes, within these cultures. Experiments were performed on DIV14.

2.2.2.5.2 Primary astrocytic cultures

Cortices were isolated from mice at postnatal days two to five (P2-P5), equivalent to the preparation primary neuronal cultures (2.2.2.5.1) but with the following modifications: The hippocampus was removed and discarded during dissection. The cortex' tissue pieces were washed in a 15 mL falcon tube three times with 5 mL HBSS (-Ca^{2+}/Mg^{2+}) and digested for 15 min at 37 °C in 5 mL of the synthetic trypsin substitute TrypLE Express Enzyme solution (TrypLE; Thermo Fisher, 12605036) supplemented with 375 U/mL DNase I. After additional three washing steps with HBSS, the cells were dissociated with siliconized Pasteur pipettes as described, but in 2 mL mCCM supplemented with 375 U/mL DNase I. The homogeneous cell suspension was filled up to 15 mL with mCCM and centrifuged. Sedimented cells were collected in 5 mL or 3 mL mCCM per *Rab35* WT or icKO cortex, respectively. The suspension was filtered through a 70 µM Nylon cell strainer (Sigma, 431751), and each 10 mL were plated per 10 cm cell culture dish.

On DIV1 the dishes were rinsed with D-PBS (-Ca^{2+}/Mg^{2+}; Thermo Fisher, 14190169) and supplied with 10 mL fresh mCCM containing 0.4 µM TMX. The cultures were grown until confluency and then passaged on DIV7 to DIV8 to smaller cell culture dishes or coverslips. In brief, 10 cm cell culture dishes were rinsed once with D-PBS, before trypsinization in 0.5 mL TrypLE for 5 to 8 min in a CO_2-incubator at 37 °C. Trypsinization was stopped by adding 4.5 mL mCCM and the cell suspension was transferred to 15 mL falcons. The cell concentration was determined by cell counting and adjusted with mCCM to the desired seeding density (2-27). Cells were seeded on plastic cell culture dishes or wells for biochemical assays. For ICC, PLL-coated glass coverslips (see 2.2.2.5.1) were used. To achieve a comparable confluency on the day of experiment, *Rab35* icKO cells were seeded with an increased density compared to WT cells. The medium was exchanged every three to four days and experiments were performed on DIV20 to DIV22. For serum-starvation, cells were washed one time with D-PBS and cultured in mCCM without FBS for 12 h prior to harvest. Control (serum-fed) cells were supplied with fresh FBS-containing medium instead.

Table 2-27: Seeded cell numbers and medium volumes of astrocytic cultures after passaging.

Dish/ well/ coverslip	Cell number [x 10^3]		Medium volume [mL]
	WT	*Rab35* icKO	
6 cm cell culture dish	360	900	5
6-well	120	300	2
24 mm coverslip	30	80	

2.2.2.5.3 Primary oligodendrocytic (precursor) cell cultures

Primary oligodendrocytic precursor cell (OPC) cultures were prepared using immunopanning-mediated purification from mouse cortices according to the protocol of Emery and Dugas (2013). Mature myelinating oligodendrocytes were obtained by differentiation induction of OPCs in culture.

In brief, cortices from P6 to P8 mouse pups were isolated as described (2.2.2.5.1) and collected in 3.5 cm cell culture dishes containing 2 mL ice-cold D-PBS -Ca^{2+}/Mg^{2+}. After dissection of all cortices, each two were transferred to 100 µL D-PBS -Ca^{2+}/Mg^{2+} in another 3.5 cm dish and cut into pieces of around 1 mm^3. The absence of calcium and magnesium is crucial to promote the subsequent enzymatic digestion. For this, 20 U/mL Papain (Worthington Biochemical, LS003126) were dissolved in equilibrated Papain buffer by incubation at 37 °C for 15 min. In contrast to the serine protease trypsin, papain is a cysteine protease and less damaging during tissue digestion. This leads to a comparably high amount

of morphologically intact cells, particularly important for immunopanning. The enzyme was activated by the addition of 0.2 mg/mL L-cysteine (Sigma-Aldrich C-7477) and supplemented with 250 U/mL DNAse I (Worthington Biochemical, LS002007).

The cortex tissue was supplied with each 3 mL of sterile filtered papain-containing digestion solution per dish and incubated for 90 min at 37 °C in a 5 % CO_2-incubator. The tissue suspension of each three dishes was pooled and transferred into a 15 mL falcon. After the tissue had settled down, the supernatant was aspirated and washed with 2 mL of equilibrated low-ovomucoid solution (LOS), supplemented with 125 U/mL DNAse I, to stop the papain activity. The tissue was dissociated mechanically to single cells by gentle trituration in 3 mL LOS for eight times with a 1 mL plastic tip pipette. When the remaining tissue pieces were settled down, 1 mL of cell suspension supernatant was transferred into a new tube and 1 mL of fresh LOS was added to the remaining tissue for another round of trituration. This procedure was repeated six times until the tissue was fully dissociated and entirely transferred as a homogeneous suspension to the new tube. The cells were pelleted by centrifugation for 15 min at RT and 400 x g and washed in 6 mL equilibrated high-ovomucoid solution (HOS) for full papain inactivation. After another round of centrifugation, the cells were collected in 15 mL immunopanning buffer, filtered through a 70 µM Nylon cell strainer (Sigma, 431751) and applied to the prepared immunopanning dishes.

In three consecutive rounds of immunopanning, the cells were first two times negatively selected for microglia with an antibody against the *Griffonia* (*Bandeiraea*) *Simplicifolia* Lectin 1 (BSL1), followed by a positive selection for OPCs against the platelet-derived growth factor receptor α (PDGFRα). For each negative selection, one 15 cm cell culture dish was coated with 20 mL of 1 µg/mL BSL1 (Vector Laboratories, L1100) in D-PBS +Ca^{2+}/Mg^{2+} (Thermo Fisher, 14287080) for 2 h at RT. The dishes were rinsed three times carefully with D-PBS +Ca^{2+}/Mg^{2+}, before the cells were applied for each 15 min. For the positive selection of OPCs, 10 cm cell culture dishes were first coated with 10 mL of 3 µg/mL goat-α-rat antibody (Jackson ImmunoResearch, 112-005-167) in 50 mM TRIS-HCl pH 9.5 overnight at 4 °C. The primary antibody solution was then applied for 2 h at RT, containing 1.6 µg/mL rat-α-PDGFRα antibody (BD Pharmingen, 558774) in 0.2 % BSA (Sigma, A4161) in D-PBS +Ca^{2+}/Mg^{2+}. The cell suspension was applied for 45 min with slight agitation of the dishes every 15 min. The supernatant was discarded, and the dishes were rinsed carefully six times with D-PBS +Ca^{2+}/Mg^{2+} to remove all non-attached cells. After another wash with 10 % CO_2-equilibrated Earle's Balanced Salt solution (EBSS; Thermo Fisher, 14155063), 4 mL of 5 x 10^3 U/mL Trypsin (Sigma, T9935) in EBSS were

applied for 6 min to 8 min at 37 °C in a 5 % CO_2-incubator. The detached OPCs were collected from the immunopanning dishes in 10 mL D-PBS +Ca^{2+}/Mg^{2+} with 30 % (v/v) heat-inactivated FBS to stop the enzyme reaction. The cell solution was transferred to a 15 mL falcon-tube for centrifugation at 400 x g for 15 min at RT. After resuspension of the cell pellet in 25 µL DMEM-Sato growth medium (DSM) per cortex, the cells were counted and the cell concentration was adjusted. OPCs were seeded in 25 µL drops with a number of 20 x 10^3 cells. Cleaned 12 mm glass coverslips were used, coated overnight at 4 °C with 80 µL of 10 µg/mL Poly-D-Lysine (PDL; Sigma, P6407) in 1.5 mM boric acid pH 8.4. After cell attachment (1 hr at 37 °C and 10 % CO_2) 500 µL equilibrated DSM was supplemented with 10 µM Forskolin and each 10 ng/mL of ciliary neurotrophic factor (CNTF) platelet-derived growth factor AA (PDGF-AA) and neurotrophin-3 (NT-3) (OPC proliferation medium) , and added. Cells were cultivated in 10 % CO_2-incubators according to standard protocols. On DIV1, the coverslips were rinsed with D-PBS -Ca^{2+}/Mg^{2+} before fresh medium was applied, supplemented with 0.4 µM TMX. For experiments with oligodendrocytic cultures, OPC differentiation medium was used from DIV1 on. Here, Forskolin and CNTF to raise cAMP levels and ensure cell survival, respectively, were added to DSM. The mitogens for OPC proliferation, PDGF-AA and NT-3, were replaced by 40 ng/mL thyroid hormone triiodothyronine (T3) to induce the differentiation into mature oligodendrocytes.

DSM was prepared freshly every week and stored at 4 °C. The cultures were fed by exchanging half of culturing medium volume every two to three days and fixed on DIV7 to DIV8. Cultures were transduced or inhibitors were applied at DIV3 with ongoing application during medium exchange.

2.2.2.5.4 Primary Schwann cell mono-cultures

The preparation of Schwann cell mono-cultures was performed according to Jessen and Mirsky (Arthur-Farraj *et al*., 2011), representing an adaption of the Brockes method for the preparation and purification of Schwann cells from mice (Brockes *et al*., 1979). In brief, Schwann cells were purified from the sciatic nerve and the brachial plexus, isolated from P4 to P6 mice after decapitation. For dissection of the sciatic nerve, the dorsal skin was removed at the level of the hindlimbs. The nerve was exposed by cutting along the gluteus maximus, and isolated from its origin at the spinal cord, at the head of the thigh-bone, until its allocation into smaller cords at the knee joint. The brachial plexus was dissected by first removing the ventral skin at the upper limbs from the armpit to the elbow. By cutting along the Biceps

brachii muscles, the nerve cords were revealed underneath and then isolated from the axilla to their distal branching points at the elbow joint.

Nerves of each mouse were collected in one 3.5 cm cell culture dish containing 2 mL ice-cold Leibovitz's L-15 medium (L-15; Thermo Fisher, 11415049) and freed from remaining connective tissue and endoneurium. For digestion, clean nerves were transferred into a new dish with 3 mL L-15 supplemented with 0.1 % (w/v) Collagenase A (Sigma, 10103586001) and 0.25 % (w/v) Trypsin (Thermo Fisher, 27250018) for 1 hr at 37 °C and 5 % CO_2. After dissociation of the nerve tissue by trituration with a 200 µL Gilson pipette, the tissue solutions of each three dishes were pooled in a 50 mL falcon-tube and SC pre-differentiation medium was added in a volume ratio of 1:1. The cells were pelleted by centrifugation at RT with 400 x g for 10 min and collected in 2 mL fresh SC pre-differentiation medium for each four nerves. Prior to plating, each one 6-well per nerves from one mouse was first coated with 1 mL of 50 µg/mL PLL diluted in water (Sigma, P1274) for 3 h at RT. PLL was then aspirated and replaced by 750 µL of 100 µg/mL Laminin (Sigma, L2020) diluted in DMEM. After 1 h incubation at 37 °C the cell suspension was added.

Schwann cells were cultured in SC pre-differentiation medium with Ara-C until DIV3, when the number of fibroblasts was sufficiently reduced. The cells were then passaged to 24 mm cleaned glass coverslips, sequentially coated with 60 µL of 50 µg/mL PLL and 50 µL of 50 µg/mL Laminin. After removing the cell medium and rinsing with D-PBS -Ca^{2+}/Mg^{2+}, the cells were detached by incubating each well with 200 µL TryPLE for 5 min at 37°C and 5% CO_2. Schwann cells were collected in each 2 mL DMEM with 0.5 % (v/v) horse serum (HS) and 1 % (v/v) P/S, and pelleted by centrifugation at 400 x g at RT. The cell pellet was resuspended in 30 µL DSM per 6-well, counted and the cell concentration was adjusted. On each 24 mm coverslip, cells were seeded at a density of 15 x 10^3 cells in 15 µL. After incubation for 1 h at 37 °C in a 5 % CO_2-incubator, 500 µL equilibrated SC differentiation medium, adapted from (Jessen *et al.*, 1994; Emery and Dugas, 2013), was added to each well. Here, DSM was supplemented with 20 ng/mL Neuregulin1 (NRG1), 1 µM Forskolin, 40 ng/mL T3 and 50 µg/mL ascorbic acid for differentiation and myelination induction (Eldridge *et al.*, 1987; Arthur-Farraj *et al.*, 2011), and 0.4 µM TMX. Half of the medium was exchanged every 2-3 days. Inhibitors were applied from DIV5 on. The cells were fixed at DIV11.

2.2.2.6 Calcium phosphate transfection of primary neuronal cultures

Primary neuronal cell cultures were transfected at DIV7 using the Calcium phosphate transfection kit from Promega. The transfection mechanism is based on the calcium phosphate assay (see 2.2.2.3) (Graham and van der Eb, 1973). According to the manufacturer's instructions, plasmid DNA was first mixed with calcium chloride and then diluted in nuclease-free water (table 2-28). The mixture was applied to an equal volume of 2x phosphate-buffer (HB) under slight vortexing for the generation of calcium-phosphate-DNA-precipitates, and subsequently incubated for 20 min in the dark. Neurobasal medium A (NBA; Invitrogen, 21103) was adjusted to the osmolarity of the culturing medium using D-(+)-Mannitol. Neuronal cultures were then incubated in 1 mL/well equilibrated NBA for 20 min at 37 °C and 5 % CO_2. The transfection solution was applied in a volume of 200 µL/well and the cultures were incubated for 30 min at 37 °C and 5 % CO_2 until the precipitates were visibly settled onto the cells. The coverslips were washed twice with 2 mL osmolarity-adjusted and equilibrated HBSS (-Mg^{2+}/Ca^{2+}) and transferred back to the culture medium.

Table 2-28: Transfection reaction solution for neuronal cultures on 24 mm coverslips.

Component	Amount/well
Plasmid DNA	6 µg
2 M Calcium chloride (Promega)	125 mM
Nuclease-free H_2O (Promega)	*ad* 100 µL
2x Phosphate-buffer HB, pH 7.1 (Promega)	1x

2. 2. 2. 7 Viral transduction of cell cultures

Viral transduction of astrocytic cultures was performed with a multiplicity of infection (MOI) of 20. Cells were transduced in fresh medium in two consecutive rounds, at DIV11-12 and DIV16-17, before harvest at DIV20-22. The day before harvest, cells were supplied with fresh medium. Similarly, MEF cells were transduced in two rounds for each three days. Oligodendrocytic cultures were transduced with a MOI of 50 in fresh medium on DIV3 and DIV6 and fixed on DIV8.

2.2.2.8 BrdU treatment

Bromodeoxyuridine (BrdU) is a nucleoside analogue for thymidine that incorporates into the S-phase of the cell cycle (Miller and Nowakowski, 1988; Cavanagh *et al*., 2011). BrdU (Abcam, ab142567) was dissolved to a 10 mM stock solution in DMSO and diluted to a working solution of 10 µM in cell culture medium prior to application. The cell medium was

replaced by sterile filtered BrdU-containing medium for 36 h. The cultures were then fixed and immunolabelled using a BrdU-targeting antibody (see 2.2.2.9).

2.2.2.9 Inhibitor treatments

All compounds were dissolved in DMSO to indicated concentrations as stock solutions (see table 2-16). The used working concentrations are indicated for each experiment. For acute application, cells were treated for 1 h with indicated concentrations. For chronical treatments, Schwann cells were supplemented with inhibitors from DIV5 to DIV11. Control cells were supplemented with an equal volume of DMSO.

2.2.2.10 Immunocytochemistry (ICC)

Cell cultures, grown on coverslips, were rinsed with 1x PBS and fixed with 4 % (w/v) paraformaldehyde (PFA) with 4 % (w/v) sucrose in millipore-filtered water in defined volumes (table 2-29) for 15 min at RT. After three washes with PBS to remove remaining PFA, the cells were simultaneously permeabilized, to perforate the cell membrane, and blocked, to prevent unspecific antibody binding, for 1 h in PBS with 0.3 % (v/v) Triton X-100 and 10 % (v/v) normal goat serum (NGS) (ICC blocking solution). If secondary antibodies raised in donkey were used additionally, the incubation time with the NGS-containing ICC blocking solution was shortened to 30 min, and another 30 min incubation was performed with 10 % (v/v) normal donkey serum (NDS) in ICC blocking solution. Antibodies were specifically diluted (table 2-13) in PBS with 0.3 % (v/v) Triton X-100 and 5 % (v/v) NGS (ICC antibody solution). The coverslips were placed upside down into a drop of antibody solution on parafilm in a dark humidified chamber. After 1 h incubation at RT with primary antibodies, the coverslips were washed three times in PBS, and incubated in secondary ICC antibody solution. Where indicated, the solution was supplemented with 6 U/mL Alexa-fluorophore-conjugated Phalloidin, a high affinity F-actin probe to label the cell cytoskeleton. Excess of unbound antibodies was removed by rinsing another three times with PBS, before the coverslips were mounted on microscope slides in Immu-Mount (Thermo Fisher, 9990402) supplemented with 1 µg/mL 4',6-Diamidino-2-phenylindol (DAPI). The slides were stored at 4 °C and imaged soon after embedding.

Table 2-29: Immunocytochemistry solution volumes.

Solution	Volume per coverslip [µL]		
	6-well: Ø 24 mm	12-well: Ø 18 mm	24-well: Ø 12 mm
PFA; ICC blocking solution	1,000	750	500
ICC antibody solution	50	25	12.5

In order to label surface-residing proteins only, the detergent Triton-X100 was omitted from the ICC blocking and primary antibody solutions. The cells were then post-fixed for 15 min at RT with 2 % (w/v) paraformaldehyde (PFA) and 2 % (w/v) sucrose, and finally incubated with detergent-containing solutions, according to the standard protocol, for subsequent immunolabeling of corresponding total protein levels using distinct primary and secondary antibodies.

Intracellular membrane lipids were immunolabelled using either a specific primary antibody (PI(4)P) or the recombinantly expressed and purified lipid-binding domain chimera eGFP-2xFYVE (Hrs) (Gillooly *et al*., 2003) which is subsequently targeted using a GFP-recognizing antibody. Therefor a modified ICC protocol was performed according to Hammond and colleagues (2009) to ensure preservation of endomembranes. The cells were fixed with low concentrations of 2 % PFA fixative to prevent osmotic swelling. After three times wash with PBS, a non-phosphate-containing PIPES-based buffer (PIB) was used for all subsequent steps, as free phosphates would otherwise compete with the phosphor-lipids for probe binding. The cells were permeabilized in PIB for 5 min at RT with 20 µM Digitonin, a cholesterol-selective detergent which perforates the cholesterol-rich plasma membrane (Lange, 1991) while internal membranes stay intact. This was followed by three thorough washes with PIB to get rid of remaining Digitonin, which would affect the efficiency of lipid staining during longer exposure. The cells were simultaneously blocked and labelled for 45 min with 0.025 µg/µL eGFP-2xFYVE (Hrs) in PIB supplemented with 5 % (v/v) NGS. In addition, the solution was supplemented with 50 mM ammonium chloride, in order to quench the remaining free aldehyde groups from the PFA fixation with amines and thus, prevent non-specific binding and autofluorescence. After washing in PIB according to the published protocol, primary and secondary antibodies were applied in 5 % (v/v) NGS in PIB for 1 h and 45 min, respectively. The volume of antibody solutions was increased by 20 % compared to the detergent-based solutions (table 2-29) to compensate for the increased surface tension and thus, ensure antibody decoration of the whole coverslip. The coverslips were then post-fixed

for 5 min with 2 % PFA fixative, and washed with PBS, three times with 50 mM ammonium chloride, and once without. Mounting was performed as described above.

Autophagosomes were visualized by immunodetection of the transiently autophagosomal-associated protein LC3 (Kaminskyy *et al*., 2011; Kabeya *et al*., 2000). Here, the fixation duration was prolonged to 30 min. Triton X-100 was omitted from the PBS-based solutions and permeabilization was performed equivalent to the lipid staining protocol by using Digitonin, to preserve the autophagosomal membranes.

For immunolabelling of BrdU, the cells were washed twice with 1x PBS and three times with 1x PBS for 2 min each, before fixation with 4 % PFA-fixative for 15 min at RT. After another three washes with PBS for each 2 min, first 0.1 % (v/v) Triton X-100 in PBS for 20 min, then 2 N HCl for 30 min was added. The coverslips were then washed another three times with PBS. ICC blocking and antibody solutions were applied according to the standard protocol (table 2-29).

2.2.2.11 Confocal microscopy and immunocytochemistry analysis

Immunolabelled or fluorescently tagged proteins in fixed cultures were imaged using a Zeiss laser scanning microscope (LSM710) with a 63x 1.4 NA (numerical aperture) oil objective routinely, or a 40 x 1.3 NA oil objective for neuronal cultures. Excitation was performed with an Argon laser at 488 nm, a DPSS laser at 561 nm and a Helium Neon laser at 633 nm for Alexa-Fluor488/eGFP, Alexa 568/mCherry and Alexa 647, respectively. Corresponding emission was detected between 503-553 nm, 581-626 nm and 649-700 nm, respectively. Images were acquired with the Digital microscope camera AxioCam (Zeiss), controlled by the Imaging-Software ZEN (Zeiss), and analyzed using ImageJ software. Single cell masks were routinely generated using Phalloidin signals and transferred to the channel of interest to measure mean fluorescence intensity per cell in the case of diffuse immunolabeling. For synaptic stainings, a synapsin-based bouton mask was used to measure mean fluorescence intensities in presynapses only. For rare punctate staining in cells, or if background subtraction was required, the sum intensities of ROIs (region of interest = fluorescent signal minus background signals) was measured and divided by the cell area. For LC3, background subtraction of diffuse cytoplasmic staining, representing LC3-I signals, was performed to reveal autophagosomal membrane associated LC3-II -positive puncta only. For eGFP-FYVE(Hrs) signals, a background threshold was determined in samples, acutely treated with the PI(3)P-synthesizing VPS34 inhibitor VPS34-IN1. HeLa cells or astrocytes immunolabeled for lipids were imaged using a z-stack series of usually seven slices with

0.5 µm intervals. Prior to fluorescence intensity analysis, the slices were summed up using the ImageJ ‘z-projection’ tool with ‘max intensity’. P0-protein immunostainings in Schwann cell mono-cultures were imaged with a 10x 0.3 NA air objective. Here, sum intensities per image (10 images per condition and experiment) were normalized by the number of DAPI-positive cell nuclei per image.

For all immunostainings, at least 10 images per condition were acquired, evaluated and averaged for each experiment. Statistical analysis with the mean values of independent experiments.

2.2.2.12 Live-cell imaging and electrical field stimulation of primary neuronal cultures

Live-cell imaging was performed on DIV14 using a pHluorin-based assay (Miesenböck *et al.*, 1998), around 7 days post-transfection with the pHluorin-construct. The construct encoded for a pH-dependent eGFP (pHluorin), with a pK_a of 7.1, excitation at 455-485 nm and emission at 510–555 nm (Sankaranarayanan *et al.*, 2000), coupled to the luminal terminus of the presynaptic vesicle protein Syt1. During electrical field stimulation, neuronal depolarization and thus, Ca^{2+} influx in the presynapse triggers exocytosis of synaptic vesicles (SVs), i.e SV fusion with the plasma membrane. Thereby, pHluorin is exposed to the physiological pH of the extracellular buffer solution and de-quenched. Subsequent endocytic retrieval of SVs, and therefore Syt1-pHluorin from the plasma membrane results in a re-quench due to subsequent reacidification of the vesicular lumen (3 - 4 s; Atluri and Ryan, 2006). Therefore, fluorescence measurements using a GFP-filter setup allow to monitor recycling of synaptic vesicle (proteins) and endocytic retrieval kinetics.

The neuronal cultures on coverslips were stimulated in a stimulation quick change chamber (Warner Instruments, RC-47FSLP) in 500 µL imaging buffer at 37 °C. The imaging buffer provided essential ions like Na^+, K^+ and Mg^{2+} on the one hand, and contained the glutamate receptor antagonists APV (NMDA receptors) and CNQX (AMPA receptors) on the other, to prevent postsynaptic responses and recurrent network excitation. Stimulation was performed with the MultiStim SYSTEM-D330 (Harvard Apparatus) by applying electric field pulses of 5 Hz for 40 s at 100 mA, with a pulse duration of 1 ms. Imaging was performed using a Nikon Eclipse Ti microscope, equipped with an incubator for temperature control (Okolab), a 200 Watt mercury lamp (Lumen 200, Prior), the eGFP filter set (Semrock, F36-526), and operated by ImageJ-based MicroManager 4.11 software. The samples were illuminated with 100 ms exposure time. Recording were done using a 40x oil-immersion objective and the PerfectFocus Autofocus system (Nikon). Images were acquired with a

sCMOS camera (Neo, Andor) controlled by the ImageJ plugin "Time Series Analyzer" at a frame rate of 0.5 Hz for 2 min, starting 10 s prior to stimulation. Evaluation of time-series fluorescence intensities from hand-masked boutons was performed using Image J. The fluorescence intensity course over time of around 50 boutons per image-series were averaged, background subtracted and corrected for bleaching. The bleaching factor was calculated from the mono-exponential decay of the fluorescence intensity trend prior to stimulation. For analysis of the relative fluorescence increase upon stimulation, representing the apparent SV release, the peak of fluorescence upon stimulation (F_{max}) was normalized to the mean initial fluorescence (F_0) prior to stimulation (F_{max}/F_0). In order to determine the endocytic time constant (τ), the initial fluorescence F_0 was subtracted from the fluorescence F at each time-point (t) to obtain the absolute change in fluorescence $\Delta F(t)$ ($F-F_0$). ΔF was then normalized to ΔF_{max} ($\Delta F/\Delta F_{max}$) to obtain relative values for the fluorescence time course scaled between 1 (F_{max}) and 0 (F_0). This allowed for a mono-exponential fit of the decay using GraphPad Prism 5 software to calculate τ:

(IV) $$(\Delta F/\Delta F_{max})(t) = y_0 + A * e^{(\frac{-t}{\tau})}$$

$(\Delta F/\Delta F_{max})(t)$- Normalized fluorescence intensity course over time; y_0- extreme value approached at t_{max}; $A = F(t)_{max}$ (= 1); τ – endocytic time constant (t at F(t) = 1/e)

The mean data from 5 to 7 image-series per experiment were averaged, and statistic was performed on the mean curves from independent experiments.

2.2.2.13 Ultrastructural analysis of HRP-uptake in neuronal cultures by electron microscopy

Horse-radish peroxidase (HRP) is a glycoprotein and was used in this assay as a fluid phase marker, uptaken from the extracellular medium by synapses during endocytosis (Clayton *et al*., 2008). HRP can be detected by oxidation of diamino-benzidine with hydrogen peroxide (Graham and Karnovsky, 1966). Oxidized diamino-benzidine-precipitates are converted to an electron-dense product (osmium-black) in the presence of Tetraosmium (OsO_4) (Johansson and Backman, 1983).

Cultured hippocampal neurons grown on coverslips were preincubated with 10 mg/mL Type VI HRP (Sigma, P8375) in 1x imaging buffer for 5 min and then stimulated with high-potassium imaging buffer including HRP for 90s. Following stimulation, cultures were washed with imaging buffer for 5 minutes and fixed with 2% (w/v) glutaraldehyde in 1x PBS for 40 minutes.

Electron microscopy was performed by Dr. Dmytro Puchkov from the EM facility at Leibniz Research Institute for Molecular Pharmacology (FMP, Berlin). Following fixation and one wash with PBS, neurons were incubated for 20 min in 0.1 M glycine in PBS to quench remainder of glutaraldehyde. HRP was visualized by incubating the fixed cultures for 25 min in 3,3′-diaminobenzidine tetrahydrochloride (DAB; 0.75 mg/mL) in 0.05 M TRIS-HCl, pH 7.6, containing 0.01 % (w/v) hydrogen peroxide. Neurons were washed in PBS, post-fixed with 1% (w/v) OsO_4 for 1 h, washed with distilled water, dehydrated, and embedded into Epoxy resin. Coverslips were cracked away by liquid nitrogen and sections of 60 nm thickness were viewed with a Zeiss EM900 transmission electron microscope. Morphometric analysis of synaptic boutons terminals was performed using ImageJ software. Vesicles were considered as HRP-positive if the intensity of DAB labeling in the vesicle lumen was at least three times higher than background labeling. Excitatory synapses were taken for analysis. 80 synapses per genotype were analyzed. Regular shaped vesicles smaller than 50 nm in diameter and 2,000 nm^2 in cross-section area were counted as synaptic vesicles. All other larger vesicles observed in synaptic terminals were classified as endosomes of different sizes.

2.2.3 Biochemical methods

2.2.3.1 Harvest of mammalian cells

Mammalian cells were harvested with a non-ionic and therefor non-denaturating detergent-based buffer. It lyses the cell membrane and releases the cytoplasmic proteins, which are kept in solution due to the physiological pH and the stabilizing salt and metal ions provided by the buffer. All steps of cell lysis were performed on ice in order to prohibit protease activity and therefor protein degradation within the cell lysates. In addition, mammalian protease inhibitor cocktail (PIC), and the serin- and cysteine protease inhibitor phenylmethylsulfonyl fluoride (PMSF), with a half-life of 30 min in water, were always added freshly to the lysis buffer prior to use. The phosphatase inhibitor cocktails 2 and 3 (Sigma, P5726, P0044) were applied when the phosphorylation status of lysate proteins was meant to be analyzed, to inhibit effects from massive dephosphorylation during lysis. The lysis buffer was applied in defined volumes for the different confluent cell cultures (table 2-30), depending on the cell type, the surface area of the culture dish and the required minimal protein concentration for the corresponding experiment. Cultures were grown on 6 cm dishes or 6-well plates for lysate protein analysis by SDS-PAGE and Western Blot. For affinity purification assays, 10 cm or 15 cm culture dishes were used to achieve high protein

amounts and a protein concentration of around 5 µg/µL with the corresponding lysis buffer volumes (table 2-30).

Mammalian cell cultures were rinsed once with ice-cold autoclaved 1x PBS before 1x cell lysis buffer was applied. The cells were collected in buffer with a cell scraper and the suspension was transferred to an Eppendorf tube. Lysis was performed by incubation for 20 min on ice with gentle inversions every 5 min. Remaining intact cells were pelleted together with the membrane fraction by centrifugation at 17,000 x g for 5 min at 4 °C in a tabletop cooling centrifuge (Eppendorf). For general analysis of protein content by SDS-PAGE and Western Blot, the protein concentration of the supernatant was directly determined by Bradford Assay, adjusted to the desired protein concentration of 1 µg/µL to 2 µg/µL with lysis buffer and prepared for SDS-PAGE.

For affinity purification assays, the lysates were further cleared from potentially interfering smaller membrane pieces. Therefore, ultracentrifugation at 180,000 x g for 15 min at 4 °C in a TLA110 rotor (Sorvall) was performed. The supernatants were then freshly supplied with 1 mM PMSF. After determination and adjustment of the protein concentration, the samples were used as “inputs” in the corresponding assays.

Table 2-30: Volumes of lysis buffer used for different cell cultures.

Cell culture dish	Lysis buffer volume [µL]		
	Astrocytes	**HEK cells**	**eGFP-Rab35^{endo} KI HeLa cells**
6-wells	40	200	
6 cm	80	350	
10 cm		300	
15 cm			300

2.2.3.2 Determination of protein concentration

The protein concentration of cell lysates was determined using the Bradford protein assay. It is based on an equilibrium shift of Coomassie brillant Blue G250 upon protein binding, from a stable double protonated red into a stable unprotonated blue form with an absorbance maximum of 595 nm (Bradford, 1976). In this assay, 1 µL of cell lysate was added to 1 mL of 1x Bradford solution diluted in millipore-filtered water. Each three replicates were analyzed per sample. The mixtures were incubated for 5 min at RT in the dark. The absorbance at 595 nm was measured using a photometer (BioPhotometer Plus, Eppendorf). Samples were blanked with 1 µL lysate buffer in Bradford solution. A BSA (bovine serum albumin) standard curve, i.e. the extinction of samples with known BSA

concentrations from 1 µg to 10 µg, served as a reference. The lysate protein concentration was calculated using the parameters from the linear regression of the standard curve. Alternatively, samples were measured in a 96-well plate in 250 µL 1x Bradford solution using the SPECTROstar^{Nano} microplate reader (BMG LABTECH) and evaluated using MARS Data Analysis Software (BMG LABTECH)

2.2.3.3 SDS-PAGE

The discontinuous Sodium dodecyl sulfate - Polyacrylamide gel electrophoresis (SDS-PAGE) was performed according to Laemmli (1970), in order to analyze the protein levels of cell lysates or other samples by protein fractionating according to their molecular weight. All reagents, including the SDS-running buffer, SDS-sample buffer and the gel components were prepared according to the Laemmli buffer system. The gel electrophoresis chamber Mini Protean Tetra Cell System (Bio-Rad), and corresponding plates, combs and pouring stations were used for gel preparation (table 2-31) with 1 mm thickness, and a polyacrylamide concentration according to the molecular weight of the proteins of interest. To ensure a straight passage between stacking and separating gel, a layer of 2-Propanol was added on top of the separating gel during polymerization incubation, and washed off twice with water before the stacking gel was poured.

Table 2-31: SDS-PAGE gel preparation.

Components	**Separating gels**			**Stacking gel**
	8 %	**10 %**	**12 %**	
1x buffer	Separating gel buffer; pH 8.8			Stacking gel buffer; pH 6.8
Acrylamide/Methylen bisacrylamide - 37.5:1 (v/v)	8 %	10 %	12 %	3 %
TEMED (v/v)	0,1 %			
APS (w/v)	0,1 %			

The samples with desired protein amounts (20 µg to 40 µg) were mixed with 6x SDS-sample buffer and boiled for 5 min at 95 °C in a heating block. This step results in protein denaturation, mediated by the disulfide bond-reducing reagent 2-Mercaptoethanol and the anionic detergent SDS. The latter binds to proteins in a ratio of around 1.4 g per 1 g protein, and thereby leads to an equal negative charge of all proteins. Thus, the protein mobility through the gel from cathode to anode is dependent on their molecular weight only. After centrifugation at 17,000 x g, samples were loaded into the equilibrated gel pockets in volumes of 20 to 40 µL. Gels were run in electrophoresis chambers filled with 1x SDS-running buffer.

As a reference, 0.5 µg of a protein marker was used. To achieve approximately equal sample volumes per gel, 1x sample-buffer was added to empty pockets as well as to pockets containing the low volume of protein marker. Electrophoresis was started with 90 V corresponding to a current of around 10 mA/gel, until the migration front accumulated at the edge between stacking and separating gel. With the passage of the samples to the separating gel, the voltage was increased to 130 V. The electrophoresis was stopped as soon as the bromophenol blue frontline of the sample buffer reached the bottom of the gel. For detection of proteins the gels were stained with Coomassie or further processed by immunoblotting.

2.2.3.4 Coomassie staining of SDS-gels

SDS-polyacrylamide gels were incubated in Coomassie staining solution for 2 h at RT, to visualize the fractionated proteins by its electrostatic interaction with Coomassie blue G-250 dye. Background staining of the gel was removed by two consecutive incubation rounds in Coomassie destain solution, first overnight and then for 2 h at RT.

2.2.3.5 Immunoblotting

For the selective detection of proteins, immunoblots (Western Blots) were performed. First, the separated and negatively charged proteins were transferred from SDS-polyacrylamide gels to nitrocellulose membranes (Amersham Protran 0.2 NC; GE Healthcare) by application of an electric current, using the tank electroblotting Mini Trans-Blot system (Bio-Rad). The SDS-polyacrylamide gel, the membrane and four sheets of Whatman paper (Grade GB003; Sigma, WHA10427826), all equally sized, were equilibrated in 1x Transfer buffer containing 10 % Methanol. They were subsequently arranged in a stack between two sponges, starting with two Whatman papers followed by the membrane, the gel and two Whatman papers on top. After removing air bubbles between the layers, the stack was placed into the blotting chamber with the gel at the side of the cathode and the membrane towards the anode. Transfer was performed at 4 °C for 2 h by applying a constant voltage of 110 V for 90 min. In order to verify transfer performance and equal protein loading among the samples, the membrane was reversibly stained with the protein binding Ponceau S-staining solution for 20 min and subsequent removal of background staining by three washes with Ponceau destaining solution. The membrane was imaged and, if necessary, cut at distinct molecular weights for the parallel detection of differently sized proteins. Ponceau S staining, which would interfere with antibody detection, was removed by several washes with PBS. All subsequent incubations were performed on a lab shaker.

For qualitative protein analysis or the detection of weak antibody signals, chemiluminescence detection was used. The membrane was blocked with 5 % (w/v) milk in PBS for 1 h, to prevent unspecific antibody-binding. Primary antibody solution was applied for 2 h at RT or overnight at 4 °C. After four times wash for 5 min with PBS-T, horseradish peroxidase (HRP)-conjugated secondary antibodies were applied in blocking buffer for 1 h. The membrane was rinsed two times for 5 min with PBS-T and another two times with PBS. An enhanced chemiluminescent substrate (Amersham ECL; GE Healthcare, RPN223) for detection of the secondary antibody-coupled HRP was used. This solution contains luminol and becomes oxidized and therefore chemiluminescent by HRP-mediated catalysis. The chemiluminescence reaction was detected with the Bio-Rad ChemiDoc™-System and recorded with Image Lab software (Bio-Rad).

For the quantitative analysis of protein levels, IRDye-conjugated secondary antibodies were used. To not interfere with the fluorescence detection, the commercial Odyssey blocking buffer from LI-COR was used instead of milk, undiluted for blocking or 1:1 diluted in PBS-T as a secondary antibody solution. Fluorescent signals were detected with the LI-COR Odyssey® Fc Imaging system and recorded and evaluated with Image Studio Lite software (LI-COR).

2.2.3.6 Affinity purification using nucleotide-loaded GST-recombinant Rab proteins

2.2.3.6.1 Recombinant protein expression in bacteria

For the expression of recombinant GST-fusion proteins, based on the T7-expressionsystem (Studier und Moffatt, 1986) in *E. coli* BL21(DE3), 50 mL LB-medium with 100 µg/mL ampicillin was inoculated with glycerol stocks of the corresponding pGEX4-T constructs and cultivated overnight as described above. The next morning, 500 mL 2x yeast extract tryptone (2x YT) medium with 100 µg/mL ampicillin were inoculated with 10 % of the pre-culture. The bacteria suspension was grown at 37 °C in a bacteria flask shaker for around 1 h to 1.5 h until a density of OD_{600} of 0.5 to 0.7 was reached. Recombinant protein expression was then induced by applying 500 µM Isopropyl-β-D-thiogalactopyranosid (IPTG) for 3 h at 30 °C.

For the less soluble GST-Rab fusion proteins, *E. coli* Rosetta (DE3) strains with additional eukaryotic tRNA-codons rarely used in *E. coli* (Tegel *et al*., 2010) were used. This strain expresses an additional antibiotic resistance gene and was therefore cultivated in the presence of 68 µg/mL chloramphenicol in addition to ampicillin. For protein expression, 100 µM IPTG in combination with a low temperature incubation of 20 °C were used. These

slow-expressing conditions were chosen to avoid the accumulation of instable or denaturated protein within inclusion bodies. To still achieve a sufficient amount of stable proteins in the bacterial cytoplasm, the incubation duration was prolonged to 20 h.

The bacteria were then pelleted via centrifugation at 4,000 x g for 15 min at 4 °C and resuspended in volume of 5 mL to 20 mL ice-cold PBS, depending on the expected yield. Dissolved pellets were stored at -20 °C as 5 mL aliquots for one-shot thawing prior to use.

2.2.3.6.2 Nucleotide-free affinity purification of recombinant GST-fusion Rab proteins from bacterial lysates

For nucleotide-mediated affinity purification assays, GST-coupled Rab proteins were extracted nucleotide-free from bacterial lysates by the presence of EDTA during cell lysis. This chelator complexes Mg^{2+}, the essential co-factor of nucleotide-binding to GTPases, and thus, increases the off rate of already bound nucleotides on the one hand, while inhibiting *de novo* binding of GTP on the other (Burstein and Macara, 1992). Nucleotide-free Rab proteins were purified using a glutathione-sepharose assay, in which the tripeptide Glutathione (Glutamine-Cysteine-Glycine) is immobilized by its sulfhydryl group to cross-linked beaded agarose. This sepharose serves as a specific substrate for the glutathione S-transferase (GST). Thus GST-fusion proteins are specifically captured by this enzyme-substrate binding reaction.

For the purification of around 1 mg recombinant protein, one aliquot of bacterial pellet was thawed on ice and filled up to a volume of 25 mL with PBS, freshly supplemented with 2 mM EDTA, 50 U Cyanase^{TM} Nuklease (Serva, 18542), 0.5 mg/mL Lysozyme (Roth, 8259), 1 mM PMSF and one tablet per 50 mL of EDTA-free Protease Inhibitor Cocktail (Sigma, 11873580001). In order to increase the stability of the recombinant Rab-proteins, 150 mM NaCl was added. The samples were incubated for 15 min at 4 °C on a tube rotator (VWR), followed by sonification in order to break the cell wall. Sonification was performed in two cycles of each 2 min with 30 % power every 2nd minute (Branson digital sonifier 450). For perforation of the cell membrane, 1 % (v/v) TritonX-100 was added and the lysates were incubated for another 15 min rotating at 4 °C. The lysates were cleared from cell debris by centrifugation in a SS-34 rotor (Sorvall) at 35,000 x g and 4 °C for 15 min. Glutathione-sepharose beads were equilibrated by adding 10 mL ice-cold PBS to 300 µL of a 50 % (w/v) GST-bind resin slurry (Millipore, 70541). The beads were pelleted at 3,000 x g for 3 min at 4 °C, PBS was aspirated, and the lysate supernatant was applied. GST-fusion proteins were coupled to the beads by an incubation for 2 hr at 4 °C on a tube rotator. The beads were washed three times with ice-cold PBS as described above, and stored under phosphate-free

conditions in 500 µL of 20 mM HEPES pH 7.5 with 5 mM EDTA at 4°C until usage for 15 h maximum.

The protein concentration of the bead-suspension was estimated from a 1:10 dilution using the Bradford assay. As this method is often inaccurate for proteins immobilized on agarose beads, the samples were additionally analyzed by SDS-PAGE and subsequent Coomassie-staining. Therefor volumes with estimated protein concentrations of 2, 4 and 8 µg were loaded. The integrated density of each GST-fusion protein was determined by Coomassie-staining using the Image Lab software (Bio-Rad). The calculated protein concentration was then adjusted according to the GST-control in order to use equal amounts of recombinant proteins in the subsequent affinity purification assay.

2.2.3.6.3 Affinity purification using nucleotide-loaded GST-fusion proteins

For GST-mediated pulldown assays, each 100 µg of bead-coupled GST-fusion proteins was first washed three times in ice-cold 500 µL lysis buffer, supplemented with 5 mM EDTA and without $MgCl_2$. Therefor the beads were pelleted at 3,000 x g for 2 min at 4 °C, the washing solution was aspirated, and fresh buffer was applied. Immobilized GST-Rab proteins were then loaded with either 1 mM GTPyS (Sigma, G8634), a non-hydrolyzable GTP-analogue, or GDP (Sigma, G7127) in 50 µL lysis buffer (without $MgCl_2$) for 15 min at 30 °C with slight agitation on a Thermomixer 5437 (Eppendorf). GST-control beads were instead incubated with 5 mM EDTA as a control. Afterwards, $MgCl_2$ was added to a final concentration of 10 mM, in order to activate and strengthen the nucleotide binding. After incubation of 10 min at 4 °C lysate inputs were applied.

HEK cells were harvested as described (2.2.3.1), 24 h post-transfection with calcium phosphate. Cleared and concentration-adjusted lysate inputs, supplemented with fresh PMSF, were distributed each on GTP-loaded-Rab, GDP-loaded-Rab- and pure GST-coupled beads. GTPyS or GDP were added to a final concentration of 1 mM. GST-control beads were supplied with 5 mM EDTA. Around 5 % of the total protein amount of each sample served as the input reference and was kept separately on ice during the assay. For affinity purification, the lysate inputs were incubated with immobilized GST-fusion proteins for 90 min on a tube rotator at 4 °C. The beads were pelleted and, after discarding the supernatant, washed three times by rotation for 10 min. Therefor lysis buffer with reduced concentrations of 50 mM KCl and 0.5 (v/v) % TritonX-100 was used, in order to remove unspecifically bound proteins. A final wash was performed without detergent. In order to avoid the disengagement of bound nucleotides, the washing buffers were additionally supplemented with either 0.1 mM GTPyS

or GDP to achieve an excess of free nucleotides in the solutions. After complete removal of buffer using a Hamilton pipette, the proteins were eluted in 30 µL of 1x SDS-sample buffer at 95 °C for 5 min. The beads were then pelleted by centrifugation at 17,000 x g, and the protein-containing supernatant was analyzed by SDS-PAGE and immunoblotting.

2.2.3.7 Affinity purification using magnetic agarose beads

For (co-)immunoprecipitation of eGFP-fusion proteins, GFP-Trap®_MA beads (Chromotek, gtma) were used. These types of magnetic agarose beads are coupled to a single variable domain (V_HH), which binds GFP with a high affinity. The domains are known as nanobodies and derived from Alpaca single heavy chain antibodies. A magnetic rack is used for sedimentation of the beads.

Lysates were prepared from eGFP-Rab35^{endo} KI HeLa cell as described (2.2.3.1), 24 h post-transfection with calcium phosphate, and applied to 20 µL of lysis buffer-equilibrated GFP-Trap® MA beads. The protein concentration of the lysate input has been again adjusted to around 5 µg/µL and a small sample volume was kept separately as the input reference. The lysates were incubated with the beads for 90 min rotating at 4 °C before the supernatant was discarded. Beads were then washed three times with lysis buffer with 50 mM KCl and 0.5 % TritonX-100, and once without detergent. Proteins were eluted from the beads in 30 µL 1x SDS-sample buffer at 95 °C for 5 min. The beads were finally sedimented by centrifugation at 17,000 x g for 5 min and the supernatant was analyzed by SDS-PAGE and immunoblotting.

2.2.3.8 Proximity-dependent biotin identification (BioID)

2.2.3.8.1 BioID in HEK cells

In order to identify potential interaction partners of a protein of interest (POI), proximity-dependent biotin identification (BioID) was performed according to Roux *et. al.* (2012). This assay is based on the prokaryotic biotin protein ligase BirA from *E. coli*, which biotinylates specific substrate peptides. The enzyme first combines biotin and ATP to form biotinoyl-5'-AMP (bioAMP), which is then added to a specific lysine residue within the biotin acceptor tag, a minimal recognition sequence of the substrate. For the BioID assay, a promiscuous form of BirA, BirA*, with a low affinity to bioAMP is used. It releases the generated bioAMP into the cell environment. Free bioAMP will readily react with primary amines and thereby unspecifically biotinylates proteins within the proximity of BirA*. In this assay, a POI is fused C-terminally to BirA* and introduced into mammalian cells, which are supplemented with biotin-containing culturing medium. Subsequently, proteins within the

proximity of the expressed BirA*-POI chimera get biotinylated. These proteins can be captured from lysates using immobilized streptavidin, a biotin binding protein with a high affinity (K_d= 10 – 15 mM). As a control for POI-independent biotinylation, lysates from cells that express the construct encoding for BirA* only are used. Overexpression of BirA* on its own results in a random biotinylation, especially of proteins involved in the process of translation or other biosynthetic pathways, which can be thus excluded as POI-relevant.

In brief, 6 cm dishes of HEK cells were transfected using JetPrime with a construct containing either mycBirA*-POI (Rab35) or myc-BirA* alone. The medium was exchanged after 4 h for fresh mCCM, supplemented with 50 µM biotin (Sigma, B4639). 24 h post-transfection, lysate inputs were prepared as described. Streptavidin-coupled agarose beads (Millipore, 69203) were equilibrated by washing 200 µL bead-slurry (50 % (w/v)) with 500 µL lysis buffer for three times. Cell lysate, adjusted to a protein concentration of 3 to 4 µg protein/µL, was applied in a volume of 250 µL and affinity binding was performed at 4 °C overnight on a rotating shaker.

The next morning, the beads were collected and extensively washed in six consecutive rounds for each 8 min rotating at RT. Four different denaturating washing buffers were used to remove unspecifically bound proteins thoroughly, without impairing the high affinity streptavidin-biotin interaction. A SDS-containing buffer (BioID- wash buffer 1) was applied first for two times, followed by a high-salt buffer (BioID- wash buffer 2) and a lithium chloride buffer (BioID- wash buffer 3), supplemented with the detergents TritonX-100 and NP-40, respectively. The physiological BioID- wash buffer 4 was applied twice in order to remove detergents and lithium chloride remnants, before the specifically bound protein fraction was eluted by incubation in 60 µL 1x SDS-sample buffer at 95 °C for 5 min. The sample buffer has been supplemented with an excess of biotin (30 mM), to facilitate the release of biotinylated proteins by the free biotin competing for the streptavidin binding sites.

After pelleting the beads at 17,000 x g for 5 min, the supernatant was collected and 50 % of the volume was loaded on a 4-15 % gradient Mini-PROTEAN® TGX™ Precast Protein Gel (Bio-Rad, #4561086) for SDS-PAGE. The gels were then either processed for immunoblot detection of proteins, or for Coomassie staining and further protein analysis by mass spectrometry.

2.2.3.8.2 Label-free quantification of BioID samples by mass spectrometry (LC-MS/MS)

Mass spectrometry was performed by Heike Stephanowitz from the Eberhard Krause laboratory, the mass spectrometry facility at Leibniz Research Institute for Molecular

Pharmacology (FMP, Berlin). For liquid chromatography (LC)–mass spectrometry (MS)/MS analysis, Coomassie-stained lanes of label free BioID samples (BirA*Rab35 vs. BirA*) were cut into each 15 gel pieces per sample and digested in-gel by trypsinization, essentially as described (Lange *et al*., 2010). Peptides were analyzed by a reversed-phase capillary liquid chromatography system (Ultimate 3000 nanoLC system, Thermo Fisher) connected to an Orbitrap Elite mass spectrometer (Thermo Fisher). Identification and quantification of proteins were performed using MaxQuant (version 1.5.2.8) software, searched against the HUMANswiss database (april, 2014) and summarized with the software Scaffold (Proteome Software). The mass tolerance of precursor and sequence ions was set to 10 ppm and 0.35 Da, respectively. Methionine oxidation and the acrylamide modification of cysteines were used as variable modifications. Proteins with at least two detected peptide sequences (razor unique peptides) with a minimum length of 7 amino acids were counted as biotinylated and specifically bound. False discovery rates were estimated to be less than 1%, based on matches to reversed sequences in the concatenated target-decoy database. Enrichment of proteins in the Rab35-BioID sample was calculated as follows: The label free quantification (LFQ)-intensity for each protein (defined by the number and abundance of detected peptides) was compared between the Rab35-BioID- and the control BioID-sample (BirA*). Proteins were considered as enriched, if the LFQ-intensity ratio of Rab35-BioID/BioID was greater than 5, or if exclusively detected in the Rab35-BioID sample.

2.2.4 Schwann cell-specific Rab35 ablation

All work was performed by Prof. Dr. A. Bolino and her team (F. Grandi, M. Mignanelli and R. Di Guardio) from the INSPE in Milan, Italy.

2.2.4.1 *In vivo* analysis of Schwann cell-specific *Rab35* knockout (cKO^{SC}) mice

Rab35 cKO^{SC} with conditional ablation of Rab35 in Schwann cells (*Rab35*$^{Fl/Fl}$ x P0-Cre) were always compared with phenotypically normal control mice (*Rab35*$^{Fl/Fl}$ or *Rab35*$^{Fl/+}$). Semithin section and ultrastructural analyses of sciatic nerves were performed as described previously (Wrabetz *et al*., 2000). Morphometric analysis was performed on digitalized images of cross sections obtained from sciatic nerves with a 100x objective and a Leica DFC300F digital camera (Milan, Italy). At least five images per animal were analyzed using the Leica QWin software (Leica Microsystem) to calculate the g-ratio (axon diameter over fiber (myelin + axon) diameter), while aberrant-myelinated fibers (tomacula,

outfoldings, degenerations) were excluded. To estimate the percentage of myelinated fibers that carried alterations, the entire nerve section was reconstructed, and the total number of myelinated fibers was assessed. For morphometric analysis on ultrastructural sections, 20-40 images per animal were taken using TALOS L120C transmission electron microscope (Thermo Fisher) at 120 kV and a 3,400x objective (for P20).

Sciatic nerve lysates were prepared for immunoblot analysis using a lysis buffer containing 2% (w/v) SDS, 50 mM TRIS buffer pH 8.0, 150 mM NaCl, 10 mM NaF, 1 mM $NaVO_3$, complete protease and phosphatase inhibitors (Roche). Protein quantification was performed using a BCA assay (Pierce, Thermo Fisher). Rapamycin (LC Laboratories) was dissolved in Ethanol and administered once daily by intraperitoneal injection 5 days a week at a final concentration of 10 mg/kg in a vehicle solution containing 5% (w/v) Polyethylene glycol 400 (PEG 400), 5% (v/v) TWEEN-80 and 0.9% (w/v) NaCl as reported (Goebbels *et al*., 2012).

2.2.4.2 *Ex vivo* analysis of Schwann cell-specific *Rab35* knockout (cKO^{SC}) mice

Myelin-forming Schwann cell (SC)/DRG neuron co-culture explants were established from E13.5 mouse embryos (Taveggia and Bolino, 2018). Organotypic explants were kept in Neurobasal (NB) medium supplemented with 50 ng/mL NGF-2.5S and B27 for 8-9 days prior to induce myelination in C-media supplemented with 50 µg/mL ascorbic acid for additional 15 days (Sigma). For immunohistochemistry, co-culture explants were fixed for 15 min in 4 % (w/v) paraformaldehyde, permeabilized for 5 min in ice-cold methanol at -20°C, and then blocked for 20 min with 10 % (v/v) NGS and 1% (w/v) BSA. Anti-MBP primary antibody was applied for 1 hour at room temperature in 1x PBS and Anti-NF-M antibody overnight in 5 % (w/v) BSA, 1 % (v/v) NGS and 0.6% (v/v) TritonX-100 in 1x PBS at 4 °C. Coverslips were washed and incubated for 30 min with secondary antibodies prior to another wash and mounting. A fluorescence microscope was used to quantify the number of MBP-positive myelinated segments in at least 5-10 random fields per coverslip. The mean of each coverslip was used as "n" for statistical analysis. To quantify the myelinated fibers that carried abnormalities, at least 300 MBP-positive myelinated fibers were evaluated, from "n" different SC/DRG explant coverslips using a TCS SP5 laser-scanning confocal microscope (Leica).

2.2.5 Statistical analysis

All data are represented as mean ± standard deviation (SD) for n = 2 independent experiments or mean ± standard error of the mean (SEM) for n > 2 independent experiments and are normalized where indicated. In *in vivo* experiments the number of animals is given. GraphPad Prism 5 and ‘R‘ software were used to perform statistical analysis. If not otherwise indicated, normalized data were analyzed using a one-sample two-tailed student’s t-tests, with prior testing of a Gaussian distribution using the Kolmogorov-Smirnov (KS) test (Smirnov, 1944). For data sets from more than two different genotypes, depicted p-values were corrected for multiple testing using Holm’s multiple comparison test (Holm, 1979). Level of significances are depicted in each graph: *$p < 0.05$, **$p < 0.01$, ***$p < 0.001$, ****$p<0.0001$. Exact p-values are provided in the respective figure legends for $p > 0.05$.

3. Results

Myelination, the glial membrane ensheathment of axons, not only facilitates axonal conductance by electrical insulation but is also important for maintaining axonal integrity and providing trophic support for neurons (Fünfschilling *et al*., 2012; Nave and Werner, 2014). In consequence, pathological conditions in which myelin homeostasis is impaired often lead to severe axonal degeneration (Bjartmar *et al*., 1999; Reilly *et al*., 2011). Myelin homeostasis is tightly regulated by a cohort of extrinsic and intrinsic factors and proteins. So far, at least 80 different mutated genes have been identified to cause the heterogeneous, most commonly inherited peripheral neuropathy group of CMT diseases (Rossor *et al*., 2013; Saporta *et al*., 2014; Pareyson *et al*., 2017). Among these, proteins that have been primarily associated with demyelination are essential myelin components, but also regulators of endomembrane trafficking or cell signaling pathways, such as phosphatidylinositides (PI) –catalyzing or -binding proteins (Suter, 2007; Rossor *et al*., 2013). Interestingly, the Ras-related GTPase Rab35 has been recently linked to myelin formation by oligodendrocytes. Rab35 is reported to negatively regulate oligodendrocyte differentiation and myelination via an ACAP2-ARF6 dependent, but otherwise still elusive mechanism (Miyamoto *et al*., 2014). On the other hand, Rab35 and its GAPs TBC1D10A-C were observed to mediate secretion of myelin proteins from late endosomal MVBs (Hsu *et al*., 2010). However, effector proteins downstream of Rab35 and the consequence of Rab35 depletion on myelin formation were not further investigated in that context. In this study, we aimed to unravel the function of Rab35 in myelin regulation, using a novel mouse model that allows for acute depletion of protein levels.

3.1 Rab35 represses myelin formation and interacts with CMT-associated MTMR-complexes

3.1.1 Generation of tamoxifen-inducible conditional *Rab35* knockout mice

In order to elucidate the role of Rab35 in myelin regulation, we aimed to acutely deplete its protein levels using a knockout (KO) approach. We took advantage from a “floxed” Rab35 (*Rab35*$^{Fl/Fl}$) mouse, generated and kindly provided by Prof. Dr. Arnaud Echard (Institut Pasteur, Paris, France), Dr. Genaro Patiño López (formerly: NIH, Bethesda, USA) and Prof. Dr. Stephen Shaw (formerly: NIH, Bethesda, USA). In these mice, *Rab35* exons number 2 and 3 are flanked by loxP insertions, specific recognition and targeting sites of Cre-recombinases. Cre-mediated recombination in these mouse cells results in the deletion of the 2nd and 3rd *Rab35* exon from the genome, and finally in an early termination of *Rab35* gene transcription. Ubiquitous knockout of Rab35 *in vivo*, by breeding *Rab35*$^{Fl/Fl}$ mice with a Cre recombinase under the

control of a ß-actin promoter, results in early embryonic lethality of mice (unpublished, with courtesy of Dr. Genaro Patiño López). Therefore, we generated tamoxifen-inducible conditional Rab35 knockout (icKO) mice by crossing *Rab35*$^{Fl/Fl}$ mice with the transgenic *Cre-ER*^{TM} -mouse line (Danielian *et al*.1998; Hayashi and McMahon, 2002). These mice encode for a chimera of the Cre recombinase and a mutant, tamoxifen-responsive form of the estrogen receptor ligand-binding domain (LBD-ER^{TM}), ubiquitously expressed under the control of a CAG-promoter (Fig. 3-1a). Upon tamoxifen binding, the cytoplasmically sequestered Cre-LBD-ER^{TM} (Cre^{ER}) is released from the chaperone protein Hsp90, translocates to the nucleus and introduces the gene knockout (Fig. 3-1b). Primary cell cultures were prepared from *Rab35*$^{Fl/Fl}$ or *Rab35*$^{Fl/Fl}$ x CAG-*Cre*^{ER} littermates, cultured in the presence of tamoxifen and referred to as wild type (WT) or icKO cultures, respectively. Sufficient Rab35 depletion, for instance in primary astrocytic cultures, was achieved by constant tamoxifen application (0.4 µM) starting at DIV1 (Fig. 3-1d).

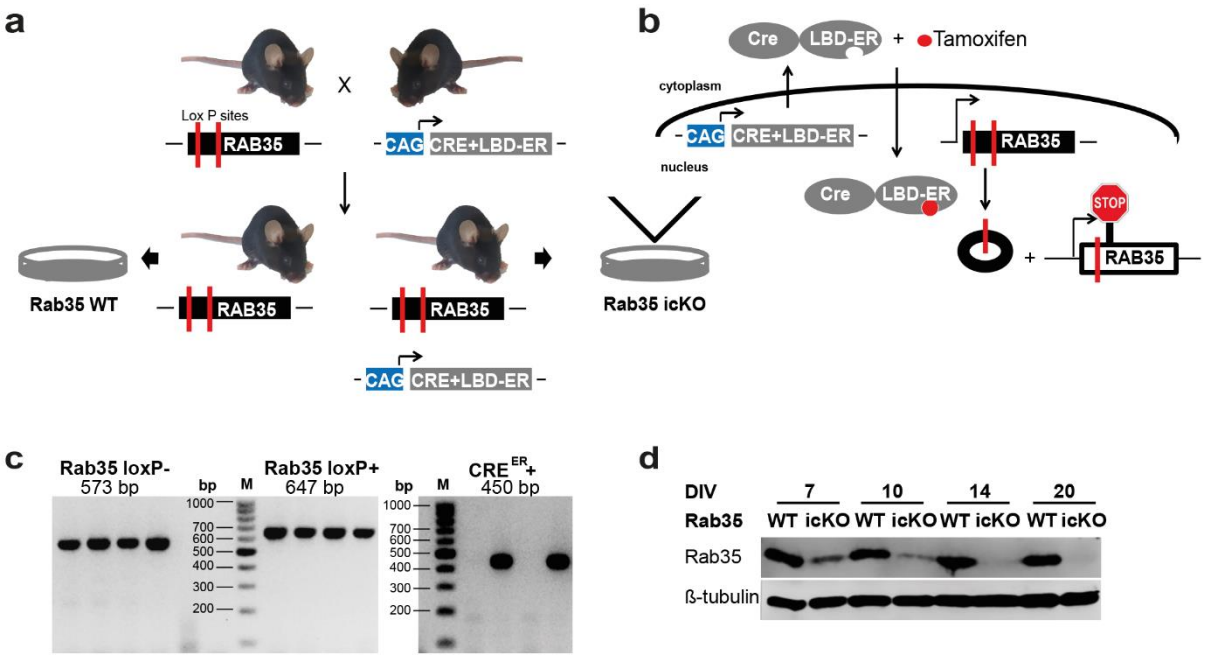

Figure 3-1: Generation of conditional *Rab35* knockout mice for tamoxifen-inducible Rab35 depletion *in vitro*. (a) Tamoxifen-inducible conditional Rab35 knockout (icKO) mice were generated by crossing *Rab35*$^{Fl/Fl}$ mice with CAG-*Cre*^{ER} mice, which express Cre-ER^{TM} (Cre^{ER}) recombinase under CAG promoter control. Littermates from backcrossed F_2-generation were used to prepare primary cultures of Rab35 wildtype (WT) and inducible conditional knockout (icKO) cells from *Rab35*$^{Fl/Fl}$ and *Rab35*$^{Fl/Fl}$ x CAG-*Cre*^{ER} mice, respectively. Both cultures were supplemented with tamoxifen. CRE+LBD-ER – Chimera of *CRE* and the ligand-binding domain of estrogen receptor. **(b)** Tamoxifen application induces Rab35 depletion in *Rab35* icKO cultures only. Cytoplasmically sequestered Cre^{ER} can translocate to the nucleus upon tamoxifen binding to its LBD-ER. Cre-mediated recombination results in an early transcriptional termination of Rab35. **(c)** PCR-amplification products from mouse biopsy DNA to reveal the genotypes for further breeding and primary cell culture preparation. From the left: Amplified DNA-fragment from *Rab35* without (-) or with (+) inserted loxP-sites, and from *Cre*^{ER}-locus in *Cre*-positive animals. **(d)** Primary cultures of astrocytes were

supplemented with tamoxifen from DIV1 on, and lysed at DIV7, 10, 14 and 20. Acute depletion of Rab35 at DIV14 and DIV20 was confirmed by immunoblotting. ß-tubulin served as a loading control.

3.1.2 Rab35 depletion does not impair synaptic vesicle recycling in neuronal cultures

Rab35 is reported to direct SVs to an endosomal recycling route upon endocytosis in NMJs of *D. melanogaster*, which promotes the formation of endosomal-like compartments in presynapses and eventually increases neurotransmitter release (Uytterhoeven *et al*., 2011). We investigated the synaptic vesicle recycling in primary cultures of hippocampal neurons from *Rab35* icKO mice in order to unveil a function of the small GTPase in presynapses of mammalian cells. We analyzed the presynaptic steady-state surface and total levels of two SV proteins, synaptotagmin1 (Syt1) and synaptophysin (Syph), by immunocytochemistry (Fig. S1a-e), and the endocytic retrieval of Syt1-pHluorin upon neuronal activity (Fig. S1f-h). However, we did not detect any alterations in neuronal cultures depleted of Rab35. In addition, we analyzed the abundance of endocytic compartments in presynapses after neuronal stimulation by ultrastructural analysis, performed by Dr. Dmytro Puchkov (FMP Berlin), for a potential increase in the formation of endosomes (Fig. S1i,j). However, neither the number of SVs nor of endosomal-like vesicles (ELVs) was different in the absence of Rab35. These data indicate, that Rab35 is not essential for proper SV recycling in mammalian neuronal cultures.

3.1.3 Characterization of *Rab35* icKO oligodendrocytic cultures

Rab35 has been reported to promote the secretion of myelin proteins on the one hand but to repress OL differentiation and myelination on the other (Miyamoto *et al*., 2014). We made use of primary *Rab35* icKO oligodendrocytic mono-cultures in order to investigate *in vitro* myelination upon acute Rab35 depletion by gene knockout. Mono-cultures of oligodendrocytes are described to form *in vitro* ‘myelin sheets’ that resemble *in vivo* sheaths in their molecular composition, even in the absence of neuronal co-culturing (Aggarwal *et al*., 2011).

Cultures of myelinating oligodendrocytes were obtained by the differentiation of oligodendrocytic precursor cells (OPCs), isolated from *Rab35* icKO and WT mice by immunopanning. OPC cultures were supplemented with tamoxifen for knockout induction and first kept under proliferating conditions by the presence of mitogens. Rab35-depleted NG2-positive OPCs displayed an increased cell size (Fig. 3-2d,e). In addition, a strongly reduced cell number was observed in *Rab35* icKO cultures. In order to dissect if the latter was resulting from either reduced proliferation or increased cell death, we supplemented the cultures for 36 h with BrdU. As an analogue of the nucleoside thymidine, BrdU is incorporated into

replicating DNA and can be visualized by immunolabelling. In *Rab35* icKO cultures only 38 % of cells were positively stained for BrdU whereas a cell fraction of 85 % was actively proliferating in WT cultures in the considered time window (Fig. 3-2a,b). Moreover, 65 % of cells depleted of Rab35 showed positive signals for cleavage-activated Caspase-3, a major apoptotic effector protease that serves as an indicator for apoptotic cell death activation (Kaiser *et al*., 2008). In *Rab35* WT cultures 15 % of the cells were apoptotic only (Fig. 3-2a,c). All cells in these cultures were either labeled for BrdU or Caspase-3, or both. Considering the overlapping fraction of BrdU- and Caspase-3- positive cells with none or only 3 % in *Rab35* WT and icKO cultures, respectively, could suggest that impaired proliferation in Rab35-depleted OPCs might underlie the increased apoptotic induction. On the other hand, a direct involvement of Rab35 in the suppression of apoptosis or apoptotic degradation was recently reported (Wheeler *et al*., 2015; Haley *et al*., 2018).

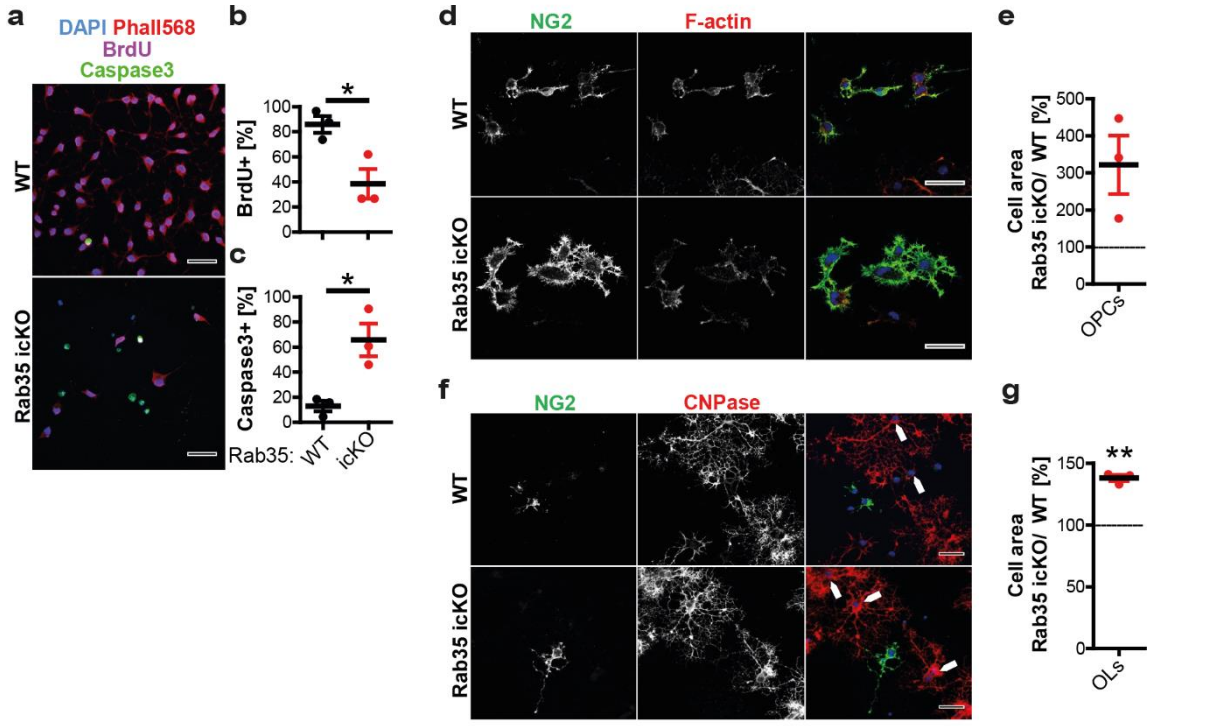

Figure 3-2: Primary *Rab35* icKO OPCs display less proliferation, more apoptotic induction and an increased cell area. (a-c) Immunostainings of oligodendrocytic precursor cells (OPCs) from *Rab35* icKO and WT mice, cultured in the presence of tamoxifen and mitogens. Proliferating OPCs, supplemented with BrdU for 36 h, and subsequently immunostained for BrdU (magenta) and cleavage-activated Caspase-3 (green). *Rab35* icKO OPC cultures display less proliferation and more apoptotic induction than *Rab35* WT cells; (n = 3 independent experiments). (a) Representative confocal images. Phalloidin (red) and DAPI (blue) labelled the total cell fraction; Scale bars, 30 µm. (b,c) Calculated cell fractions positively labelled for (b) BrdU or (c) Caspase-3; (mean ± SEM; two-tailed paired student's t-test; *p < 0.05). **(d-g)** *Rab35* icKO cells have an increased cell area. (d) Proliferating OPCs, immunolabelled for the OPC marker NG2 (green) and Phalloidin-AlexaFluor568 (red). Scale bars, 30 µm (e) The NG2-masked cell area is threefold increased in *Rab35* icKO OPCs compared to WT cells (100 %); (n = 3 independent experiments; p = 0.1). (f) Primary oligodendrocytes (OLs), differentiated in culture, and immunolabelled for OPC marker NG2 (green) and oligodendrocytic marker CNPase (red); Scale bars: 30 µm. (g) The CNP-masked somata of *Rab35* icKO OLs

are larger than of WT cells (100 %); (mean ± SEM; n = 3 independent experiments; one sample two-tailed student's t-test with a theoretical mean of 100; **p < 0.01).

Since we aimed to investigate cultures with a sufficient number of myelinating oligodendrocytes, we induced differentiation of primary OPCs already at DIV1 in parallel to knockout induction, to circumvent proliferating and hence, survival defects upon Rab35 depletion. At DIV8, differentiated oligodendrocytes (OLs) could be identified in both cultures by loss of NG2- and gain of CNPase expression. Similar to OPCs, *Rab35* icKO OLs were marked by an increased cell soma area (Fig. 3-2f,g). To investigate the *in vitro* myelin sheet formation, OL cultures were immunolabelled for the myelin compaction protein MBP. Strikingly, *Rab35* icKO cultures displayed an increased MBP-positive area per cell compared to WT oligodendrocytes (Fig 3-3 a,b). In addition, mean fluorescence intensities of the myelin compaction protein, PLP, and two proteins associated with non-compacted myelin, MAG and CNPase, were significantly increased upon Rab35 depletion (Fig 3-3 c,d). Hence, by acute Rab35 depletion upon differentiation induction, we could confirm a negative regulatory function for the small GTPase in myelin sheet formation.

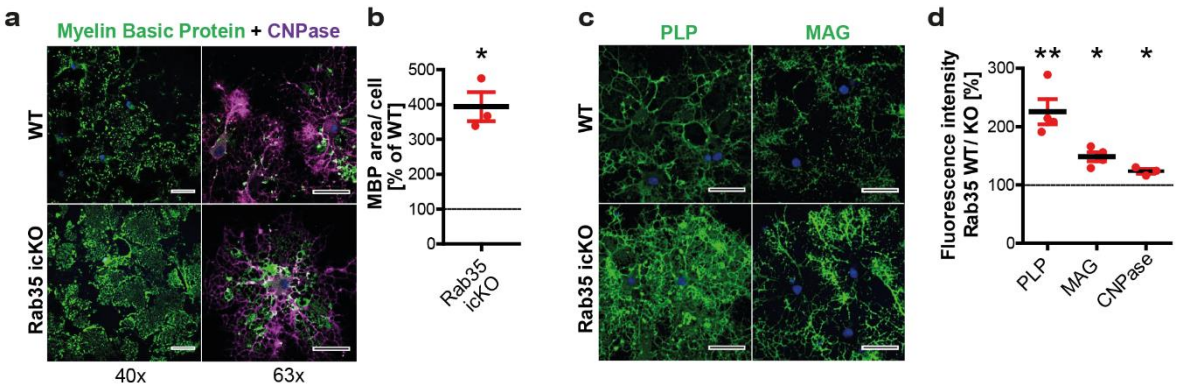

Figure 3-3: Elevated *in vitro* myelination in *Rab35* icKO oligodendrocytic cultures. Differentiated oligodendrocytes (OLs) immunostained for myelin proteins. **(a, b)** *Rab35* icKO oligodendrocytic cultures produce an increased area of MBP-positive myelin sheets *in vitro*. (a) Representative confocal images with lower (left) and higher (right) magnification of primary OLs immunolabelled for myelin compaction protein MBP (green) and oligodendrocytic marker protein CNPase (magenta); Scale bars: 30 µm. (b) Quantification of the MBP-positive area normalized to the number of cells per image, and WT cultures (100 %) in n = 3 independent experiments. **(c, d)** Increased fluorescence intensity of myelin marker proteins PLP, MAG and CNPase in OLs depleted of Rab35. (c) Confocal images of primary OLs immunolabelled for PLP (left) and MAG (right), shown in green; Scale bars: 30 µm. (d) Mean fluorescence intensities in Phalloidin-based cell masks and normalized to WT cultures (100 %); (mean ± SEM; n = 4 (PLP, MAG) or 3 (CNPase) independent experiments; one sample two-tailed student's t-test with a theoretical mean of 100; *p < 0.05, **p < 0.01).

3.1.4 Active Rab35 interacts with MTMR pseudophosphatases

Rab35 is implicated in the regulation of diverse cell physiological pathways. However, only a few effector proteins have been identified so far (Chaineau *et al*., 2013). The function of Rab35 in myelination is proposed to be either mediated by a still elusive mechanism involving ACAP2 and ARF6 (Miyamoto *et al*., 2014), or via exosome secretion with not yet identified effector proteins (Hsu *et al*., 2010). We asked if additional, so far unknown Rab35-interaction partners could reveal more insight into the mechanism of myelin-regulation by Rab35. For this purpose, we performed an unbiased proteomic screen using a BioID assay according to Roux and colleagues (2012). Rab35 was C-terminally fused to the mutant biotin protein ligase BirA*, which promiscuously biotinylates proteins in its close proximity, and was overexpressed in HEK cells. First, by immunoblot detection we analyzed the biotinylated protein fraction, captured by Streptavidin-mediated affinity purification from lysates of BirA*-Rab35-expressing cells, and compared to BirA* or mock-transfected ones. This confirmed functional biotinylation by the Rab35 chimera, when cells were cultured in the presence of biotin for 24 h before lysis (Fig. 3-4a). Using mass spectrometry (LC-MS/MS), performed by the lab of Dr. Eberhard Krause (FMP, Berlin), we analyzed the biotinylated protein fractions from BirA*-Rab35- (Rab35-BioID sample) compared to BirA*- expressing cells (BioID) by label-free quantification (LFQ) (Fig. 3-4b). Potential Rab35-interacting proteins were determined by dividing the LFQ-intensity of each protein in the Rab35-BioID fraction by its intensity in the BioID-fraction. We could identify 150 proteins enriched in the Rab35-BioID sample (Suppl. table S1, S2). Among those were two members from the same small protein family, which are both strongly associated with myelin homeostasis. MTMR5 and MTMR13, two pseudophosphatases from the myotubularin-related phosphatidylinositol (MTMR) phosphatase family, were 30-fold enriched or detected selectively in the Rab35-BioID sample, respectively (Fig. 3-4c). Interestingly, the fly homologue of both proteins, Sbf, has been detected in a previous study in the Rab35-affinity purified fraction from fly lysates (Gillingham *et al*., 2014).

Since missense mutations in either of these proteins result in the demyelinating peripheral neuropathy Charcot-Marie-Tooth disease type 4B in humans (Senderek *et al*., 2003; Nakhro *et al*., 2013), we hypothesized that Rab35 by interacting with these CMT-associated MTMR proteins might be involved in PNS myelin homeostasis as well. To investigate this hypothesis, we first further analyzed this potential interaction.

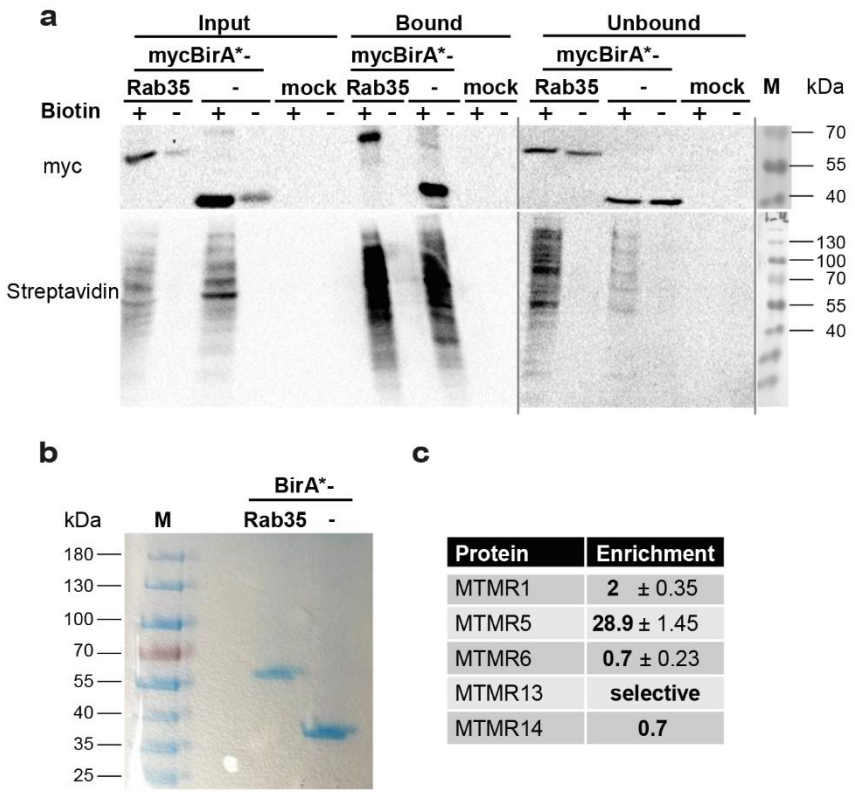

Figure 3-4: BioID-screen in HEK cells reveals novel interactors for Rab35. (a) mycBirA*Rab35 displays functional biotinylation in HEK cells. Streptavidin-mediated affinity capture and –HRP-immunoblot analysis reveals biotinylated proteins in lysates from BirA* or BirA*Rab35 but not mock-transfected cells, and upon biotin supplementation only. **(b)** Coomassie blue-stained SDS-PAGE gel of streptavidin-captured biotinylated protein fractions prior to analysis via mass spectrometry. **(c)** MTMR5 and MTMR13 are specifically associated with BirA*Rab35. The protein-specific ratio of label free quantification (LFQ)-intensity detected in BirA*Rab35-, divided by the BirA*-sample, was used to express the enrichment of proteins in n = 2 independent experiments (mean ± SD). MTMR13 was detected in association with BirA*Rab35 only. All Rab35-enriched proteins are listed in table S1 and S2.

MTMR13 and its closest relative MTMR5 are multi-domain proteins. Their N-terminal DENN domain is a typical motif for GEFs that promote GDP to GTP exchange of Rab proteins. Rab21 and Rab28 are already identified for being regulated by this MTMR-DENN domain (Yoshimura *et al*., 2010; Jean *et al*., 2012). In order to reveal if the pseudophosphatases function as GEFs for Rab35 as well, we performed affinity purification with recombinantly expressed GST-Rab35, either activated or inactivated by loading with GTPγS or GDP, respectively. Due to a lack of an antibody for endogeneous detection, we used lysates from HEK cells that overexpressed FLAG-MTMR13 as a bait. First, we could confirm the association of MTMR13 with Rab35. Interestingly, the relative amount of bound MTMR13 was five-fold higher in Rab35^GTPγS than in ^GDP (Fig. 3-5a,b). As GEFs bind Rabs in their GDP-bound form, this finding excluded the possibility of MTMR13 to function as a GEF for Rab35, in line with the interaction of their fly homologue proteins (Gillingham *et al*., 2014). In addition, we made use

of a Rab35 deletion mutant that lacks 20 amino acids at the C-terminus and is presumed to form more stable complexes with GEF proteins *in vitro* (Wu *et al*., 2011). In contrast, MTMR13 bound to GST-Rab35(ΔC) with an even higher relative binding preference of more than ten times for GTPyS- over the GDP-loaded form (Fig. 3-5b). Despite of the observed lower overall binding affinity of MTMR13 to GST-Rab35(ΔC), we used the latter in all following assays to better discriminate nucleotide-dependent and hence, specific binding for other proteins as well. First, using different GST-chimera of other prominent intracellular trafficking Rab proteins side-by-side, we could confirm that binding of MTMR13 is specific to Rab35 only. Neither GST- Rab1A, -Rab5, -Rab7 nor -Rab11 could capture overexpressed MTMR13 (Fig. 3-5c,d).

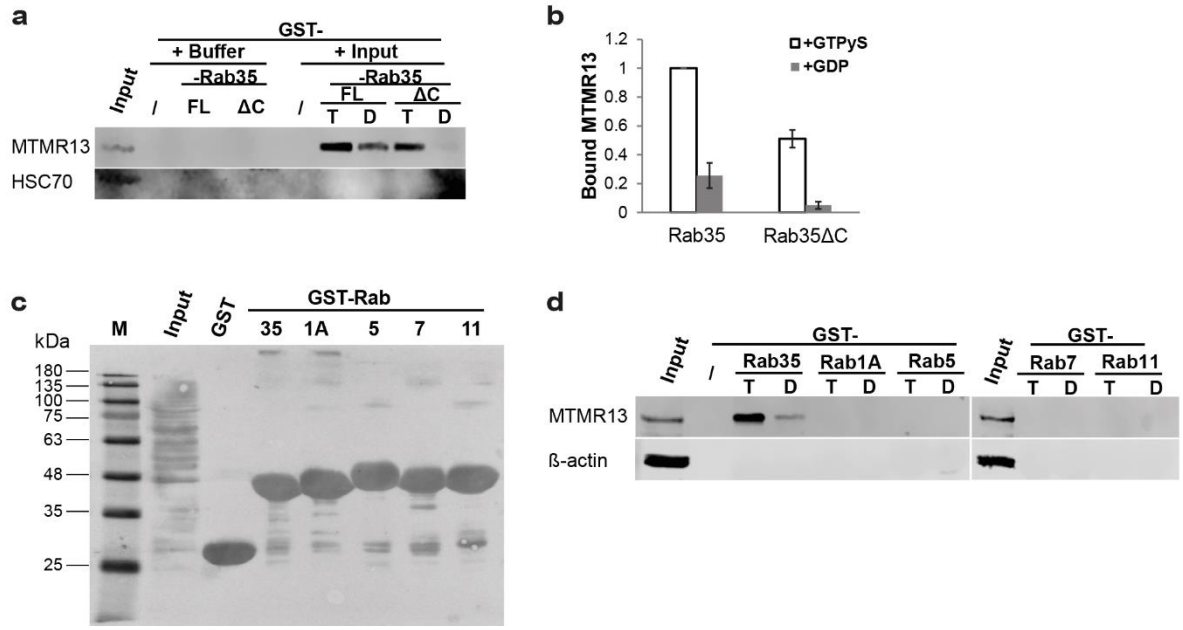

Figure 3-5: MTMR13 specifically interacts with active Rab35. (a, b) FLAG-MTMR13 was affinity captured from HEK cell lysates using GST-chimera of Rab35 and Rab35ΔC (-20 aa) loaded with GTPγS (T) or GDP (D). (a) Representative immunoblot of MTMR13-detection using a FLAG-antibody, and HSC70 as a negative binding control. Input: 5 % of total protein. (b) Bound MTMR13 fraction, normalized to GTPγS-loaded GST-Rab35, (mean ± SD) from n = 2 independent experiments. MTMR13 binds preferentially to GTPγS- over GDP-loaded Rab35 (GTPγs/GDP: Rab35 - 5x, Rab35ΔC - 12x). **(c, d)** MTMR13 binds selectively to Rab35 but not Rab1A, Rab5, Rab7 or Rab11. Affinity chromatography as in (a,b) using different GST-Rab chimera as a prey. (c) Representative blotting membrane of affinity captured protein fractions, visualized by Poinceau-S staining, verifies comparable protein amounts of GST-Rab chimera. (d) Representative immunoblot from n = 6 independent experiments for MTMR13 detection. ß-actin served as negative binding control; 5 % Input; T – GTPγS, D – GDP.

Next, we performed this assay including MTMR5 and a set of eGFP-fused active MTM(R) phosphatases. MTMR5 displayed a similar binding preference to GST-Rab35^GTPγS over ^GDP as observed for MTMR13, though with a lower enrichment considering the high expression levels (Fig. 3-6). However, neither MTM1, MTMR1 nor

MTMR2 could be eluted from any Rab35-bound fraction, indicating a specific interaction of Rab35 with the MTMR pseudophosphatases.

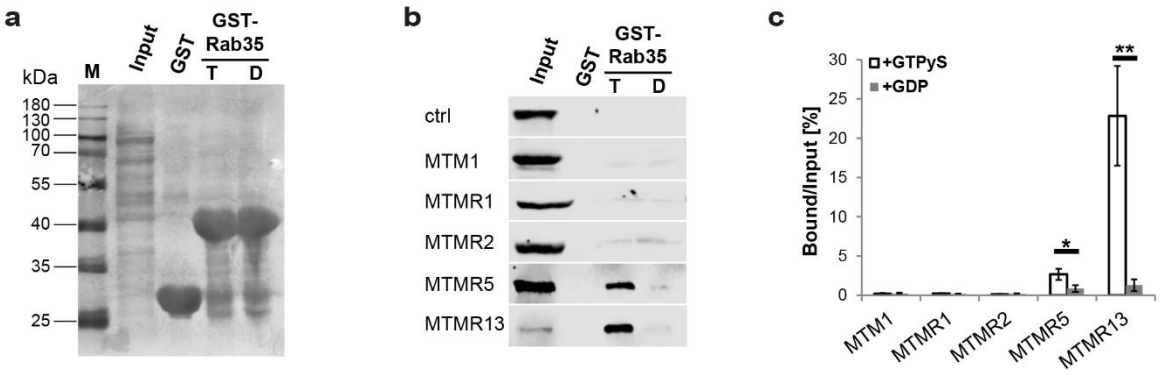

Figure 3-6: Rab35 interacts specifically with the pseudophosphatases MTMR13 and MTMR5. Affinity purification of lysates from HEK cells overexpressing eGFP- MTM1, MTMR1, MTMR2, MTMR5, or FLAG-MTMR13 using GST-Rab35^GTPγS (T) or ^GDP (D). **(a)** Representative Ponceau S stained blotting membrane shows comparable protein amounts of applied GST-Rab35^GTPγS, ^GDP and GST. **(b)** Representative immunoblots. MTM(R)-detection with antibodies against GFP- or FLAG-epitope. Overexpressed eGFP served as a negative control (ctrl); 5 % Input. **(c)** Bound protein fractions (depicted relative to the input) show specific binding of MTMR5 and MTMR13 to Rab35-GTPγS, but not MTM1, MTMR1 or MTMR2; (mean ± SEM from MTM1: n = 4, MTMR1: n = 5, MTMR2: n = 7, MTMR5: n = 4, and MTMR13: n = 10 independent experiments; two-tailed paired student's t-test; *$p < 0.05$, **$p < 0.01$).

In contrast to small GTPases which mainly interact with other proteins via their conserved globular G-domain (Milburn *et al*., 1990; Wittinghofer and Vetter, 2011), MTMR13 and -R5 are large multi-domain proteins. Besides the N-terminal GEF domain they harbor two lipid-binding domains, PH-GRAM and PH, the inactive protein tyrosine phosphatase domain (iPTP) with unknown function, and a coiled-coil (CC) region for oligomerization (Fig. 3-7a) (Goryunov *et al*., 2008). In order to further dissect the nature of interaction between Rab35 and these closely homologous pseudophosphatases, we aimed to map the MTMR-domain which confers binding to Rab35. Due to the close domain homology of both pseudophospatases, we focused on MTMR13 which possessed the stronger binding affinity to Rab35 in our previous assays. We generated constructs encoding for mCherry-fused single domains of MTMR13, with the exception of the coiled coil region that was not soluble on its own, and therefore expressed in conjunction with the inactive PTP domain. The constructs were introduced into a TALEN-edited HeLa knock-in (KI) cell line which expresses endogeneous Rab35 with an N-terminal eGFP-tag (eGFP-Rab35^{endo}), generated in the lab of Arnaud Echard (Cauvin *et al*., 2016). eGFP-Rab35^{endo} protein was captured from lysates using GFP-nanotrap magnetic beads. Bound fractions were then analyzed for overexpressed MTMR13 full-length or single domains by immunoblotting for mCherry. Importantly, full-length MTMR13 also bound to the

endogeneously expressed Rab35 (Fig. 3-7b). From the single MTMR13-domains, the iPTP domain was detected in the Rab35-bound fraction only. Surprisingly, the conjunction peptide of iPTP and CC region could not be captured. This might result from sterical interference by the CC region in this construct. Nevertheless, selective binding to the inactive PTP domain provides a possible explanation for the observed pseudophosphatase-specific MTMR protein association of Rab35.

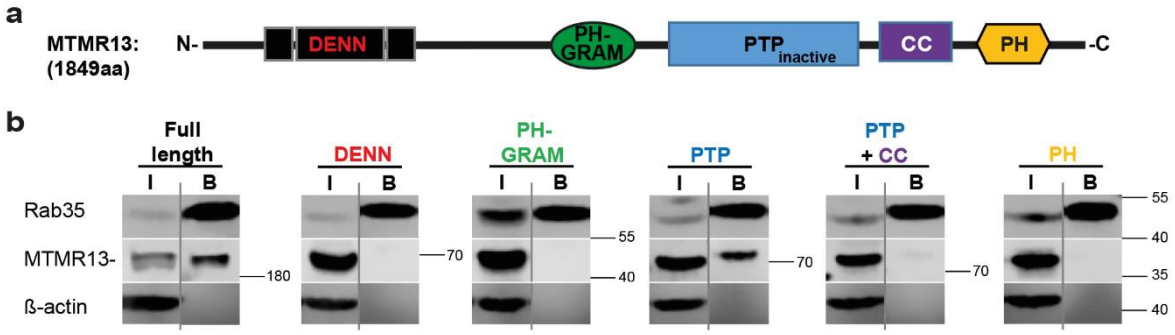

Figure 3-7: Rab35 binds to the inactive PTP domain of MTMR13. (a) Schematic presentation of the full-length multi-domain protein MTMR13, adapted from Goryunov *et al.*, (2008). **(b)** eGFP-Rab35^{endo} knock in (KI) HeLa cells, expressing mCherry-tagged MTMR13 full-length (FL) or single domains, were lysed and subjected to affinity capture using GFP-nanotrap magnetic beads. Representative immunoblot shows binding of mCherry-MTMR13 FL and -PTP domain to affinity captured endogeneously expressed Rab35. (5 %) Input (I) and bound (B) protein fractions were analyzed using antibodies against GFP, RFP, or ß-actin as a control.

3.1.5 Rab35 can recruit MTMR phosphatase complexes

The GTP-loading state of Rab GTPases represents their active form. Accordingly, we could also observe MTMR13-binding to a constitutively active mutant Rab35Q67L (CA), upon co-overexpression and affinity purification using nanotrap beads against the epitope-tag of the latter (Fig. 3-8b). In their active state, Rab proteins can either interact with effector proteins downstream or with their regulatory Rab GTPase activating proteins (GAPs) upstream (Pfeffer and Aivazian, 2004; Blümer *et al.*, 2013). However, Rab GAPs are usually characterized by TBC domains that mediate their binding to Rab proteins (Barr and Lambright, 2010). Our finding that Rab35 binds to the inactive PTP domain of MTMR13, and the fact that a TBC sequence has not been identified so far in MTMR5 or MTMR13 let us suggest a potentially upstream regulatory function of Rab35 in this interaction. In order to confirm this hypothesis, we aimed to dissect the influence of active Rab35 on the cellular localization pattern of MTMR13 by confocal microscopy. Localization studies of MTMRs are rare. MTMR13 and MTMR5 are mainly described as complex interaction partners for MTMR2 (Berger *et al.*, 2003; Kim *et al.*, 2003b; Robinson and Dixon, 2006), that is assigned to function at late endosomes (Cao *et al.*, 2008). As Rab35 was recently identified on LAMP-positive late endosomal/

lysosomal membranes as well (Hsu *et al*., 2010; Wheeler *et al*., 2015), we made use of LAMP-1 co-immunostaining to identify these compartments (Johansson *et al*., 2005; Schröder *et al*., 2007). First, we analyzed the localization of endogeneously expressed Rab35 in eGFP-Rab35^{endo} KI HeLa cells by probing the eGFP-epitope. We could observe signals at the plasma membrane and at perinuclear puncta that partially overlapped with LAMP-1 (Fig. 3-8a). In addition, overexpression of the GTP-locked mutant Rab35CA in HeLa cells resulted in a similar localization pattern (Fig. 3-8c). Co-expression of Rab35 with MTMR13 did not alter the localization of the small GTPase, but interestingly the pseudophosphatase was translocated. Overexpression of FLAG-MTMR13 on its own resulted in a diffuse cytoplasmic localization pattern (Fig. 3-8d), consistent with earlier observations (Robinson and Dixon, 2006). In contrast, in the presence of Rab35CA we detected FLAG-positive fluorescent signals at the plasma membrane, and discrete perinuclear puncta (Fig. 3-8e) that partially co-localized with LAMP-1 (Fig. 3-8f). These data strongly suggest that Rab35 acts upstream in this interaction and can recruit MTMR13 to late endosomal/ lysosomal compartments.

Complex formation between an active and an inactive MTMR phosphatase by heterodimerization is accompanied by changes in their localization, lipid specificity and phosphatase activity. This has led to the assumption that pseudophosphatase members of the MTMR family act as recruitment factors for their respective active partner and thereby mediate their specific function (Caldwell *et al*., 1991; Kim *et al*., 2003b; Mochizuki and Majerus, 2003; Berger *et al*., 2006b; Zou *et al*., 2009, 2012). MTMR5 and MTMR13 form both active complexes with MTMR2, which increases the phosphatase activity of the latter towards PI(3)P and PI(3,5)P_2 *in vitro* (Kim *et al*., 2003b; Berger *et al*., 2006b). Moreover, missense or nonsense mutations in one of these pseudophosphatases largely phenocopy loss of function mutations of MTMR2 in humans (Azzedine *et al*., 2003; Senderek *et al*., 2003; Nakhro *et al*., 2013). In order to unveil if these complexes are still formed when MTMR5 or MTMR13 are bound to Rab35, we performed GST-Rab35-mediated affinity purification from HEK cells that co-express MTMR2 with MTMR13 or MTMR5. Indeed, in the presence of MTMR13 or MTMR5, but not their epitope-tags alone as a control, MTMR2 was detected in the bound fraction of Rab35^GTPyS (Fig. 3-9, 3-10). Next, we replaced the active phosphatase MTMR2 by its closest homologues MTMR1 and MTM1. Surprisingly, also MTMR1 specifically bound to Rab35^GTPyS upon co-expression with MTMR13, whereas MTM1 did not (Fig. 3-9c,d). Thus, MTMR1 is as an additional, so far unknown complex partner of MTMR13. In sum, these data reveal that Rab35 can bind and recruit MTMR pseudophosphatases and via these also active MTMR phosphatases.

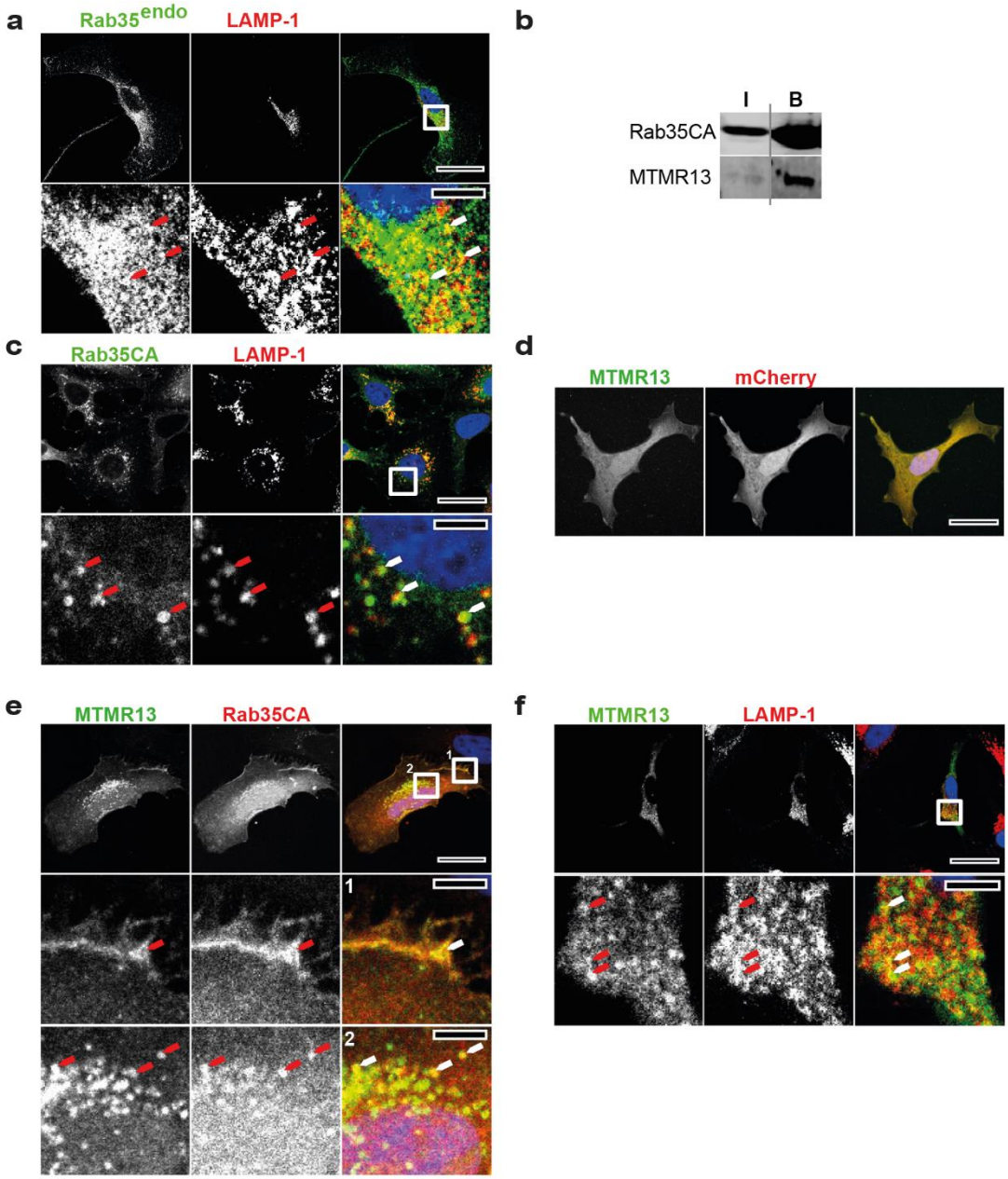

Figure 3-8: Active Rab35 recruits MTMR13. (a) Immunostaining of eGFP-Rab35^{endo} HeLa KI cells for GFP (green) and LAMP-1 (red) shows partial overlap; Scale bars: 30 µm (upper), 5 µm (lower). **(b)** MTMR13 binds to Rab35CA. Lysates from HeLa cells that co-expressed FLAG-MTMR13 and constitutively active eGFP-Rab35 (Rab35CA) were affinity purified using GFP-nanotrap magnetic beads. Representative immunoblot with (5 %) Input (I) and bound protein fractions (B) analyzed by immunoblotting using antibodies for the eGFP- and FLAG-epitope. **(c-f)** Confocal images of HeLa cells expressing constitutively active eGFP-Rab35 (Rab35CA) or FLAG-MTMR13, or both. Cells were immunostained for GFP, LAMP1 and FLAG. Arrows mark examples of co-localizing puncta. White squares in upper panels are shown in inserts in lower panels; Scale bars: 30 µm (top), 5 µm (bottom). (c) eGFP-Rab35 (Rab35CA) (green) localizes to perinuclear LAMP1 overlapping (red)-positive puncta. (d) FLAG-MTMR13 is diffusively localized to the cytoplasm when co-expressed with mCherry as a control protein (red). (e, f) Co-localization of MTMR13 (green) with (d) Rab35CA (red) at the plasma membrane (top-1) and in perinuclear puncta (bottom-2), that (f) contained LAMP-1 (red).

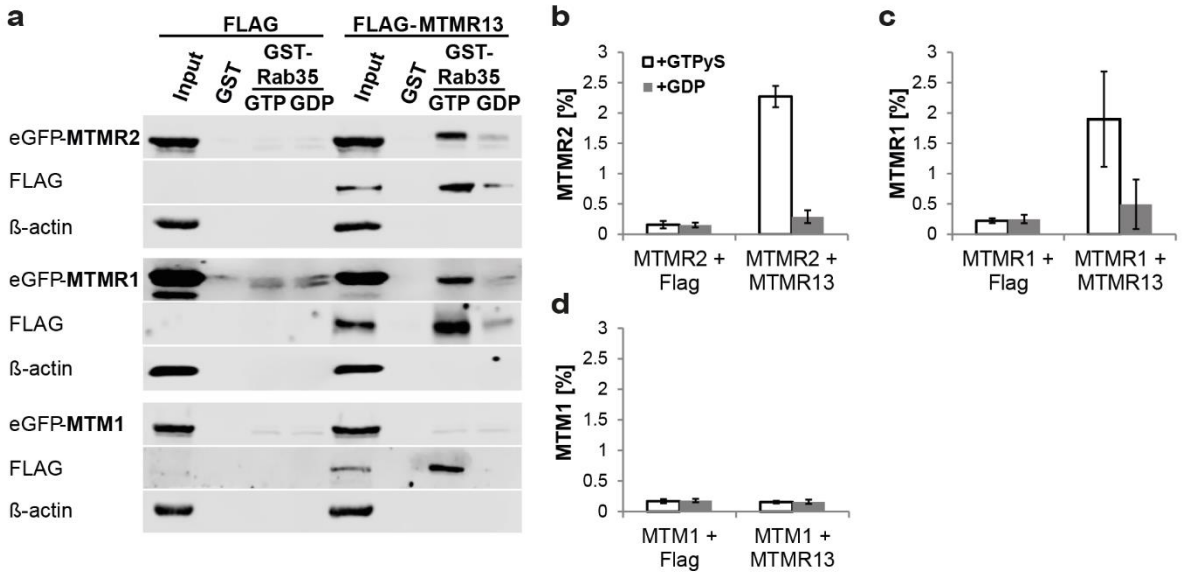

Figure 3-9: Active Rab35 interacts with MTMR1 and MTMR2 via MTMR13. Lysates from HEK cells co-expressing eGFP- MTM1, -MTMR1 or -MTMR2 with FLAG-MTMR13 or FLAG (as a control) were incubated with nucleotide-loaded GST-Rab35. The bound fraction was analyzed by immunoblotting with antibodies against GFP, FLAG, and ß-actin. **(a)** Representative immunoblot. 5 % Input; T – GTPγS, D – GDP. **(b-d)** Quantification of the bound protein fraction relative to the input (mean ± SEM) shows specific association for (b) MTMR2 (n = 3) and (c) MTMR1 (n = 4) to GTPγS-loaded Rab35 when co-expressed with FLAG-MTMR13, but not (d) MTM1 (n = 4 independent experiments).

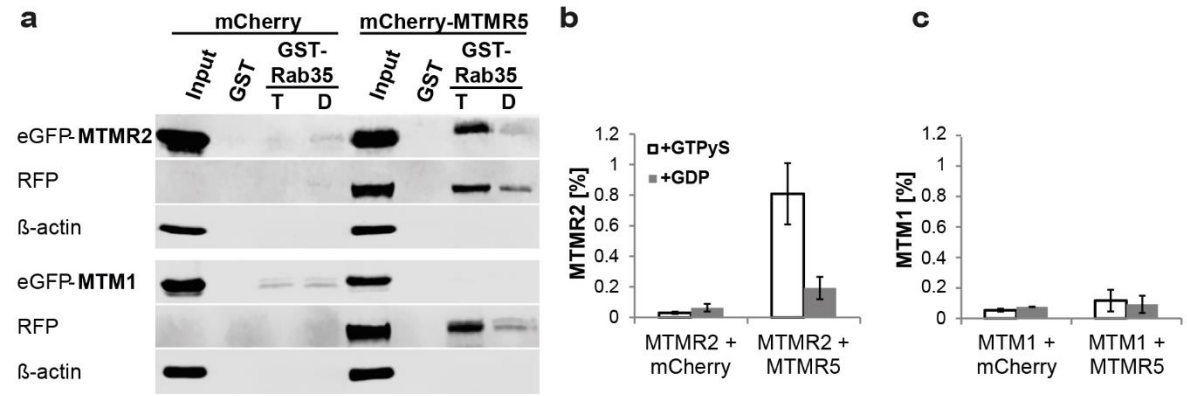

Figure 3-10: MTMR2 binds to active Rab35 via MTMR5 as well. eGFP- MTM1 or -MTMR2 were co-expressed with mCherry-MTMR5 or mCherry (as a control) in HEK cells. Lysates were incubated with nucleotide-loaded GST-Rab35 and analyzed by immunoblotting with antibodies against GFP, RFP, and ß-actin. **(a)** Representative immunoblot. 5 % Input; T – GTPγS, D – GDP. **(b, c)** Quantification of the bound protein fraction relative to the input (mean ± SEM) shows specific association of (b) MTMR2 (n = 3), but not (c) MTM1 (n = 4 independent experiments) to GTPγS-loaded Rab35, when co-expressed with mCherry-MTMR5.

3.1.6 Loss of MTMR2 phenocopies Rab35 depletion in oligodendrocytic cultures

So far, we could show a novel interaction between Rab35 and CMT-associated MTMR proteins that have been strongly associated with myelin homeostasis regulation in the PNS. Nevertheless, MTMR proteins including MTMR2, are ubiquitously expressed and also in CNS cells (Laporte *et al*., 1998; Berger *et al*., 2002; Bolino *et al*., 2002) (and see below). We were interested, if the observed increase in myelin protein expression in Rab35-depleted cells *in vitro* could result from an impaired recruitment of active MTMR complexes. To address this question, we made use of lentiviral transduction with shRNA to deplete the active phosphatase MTMR2 in differentiated oligodendrocytes in culture. Due to the lack of a functional antibody for immunocytochemistry, successful knockdown of mouse MTMR2 with this approach was confirmed in mouse embryonic fibroblast (MEF) cultures by immunoblotting (Fig. 3-11a). Indeed, shRNA-mediated knockdown of MTMR2 in WT oligodendrocytic cultures caused an increase of MAG and PLP-fluorescence intensities compared to WT cells transduced with non-targeting (scrambled) shRNA. Moreover, for both proteins the increase in protein levels was comparable to the mean increase observed in *Rab35* icKO cells transduced with control shRNA (Fig. 3-11b,c,d). MTMR2 knockdown in *Rab35* icKO oligodendrocytes resulted in partially elevated protein levels compared to the single depletion of either Rab35 or MTMR2. These results might implicate that the involvement of Rab35 in oligodendrocytic myelination is mediated by active MTMR complexes.

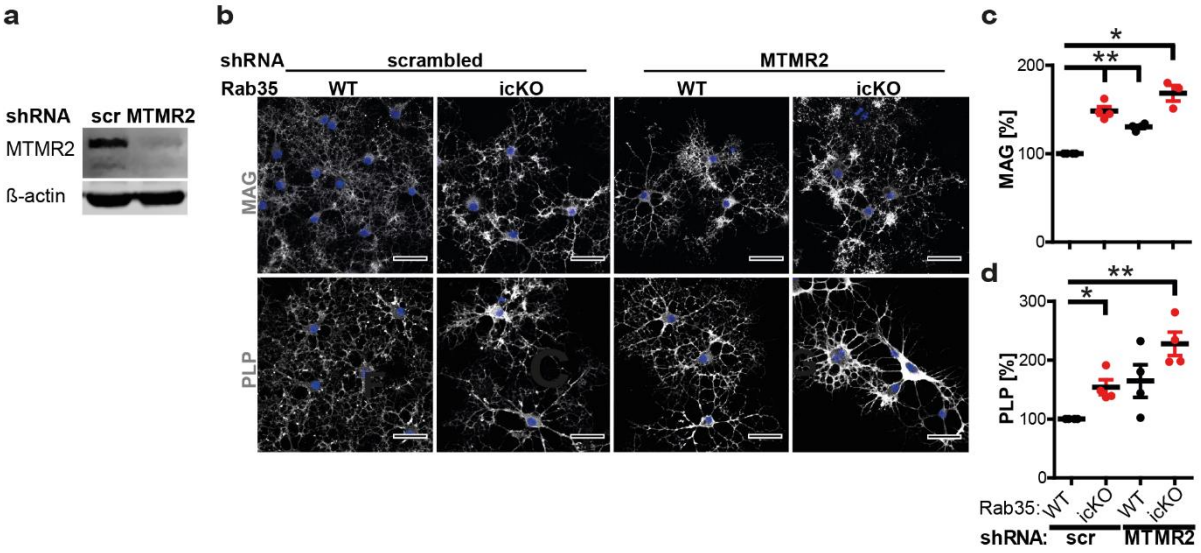

Figure 3-11: MTMR2 depletion phenocopies loss of Rab35 with increased *in vitro* myelination in oligodendrocytic cultures. (a) Transduction with shRNA depletes MTMR2 protein levels in mouse cells. Mouse embryonic fibroblast (MEF) cell cultures were transduced with non-targeting scrambled or MTMR2-targeting shRNA using a lentiviral system. Representative immunoblot of MEF lysates probed for MTMR2 and ß-actin as a loading control. **(b-d)** Oligodendrocytic (OL) cultures were transduced at DIV3 with lentiviral non-targeting scrambled or MTMR2-targeting shRNA and fixed at DIV7. (b) Representative confocal images of immunolabelling for MAG (upper) and PLP (lower) (grey); Scale bars: 30 µm. (c,d) Mean

fluorescence intensities, normalized to WT + scr (100%), of (c) MAG and (d) PLP, are elevated upon shRNA-mediated knockdown of MTMR2 in *Rab35* WT and icKO cells; (mean ± SEM; n = 4 independent experiments; one sample two-tailed student's t-test for each genotype compared to control (*Rab35* WT + scr) with a theoretical mean of 100, followed by p-value correction for multiple testing using Holm's Multiple Comparison Test; *p < 0.05, **p < 0.01, PLP: WT + scr vs. WT + shMTMR2: p = 0.1013).

3.2 Rab35 represses mTORC1 via MTMR-mediated lipid regulation, and controls PNS myelination *in vivo* and *in vitro*

3.2.1 Focal hypermyelination upon loss of Rab35 in Schwann cells *in vivo*

We could identify Rab35 as a potential regulator of active MTMR complexes and observed that depletion of MTMR2 mimics the effect of Rab35 loss on *in vitro* myelination of oligodendrocytes. However, distinct MTMR family proteins are strongly associated with the regulation of PNS myelination. Loss of function or missense mutations in either MTMR2, -R5 or -R13 cause the peripheral demyelinating neuropathy CMT4B (Senderek *et al*., 2003; Bolino *et al*., 2004; Nakhro *et al*., 2013). Thus, we hypothesized that the small GTPase could regulate PNS myelination as well. Therefore, in collaboration with Prof. Dr. A. Bolino (INSPE, Milan, Italy), we generated a conditional Rab35 knockout mouse that is specifically depleted of Rab35 in Schwann cells. The "floxed" Rab35 mice (*Rab35*$^{Fl/Fl}$) were bred with a mouse line that expresses a Cre-recombinase under control of the myelin protein 0 (P0)-promoter (P0-*Cre*) as early as embryonic day E13.5 (Feltri *et al*., 1999) (Fig. 3-12a). Successful recombination *in vivo* was confirmed by a mean reduction in Rab35 protein levels of 75 % in sciatic nerve (SN) lysates of *Rab35* cKO^{SC} (*Rab35*$^{Fl/Fl}$ x P0-*Cre*) compared to Ctrl animals (*Rab35*$^{Fl/Fl}$) (Fig. 3-12b,c). As the detected residual protein amount of 25 % only, is presumably representing levels in SN axons and fibroblasts, Rab35 is comparably high abundant in Schwann cells. Importantly, *Rab35* cKO^{SC} sciatic nerves from mice of different postnatal days (P), investigated by semi-thin section analysis, displayed striking myelin alterations in form of tomacula, outfoldings and myelin degeneration, that were not observed in Ctrl mice of any age. In contrast, in *Rab35* cKO^{SC} nerves, these forms of abnormal myelin morphologies were observed already at P20, of progressive worsening with ageing, and resulted in a mean fraction of around 30 % altered myelinated fibers in 3 month old mice (Fig. 3-12d,e,f). The number of myelin layers wrapped around an axon per internode is tightly regulated and highly correlated to the axon diameter as expressed by a relatively constant g-ratio for healthy myelinated fibers between 0.6 and 0.7, slightly increasing with the axonal diameter and the age of the animal (Rushton, 1951; Berthold *et al*., 1983; Friede and Beuche, 1985).

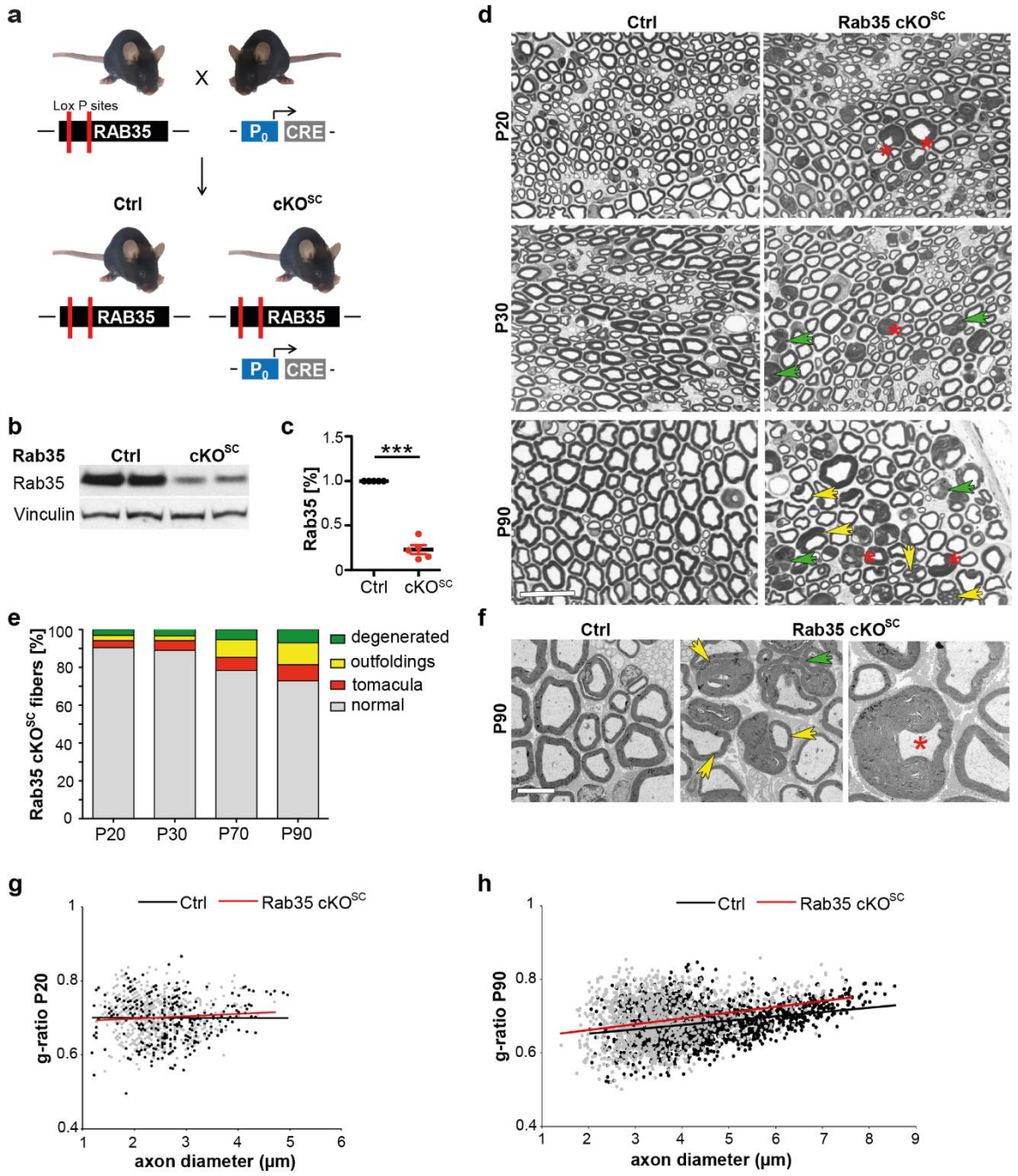

Figure 3-12: Loss of Rab35 in Schwann cells causes focal hypermyelination *in vivo*. Performed by the laboratory of Prof. Dr. A. Bolino (INSPE, Milan, Italy): **(a)** Schwann cell-specific Rab35 knockout (cKO^{SC}) mice were generated by crossing *Rab35*$^{Fl/Fl}$ mice with transgenic mice that encode a Cre recombinase under control of the Schwann cell-specific P0-promotor (P0-*Cre*). *Rab35* Ctrl – *Rab35*$^{Fl/Fl}$; *Rab35* cKO^{SC} - *Rab35*$^{Fl/Fl}$ x P0-*Cre*. **(b, c)** Reduced Rab35 protein expression in sciatic nerve lysates from *Rab35* cKO^{SC} mice at postnatal day (P) 30. (b) Representative immunoblot for Rab35. Tubulin was used as a loading control. (c) Rab35 protein levels, normalized to Tubulin and Ctrl levels (= 100 %), were reduced to 25 % in *Rab35* cKO^{SC} sciatic nerve lysates; (mean ± SEM; n = 5 independent experiments; one sample two-tailed student's t-test with a theoretical mean of 100; $^{***}p < 0.001$). **(d)** Semithin section analysis of *Rab35* cKO^{SC} sciatic nerves at P20, P30 and P90 revealed myelinated fibers carrying myelin degenerations (green arrows), tomacula (red asterisks) and myelin outfoldings (yellow arrows); Scale bar: 20 µm. **(e)** Quantification of the fraction of aberrant myelinated fibers (% of total) in *Rab35* cKO^{SC} sciatic nerves at P20, P30, P70 and P90, reveals increasing abundance of alterations in aged animals. Ctrl fibers were 0 % aberrantly myelinated; (mean; n = 5 (P20) and 4 (P30, P70, P90) animals per genotype). **(f)** Example images of ultrastructural

analysis of *Rab35* Ctrl and cKO^{SC} sciatic nerves depicting myelin outfoldings (yellow arrows), myelin degeneration (green arrows) and a tomaculum (red asterisk); Scale bar: 5 µm. (**g, h)** Quantification of the g-ratio by ultrastructural analysis, as a function of axonal diameter in sciatic nerves at (g) P20 (n=5 animals per genotype) or (h) P90 (n= 4 animals per genotype). No significant differences in *Rab35* cKO^{SC} compared to Ctrl at P20 or P90, except for fibers larger than 5 µm at P90 which displayed a significantly increased g-ratio (two-tailed nonparametric Mann-Whitney test; $^{**}p < 0.01$).

The g-ratio is calculated by dividing the axonal diameter by the fiber (axon + myelin) diameter. By analyzing the remaining fraction of non-altered fibers in *Rab35* cKO^{SC} sciatic nerves, no change in the number of myelinated axons and largely unaltered g-ratios were observed at P20 and P90 (Fig. 3-12g,h). At P90 only, fibers with an axonal diameter greater than 5 µm displayed reduced myelin thickness, represented by an increase in the g-ratio compared to Ctrl nerves (Fig. 3-12h). In sum, these data reveal that loss of Rab35 in Schwann cells results in focal hypermyelination in form of redundant-focally folded myelin sheaths including myelin outfoldings, reminiscent to *MTMR2* KO and *MTMR13* KO mice (Bolino *et al*., 2004; Robinson *et al*., 2008; Tersar *et al*., 2007; Ng *et al*., 2013). Notably, signs of hypomyelination in aged animals have also been observed in *MTMR13* KO mice (Robinson *et al*., 2008; Ng *et al*., 2013).

3.2.2 Depletion of Rab35 and/ or MTMR2 results in mTORC1 hyperactivity

We aimed to investigate the underlying molecular mechanism by which Rab35 and active MTMR complexes could regulate myelination. Interestingly, focal hypermyelination in peripheral nerves is also a hallmark in transgenic mice with overactivated PI3K/AKT/mTOR signaling in Schwann cells (Goebbels *et al*., 2012; Beirowski *et al*., 2017). Rab35 has been implicated in AKT activation, though with contrasting findings from different cell types (Allaire *et al*., 2013; Wheeler *et al*., 2015; Zheng *et al*., 2017). In addition, overexpression of MTMR2 is reported to result in sustained AKT activation (Berger *et al*., 2011), though CMT4B mouse models do not display altered AKT activity (Ng *et al*., 2013; Bolino *et al*., 2016).

In order to analyze if depletion of Rab35 and/ or the active phosphatase MTMR2 affects PI3K/AKT/mTOR signaling, we first made use of a mammalian cell line as an easily genetically manipulatable system. We performed siRNA-mediated depletion of Rab35 and its indirect interaction partner, the active phosphatase MTMR2, in HEK cells, which sufficiently reduced the levels of each protein to less than 20 % (Fig. 3-13a,b,c). The cell lysates were analyzed by immunoblotting for activation of the main signaling pathway-components AKT and mTOR, displayed by the ratio of phosphorylated over total protein levels (Fig. 3-13a). In neither of the knockdown conditions, Rab35, MTMR2, or both, we could observe alteration in AKT

activation (Fig. 3-13d). In contrast, activation of the kinase complex mTORC1, downstream to and indirectly regulated by AKT upon mitogen and growth factor stimulation (Inoki *et al*., 2002), is elevated in Rab35- and MTMR2-depleted cells. In both conditions, the ratio of the phosphorylated mTORC1-target p70 S6 Kinase 1 (p-S6K) to total S6K levels is increased by twofold (Fig. 3-13e). Cells depleted of Rab35 and MTMR2 display an even higher increase in the ratio of p-S6K/ S6K. Additionally, the levels of S2448-phosphosporylated mTOR, a specific mTORC1-phosphorylation site for S6K in a presumable positive feedback-loop (Chiang and Abraham, 2005; Copp *et al*., 2009; Rosner *et al*., 2010), display a similar tendency as depicted by the ratio of p-mTOR/ mTOR protein levels (Fig. 3-13f). This suggests that both, Rab35 and MTMR2 repress mTORC1 activity, independent of the PI3K/AKT axis in mammalian cells.

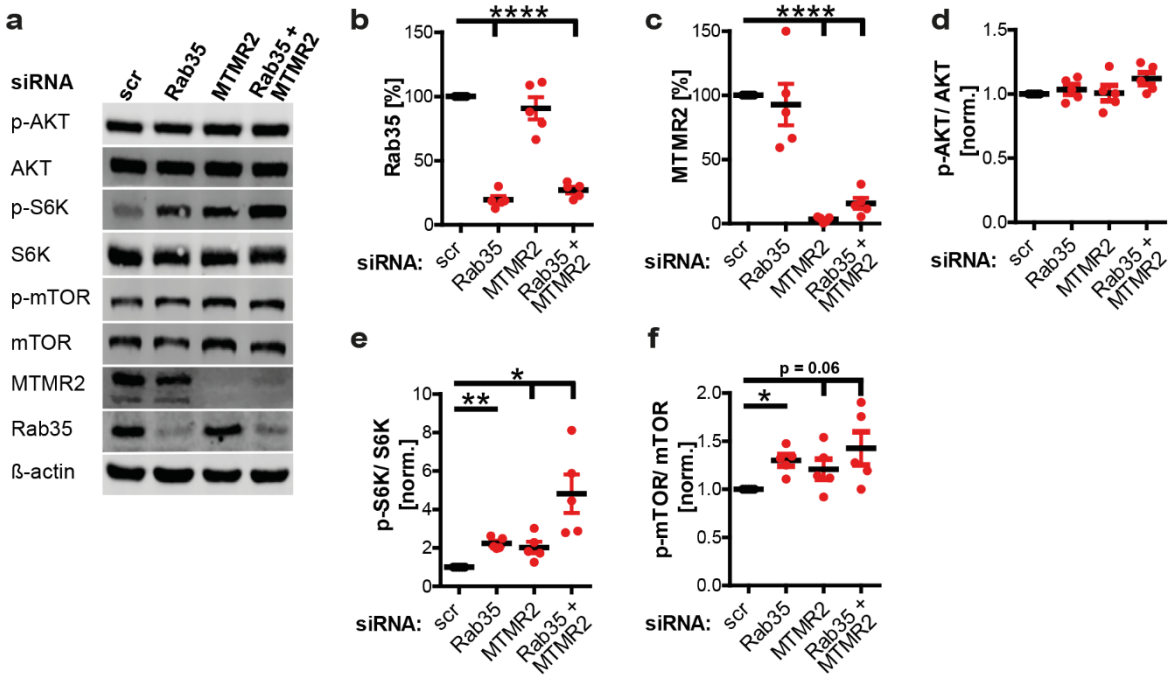

Figure 3-13: Depletion of Rab35 and/ or MTMR2 in HEK cells results in mTORC1 hyperactivation. Lysates of HEK cells depleted of Rab35, MTMR2, or both by siRNA-mediated knockdown were analyzed for proteins of the PI3K/AKT/mTOR pathway by immunoblotting. Scrambled siRNA (scr) transfected cells were used as controls. **(a)** Representative immunoblot for S473-phospho AKT (p-AKT), total AKT, T389-phospho p70 S6 Kinase (p-S6K), total p70 S6K (S6K), S2448-phospho mTOR (p-mTOR), total mTOR, Rab35 and MTMR2. ß-actin served as a loading control. **(b-f)** Quantification from n = 5 independent experiments. (b) Rab35 and (c) MTMR2 are efficiently depleted upon siRNA-mediated knockdown. (d) p-AKT/ AKT ratio normalized to scrambled siRNA (scr) (=1) is not altered in any condition; (siRNA: Rab35, p = 0.93502; MTMR2, p = 0.9073; Rab35 + MTMR2, p = 0.18496). (e) p-S6K/ total S6K ratio normalized to scrambled siRNA (scr) control (=1) as a readout for mTORC1 activity, is significantly increased upon depletion of MTMR2 or Rab35, or both. (f) p-mTOR / total mTOR ratio normalized to scrambled siRNA (scr) control is elevated in all knockdown conditions (p = 0.0688); (mean ± SEM; one sample two-tailed student's t-test with a theoretical mean of 100 (b,c) or 1 (d-f), for all conditions normalized to scr, followed by p-value correction for multiple testing using Holm's Multiple Comparison Test; *p < 0.05, **p < 0.01; ****p < 0.0001).

3.2.3 Rab35 represses mTORC1 activity via MTMR2

Since hyperactivation of mTORC1 in myelinating glial cells of the CNS and PNS causes a strong impairment of myelin homeostasis *in vivo* (Narayanan *et al*., 2009; Goebbels *et al*., 2010; 2012; Beirowski *et al.,* 2017; Figlia *et al*., 2017), we aimed to test if the observed repression of mTORC1 activity by Rab35 and MTMR2 is also displayed in cells of the nervous system. To that end, we made use of primary astrocytic cultures, proliferating CNS-derived cultures that provide a sufficient number of cells for lysate protein level analysis by immunoblotting. Indeed, in *Rab35* icKO cultures we could detect a mean increase of 50 % for p-S6K/ S6K protein levels at steady state (+ FBS) (Fig. 3-14a,b). Serum starvation, the withdrawal of the major source for growth factors and mitogens, down-regulates PI3K class I- and thereby AKT- signaling. When cultures were serum-starved for 12 h before lysis (- FBS), hyperactivation of mTORC1 is still observed in *Rab35* icKO compared to WT cultures (Fig. 3-14a,b), indicating that altered mTORC1 regulation is independent of AKT activation. Accordingly, p-AKT protein levels are not increased in *Rab35* icKO cultures (Fig. 3-14c,d). In contrast, a robust decrease of p-AKT/ AKT protein levels is detected upon acute Rab35 knockout. This result is consistent with a previous study that claims a promoting function of Rab35 in PI3K-mediated AKT activation (Wheeler *et al*., 2015). In sum, our data confirm a negative regulatory role for Rab35 in mTORC1 activation in cells of the nervous system, independent of the PI3K/AKT axis.

As a signaling hub at which external and internal cues such as nutrient, energy and oxygen availability are integrated, mTORC1 is an important master regulator in the control of the cell anabolic *versus* metabolic state. Upon activation in favorable environmental conditions, for instance by nutrient or energy availability, this complex promotes protein and lipid synthesis, thus cell growth, and simultaneously downregulates autophagy and lysosome biogenesis (Laplante and Sabatini, 2012). Similar to primary *Rab35* icKO OPCs and oligodendrocytes, and consistent with the established function of mTORC1 activity in the regulation of cell size in different eukaryotic cell types (Fingar *et al*., 2002; Laplante and Sabatini, 2012), we could detect a significant enlargement of *Rab35* icKO astrocytes in cultures (Fig. 3-15a,b).

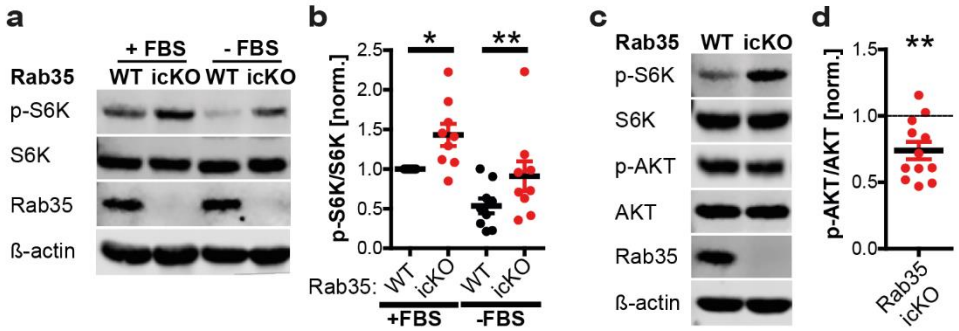

Figure 3-14: mTORC1 hyperactivation in primary *Rab35* icKO cells is independent of AKT. (a, b) mTORC1 hyperactivity in *Rab35* icKO astrocytes independent of growth factor stimulation. Astrocytic cultures were either serum-fed (+ FBS) or serum-starved (- FBS) for 12 h before lysis. (a) Representative immunoblot probed with antibodies against p-S6K1, total S6K1, and ß-actin used as a loading control. (b) p-S6K/ total S6K ratio as a readout for mTORC1 activity, normalized by setting WT + FBS to 1, is increased in *Rab35* icKO cells under both conditions (n = 9 independent experiments). **(c, d)** mTORC1 hyperactivity in *Rab35* icKO astrocytes is independent of p-AKT. (c) Representative immunoblot of WT and *Rab35* icKO astrocytes for p-S6K, total S6K, p-AKT and total AKT, and for Rab35 and ß-actin as controls. (d) p-AKT/ AKT is decreased in *Rab35* icKO astrocytes compared to WT (set to 1); (mean ± SEM; n= 12 independent experiments; one sample two-tailed student's t-test with a theoretical mean of 1; *p < 0.05; **p < 0.05).

Next, we probed astrocytic lysates for the autophagic marker protein LC3/ATG8 by immunoblotting. In *Rab35* icKO lysates, we observed a significant reduction of protein levels for both, the cleaved cytosolic form LC3-I and the phosphatidylethanolamine-conjugated LC3-II that is associated to autophagosomal membranes (Kabeya *et al*., 2000), to 60 % and 80 % of WT levels, respectively (Fig. 3-15c,d). In contrast, the ratio of the autophagosome-associated LC3-II over cytosolic LC3-I levels is increased upon Rab35 depletion, at steady state (+ FBS) by 40 % and upon serum-starvation (-FBS) by 200 % (Fig. 3-15c,e). This implicates that autophagy is starvation-induced with a higher rate in *Rab35* icKO than WT cultures, with 4- and 2.5-fold, respectively (Fig. 3-15e). Moreover, comparable results were obtained by immunolabelling for LC3, using short-term digitonin permeabilization to preserve autophagosomal membranes (Kaminskyy *et al*., 2011). Background subtraction of diffuse cytoplasmic (LC3-I) signals revealed a significantly increased intensity of LC3-II punctate signals, representing autophagosomal structures (Kabeya *et al*., 2000; Kaminskyy *et al*., 2011), in *Rab35* icKO astrocytic cultures at steady state and under starvation conditions (Fig. 3-15f,g). These might indicate increased formation or impaired maturation and thus, degradation of autophagosomes. In agreement, a function of Rab35 in the maturation of autophagosomes is reported (Minowa-Nozawa *et al*., 2017). In contrast, the prominent down-regulation of LC3 protein levels is likely caused by hyperactivation of mTORC1. The complex inhibits the nuclear translocation of TFEB, a master transcription factor for LC3 and lysosomal biogenesis (Settembre *et al*., 2011; Martina *et al*., 2012). Despite of that, we could not detect any overt

alterations in compartments of the endo-/lysosomal system. EEA1-positive early endosomal, Rab7-positive late endosomal, LAMP-1-positive late endosomal/lysosomal and LAMP2-positive lysosomal compartments appeared normal in shape and abundance in *Rab35* icKO astrocytes (Fig. 3-16).

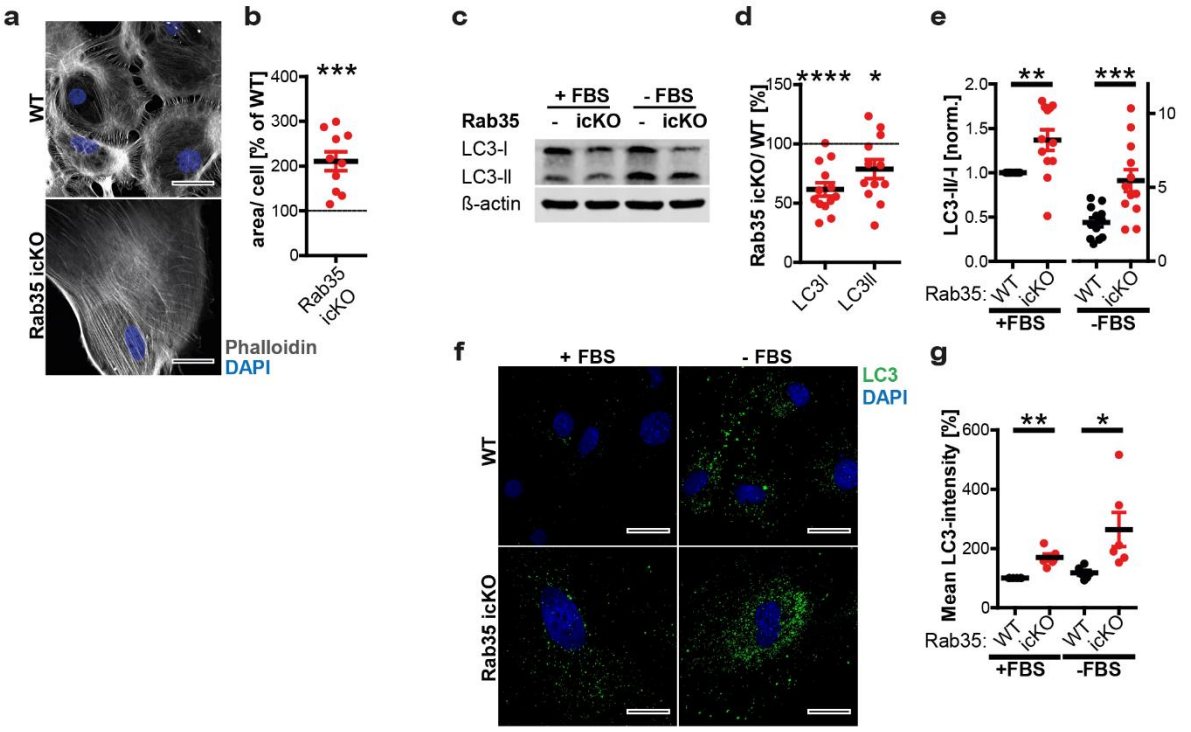

Figure 3-15: *Rab35* icKO astrocytes in culture have an increased cell area and elevated autophagosome levels. (a, b) The cell area of cultured astrocytes was visualized using Phalloidin-AlexaFluor568 (grey) and analyzed by confocal imaging. (a) Representative confocal images with DAPI (blue) to visualize cell nuclei, Scale bar: 30 µm. (b) Quantitative determination of the cell area, using Phalloidin as a mask and normalized to WT (100 %). (n = 10 independent experiments) **(c-e)** Reduced steady-state levels of LC3 are accompanied by an increased ratio of LC3-II/-I in Rab35 icKO astrocytes. (c) Representative immunoblot of lysates from *Rab35* WT and icKO cultures, supplemented with (+FBS) or without serum (-FBS) for 12 h before lysis, probed for cytosolic LC3-I and autophagosomal membrane-associated LC3-II, and ß-actin as loading control. (d) Quantification of steady state (+ FBS) LC3-I and LC3-II levels presented in c), normalized to the loading control and WT levels (100 %); (n = 13 (I) and 12 (II) independent experiments) (e) LC3-II/ LC3-I protein ratio, normalized to *Rab35* WT +FBS (=1) as a readout for autophagosome formation. Note the differently scaled y-axes for '+FBS' (left) and '-FBS' (right); (n = 12 independent experiments). **(f, g)** More autophagosomes in *Rab35* icKO cells. Astrocytic cultures were supplemented with or without FBS for 12 h before fixation and immunolabelled for LC3. (f) Representative confocal images with LC3-II (green) and DAPI-visualized cell nuclei (blue). Scale bar: 30 µm. (g) The mean LC3-II fluorescence intensity in Phalloidin-labelled cells, normalized to *Rab35* WT +FBS (100 %), is significantly increased in *Rab35* icKO cultures under both conditions; (n = 12 independent experiments). (mean ± SEM; one sample two-tailed student's t-test with a theoretical mean of 100 (b, d, g) or 1 (e), comparing genotypes in each condition; $^{*}p < 0.05$, $^{**}p < 0.01$; $^{***}p < 0.001$; $^{****}p < 0.0001$).

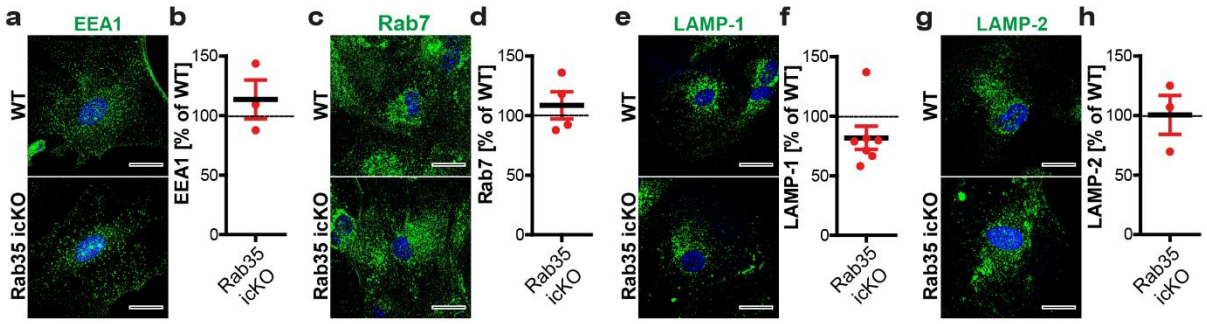

Figure 3-16: Rab35 loss does not cause major alterations in the endo-/lysosomal system. Representative confocal images and quantitative analysis of steady-state levels of **(a, b)** early endosomal antigen 1 (EEA1), **(c, d)** late endosomal Rab7, **(e, f)** late endosomal/ lysosomal LAMP-1, and **(g, h)** the lysosomal marker LAMP-2 (green) in *Rab35* WT and icKO astrocytic cultures. Sum intensities were normalized to the Phalloidin-labelled cell area and depicted as a fraction of *Rab35* icKO to WT signals (100 %); Scale bars: 30 µm; (mean ± SEM; n = 3 (EEA1), 4 (Rab7), 7 (LAMP-1) and 3 (LAMP-2) independent experiments; one sample two-tailed student's t-test with a theoretical mean of 100; EEA1: p = 0.4956, Rab7: p = 0.5061, LAMP-1: p = 0.1104, LAMP-2: p = 0.9769).

To corroborate the results obtained from HEK cells, we aimed to investigate if downregulation of MTMR2 elevates mTORC1 activity in cells of the nervous system as well. First, we confirmed the expression of MTMR2 in lysates of primary astrocytic cultures (Fig. 3-17a). Surprisingly, we could detect significantly reduced MTMR2 levels of 25 % on average in *Rab35* icKO compared to WT cells (Fig. 3-17b). A reduction in MTMR2 is also reported in tissue from *MTMR13* KO mice and *vice versa*, *MTMR2* KO mice display reduced protein levels of MTMR13 (Robinson *et al*., 2008; Ng *et al*., 2013). This is presumed to reflect a decreased protein stability in the absence of the MTMR complex partner and thus, a strong interdependence, which was also observed for other complex-forming MTMRs (Robinson *et al*., 2008; Zou *et al*., 2009, 2012; Gupta *et al*., 2013; Ng *et al*., 2013).

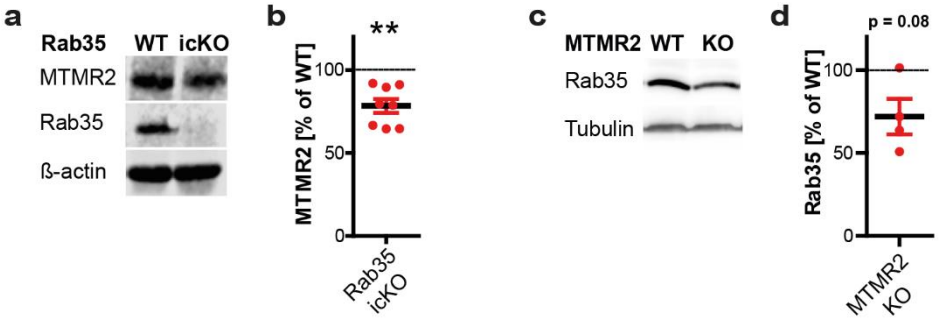

Figure 3-17: Interdependence of Rab35 and MTMR2 protein levels. (a, b) MTMR2 protein levels are reduced in *Rab35* icKO astrocytic cultures. (a) Representative immunoblot of MTMR2 and Rab35 detection. ß-actin was used as a loading control. (b) Quantification of MTMR2 protein levels in *Rab35* icKO astrocytes, normalized to the loading control and depicted as a fraction of WT levels (100 %); (n = 8 independent experiments). **(c, d)** Performed by the laboratory of Prof. Dr. A. Bolino (INSPE, Milan, Italy): Rab35 protein levels are reduced in *MTMR2* KO mice. Sciatic nerves from *MTMR2* WT (*MTMR2*$^{+/+}$) and KO (*MTMR2*$^{-/-}$) mice were lysed and analyzed by immunoblotting. (c) Representative immunoblot for Rab35, and tubulin as

a loading control. (d) Quantification of Rab35 level in *MTMR2* KO mice, with *MTMR2* WT levels set to 100 %; (n = 4 animals/ genotype); (mean ± SEM; one sample two-tailed student's t-test with a theoretical mean of 100; d: p = 0.079; $^{**}p < 0.01$).

Therefore, our data might indicate an interdependence of Rab35 and MTMR2 protein levels. Notably, this hypothesis was further strengthened by the observation, in collaboration with Prof. Dr. A. Bolino (INSPE, Milan, Italy), that *vice versa* Rab35 protein levels are reduced in tissue from *MTMR2* KO mice (Fig. 3-17c,d).

Next, we analyzed mTORC1-activation upon MTMR2 depletion in astrocytic cultures. By lentiviral transduction with MTMR2-targeting shRNA, protein levels were sufficiently reduced in these cells as well (Fig. 3-18a,b). Quantification of the p-S6K/ S6K ratio, as a readout for mTORC1 activation, revealed a 50 % mean increase in MTMR2 shRNA- compared to scrambled shRNA- transduced WT cultures. This increase was comparable to Rab35-depleted cultures, transduced with scrambled shRNA. In three out of six experiments, an further increase of p-S6K was observed in astrocytes depleted of both, MTMR2 and Rab35 (Fig. 3-18a,d). Nevertheless, AKT activation was notably unaffected by MTMR2 knockdown in both, *Rab35* WT and icKO cells (Fig. 3-18c).

In sum, these data confirm that MTMR2 represses mTORC1 activity independent of AKT activation in cells of the nervous system as well, similar to Rab35.

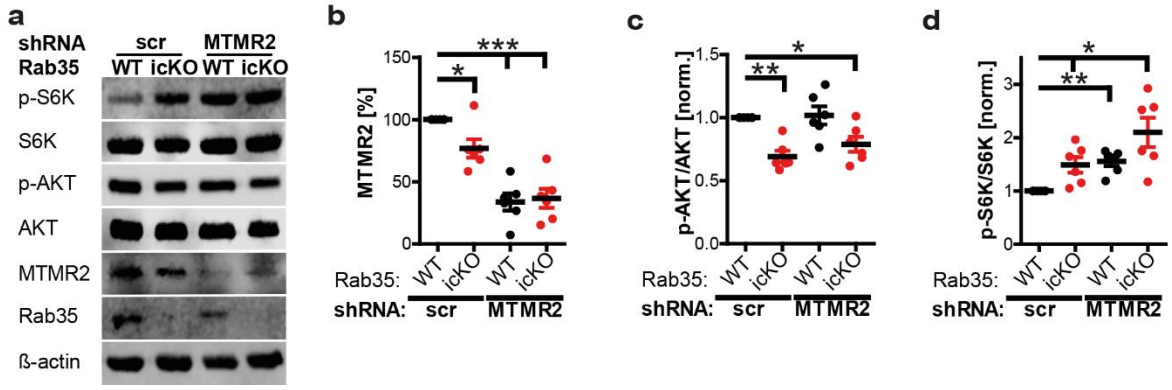

Figure 3-18: Loss of MTMR2 results in mTORC1 hyperactivity in primary astrocytic cultures. Lysates from lentiviral-transduced *Rab35* WT or icKO astrocytes with shRNA targeting MTMR2 or non-targeting scrambled (scr) control shRNA were analyzed by immunoblotting; (n = 6 independent experiments). **(a)** Representative immunoblot probed with antibodies for p-S6K, total S6K, p-AKT, total AKT, MTMR2 and ß-actin (loading control). **(b)** Efficacy of MTMR2 knockdown. MTMR2 levels are normalized to ß-actin and WT + scr control (100 %). **(c)** p-AKT/ AKT ratio, normalized to WT + scr control (= 1), is not altered upon MTMR2 knockdown (WT + MTMR2 shRNA: p = 0.8170). **(d)** pS6K/ total S6K ratio, normalized to WT + scr (= 1) as a readout for mTORC1 activity, is significantly increased upon MTMR2 knockdown in WT cells, comparable to the level in *Rab35* icKO (+scr) lysates. Double depletion of MTMR2 and Rab35 partially elevates mTORC1 activity; (mean ± SEM; one sample two-tailed student's t-test with a theoretical mean of 100 (b) or 1 (c,d), followed by p-value correction for multiple testing using Holm's Multiple Comparison Test; $^{*}p < 0.05$, $^{**}p < 0.01$; $^{***}p < 0.001$).

Next, in order to dissect whether increased mTORC1 activity *in vivo* is underlying the striking phenotype of focal hypermyelination in *Rab35* cKO^{SC} mice, sciatic nerves were lysed at postnatal day (P)30, after the peak of PNS myelination (P10-P21), and analyzed by immunoblotting. In *Rab35* cKO^{SC} nerves, both, phosphorylated S6K and its target the ribosomal protein S6 were increased by a mean of 50 % and 250 %, respectively (Fig. 3-19a,b). As expected from our *in vitro* data, the ratio of p-AKT/ AKT levels was unaltered (Fig. 3-19c). In addition, activation of the MAPK pathway component ERK, an alternative upstream activator of mTORC1 that is also implicated in myelin regulation (Ma *et al*., 2005; Newbern *et al*., 2011; ; Sheean et al., 2014; Furusho *et al*., 2017), was unchanged upon Rab35 depletion as well (Fig. 3-19b). These data confirm that Rab35 depletion in the PNS results in mTORC1 hyperactivity *in vivo*, independent of PI3K/AKT- and MAPK/ERK-dependent mTORC1 regulation.

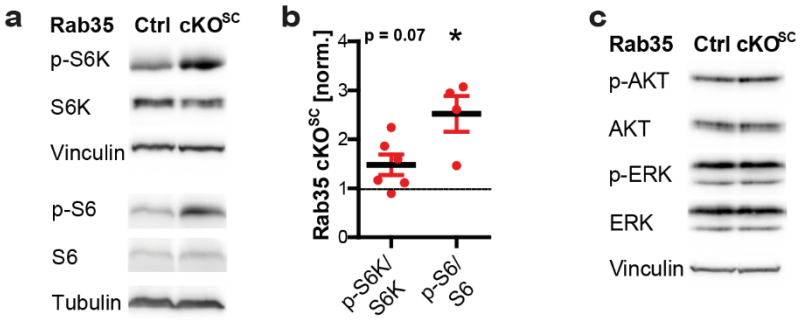

Figure 3-19: mTORC1 is hyperactivated *in vivo* in sciatic nerves from *Rab35* cKO^{SC} mice. Performed by the laboratory of Prof. Dr. A. Bolino (INSPE, Milan, Italy): Sciatic nerves from P30 *Rab35* Ctrl and cKO^{SC} mice were lysed and analyzed by immunoblotting. **(a)** Representative immunoblot for p-S6K, total S6K, p-S6 and total S6 as a readout for mTORC1 activity. Vinculin and Tubulin were used as loading controls. **(b)** Mean ratio of p-S6K/ S6K and p-S6/S6 in *Rab35* cKO^{SC} sciatic nerves, normalized to Ctrl (= 1), is 1.5-fold and 2.5-fold increased, respectively; (mean ± SEM; one sample two-tailed student's t-test with a theoretical mean of 1; p-S6K/ S6K: n = 6 animals/genotype, p=0.0706; p-S6/ S6: n = 4 animals/genotype, $^{*}p < 0.01$). **(c)** Immunoblot for p-AKT, total AKT, T202/Y204-phosphorylated ERK1/2 (p-ERK) and total ERK in sciatic nerve lysates. No alterations were observed. Vinculin was used as a loading control.

Next, we aimed to test the hypothesis that repression of mTORC1 activity is mediated by Rab35-dependent recruitment of active MTMR phosphatases. To that end, we analyzed mTORC1 activation upon overexpression of MTMR2 in cells depleted of MTMR2 or Rab35. Indeed, introducing an excess of siRNA-resistant mouse MTMR2 caused reduced hyperactivation of mTORC1 in form of ameliorated p-S6K/ S6K protein levels in MTMR2 and notably also Rab35 knockdown cells (Fig. 3-20a,b). These results indicate that Rab35 represses mTORC1 activity by the recruitment of active MTMR complexes.

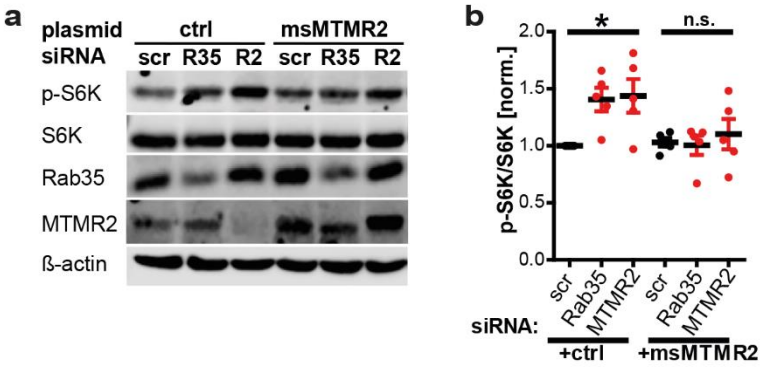

Figure 3-20: MTMR2 re-expression rescues mTORC1 hyperactivity caused by Rab35 reduction. Lysates of HEK cells depleted of Rab35 or MTMR2 by siRNA-mediated knockdown were transfected with plasmids encoding either eGFP (ctrl) or siRNA-resistant mouse MTMR2 (msMTMR2) and analyzed by immunoblotting. **(a)** Representative immunoblot for p-S6K, total S6K, Rab35 and MTMR2. ß-actin was used as loading control. **(b)** p-S6K/ total S6K, normalized to scr + ctrl (=1), is significantly increased for Rab35 and MTMR2 in ctrl- but not msMTMR2-overexpressing cells; (mean ± SEM; n = 5 independent experiments; one sample two-tailed student's t-test with a theoretical mean of 1 for targeting siRNA samples compared with scr within each overexpression condition, followed by p-value correction for multiple testing using Holm's Multiple Comparison Test; $^{*}p < 0.05$).

3.2.4 Accumulation of PI(3)-phosphates causes mTORC1 hyperactivity in the absence of Rab35

Active MTMR phosphatases possess specificity to dephosphorylate PI(3)P and PI(3,5)P_2 in complex with their pseudophosphatase partners (Caldwell *et al*., 1991; Kim *et al*., 2003b; Berger *et al*., 2006b; Zou *et al*., 2012). Thus, we hypothesized that impaired recruitment of MTMR phosphatases by Rab35 depletion could conceivably lead to imbalanced levels of these phosphatidylinositol (PI) species. As no functional probes for quantitative monitoring of PI(3,5)P_2 in eukaryotic cells are available so far (Hammond *et al*., 2015), we focused on PI(3)P. This lipid is detectable by the use of a PI(3)P-binding FYVE-tandem domain of Hrs, fused to eGFP (eGFP-2xFYVE) (Gillooly *et al*., 2003). Additionally, PI(3)P levels can also reflect imbalanced PI(3,5)P_2 abundance, as it serves as the only known precursor for its synthesis by PIKfyve (Sbrissa *et al*., 1999; Zolov *et al*., 2012). We used HeLa cells as a more convenient cell type for confocal microscopy than HEK cells, due to a better adhesion and shape preservation during immunocytochemistry. Importantly, siRNA-mediated depletion of Rab35 resulted in increased p-S6K level in HeLa cells as well (Fig. 3-21a). Next, we probed HeLa cells depleted of MTMR2 and Rab35 after fixation with recombinantly expressed eGFP--2xFYVE and subsequently immunolabelled the cultures with an antibody recognizing the eGFP-epitope (Hammond *et al*., 2009). As expected due to the knockdown of MTMR2, significantly increased PI(3)P levels were observed (Fig. 3-21b,c). We identified these puncta as PI(3)P-specific by acute inhibition of the main PI(3)P-synthesizing enzyme VPS34 using

10 µM VPS34-IN1 for 1 h prior to fixation, which completely abrogated the signal, in line with previous work (Bago *et al*., 2014). Strikingly, an increase in PI(3)P puncta was also observed in *Rab35* icKO primary astrocytic and oligodendrocytic cultures without simultaneous depletion of MTMR2 (Fig. 3-22). This indicates that the absence of Rab35 indeed causes an accumulation of PI(3)P, and maybe PI(3,5)P_2, which likely results from the impaired recruitment of 3'-phosphatases such as MTMR2.

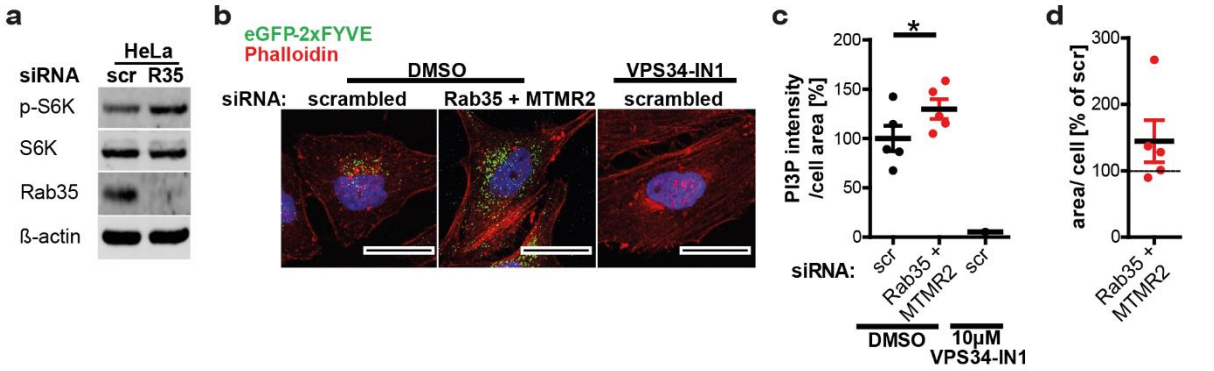

Figure 3-21: Elevated PI(3)P levels in HeLa cells depleted of Rab35 and MTMR2. (a) Immunoblot for Rab35, p-S6K and total S6K protein levels confirms upregulation of mTORC1 activity in HeLa cells depleted of Rab35 using siRNA-transfection. **(b, c)** HeLa cells were treated with non-targeting scrambled (scr) control siRNA or siRNAs specific for Rab35 and MTMR2, and immunolabelled for PI(3)P using recombinant eGFP-2xFYVE as a probe. As a control for specific labeling, 10 µM VPS34-IN1 was acutely applied to scr 1 h before fixation for acute VPS34 inhibition. (b) Representative confocal images of siRNA transfected HeLa cells stained for PI(3)P (green) and F-actin by fluorescently-labelled phalloidin (red); Scale bars: 30 µm. (c) Quantification of PI(3)P levels as the sum intensity of eGFP-2xFYVE-positive puncta normalized to the cell area and scr + DMSO control conditions (100 %). (d) Depleted HeLa cells tend to an increased cell area. Quantification of Phalloidin-masked cell area in Rab35- and MTMR2- co-depleted cells and normalized to scr. (mean ± SEM; n = 5 independent experiments; two-tailed paired student's t-test with a theoretical mean of 100; d: $p = 0.2340$; $^{*}p < 0.05$).

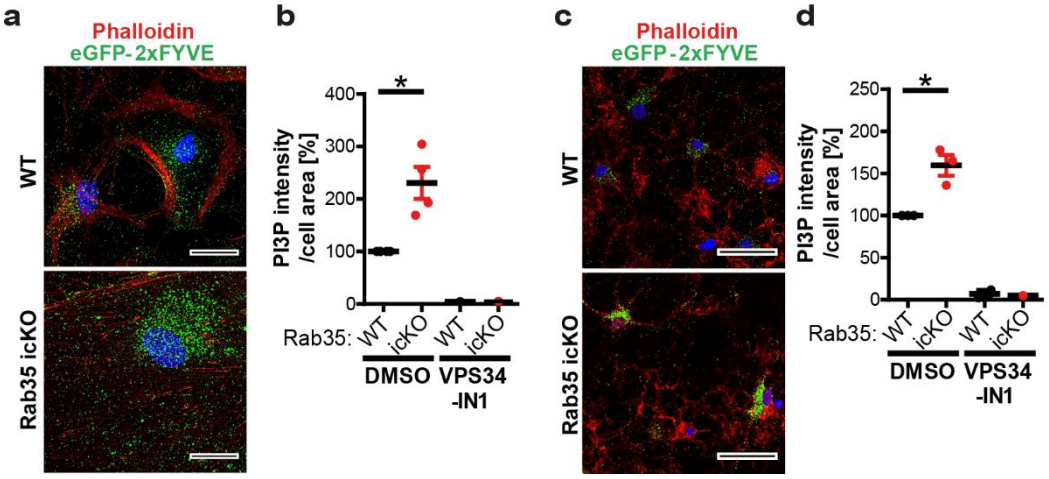

Figure 3-22: PI(3)P accumulation in primary *Rab35* icKO cells. Primary *Rab35* icKO cells were fixed and immunolabelled for PI(3)P (green) using recombinant eGFP-2xFYVE and F-actin (red). Representative confocal images of primary **(a)** astrocytic and **(c)** oligodendrocytic cultures; Scale bars: 30 µm. Quantification of mean PI(3)P fluorescence intensity, normalized to the cell area and WT cells (= 100 %) for **(b)** astrocytic cultures (n = 4 independent experiments) and **(d)** oligodendrocytic cultures (n = 3 independent

experiments). Acute VPS34 inhibition (10 µM VPS34-IN1) completely abrograted eGFP-2xFYVE puncta (n = 1 experiment each); (mean ± SEM; one sample two-tailed student's t-test with a theoretical mean of 100; $^{*}p < 0.05$).

MTMR2 is presumed to act on lipid levels at late endosomal/ lysosomal compartments (Cao *et al*., 2008). In addition, we had observed recruitment of the MTMR2-complex partner MTMR13 to these organelles by Rab35. Hence, we further investigated the PI(3)P levels specifically at these late endo-/ lysosomal sites by co-immunolabelling of HeLa cells for PI(3)P and the late endosomal marker protein CD63 (Kobayashi *et al*., 2000). Interestingly, PI(3)P levels at CD63-positive late endosomal compartments were significantly increased by around 25 % upon knockdown of either Rab35, MTMR2, or both (Fig. 3-23).

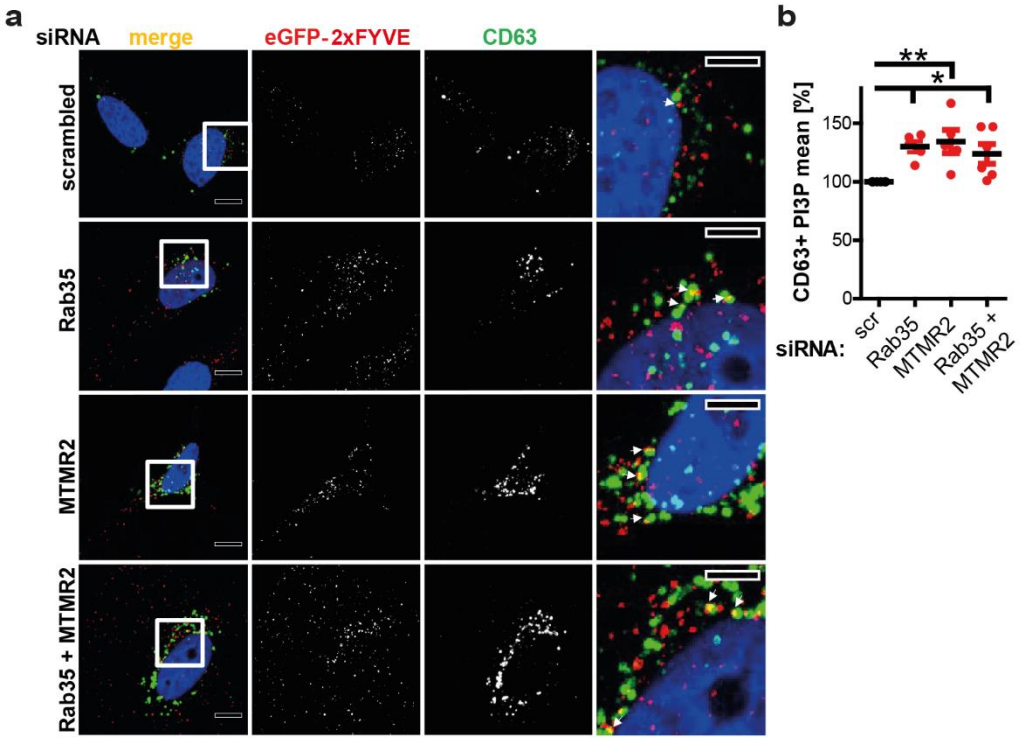

Figure 3-23: Depletion of Rab35 and/ or MTMR2 causes PI(3)P accumulation on late endosomes/ lysosomes. HeLa cells depleted of Rab35, MTMR2, or both, by siRNA-mediated knockdown, were immunolabelled for PI(3)P and the late endosomal/ lysosomal marker protein CD63, and analyzed by confocal imaging. **(a)** Representative confocal images of HeLa cells immunostained for PI(3)P (red) and CD63 (green). Cell nuclei were visualized with DAPI (blue). White arrows indicate examples of co-localization. Scale bars: 10 µm (left), 5 µm (right). **(b)** The mean intensity of PI(3)P in CD63-positive ($CD63^{+}$) compartments is depicted as a fraction of control cells (scr ; 100 %); (mean ± SEM; n = 5 independent experiments; one-way ANOVA followed by Dunnett's Multiple Comparison Test; $^{*}p < 0.05$; $^{**}p < 0.05$).

Given the fact that mTORC1 is recruited to and activated at late endosomal/ lysosomal organelles (Sancak *et al*., 2008; 2010), and both lipid substrates of the MTMR2 phosphatase,

PI(3)P and PI(3,5)P_2, are reported signaling lipids in PI3K/AKT-independent activation of mTORC1 (Byfield *et al*., 2005; Nobukuni *et al*., 2005; Jaber *et al*., 2011; Bridges *et al*., 2012; Jin *et al*., 2014; Mohan *et al*., 2016; Yoon *et al*., 2016; Hong *et al*., 2017), we hypothesized that hyperactivation of mTORC1 in MTMR2- and Rab35-depleted cells is due to the observed imbalance of PI(3)P levels. According to this hypothesis, normal activation of mTORC1 should be re-stored by interfering with the cellular PI(3)P production. To test this, we first depleted PI(3)P levels in *Rab35* WT and icKO astrocytic cultures using acute inhibition of VPS34 by treatment with 5 µM or 10 µM VPS34-IN1 for 1 h and analyzed mTORC1 activation. Strikingly, the significant increase in p-S6K/ S6K protein levels in *Rab35* icKO compared to WT lysates in control conditions was completely abrogated upon treatment with VPS34-IN1 (Fig. 3-24a,b). The same effect was observed upon treatment of cultures with two other specific VPS34 inhibitors, SAR405 (Ronan *et al*., 2014) or Compound-19 (Bilanges *et al*., 2017) (Fig. 3-24a). Moreover, WT-comparable mTORC1 activity was also re-stored by acutely treating *Rab35* icKO astrocytic cultures with VPS34-IN1, which were simultaneously depleted of MTMR2, (Fig. 3-24c,d). This finding indicates that the accumulation of PI(3)-phosphates in the absence Rab35 and MTMR2 could be the underlying cause for mTORC1 hyperactivity.

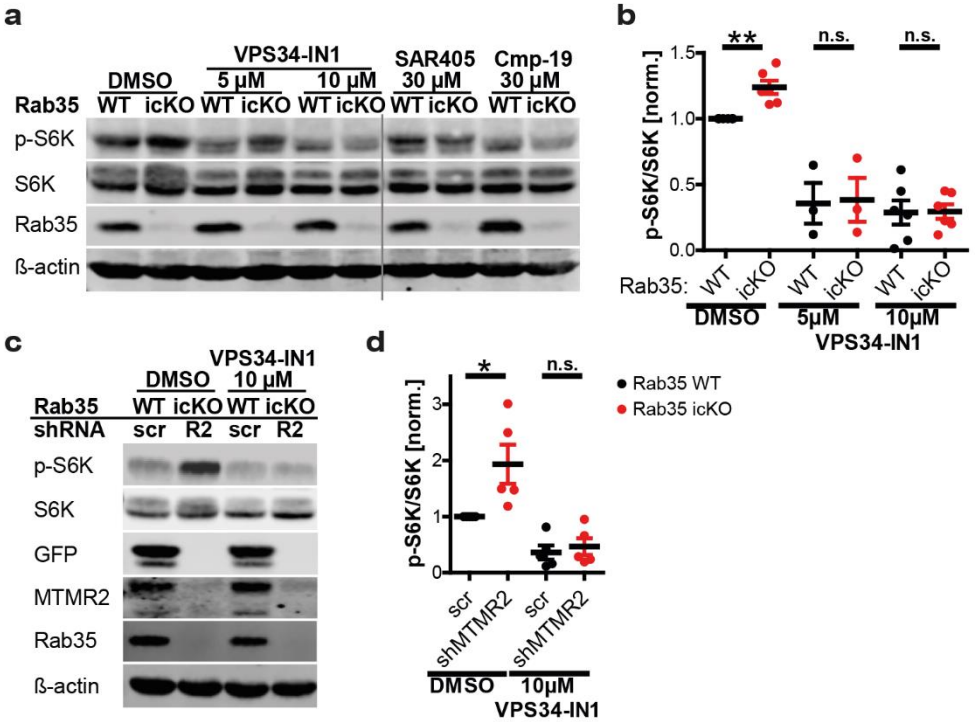

Figure 3-24: Pharmacological inhibition of PI(3)-phosphate synthesis rescues mTORC1 hyperactivity upon Rab35- and MTMR2-depletion. (a,b) Inhibition of VPS34-dependent PI(3)-phosphate synthesis rescues mTORC1 hyperactivity in *Rab35* icKO astrocytes. Astrocytic cultures were treated with indicated concentrations of the selective VPS34 inhibitors VPS34-IN1, SAR405, or Compound-19 (Cmp-19) or with DMSO for 1 h prior to lysis. (a) Lysates were analyzed by immunoblotting for Rab35, total S6K and pS6K as a readout for mTORC1 activity. ß-actin was used as a loading control. (b) The significant increase in the ratio of p-S6K to total S6K, normalized to WT cells (= 1) in *Rab35* icKO cells is ameliorated upon inhibitor

treatments; (n = 6 (10 µM VPS34-IN1) and 3 (5 µM VPS34-IN1) independent experiments). **(c, d)** VPS34 inhibition rescues mTORC1 hyperactivation in Rab35- and MTMR2-depleted primary astrocytes. Astrocytic cultures were transduced with lentiviruses containing non-targeting scrambled (scr) control shRNA (co-expressing eGFP) or shRNA targeting MTMR2, treated with DMSO or 10 µM VPS34-IN1 for 1 h before lysis, and analyzed by immunoblotting. (c) Representative immunoblots for p-S6K, S6K, eGFP (scr), MTMR2 and Rab35. (g) Quantification of p-S6K/ S6K, normalized to control (WT + scr + DMSO = 1); (n = 5 independent experiments); (mean ± SEM; one sample two-tailed student's t-test with a theoretical mean of 1, comparing the genotypes in each treatment condition; $^{*}p < 0.05$; $^{**}p < 0.01$).

So far, our data reveal a novel physiological pathway in which Rab35-mediated recruitment of active MTMR complexes to lysosomes limits mTORC1 activity by dephosphorylating PI(3)P, and likely PI(3,5)P_2, which serve as a platform for the recruitment and activation of the cell signaling complex.

3.2.5 Counteracting mTORC1 hyperactivity ameliorates myelin abnormalities upon Rab35 depletion

mTORC1 has a dual role in Schwann cells. It inhibits the cell cycle exit and is reported to repress KROX20 on the one hand, and promotes myelin lipid synthesis and myelin protein expression on the other (Norrmén *et al*., 2014; Beirowski et al., 2017; Figlia *et al*., 2017; Jiang *et al.*, 2018). Thus, mTORC1 activity in Schwann cells must be physiologically tightly regulated and alterations result in time- and dosage-dependent effects (Figlia *et al.*, 2018).

To corroborate the hypothesis that mTORC1 activity is causative for the observed focal hypermyelination in *Rab35* cKO^{SC} mice, our collaboration partners (Prof. Dr. A. Bolino, INSPE, Italy) prepared embryonic explants of myelin-forming Schwann cell/dorsal root ganglion (DRG) neuron co-cultures, and analyzed axonal myelination in the absence of Rab35 *ex vivo*. Surprisingly, the number of MBP-positive myelin segment was reduced to 40 % in *Rab35* cKO^{SC} explants (Fig. 3-25c,d). Furthermore, more than 50 % of the MBP-positive fibers possessed structural myelin abnormalities in *Rab35* cKO^{SC} co-cultures (Fig. 3-25e,f), reminiscent of *in vitro* myelin outfoldings in *MTMR2* and *MTMR13* KO explants (Bolis *et al*., 2009; Robinson *et al*., 2018). Importantly, when co-cultures were treated with Rapamycin, a specific mTORC1-component FKBP12 inhibitor (Sehgal *et al*., 1975; Sabatini *et al*., 1994), the reduced abundance of myelin segments was fully rescued and aberrant myelin formation strikingly ameliorated (Fig. 3-25d,f). This confirms that increased mTORC1 underlies the altered myelin homeostasis in *Rab35* cKO^{SC} explants.

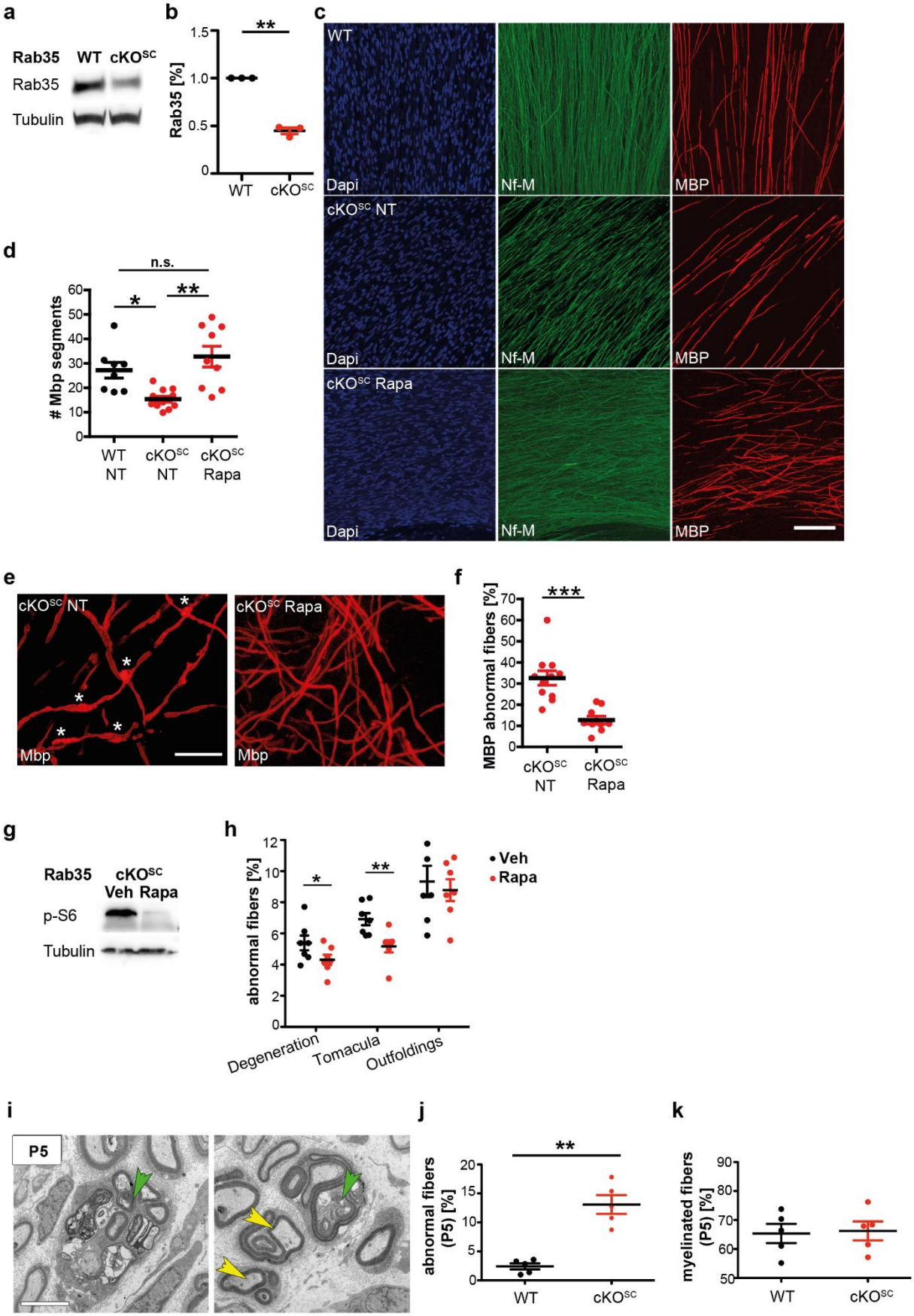

Figure 3-25: Repression of mTORC1 hyperactivity ameliorates aberrant myelination in the absence of Rab35 ex vivo and in vivo. Performed by the laboratory of Prof. Dr. A. Bolino (INSPE, Milan, Italy): Schwann cell/ DRG neuron co-culture explants were prepared from *Rab35* Ctrl and cKO^{SC} mouse embryos. **(a, b)** Loss of Rab35 in co-culture explants. (a) Representative immunoblot for Rab35 and Tubulin as control

protein. (b) Rab35 protein levels, normalized to Tubulin and WT levels (= 100 %); (mean ± SEM; n = 6 coverslips/DRG explants; one sample two-tailed student's t-test with theoretical means of 100; $^{**}p < 0.01$). **(c, d)** *Rab35* WT and cKO^{SC} mouse explants were fixed and immunolabelled. (c) Representative confocal images of Myelin-forming Schwann cell/ DRG neuron co-culture explants, with axonal marker Nf-M (green), myelin segment marker MBP (red) and DAPI (blue) to visualize Schwann cell nuclei. Scale bar: 7 µm (d) The number of MBP-positive myelin segments is reduced by 40 % in untreated (NT) *Rab35* cKO^{SC} co-culture explants compared to WT cultures. Rapamycin treatment (Rapa) of *Rab35* cKO^{SC} co-cultures rescued the number of myelin segments; (mean ± SEM; n = 12 (WT), 10 (cKO^{SC} – NT) and 8 (cKO^{SC} +Rapa) coverslips/DRG explants; two-tailed paired student's t-test; $^{*}p < 0.05$, $^{**}p < 0.01$). **(e, f)** Myelin abnormalities in *Rab35* cKO^{SC} are ameliorated by treatment with Rapamycin. (e) Higher magnification images of MBP staining in untreated and Rapamycin-treated *Rab35* cKO^{SC} cells. Asterisks mark myelin abnormality examples. Scale bars: 4 µm (f) The fraction of MBP-positive fibers carrying myelin abnormalities, with a mean of 50 % in *Rab35* cKO^{SC} –NT cultures, was reduced to 30 % in cKO^{SC} +Rapa; (mean ± SEM; n = 6 coverslips/DRG explants; two-tailed paired student's t-test; $^{***}p < 0.001$). **(g, h)** Focal hypermyelination in *Rab35* cKO^{SC} sciatic nerves is ameliorated upon Rapamycin treatment *in vivo*. (g) Repressed mTORC1 activation by Rapamycin treatment in sciatic nerves. Immunoblot for p-S6 in sciatic nerve lysates from *Rab35* cKO^{SC} mice treated with vehicle (Veh) or Rapamycin (Rapa). (h) Semithin section analysis of sciatic nerves from *Rab35* cKO^{SC} mice (P70) following vehicle or Rapamycin treatment and quantification of the percentage of fibers carrying myelin degenerations, tomacula or myelin outfoldings; (mean ± SEM; n=7 animals from each genotype; two-tailed non-parametric Mann-Whitney test; $^{*}p < 0.05$, $^{**}p < 0.01$). **(i-k)** Ultrastructural analysis of sciatic nerves at P5. (i) Representative image of *Rab35* cKO^{SC} sciatic nerves with myelin degenerations (green arrows) and myelin outfoldings (yellow arrows) already at P5; Scale bar: 4 µm. (j) *Rab35* cKO^{SC} sciatic nerves contain an increased fraction of abnormal fibers; (mean ± SEM; n = 5 animals/ genotype; two-tailed Mann-Whitney t-test; $^{**}p < 0.01$). (k) The fraction of myelinated fibers is not altered; (n = 5 animals /genotype; two-tailed Mann-Whitney t-test; p = 0.84).

In order to substantiate these findings *in vivo*, *Rab35* cKO^{SC} animals were treated with 10 mg Rapamycin per kg of body weight. Treatment was started at P12, the earliest time point, when animals were yet able to tolerate the long-term drug application. Ultrastructural analysis of sciatic nerves from *Rab35* cKO^{SC} at P70 revealed an amelioration of focal hypermyelination, particularly a significantly reduced proportion of fibers displaying tomacula and myelin degeneration (Fig. 3-25g,h). In contrast to the *in vitro* observation, myelin outfoldings were unchanged in nerves of Rapamycin-treated *Rab35* cKO^{SC} mice. Crucially, the analysis of sciatic nerves at P5 revealed an early onset of focal hypermyelination upon loss of Rab35 (Fig. 3-25i,j). As Rapamycin was applied from P12 on only, manifestation of the phenotype at that early age might be an explanation for incompletely restored myelin homeostasis in Rapamycin-treated *Rab35* cKO^{SC} mice. Earlier treatment with this inhibitor at the used dose was so far lethal. Interestingly, *in vivo*, the number of myelinated fibers in was unaltered between the genotypes (Fig. 3-25g,h).

Nevertheless, these data reveal Rab35 as an important regulator of PNS myelination, and, in agreement with our findings from other cell types *in vitro*, show that loss of Rab35 results in elevated mTORC1 activity in Schwann cells. In addition, mTORC1

hyperactivity contributes to the observed impairment of myelin homeostasis in form of focal hypermyelination in *Rab35* cKO^{SC} sciatic nerves *in vivo* and aberrant myelination *ex vivo*.

3.2.6 Interfering with PI(3)-phosphate synthesis rescues mTORC1 hyperactivity and abnormal myelin protein expression in primary cultures of *Rab35* icKO Schwann cells

Focal hypermyelination, as seen in the absence of Rab35 *in vivo* is not only a phenotypical hallmark in sciatic nerves from adult mice with mTORC1 hyperactivation (Goebbels *et al*., 2012; Beirowski *et al*., 2017; Figlia *et al*., 2017) but also from *MTMR2* KO or *MTMR13* KO animals (Tersar *et al*., 2007; Robinson *et al*., 2008; Bolino *et al*., 2004; Ng *et al*., 2013). Moreover, myelin outfoldings are observed in organotypic explants of both, *MTMR2* and *MTMR13* KO animals (Bolis *et al*., 2009; Robinson *et al*., 2018). In agreement with our data from several cell types *in vitro*, we presumed that impaired recruitment of active MTMR phosphatase complexes contributes to the observed impairment of the myelin homeostasis in the absence of Rab35. To test this hypothesis, we made use of primary Schwann cells from *Rab35* icKO mice, induced for knockout and differentiation with tamoxifen and ascorbic acid, respectively. Due to the limited amount of material in these cultures, we analyzed mTORC1 activation by immunolabelling for p-S6 and S6 protein levels. This approach revealed the expected increase in the ratio of p-S6 over S6 protein levels as a readout for mTORC1 activity in primary Schwann cells from *Rab35* icKO animals (Fig. 3-26a,b), as also recapitulated in primary astrocytic cultures (Fig. 3-26c,d). Accordingly, chronical inhibition of mTORC1 by application of 15 nM Rapamycin for six days sufficiently diminished p-S6 protein levels in *Rab35* WT and icKO Schwann cells (Fig. 3-26a,b). In addition, immunolabelling using eGFP-2xFYVE(Hrs) probe revealed increased PI(3)P levels in *Rab35* icKO Schwann cells, indicating an impaired PI(3)-phosphatase function in these cells as well (Fig. 3-27a,b). In contrast, PI(4)P levels were not altered (Fig. 3-27c,d).

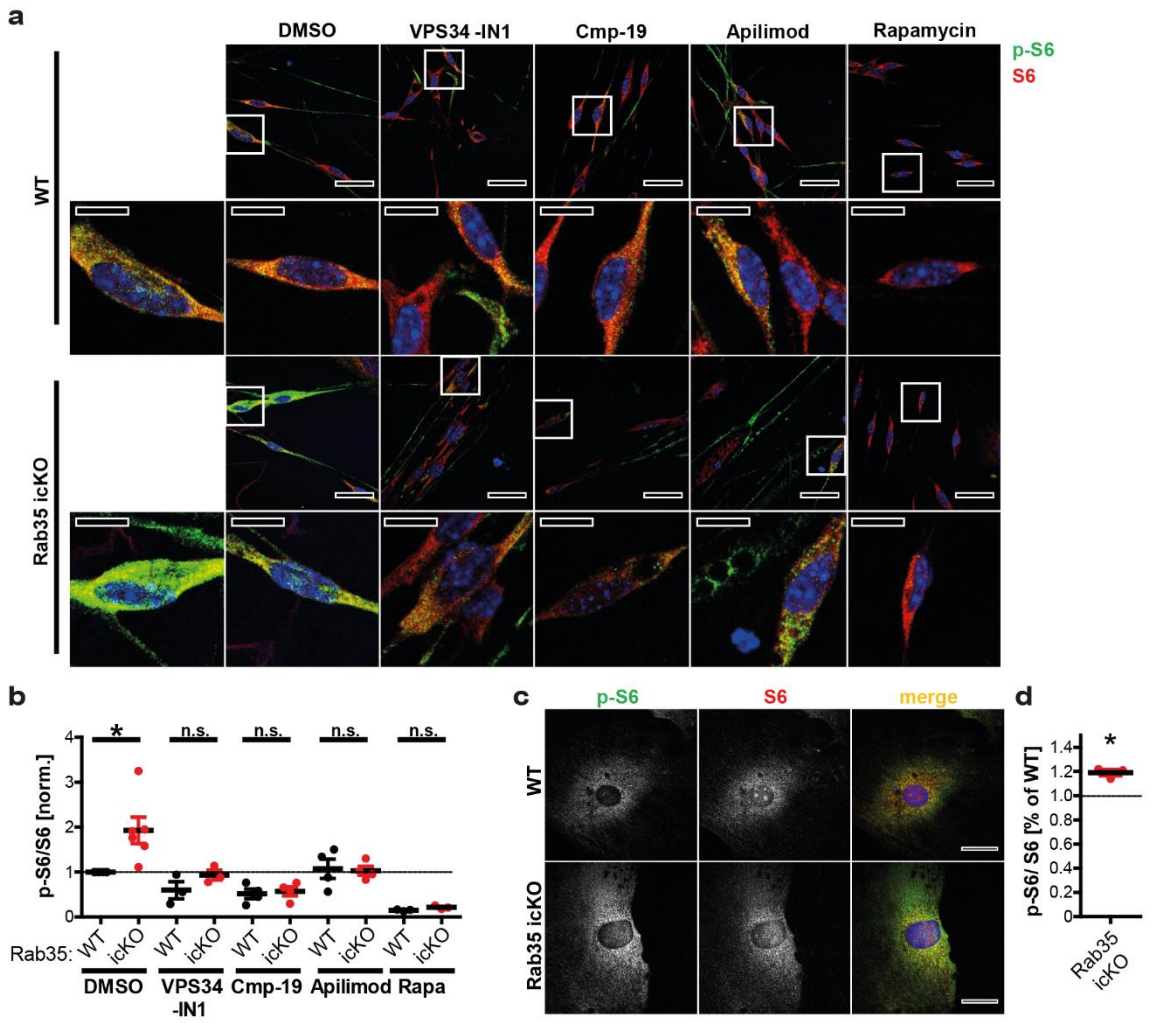

Figure 3-26: Repression of mTORC1 hyperactivity by interfering with PI(3)-phosphate synthesis in Rab35-depleted primary Schwann cells. (a,b) Primary Schwann cell cultures, prepared from tamoxifen-inducible *Rab35* icKO (*Rab35*$^{Fl/Fl}$ x *Cre*^{ER}) and WT (*Rab35*$^{Fl/Fl}$) mice, were induced for knockout and differentiation at DIV3, and chronically supplemented with DMSO, 1 µM VPS34-IN1, 2.5 µM Cmp-19, 50 nM Apilimod or 15 nM Rapamycin (Rapa) from DIV5 until fixation and subsequent immunolabelling at DIV11. (a) Representative confocal images of Schwann cells supplemented with DMSO or inhibitors, and immunolabelled for ribosomal p-S6 (green) and S6 (red) protein. Areas marked by white squares in upper images (scale bars: 30 µm) are shown as insets below (scale bars: 10 µm). (b) Quantification of mTORC1 activity by the ratio of p-S6 to S6 mean intensity in SC somata, normalized to WT + DMSO control (=1). Significantly increased mTORC1 activity in *Rab35* icKO Schwann cells is rescued in all inhibitor conditions; (n = 6 (DMSO), 4 (Cmp-19, Apilimod) and 3 (VPS34-IN1, Rapa) independent experiments). **(c, d)** Increased p-S6/ S6 protein levels in *Rab35* icKO astrocytes as a readout for mTORC1 hyperactivity. (c) Confocal images of *Rab35* WT and icKO astrocytes immunostained for p-S6 (green) and total S6 (red); Scale bar, 30 µm. (d) p-S6/ S6 ratio in Phalloidin-masked cells normalized to WT (100 %), is increased in *Rab35* icKO cells; (n= 3 independent experiments). (mean ± SEM;; one sample two-tailed student's t-test with a theoretical mean of 1, comparing the genotypes in each condition; *p < 0.05).

Our data so far indicated that accumulation of the MTMR substrate PI(3)P could be the underlying cause of increased mTORC1 activation in the absence of Rab35 and MTMR2. In order to finally test this hypothesis in Schwann cells we chronically treated *Rab35* WT and

icKO cultures with VPS34-IN1 or Compound-19 to interfere with PI(3)P and eventually $PI(3,5)P_2$ synthesis (Ikonomov et al., 2015). In addition, we made use of chronical treatment with the specific PIKfyve-inhibitor Apilimod to selectively block the $PI(3,5)P_2$ production (Gayle *et al.*, 2017). In agreement with our previous findings, VPS34-inhibitors evidently abrogated PI(3)P levels (Fig. 3-27b) and reduced mTORC1 activity to WT levels in *Rab35* icKO Schwann cells as well (Fig. 3-26b). Inhibition of PIKfyve caused an elevation of PI(3)P levels in both, *Rab35* WT and icKO Schwann cells (Fig. 3-27b), in agreement with the role of this lipid as a precursor for $PI(3,5)P_2$. In contrast, mTORC1 activity was also restored to WT levels in *Rab35* icKO SC cultures treated with Apilimod (Fig. 3-26b). These data indicate that mTORC1 hyperactivity upon Rab35 depletion is rather not elicited by the observed accumulation of PI(3)P but instead by simultaneously elevated $PI(3,5)P_2$ levels in Schwann cells.

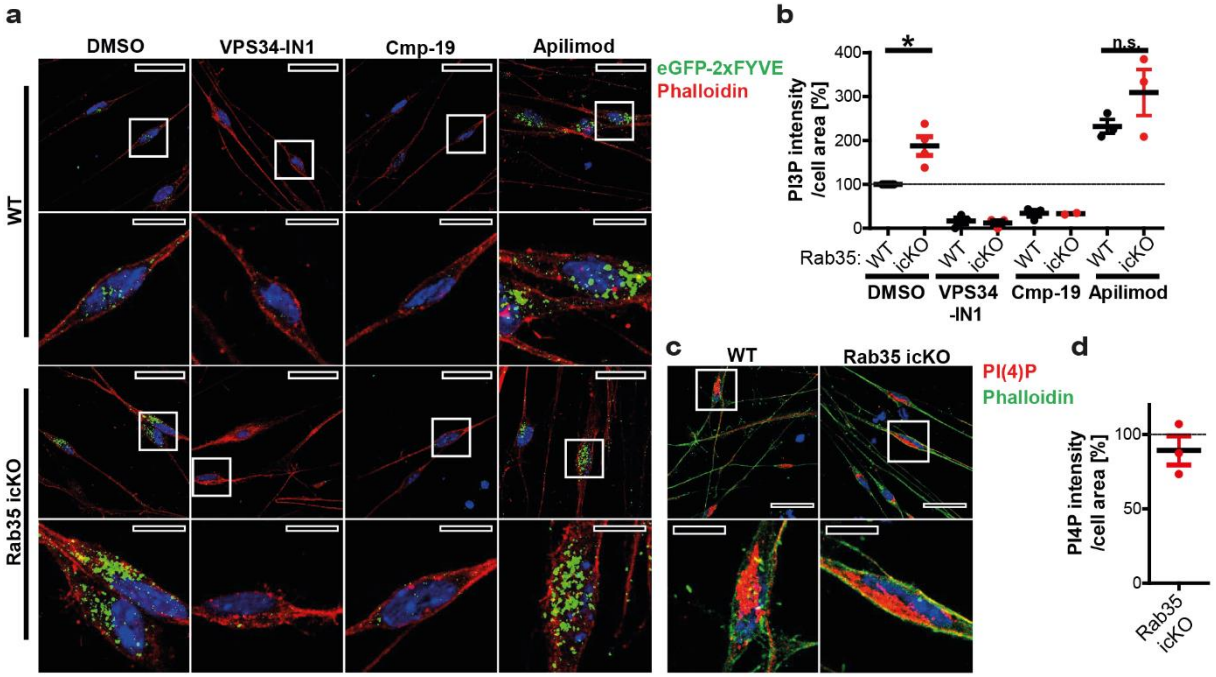

Figure 3-27: Elevated PI(3)P levels in Schwann cells depleted for Rab35. (a,b) Primary Schwann cell cultures were treated chronically with DMSO or 50 nM Apilimod for six days, or acutely (1 h) with 10 µM VPS34-IN1 or 10 µM Cmp-19 prior to fixation with subsequent immunolabelling for PI(3)P. (a) Representative confocal images of differentiated Schwann cells, immunolabelled for PI(3)P using eGFP-2xFYVE (green) and cell bodies using fluorescent phalloidin (red). Areas marked by white squares in upper images (scale bars: 30 µm) are shown as insets below (scale bars: 10 µm). (b) Quantification of PI(3)P sum intensity, normalized to the somata area and WT + DMSO control (100 %); (n = 4 (DMSO) and 3 (Apilimod) independent experiments). **(c, d)** Rab35 depletion does not alter the levels of PI(4)P in Schwann cells. (c) Representative confocal images of Schwann cells in culture, immunostained with an antibody against PI(4)P (red). Cell bodies were labelled using fluorescent phalloidin (green); Scale bars: 30 µm (upper), 10 µm (lower images). (d) The sum intensity of PI(4)P-positive puncta in *Rab35* icKO Schwann cell somata, normalized to the somata area and *Rab35* WT cells (100 %), is unaltered ($p = 0.3854$); (n = 3 independent experiments). (mean ± SEM; one sample two-tailed student's t-test with a theoretical mean of 100, comparing the genotypes in each condition; $^{*}p < 0.05$).

So far, we could observe hypomyelination in *Rab35* icKO coculture explants with early, embryonically induction of Rab35 depletion. These results would be in line with the dual role of mTORC1 in repressing differentiation induction on the one hand, and promoting myelin lipid and protein synthesis on the other (Norrmen et al., 2017; Beirowski *et al*., 2017; Figlia *et al*., 2017). Thus, we aimed to reveal the effect of late Rab35 knockout induction on myelin protein levels in Schwann cells upon simultaneous induction of differentiation and Cre-recombination. Mono-cultures of Schwann cells usually express low amounts of myelin proteins as they are not able to form "*in vitro*" myelin sheets as cultured oligodendrocytes (Arthur-Farraj *et al*., 2011; Liu *et al*., 2015b). In agreement, we observed low levels of fluorescent signals in WT SC cultures immunolabelled for myelin protein 0 (P0), one of the major myelin components in the PNS (Shy *et al*., 2006) (Fig. 3-28). Interestingly, in *Rab35* icKO cultures a high proportion of cells with strikingly elevated P0 protein levels were observed. Upon chronical treatment with Rapamycin, the mean P0 levels were indeed reduced to WT levels in *Rab35* icKO cells. Importantly, this effect was also rescued by interfering with PI(3)-phosphate synthesis using VPS34-IN1, Cmp-19 or Apilimod (Fig. 3-28b), presumably by the indirect repression of mTORC1 activation as observed under these conditions. In sum, these data indicate that Rab35 depletion in differentiated Schwann cells causes an increase in myelin protein levels *in vitro*, consistent with the myelin promoting function of mTORC1, once differentiation is induced (Beirowsky *et al*., 2017; Figlia *et al*., 2017). It additionally suggests that the observed reduction of mTORC1 repression in these cells is mainly due to an accumulation of the MTMR-phosphatase substrate $PI(3,5)P_2$.

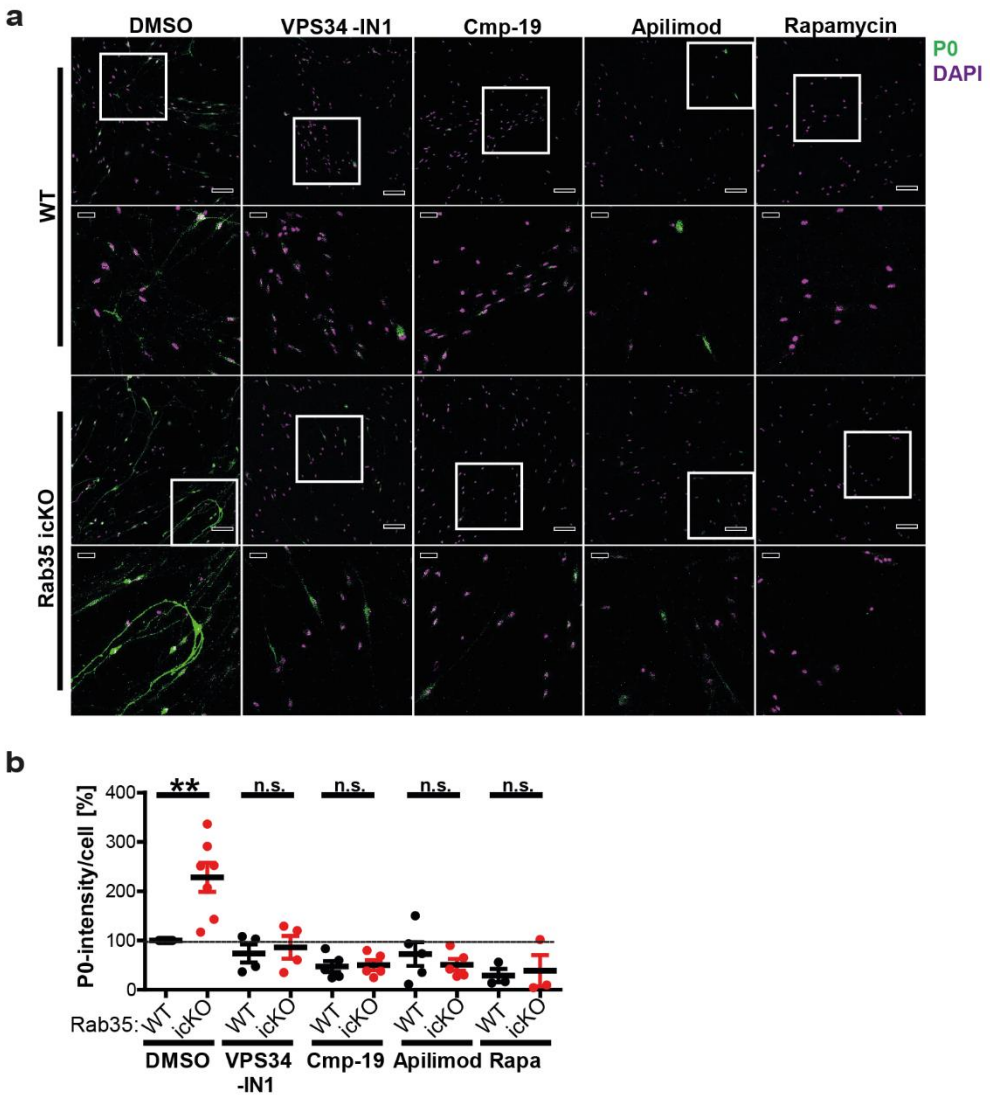

Figure 3-28: Increased myelin protein expression in *Rab35* icKO Schwann cell cultures is rescued by inhibition of mTORC1, VPS34 or PIKfyve. Primary Schwann cell cultures, induced for knockout and differentiation, were treated chronically with DMSO, 1 µM VPS34-IN1, 2.5 µM Cmp-19, 50 nM Apilimod or 15 nM Rapamycin (Rapa) for six days. Cells were fixed and immunostained. **(a)** Representative confocal images of *Rab35* WT and icKO cells immunolabelled for P0 (green). The total number of cells was visualized using DAPI (magenta). Areas marked by white squares in upper images (scale bars: 100 µm) are shown as insets below (scale bars: 30 µm). **(b)** Quantification of the sum P0 fluorescence intensity divided by the cell number, and normalized to WT + DMSO controls (100 %); (mean ± SEM; n = 7 (DMSO), 5 (Cmp-19, Apilimod), 4 (VPS34-IN1) and 3 (Rapa) independent experiments; one sample two-tailed student's t-test with theoretical means of 100 comparing WT and KO in each treatment condition; $^{**}p < 0.01$).

Collectively, our data identify Rab35 as a novel regulator of PNS myelination and reveal that elevated mTORC1 activity contributes to the impaired PNS myelin homeostasis upon loss of Rab35 *in vivo*, *ex vivo* and *in vitro*. Furthermore, repression of mTORC1 activity by Rab35 is likely mediated by PI(3)-phosphate regulation through the recruitment of active MTMR phosphatases complexes.

4. Discussion

This work unravels a novel function of Rab35 in the control of PNS myelin homeostasis. We demonstrate that loss of the small GTPase leads to a crucial impairment of Schwann cell myelination *in vivo* and *in vitro*. Furthermore, we identified Rab35 as a repressor of mTORC1 activity, which contributes to the regulation of myelin homeostasis. This action is mediated by the conversion of PI(3)-phosphates through Rab35-dependent recruitment of MTMR lipid phosphatase complexes. We observed this mechanism in different cell types, including primary cell cultures of the nervous system. Specifically in cultured Schwann cells, interfering with $PI(3,5)P_2$ synthesis ameliorates not only mTORC1 hyperactivation upon loss of Rab35 but also aberrant myelin protein levels. These data reveal insights how dysregulated PI(3)-phosphate conversion can lead to severe demyelination as displayed in CMT-disease types 4B, and thus might have therapeutic implications for the treatment of peripheral neuropathies.

4.1 Rab35 is a novel repressor of mTORC1 and controls PNS myelin homeostasis

4.1.1 mTORC1 hyperactivity in the absence of Rab35 affects PNS myelin homeostasis

Perturbances in the regulation of mTORC1 and thus dysregulation of cell metabolism is the underlying cause for several diseases, including cancer and neurodegeneration (Laplante and Sabatini, 2012; Tatebe and Shiozaki, 2017). In peripheral nerves, mTORC1 promotes proliferation of Schwann cell (SC) precursors, radial sorting of axons by immature SCs and myelin growth (Norrmén *et al.*, 2014; Figlia *et al.*, 2017). In SCs, mTORC1 is mainly activated via MAPK/ERK and PI3K/AKT signaling downstream of axonal NRG1-ligand binding to Schwann cell ErbB2/B3 receptors (Goebbels *et al*., 2012; Heller *et al*., 2014; Belin *et al.*, 2018). Expression levels of ErbB3, ERK and AKT are downregulated during the maturation of nerves, from the first to the second postnatal week in mice when myelin growth reaches a plateau (Sheean *et al*., 2014). Similarly, mTORC1 activity declines during that time and remains at relatively low levels throughout further development (Heller *et al.*, 2014; Figlia *et al.*, 2017; Beirowski *et al.*, 2017) (Figure 4-1). This mechanism seems to ensure proper axonal myelination by limiting further myelin growth. In accordance, abnormally high mTORC1 activity during adulthood results in excessive myelin growth with focal hypermyelination (Goebbels *et al*., 2012; Beirowski *et al.*, 2017; Figlia *et al.*, 2017; Jiang *et al.*, 2018). Interestingly, in disease mouse models with insufficient myelin formation, hypomyelination is ameliorated by overexpression of ErbB-activating NRG1-III or pharmacological suppression of the NRG1-III-inactivating ß-secretase ADAM17/TACE

(Scapin *et al*., 2018; Belin *et al.*, 2018). In turn, focal hypermyelination in mouse models of Charcot-Marie-Tooth (CMT) disease type 4B1 or Hereditary Neuropathy with liability to pressure palsies (HNPP) is rescued by pharmacological TACE activation (Bolino *et al*., 2016). *Rab35* cKO^{SC} mice display not only progressive focal hypermyelination (Figure 3-12), but also mTORC1 hyperactivation *in vivo* (Figure 3-19a,b). Interfering with mTORC1 activity in these mice by rapamycin treatment partially ameliorated the abundance of aberrantly myelinated fibers (Figure 3-25g,h). In agreement, the SC-specific ablation of PTEN, a negative regulator of mTORC1 activation, results in focal hypermyelination, and is ameliorated by rapamycin treatment (Goebbels *et al*., 2012). Similarly, tomacula and myelin outfoldings are observed upon genetic inactivation of TSC1 in Schwann cells (Beirowski *et al.*, 2017). Moreover, elevated MAPK/ERK signaling in SCs results in mTORC1 hyperactivity, focal hypermyelination and an increase in the myelin thickness, whereas the latter is partially mediated by mTORC1-independent ERK-targets (Sheean *et al.*, 2014). As neither AKT- nor ERK-activity was elevated in *Rab35* cKO^{SC} mice (Figure 3-19c), our data further strengthen previous suggestions that increased mTORC1 activation is the underlying cause for focal hypermyelination in transgenic mice with upregulated MAPK/ERK- or PI3K/AKT-signaling in SCs. Excessive myelin growth due to elevated mTORC1 activity can be explained by its regulatory function in the synthesis of lipids. mTORC1 promotes the activation, trafficking and maturation of SREBP transcription factors and thus, regulates the expression of enzymes involved in the lipid, fatty acid and cholesterol synthesis in different cell types (Porstmann *et al*., 2008; Düvel *et al.*, 2010; Li *et al.*, 2010; Peterson *et al*., 2011; Han *et al.*, 2015b), as well as in Schwann cells (Norrmén *et al.*, 2014). The potential upregulation of these enzymes remains to be investigated in *Rab35* cKO^{SC} mice. However, g-ratios are mainly unaltered in *Rab35* cKO^{SC} sciatic nerves and thus, do not indicate an increase in the overall myelin thickness (radial hypermyelination) which is displayed, at least for small diameter fibers (< 2 µm), in other transgenic mice with mTORC1 hyperactivation (Goebbels *et al.*, 2010; 2012; Beirowski *et al*., 2017). This might be a dosage-dependent effect of mTORC1 activity (see below). On the other hand, the underlying molecular mechanisms that mediate the formation of these common pathological features and thus, how they result from elevated mTORC1 activity, are still elusive. Interestingly, genetic ablation of different myelin proteins leads to focal hypermyelination as well (Sander *et al*., 2006; Fabrizi *et al*., 2000). This is observed in HNPP, caused by haploinsufficency of the compaction protein PMP22 (Adlkofer *et al*, 1997). Similarly, MAG-deficient mice display myelin outfoldings that eventually result in the formation of tomacula (Cai *et al*., 2002). In addition,

focal hypermyelination is caused by different mutations in P0 (Fabrizi *et al*., 2000; Kochański *et al*., 2003; Iida *et al*., 2012), whereas other mutations in the same gene result in hypomyelination as displayed in CMT1B patients (D'Antonio *et al*., 2013). The phenotypical rescue in a CMT1B mouse model by overexpression of NRG1-III is suggested to result from an improvement in the stoichiometry of myelin lipid and protein synthesis (Scapin *et al.*, 2018). Accordingly, these animals display elevated AKT- and ERK-signaling, and, presumably due to increased mTORC1 activation, an upregulation in the lipid synthesis. In turn, the balanced upregulation of myelin lipid synthesis and myelin protein expression might underly radial hypermyelination, whereas focal hypermyelination could result from an imbalanced myelin formation. An increase in mTORC1-mediated myelin lipid synthesis accompanied by physiological levels of myelin protein expression or an impaired myelin protein incorporation into the nascent sheath, as discussed below, might account for the formation of focal but not radial hypermyelination in *Rab35* cKO^{SC} mice *in vivo*.

Distinct Cre-recombinases used for conditional ablations of negative upstream regulators of mTORC1 partially account for observed differences in the extent of hypo- and hypermyelination upon mTORC1 hyperactivation *in vivo* (Figlia *et al.*, 2018). Whereas strong hypomyelination results from Cre-expression controlled by the Dhh-promoter from E12 on, an initial hypomyelination followed by focal hypermyelination is observed in conditional *TSC1* cKO^{SC} animals using a Cre recombinase expressed at E13.5 under control of the P0-promoter (Beirowski *et al.*, 2017; Jiang *et al.*, 2018). Similarly, the conditional ablation of Rab35 was controlled by a P0-*Cre* (Figure 3-12a). These mice do not display hypomyelination in sciatic nerves at early stages of development, but Rab35 depletion *ex vivo* leads to a striking reduction in myelin segment formation in SC/DRG organotypic explants (Figure 3-25a-d). This might reflect the postulated time-dependent effect on myelination by altered mTORC1 activation (Beirowski *et al*., 2017; Figlia *et al.*, 2017). The cause for such a difference in myelin formation *in vivo* and *ex vivo*, which is not reported so far in other transgenic mouse models with mTORC1 hyperactivity, remains to be investigated (Beirowski *et al.*, 2017; Figlia *et al.*, 2017; Jiang *et al.*, 2018). Despite of that, myelin segment formation was restored in *Rab35* cKO^{SC} explants to WT levels by rapamycin treatment, suggesting that mTORC1 hyperactivity is indeed causative (Figure 3-25d). Importantly, a significant number of myelin segments *ex vivo* displayed abnormal structures, resembling of focal hypermyelination *in vivo* or myelin outfoldings in explants from CMT4B mouse models, and could be rescued by rapamycin (Figure 3-25e,f). Thus, mTORC1 hyperactivation in *Rab35* cKO^{SC} explants is causative for impaired myelin formation.

The observed initial hypomyelination upon mTORC1 hyperactivation *in vivo* is attributed to an elevated proliferation of immature SCs on the one hand (Beirowski *et al.*, 2017; Jiang *et al.*, 2018), and repression of the myelination-initiating transcription factor KROX20 by the mTORC1-target S6K on the other (Figlia *et al.*, 2017). Notably, hyperproliferation of Schwann cells correlates with the extent of mTORC1 hyperactivity and thus, the impairment in myelination onset. In agreement with the fact that mTORC1 hyperactivation is more pronounced upon TSC2 than TSC1 depletion (Zeng *et al.*, 2011), *TSC2*$^{Fl/Fl}$ x P0-*Cre* mice display persistent hypomyelination into adulthood (Beirowski *et al.*, 2017). However, both, mTORC1 and Rheb are implicated in repression of the cell cycle exit by regulating the cyclin dependent kinase (CdK)-inhibitor p27kip1 for instance (Hong *et al.*, 2008; Lacher *et al.*, 2010; Ji *et al.*, 2012; Ke *et al.*, 2016; Jiang *et al.*, 2018). Thus, the observed hyperproliferation of TSC-depleted Schwann cells also results from mTORC1-independent regulation of p27kip1 by Rheb (Beirowski *et al.*, 2017). In conclusion, more moderate activity elevation of mTORC1 and Rheb in *TSC1*$^{Fl/Fl}$ x P0-*Cre* than in *TSC2* cKO^{SC} mice results in modest hyperproliferation and slightly delays the onset of myelination only (Beirowski *et al.*, 2017; Jiang *et al.*, 2018). The latter is represented by a reduced number of myelinated fibers in the first weeks postnatally, which indicates a lack of differentiated Schwann cells. However, in *Rab35* cKO^{SC} mice the number of myelinated fibers was comparable to control sciatic nerves already at P5 (Figure 3-25k). In addition, focal hypermyelination could be observed even at that young age. This difference to other mouse models with mTORC1 hyperactivity might be caused by additive effects. First, in contrast to *TSC* knockout animals, *Rab35* cKO^{SC} presumably do not display Rheb hyperactivity as neither AKT nor ERK are upregulated. Thus, less hyperproliferation than in TSC knockout animals can be expected. Second, in sciatic nerves of *TSC1*$^{Fl/Fl}$ x P0-*Cre* animals at P28, phosphorylated S6 protein levels are more than five times increased over WT levels (Beirowski *et al.*, 2017). In contrast, sciatic nerves of *Rab35* cKO^{SC} mice displayed a more moderate 2- to 3-fold increase in p-S6/ S6 levels (Figure 3-19b). Thus, lower mTORC1 hyperactivation might account for the lack of a delayed SC differentiation in these animals. Moreover, Rab35 is a known regulator of cytokinesis, due to its relevance in the cytokinetic abscission (Kouranti *et al.*, 2006; Dambournet *et al.*, 2011; Chesneau *et al.*, 2012; Fremont *et al.*, 2017). Accordingly, the rate of proliferation was markedly reduced in *Rab35* icKO OPC cultures and slowed down by more than 50 % in *Rab35* icKO astrocytes in culture (data not shown). A slower cytokinesis might counteract the increased proliferation induction upon mTORC1 hyperactivation. In sum, mTORC1 hyperactivity does not lead to hyperproliferation

or a delayed myelination onset in *Rab35* icKO mice and thus, not to early hypomyelination *in vivo*.

Interestingly, if mTORC1 hyperactivity is induced in mice upon adulthood, focal hypermyelination is accompanied by radial hypermyelination of large diameter fibers as well (Goebbels *et al.*, 2012; Beirowski *et al.*, 2017; Figlia *et al.*, 2017; Jiang *et al.*, 2018). This might indicate that mTORC1 activation upon myelin induction can cause an upregulated homeostatic wrapping of myelin layers by promoting myelin lipid as well as myelin protein synthesis. KROX20 regulates myelin protein translation during myelin induction (Jang *et al.*, 2010), and is suppressed by mTORC1. However, KROX20-independent upregulation of myelin protein expression is also reported, for instance upon NRG1 overexpression and presumably mTORC1 hyperactivation (Scapin *et al.*, 2018). In addition, an upregulation of myelin protein levels is observed upon SC-specific overexpression of hyperactive AKT *in vivo*, whereas KROX20 levels are even reduced (Domenech-Estevez *et al.*, 2016). Interestingly, in the CNS, cholesterol is critical for myelin protein synthesis (Smolders *et al.*, 2010; Mathews *et al.*, 2014), and mTORC1 was recently identified as a key player in the cholesterol-mediated regulation of myelin protein expression (Mathews and Appel, 2016). When we made use of tamoxifen-inducible *Rab35* knockout in differentiated Schwann cell mono-cultures, we could observe a large fraction of cells with abnormally high P0-protein expression *in vitro* (Figure 3-28). P0-signals in these cultures could be reduced to WT-levels by Rapamycin application, indicating that mTORC1 hyperactivity is indeed causative. Interestingly, Raptor depletion in Schwann cells *in vivo* results in lower protein levels of P0 and MBP, but not MAG, suggesting that mTORC1 does not control PNS myelin protein synthesis in general but rather the expression of distinct proteins only (Norrmén *et al.*, 2014). In contrast, in the CNS, mRNA and protein levels of almost all major myelin proteins are downregulated upon Raptor depletion, whereas MBP mRNA levels are less affected (Bercury *et al.*, 2014; Lebrun-Julien *et al.*, 2014). From these data, mTORC1 has been suggested to control translation but not transcription of MBP (Figlia *et al.*, 2018). Our data, together with earlier findings (Norrmén *et al.*, 2014), indicate that P0-protein levels are also regulated by mTORC1. Interestingly, the exit of newly synthesized P0-protein from the endoplasmatic reticulum is cholesterol-dependent (Saher *et al.*, 2009), providing a mechanism by which mTORC1 activation could specifically promote P0-protein synthesis. Thus, inducing mTORC1 hyperactivity after KROX20-mediated P0- and MBP-transcription initiation could result in a more balanced upregulation of myelin lipid and protein synthesis and thus, to radial hypermyelination as well. To confirm this hypothesis, the levels of other myelin proteins in

Rab35-depleted SCs need to be analyzed. In addition, ultrathin sections of sciatic nerves from *Rab35* cKO^{SC} mice could be analyzed by immunogold labelling for the abundance and incorporation of myelin proteins into aberrantly myelinated sheaths *in vivo*.

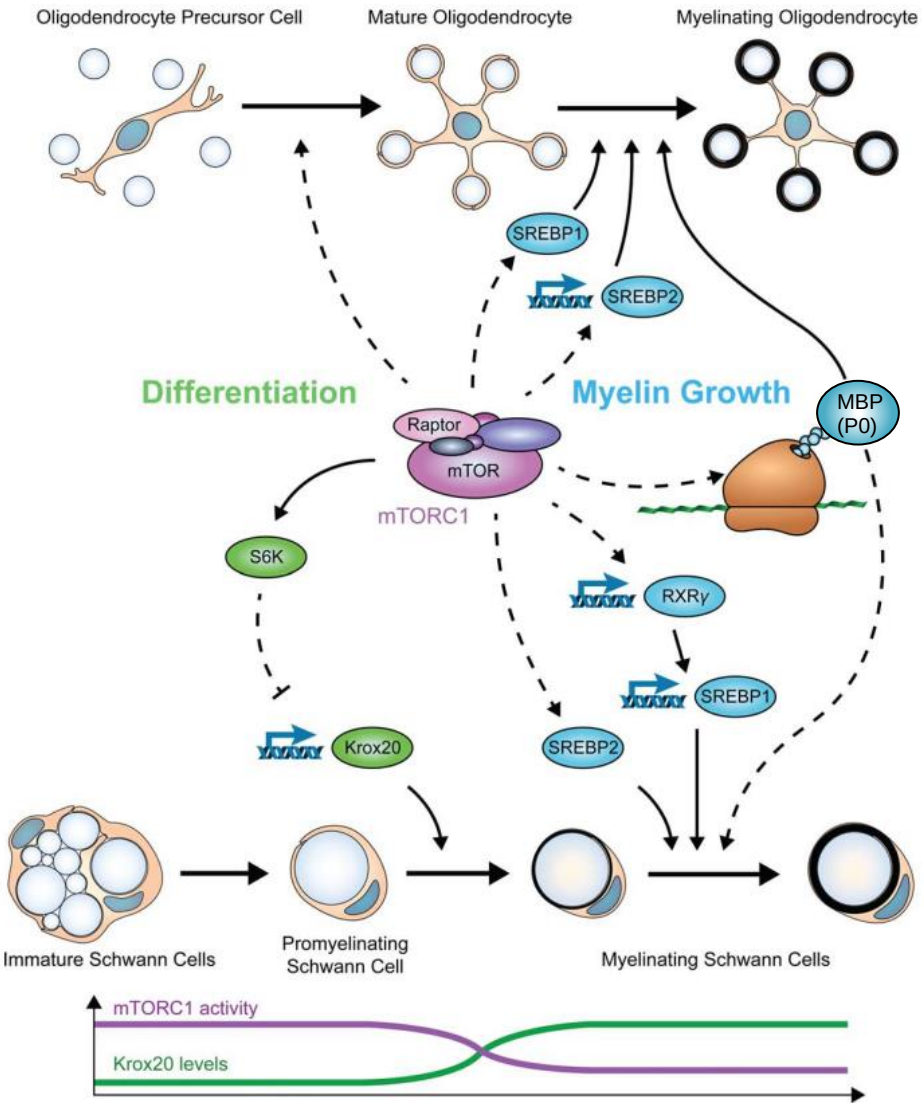

Figure 4-1: Regulation of myelin homeostasis by mTORC1 in CNS and PNS. mTORC1 is proposed to delay the myelination onset in Schwann cells by S6K-mediated repression of KROX20 transcription and inhibition of the cell cycle exit. In the CNS, differentiation of OLs is presumed to be potentiated by mTORC1. After onset of myelination, mTORC1 promotes myelin growth by transcriptional upregulation of lipid- and cholesterol synthesizing enzymes via SREBPs, and presumably by promoting myelin protein synthesis. In the PNS, mTORC1 activity declines in pro-myelinating Schwann cells, and remains at low levels in mature myelinating Schwann cells. Modified from (Figlia *et al*., 2018).

So far, myelin degeneration has not been reported as a frequent morphological feature that accompanies focal hypermyelination. However, myelin degeneration in *Rab35* cKO^{SC} was slightly ameliorated by Rapamycin treatment, indicating a link to mTORC1 hyperactivation. Re-activation of mTORC1 is observed upon nerve injury and critical for

proper myelin clearance, SC dedifferentiation and re-myelination (Norrmén *et al.*, 2018). In turn, abnormally increased mTORC1 activity might induce myelin breakdown and thus, myelin degeneration even in the absence of a nerve damage. On the other hand, autophagy is required for proper myelin clearance (Gomez-Sanchez *et al.*, 2015). Our data from astrocytic cultures and recent studies (De Leo *et al.*, 2016; Minowa-Nozawa *et al.*, 2017) indicate that autophagy might be impaired in the absence of Rab35. Thus, defective debris clearance could contribute to the progressive abundance of this pathological feature in *Rab35* cKO^{SC} sciatic nerves.

Finally, despite of the significant rescue of myelin segment formation *ex vivo* and P0-protein levels *in vitro* by mTORC1 inhibition in Rab35-depleted SCs, aberrant myelination *in vivo* is only partially ameliorated. Tomacula displayed the strongest reduction upon Rapamycin treatment, in accordance with the major role of mTORC1 in bulk membrane formation (Goebbels *et al.*, 2012; Beirowski *et al.*, 2017; Jiang *et al.*, 2018). Myelin degeneration and outfoldings are less efficiently rescued, which might be explained by the early onset of the phenotype and the comparably late Rapamycin application. These features, but not tomacula, are already observed at P5 with a strikingly high abundance compared to Control animals (Figure 3-25j). In contrast, Rapamycin treatment was performed from P12 on, as earlier application affected the survival of the mice. This problem might be circumvented by a 50 % reduction of the Rapamycin dosage, which is reported to be well tolerated by young mice already at P3 (Lebrun *et al*., 2014; Figlia *et al*., 2017). In addition, other processes independent of mTORC1 but regulated by Rab35 and required for the maintenance of myelin homeostasis might contribute to the demyelination in *Rab35* cKO^{SC} animals as further discussed in section 4.4.

4.1.2 Rab35 represses mTORC1 activity independent of growth factor stimulation

mTORC1 is a conserved and central signaling hub for the switch of cellular anabolism and catabolism, controlled by a cohort of extrinsic and intrinsic mechanisms to regulate cell growth and survival. In this study, we observed elevated mTORC1 activity upon depletion of Rab35 in several cell types. siRNA-mediated knockdown of Rab35 in HEK (Figure 3-13e,f) or HeLa cells (Figure 3-21a), or its acute depletion in primary astrocytic cultures (Figures 3-14a,b; 3-26c,d) or Schwann cells, *in vitro* (Figure 3-26a,b) as well as *in vivo* (Figure 3-19a,b), resulted in hyperactivation of mTORC1. Rab35 has been implicated in regulation of the mTORC1-upstream activator AKT in different tissues. Its absence is reported to cause elevated EGFR recycling to the surface instead of degradation and thus, increased AKT

activation in different cancer cell lines (Allaire *et al.*, 2013; Duan *et al.*, 2016; Zheng *et al.*, 2017; Ye *et al.*, 2018). In contrast, Rab35 is also presumed to facilitate PI3K activity and eventually AKT phosphorylation in somatic cancer or HEK cells, as well as upon ROS (reactive oxygen species) production in a breast cancer cell line (Wheeler *et al.*, 2015; Deng *et al.*, 2016). In these studies, less AKT activation was reported in the absence of Rab35, whereas overexpression of the constitutively active mutant Rab35Q67L enhanced AKT phosphorylation. In accordance, we observed reduced AKT phosphorylation upon acute depletion in *Rab35* icKO primary astrocytes in culture (Figure 3-14c,d). Simultaneously, these cells display an upregulation in mTORC1 activity. This indicates an additional role of Rab35 in the repression of mTORC1, independent of its function in the activation of AKT. This hypothesis is corroborated by the fact that downregulation of RTK-mediated PI3K/AKT signaling by serum-starvation leads to reduced mTORC1 activity but does not compensate the significant hyperactivity in *Rab35* icKO compared to control cells (Figure 3-14b). Furthermore, elevated mTORC1 activity *in vivo*, in sciatic nerve tissue of *Rab35* icKO^{SC} mice is not caused by RTK-overactivation as neither AKT- nor ERK-phosphorylation is increased (Figure 3-19c,d). Thus, we conclude that Rab35 represses mTORC1 independent of growth factor receptor signaling.

mTORC1 promotes cell growth on the one hand and represses autophagy on the other (Laplante and Sabatini, 2012). In agreement, cultured cells depleted of Rab35 display an increased cell area (Figures 3-15a,b; 3-21d). Despite of the established function of mTORC1 in the transcriptional repression of lysosomal and autophagic biogenesis via TFEB (Settembre *et al.*, 2011; Martina *et al.*, 2012), the abundance of lysosomal compartments is not altered in *Rab35* icKO astrocytic cultures (Figure 3-16e-h). Notably, recent studies revealed, that inactivation of mTORC1 does not necessarily result in an increased number of lysosomes, as represented by unaltered LAMP-1 and LAMP-2 levels. Instead, enhanced lysosomal function by an increased lysosomal pH and TFEB-mediated upregulation of hydrolytic lysosomal enzymes was observed (Zhou *et al.*, 2013; Puertollano *et al.*, 2014). Thus, investigating the lysosomal functionality could reveal more insight into the effect of mTOR1 hyperactivity on protein degradation in our cells. On the other hand, LC3-levels are reduced as expected (Figure 3-15c,d). In contrast to the conserved role of mTORC1 in the downregulation of autophagy (Hosokawa *et al.*, 2009; Jung *et al.*, 2009), we observed an increased number of autophagosomes in the absence of Rab35 (Figure 3-15c-g). This might reflect a block in autophagosome maturation or clearance, for instance due to impaired fusion with lysosomes. Interestingly, a similar phenotype has been recently observed in *Rab35* knockout HeLa cells

and was assigned to a function of Rab35 in mediating NDP52-dependent autophagosome maturation (Minowa-Nozawa *et al.*, 2017). In addition, the Rab35 effector protein, OCRL, has been implicated in autophagosome-lysosome fusion (De Leo *et al.*, 2016). Measuring the autophagic flux would reveal if impaired autophagosome maturation or clearance is indeed a consequence in *Rab35* cKO primary astrocytes. On the other hand, VPS34-complex I -mediated PI(3)P production is a crucial promoter for autophagosome formation (Vergne *et al.*, 2009; Jaber *et al.*, 2012; Ronan *et al.*, 2014), and we could observe increased VPS34-synthesized PI(3)P-levels in the absence of Rab35 (Figures 3-22; 3-27a,b). The complex should be at least partially inhibited by mTORC1 activity (Martina *et al.*, 2012; Yuan *et al.*, 2013), but an impairment in PI(3)P hydrolysis due to a loss of different MTMR phosphatases, such as MTMR14, -R3, -R9 and -R8, indeed results in enhanced autophagy initiation (Vergne *et al.*, 2009; Taguchi-Atarashi *et al.*, 2010; Cebollero *et al.*, 2012; Zou *et al.*, 2012). It would be thus worth to investigate, if the loss of Rab35 increases PI(3)P-levels at autophagosomal membranes as well.

In sum, catabolic pathways are not dramatically downregulated in the absence of Rab35 despite of mTORC1 hyperactivity. mTORC1-independent targets of Rab35, as well as proteins that mediate the repression of mTORC1 by Rab35 might counteract the effect of mTORC1 hyperactivity on autophagy.

4.2 Rab35-dependent repression of mTORC1 is mediated by PI(3)P- and PI(3,5)P_2-hydrolyzing MTMR proteins

Several reports indicate that mTORC1 recruitment to or activation at late endosomes/ lysosomes is mediated by PI(3)P and/ or PI(3,5)P_2, independent of AKT or ERK regulation (Byfield *et al.*, 2005; Nobukuni *et al.*, 2005; Han *et al.*, 2012; Yoon *et al.*, 2016; Fang *et al.*, 2001; 2003; Xu *et al.*, 2011; Yoon *et al.*, 2011; Bridges *et al.*, 2012; Jin *et al.*, 2014). By genetic manipulations, a set of PI(3)-phosphate kinases have been identified to thereby mediate mTORC1 activation, including the PI(3)P-generating enzymes, VPS34 and class II PI3K C2α (Jaber *et al.*, 2011; Bridges *et al.*, 2012), and the PI(3,5)P_2-synthesizing PIKfyve in a complex with Fig4 and Vac14 (Bridges *et al.*, 2012; Jin *et al.*, 2014). In contrast, not much is known about the negative regulation of mTORC1 by PI(3)P- or PI(3,5)P_2-dephosphorylation.

4.2.1 MTMR proteins are novel effectors of Rab35

Active Rab35 specifically interacts with the pseudophosphatases MTMR5 and MTMR13 (Figures 3-5; 3-6), and via these also with their complex partner, the active phosphatase MTMR2 (Figures 3-9; 3-10). In addition, we identified MTMR1 as a novel complex partner of MTMR13 (Figure 3-9), and presumably also MTMR5 (data not shown). Rab35 recruits MTMR13 to LAMP-positive late endosomal/ lysosomal (LE/ Lys) membranes (Figure 3-8d-f). These compartments display PI(3,5)P_2- and PI(3)P-identity, the preferred substrates of MTMR2 (Cao *et al.*, 2008) in a complex with MTMR13 (Berger *et al.* 2006b) or MTMR5 (Kim *et al.*, 2003b). Active Rab35 and MTMR13 also colocalized at defined plasma membrane sites. This in agreement with the known localization of Rab35 (Li *et al.*, 2014), whereas a function of MTMRs at the plasma membrane remains to be investigated. Interestingly, lysosomal positioning towards the plasma membrane in response to amino acid stimulation is mediated by PI(3)P-binding proteins (Hong *et al.*, 2017). In addition, a plasma membrane pool of PI(3)P and PI(3,5)P_2 is also reported to mediate mTORC1 activation via TSC complex regulation (Bridges *et al.*, 2012; Hirsch *et al.*, 2014; Mohan *et al.*, 2016).

Furthermore, Rab35-depleted cells display accumulation of PI(3)P, which strongly indicates that PI(3)-phosphate regulating enzymes are dysregulated (Figures 3-22; 3-27a,b). The only so far known Rab35 effector that regulates PI-metabolism is the 5'-phosphatase OCRL. This enzyme preferentially dephosphorylates PI(4,5)P_2, which is for instance required for the uncoating of clathrin-coated vesicles upon endocytosis, and their eventual fusion with endosomes (Cauvin *et al.*, 2016). The subsequent conversion from PI(4)P to endosomal PI(3)P is incompletely resolved, but might be realized by class II PI3K C2α-mediated generation of PI(3,4)P_2 from PI(4)P, which is eventually converted into PI(3)P by INPP4B (Posor *et al.*, 2013). Thus, an impaired recruitment of OCRL in the absence of Rab35 would thereby not result in the observed accumulation of PI(3)P. In addition, *Rab35* icKO Schwann cells do not display altered PI(4)P levels (Figure 3-27c,d). Interestingly, overexpression of MTMR2 decreases PI(3)P levels in cultured cells (Lorenzo *et al*., 2006). Thus, we propose that the loss of Rab35 impairs the recruitment of the PI(3)P phosphatase complexes MTMR13/-R2, MTMR5/-R2, MTMR13/-R1 to lysosomal membranes and thereby causes an accumulation of PI(3)P. This hypothesis is corroborated by the finding that PI(3)P levels are increased at late endosomal/lysosomal (LE/Lys)-compartments upon depletion of Rab35, MTMR2, or both (Figure 3-23). An accumulation of PI(3,5)P_2 is also likely, though we could not investigate this directly, due to the lack of a functional probe (Hammond *et al.*, 2015). Furthermore, we observed reduced MTMR2 levels in *Rab35* icKO primary astrocytic cultures

(Figures 3-17a,b; 3-18b). In turn, sciatic nerve tissue from *MTMR2* KO mice also harbor reduced Rab35 levels (Figure 3-17c,d). A regulation of these proteins in the translational process of each other could explain this finding but a function in protein translation is neither reported for Rab35 nor MTMR2 so far. We observed that either loss of Rab35 or MTMR2 in HEK cells or primary astrocytes in culture results in increased activity of mTORC1 (Figures 3-13e,f; 3-18d). Thus, both proteins act in the repression of the core kinase complex. Moreover, simultaneous depletion of both proteins partially results in an even more severe upregulation of steady state mTORC1 activity. This argues against a genetic compensation by the reduction of MTMR2 or Rab35 in the absence of its partner protein. Intriguingly, a reduction in MTMR2 protein levels is also observed in *MTMR13* KO mice, while MTMR13 protein levels are reduced in *MTMR2* KO mice as well (Ng *et al.*, 2013). In addition, higher protein levels than expected from single overexpression of MTMR2 and -R13 are reported upon their co-expression in cell cultures (Robinson and Dixon, 2006). The same interdependence of protein levels is observed for other MTMR complex-forming members (Zou *et al.*, 2009; 2012; Gupta *et al.*, 2013), and likely reflects an increased or decreased protein stability in the presence or absence of a complex partner, respectively. Thus, the observed interdependence of Rab35 and MTMR2 strongly suggests a functional interaction, presumably by complex formation for the repression of mTORC1 activity. This hypothesis is corroborated by the finding that overexpression of MTMR2 not only ameliorates mTORC1 hyperactivation in MTMR2-depleted HEK cells, but also in cells with markedly decreased levels of Rab35 upon siRNA-mediated knockdown (Figure 3-20). Furthermore, increased mTORC1 activity in the absence of MTMR2 is also not attributed to elevated AKT activation (Figures 3-13d; 3-18c). In a recent study, overexpression of MTMR3 has been reported to interfere with mTORC1 activation, though independent of its phosphatase activity and by direct binding (Hao *et al*., 2016). If such an interaction is also true for other MTMRs should be therefore investigated, for instance in an affinity purification assay. Despite, our data rather suggest a lipid-mediated regulation by MTMR2, as mTORC1 hyperactivation is rescued by pharmacological interference with PI(3)P synthesis in *Rab35* icKO cells (Figure 3-24a,b), and in cells additionally depleted of MTMR2 (Figure 3-24c,d). However, lipid-mediated regulation of mTORC1 by MTMR2 remains to be ultimately confirmed, for instance by showing that overexpression of a phosphatase-deficient MTMR2 mutant does not rescue mTORC1 hyperactivation in MTMR2-depleted cells. So far, our findings indicate a sequential action of Rab35 and MTMR2 in repressing mTORC1 by PI(3)P- and PI(3,5)P_2-hydrolysis at lysosomal sites.

4.2.2 Rab35-dependent recruitment of MTMR phosphatase complexes

Despite of the fact that MTMR2 and its closest homologues MTM1 and MTMR1 harbor a lipid-binding domain, their association with membranes is only occasionally observed upon overexpression, and the localization pattern remains mainly cytosolic (Robinson and Dixon, 2006; Cao *et al.*, 2007; 2008). Furthermore, these phosphatases convert PI(3)P (Cao *et al.*, 2007; 2008; Ketel *et al.*, 2016; this study), whereas their PH-GRAM domain preferentially binds to PI(3,5)P_2 and PI(5)P (Berger *et al.*, 2003; Schaletzky *et al.*, 2003; Tsujita *et al.*, 2004). This indicates their membrane association might be mediated by additional factors or other proteins. For instance, constricted conditions such as a hypoosmotic shock, which increases PI(3,5)P_2 concentration, facilitate MTMR2 membrane association (Berger *et al.*, 2003). A report about ERK-mediated MTMR2-dephosphorylation and its eventual dissociation from early endosomal membranes (Franklin *et al.*, 2011; 2013) contrasts earlier findings of EGF-stimulated MTMR2 translocation to late endosomal membranes (Cao *et al.*, 2008). In the latter study, a direct interaction between VPS34 and MTM1 or MTMR2, controlled by early endosomal Rab5 or late endosomal Rab7, respectively, was proposed to mediate their recruitment (Cao *et al.*, 2007; 2008). However, these Rab GTPases activate VPS34 by disrupting the kinase-phosphatase interaction. Thus, how MTM1 and MTMR2 bind to the respective PI(3)P-positive membranes remains elusive. Interestingly, a recent study reported that Rab11 is activated by an endosomal PI(3)P pool and mediates the recruitment of MTM1 (Campa *et al.*, 2018). Here, we propose that Rab35 recruits MTMR2 and -R1 in a complex with MTMR5 or -R13. This is conceivable, as complex formation with these pseudophosphatases by oligomerization through their coiled-coil regions is known to regulate the membrane association of MTMR2 (Laporte *et al.*, 2002; Berger *et al.*, 2003; 2006b; Kim *et al.*, 2002b; 2003b; Robinson and Dixon, 2006). For instance, its localization to endomembranes is disrupted when the coiled-coil region is mutated (Kim *et al.*, 2002b). In turn, overexpressed MTMR2 translocates from the cytosol to punctate, perinuclear puncta when MTMR5 is co-expressed (Kim *et al.*, 2003b). Furthermore, the association of MTMR2 with MTMR5 or -R13 results in strikingly increased catalytic activity towards PI(3)P and PI(3,5)P2 *in vitro* (Kim *et al.*, 2003b; Berger *et al.*, 2006b). Thus, these pseudophosphatases not only recruit but also stimulate phosphatase activity of MTMR2.

We propose that membrane association of these pseudophosphatases is regulated by recruitment through Rab35, as overexpressed MTMR13 remains mainly cytosolic (Robinson and Dixon, 2005) but is translocated by active Rab35 (Figure 3-8d-f). This hypothesis is corroborated by the fact that the partial localization of MTMR13 to membrane fractions is

independent of its two lipid-binding domains, PH or PH-GRAM, whereas the inactive PTP domain alone is sufficient (Robinson and Dixon, 2006). Intriguingly, we could map the binding site of Rab35 to the PTP domain of MTMR13 (Figure 3-7). Interaction at this site can explain the specific binding of Rab35 to these pseudophosphatases, but also raises the question if other inactive MTMR members might be recruited as well. In contrast, the inactive PTP domain of MTMR13 displays the largest sequence identity with MTMR5 (57,5 %) and MTMR2 (30.1 %). Thus, the PTP domains of other MTMR pseudophosphatases have less overlap with MTMR13 than MTMR2 and are therefore similarly not expected to bind to Rab35. Furthermore, neither our interactor screen in HEK cells (Figure 3-4) nor the screen performed with *D. melanogaster* proteins (Gillingham *et al.*, 2014) indicate comparable association of other MTMR pseudophospatases with Rab35. Interestingly, the PTP domain displayed a lower binding affinity to Rab35 than full-length MTMR13. Thus, binding of Rab35 to the PTP domain could be additionally promoted by other domains of MTMR13 in its native conformation. Though, we observed reduced binding of the PTP domain to Rab35 when expressed in conjunction with the coiled-coil region, steric interference by the latter could also be an artefact of the recombinant peptide. In consequence, we propose a model in which Rab35 binds to the inactive PTP domain of MTMR13, and presumably also MTMR5. The active phosphatases MTMR2 or -R1 hetero-oligomerize with these pseudophosphatases via their coiled-coil (CC) regions, and thereby active MTMR complexes can be recruited by the small GTPase (Figure 4-2). The hypothesis that these complexes are still active when Rab35 is bound remains to be confirmed. For instance, an *in vitro* phosphatase assay with MTMRs, affinity-purified from HEK cell lysates using GST-Rab35^GTPyS as a bait, could reveal their functional activity. Alternatively, recombinantly expressed and purified MTMR1 and -R2 from *E. coli* can be used. In contrast, the large multi-domain proteins MTMR13 or -R5 are not soluble in *E. coli* (data not shown). In addition, localization studies within cells were so far limited as endogeneous levels of Rab35 are obviously not sufficient to recruit overexpressed MTMR13. Furthermore, the overexpression of all three interacting proteins impaired cell morphology and survival (data not shown). Thus, antibodies are required to detect their endogeneous localization. Alternatively, if an increased phosphatase activity upon co-overexpression of Rab35 with MTMR complexes is responsible for the lethal effect, the use of a phosphatase-inactive mutant of MTMR2 might solve this problem.

Finally, we could not yet reveal how Rab35 is recruited to lysosomal sites. In a recent study, overexpression of the long non-coding mRNA HOTAIR increased the co-locolization of Rab35 with CD63-positive LE/Lys (Yang *et al.*, 2019). In oligodendrocytes, the function

of Rab35 at LAMP-positive late endosomal MVBs during exosome secretion is negatively regulated by the GAPs TBC1D10A-C (Hsu *et al.*, 2010). Another candidate could be Folliculin, which possesses GEF activity towards Rab35 (Nookala *et al.*, 2012; Zheng *et al.*, 2017), is identified at lysosomal sites and regulates mTORC1 activity (Baba *et al.*, 2006; Hasumi *et al.*, 2009; 2014; Petit *et al.*, 2013; Tsun *et al.*, 2013; Meng and Ferguson, 2018). In addition, the Rab35-GEF DENND1A (Connecdenn1) possesses the highest binding affinity among all PI-species towards PI(3)P, and insignificantly less to PI(3,5)P_2 (Allaire *et al.*, 2010). Analyzing PI(3)P levels or mTORC1 activation in the absence of these GEFs and GAPs in primary Schwann cells could reveal their potential involvement in mediating the recruitment and regulation of Rab35 at LE/Lys.

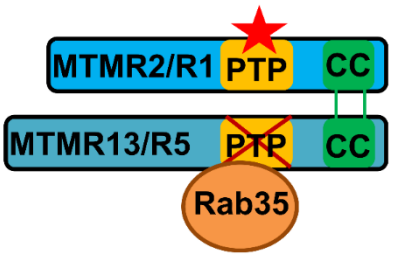

Figure 4-2: Model of interaction between Rab35 and MTMR complexes. Rab35 binds MTMR13, and presumably MTMR5 at their inactive PTP domains, and via these, to the active phosphatases MTMR2/ -R1. CC - coiled-coil region; PTP – phosphotyrosine phosphatase

4.2.3 PI(3)-phosphates in the regulation of Schwann cell myelin homeostasis

The regulation of PI signaling is strongly correlated to SC myelin homeostasis. Four CMT-disease types are caused by loss of function or missense mutations in PI(3)-phosphate catabolizing enzymes: CMT4J by Fig4, and CMT4B1, -B2 and -B3 by MTMR2, -R13 and -R5, respectively (Suter, 2007). In CMT4B1, mostly truncating or missense mutations within the highly conserved residues of the catalytic PTP- and the PH-GRAM domain of MTMR2 are causative (Berger *et al.*, 2012). CMT4J mainly results from mutations in the catalytic SAC domain of Fig4, or within its interaction domains with the scaffolding protein Vac14 (Chow *et al.*, 2007). While CMT4B is marked by redundant myelin formation, CMT4J patients display hypomyelination. The interaction of MTMR2 with Dlg-1 has been recently proposed to inhibit the delivery of membrane via vesicular structures at paranodal loops and thereby account for the occurrence of myelin outfoldings in CMT4B1 mouse models (Bolis *et al.*, 2009). Accordingly, depletion of the fusion promoter Sec8 slightly ameliorated myelin outfoldings in *MTMR2* KO cultures *in vitro* (Bolis *et al.*, 2009), but inactivation of Dlg-1 in *MTMR2* KO mice did not alter the phenotype *in vivo* (Cotter *et al.*, 2010). In addition, how

the phosphatase activity of MTMR2 could contribute in this mechanism is not revealed. Interestingly, heterozygousity of Fig4, which conversely results in reduced $PI(3,5)P_2$ levels due to the physical interdependence with PIKfyve (Vaccari *et al.*, 2011), ameliorates the phenotype of *MTMR2* KO mice *in vivo*. Also *in vitro*, the depletion of PIKfyve ameliorates myelin abnormalities in *MTMR2* KO cultures. These data indicate a striking dependency of myelin homeostasis on the phosphatase activity of MTMR2 towards $PI(3,5)P_2$.

Reminiscent of CMT4B mouse models (Bolino *et al.*, 2004; Robinson *et al.*, 2008; Ng *et al.*, 2013), sciatic nerves from *Rab35* cKO^{SC} are marked by focal hypermyelination with abundant myelin outfoldings (Figure 3-12d-f). In addition, adult mice display a reduction in the myelin thickness of large diameter nerve fibers (Figure 3-12h), which is also observed in aged *MTMR13* KO mice (Ng *et al.*, 2013; Robinson *et al.*, 2008). Moreover, in agreement with the identification of Rab35 as an upstream regulator of MTMR2, we observed increased PI(3)P levels in *Rab35* icKO Schwann cells in culture (Figure 3-27a,b). Furthermore, though a positive regulation of AKT (Berger *et al.*, 2011) or negative regulation of ERK (Franklin *et al*., 2011) signaling was presumed from MTMR2 overexpression assays in cell lines, neither *MTMR2* KO nor -*R13* KO mice display altered AKT- or ERK- activation, whereas mTORC1 activity has not been investigated yet in CMT4B mouse models (Bolino *et al.*, 2016; Ng *et al.*, 2013). Consistent with the fact, that late endosomal/ lysosomal PI(3)P activates mTORC1 activity (Byfield *et al.*, 2005; Nobukuni *et al.*, 2005; Jaber *et al.*, 2011), we observed an amelioration of mTORC1 hyperactivity in SC mono-cultures upon pharmacological interference with the main PI(3)P-synthesizing enzyme VPS34 (Figure 3-26a,b). We could not directly probe for $PI(3,5)P_2$ levels (Hammond *et al.*, 2015), but PI(3)P is the only known precursor of $PI(3,5)P_2$ and depletion of VPS34 lowers $PI(3,5)P_2$ levels by about 65% (Sbrissa *et al.*, 1999; Zolov *et al.*, 2012; Ikonomov *et al.*, 2015). In agreement, we observed a strong increase of PI(3)P levels upon pharmacological interference with PIKfyve using Apilimod. Despite of that, this condition also rescued the hyperactivation of mTORC1 and, importantly, elevated P0-protein levels in Rab35-depleted Schwann cells (Figure 3-28). This suggests that $PI(3,5)P_2$ levels, and not PI(3)P, are the main driver for mTORC1 activity in Schwann cells, and thus, presumably for myelin regulation.

Surprisingly, in a recent study, an amelioration of myelin outfoldings in *MTMR13* KO mice has not been observed upon simultaneous knockout of either VPS34 or PI3KC2ß (Robinson *et al.*, 2018). Astonishingly, additive effects in these double knockout mice were also not reported, though *VPS34* cKO^{SC} animals display a severe hypomyelination *in vivo* (Logan *et al.*, 2017). The lack of both, amelioration and exacerbation, could hint to a

compensation of class II and class III PI3K in the absence of each other, similar to the observed PI3KC2ß upregulation in the absence of -C2α in HeLa cells and fibroblasts (Tiosano *et al.*, 2019). In addition, in contrast to the presented morphometric analysis from 2- and 8-month-old *MTMR13* KO x *PI3KC2ß* cKO^{SC} animals, adult *MTMR13* KO x *VPS34* cKO^{SC} mice have not been investigated (P3 and P18 only). The authors proposed an MTMR2-independent phenotype of MTMR13, which is contrasted by the strong phenocopy in *MTMR13*- and *-R2* KO mouse nerves (Bolino *et al.*, 2004; Ng *et al.*, 2013). In addition, MTMR2 re-expression in *MTMR13* KO SC/ DRG organotypic explants did ameliorate myelin outfoldings (Robinson *et al.*, 2018). Our data, together with recent findings (Vaccari *et al.*, 2011), indicate that an alternative cross breeding of *MTMR13* KO animals with Fig4 heterozygeous mice might be a better strategy to compensate focal hypermyelination. Finally, also a reduction in PI(5)P levels due to impaired PI(3,5)P_2 dephosphorylation by MTMR2 could contribute to defective myelin formation. However, its role in myelination and membrane trafficking is less well investigated. PI(5)P is a known allosteric activator of the PH-GRAM domain (Schaletzki *et al.*, 2003), and can be converted to the PM-lipid PI(4,5)P_2 by type II PI(5)P 4-hydroxy kinase (PI5P 4K) (Rameh *et al.*, 1997; McCartney *et al.*, 2014). This might be a crucial step for the fusion of late endosomal/ lysosomal compartments with the plasma membrane, for instance during exosome secretion (see section 4.4).

We identified MTMR1 as a novel active phosphatase that interacts with MTMR13 (Figure 3-9) and most likely also with MTMR5 (data not shown). Interestingly, the pathology and onset of CMT4B1 patients is more severe than displayed in CMT4B2 patients (Pareyson *et al.*, 2019). A partial redundancy of MTMR13 and -R5 in the recruitment of MTMR2 in Schwann cells is thus highly suggestive. Could MTMR1 likewise compensate the absence of the active phosphatase MTMR2? MTMR1 has been recently implicated in muscular atrophy (Zanoteli *et al.*, 2005), and its knockdown in HeLa cells partially phenocopies MTM1 depletion with mislocalized transferrin receptors (Ketel *et al.*, 2016). However, MTMR1 is more closely related to MTMR2 than MTM1 with a sequence identity in humans of 69.7 % and 58.3 %, respectively. In addition, we could not detect any interaction between MTM1 and MTMR13 or -R5. If MTMR1 can functionally compensate the loss of MTMR2 could be investigated by analyzing PI(3)P accumulation and mTORC1 activity in the absence of both phosphatases in Schwann cells. More insight could be also revealed by comparing the modulation of MTMR2 and -R1 phosphatase activity in the presence of MTMR5 or -R13 in an *in vitro* phosphatase assay. Thus, so far, compensation of MTMR1 for -R2 can only be speculated and might also be cell type-specific.

In conclusion, we propose that impaired MTMR complex recruitment leads to an accumulation of PI(3,5)P_2, which in turn results in dysregulated mTORC1 repression, and thus, contributes to myelin abnormalities in Rab35-depleted Schwann cells (Figure 4-3). Our data indicate that increased mTORC1 activity might also contribute to the observed focal hypermyelination in CMT4B patients. The finding that Rab35 can potentially recruit different MTMR complexes can explain why *Rab35* cKO^{SC} mice display stronger focal hypermyelination including tomacula, which were recently suggested to represent a late form of myelin outfoldings (Cai *et al*., 2002), and an earlier onset of demyelination compared to *MTMR2* KO mice, in which nerve fiber abnormalities are not observed before P19 (Bolino *et al*., 2004).

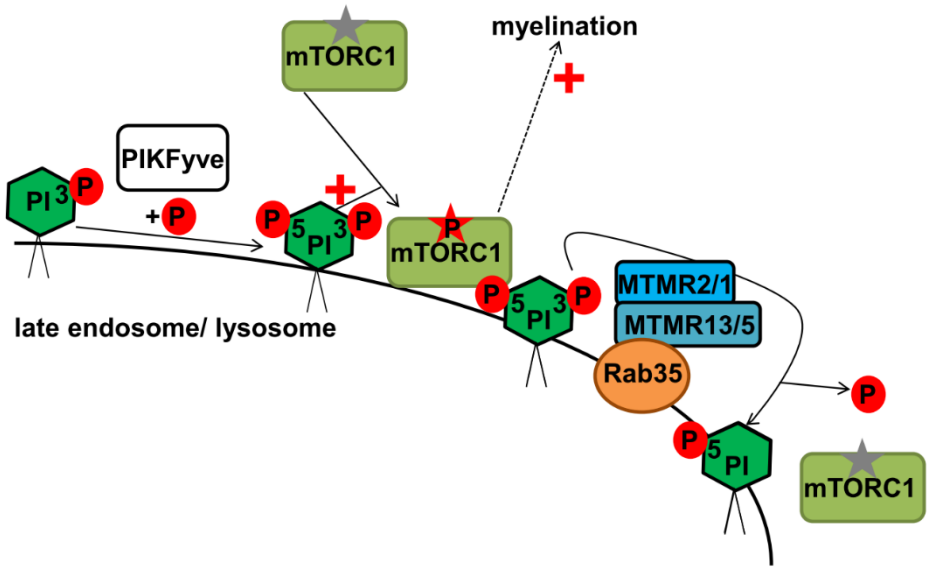

Figure 4-3: Proposed model of Rab35-dependent mTORC1 repression in Schwann cells mediated by the recruitment of PI(3,5)P_2-hydrolyzing MTMR complexes to LE/Lys. PI(3,5)P_2, generated by PIKfyve from PI(3)P, enables Raptor-binding and thereby promotes mTORC1 recruitment to the late endosomal/ lysosomal (LE/Lys) membrane. In turn, active MTMR complexes are recruited to LE/Lys by Rab35. MTMR2 (or -R1) mediated dephosphorylation of PI(3,5)P_2 facilitates the dissociation of mTORC1 from LE/Lys and thus, inactivation of the kinase complex. Thereby, sustained mTORC1 activity and consequently excessive aberrant myelin growth is repressed.

4.3 Altered myelin homeostasis in Rab35-depleted oligodendrocytes

In oligodendrocytes, shRNA-mediated depletion of Rab35 has been reported to result in impaired secretion of major myelin proteins on the one hand (Hsu *et al.*, 2010), and a gain in differentiation and myelination on the other (Miyamoto *et al.*, 2013). We could confirm the latter, as acute knockout of Rab35 in primary cultures of differentiated OLs resulted in increased *in vitro* myelin sheet formation and myelin protein abundance (Figure 3-3). Could a loss of mTORC1 repression in these cells be a causative factor? Indeed, elevated mTORC1

activation upon OL-specific upregulation of PI3K/AKT or MAPK/ERK signaling leads to radial hypermyelination in the CNS (Flores *et al*., 2008; Narayanan *et al.*, 2009; Goebbels *et al*., 2010; Ishii *et al.*, 2013; Sheean *et al.*, 2014; Furusho *et al.*, 2017), whereas features of focal hypermyelination are of lower abundance than in the PNS (Goebbels *et al.*, 2010). This difference could reflect the presumed positive effect of mTORC1 activity on myelin induction in OLs, though the underlying mechanism is not revealed yet (Figlia *et al.*, 2018; Figure 4-1). The early ablation or increased activity of Rheb in OPCs delays or prematures myelination onset, respectively (Zou *et al.*, 2014). In addition, Rapamycin treatment delays *in vitro* myelination and downregulates the transcription of myelin lipid synthesizing enzymes and major myelin proteins (Tyler *et al.*, 2009; 2011). Though mTORC1 has not yet been identified as a direct regulator of myelin protein synthesis, OL-specific Raptor depletion results in a reduction of mRNA and protein levels of major myelin proteins as well (Bercury *et al.*, 2014; Lebrun-Julien *et al.*, 2014). Similarly, downregulation of the cholesterol synthesis in oligodendrocytes results in decreased myelin gene expression *in vitro* (Smolders *et al*., 2010) and *in vivo* (Mathews *et al*., 2014). mTORC1 not only promotes cholesterol synthesis but has also been recently identified as a key player in cholesterol-regulated myelin protein expression in the CNS (Mathews and Appel, 2016). Thus, promoting myelin lipid synthesis as well as protein synthesis in OLs can account for the balanced increase in myelin growth and thus, radial hypermyelination in the CNS when mTORC1 activity is elevated. So far, we have not investigated mTORC1 activation in Rab35-depleted oligodendrocytes. Despite, our data could hint to a similar regulation of mTORC1 by Rab35 in CNS myelinating glial cells as in Schwann cells. First, as indicated from above-mentioned studies, a loss of mTORC1 repression can indeed result in hypermyelination as observed *in vitro* in *Rab35* icKO OL cultures. Second, these cells also accumulate PI(3)P (Figure 3-22c,d), suggesting an important role of Rab35 in PI(3)-phosphate conversion in oligodendrocytes as well. In addition, this regulation might also be mediated by MTMR complexes in OLs, as short-term depletion of MTMR2 phenocopies the loss of Rab35 in form of elevated myelin protein levels (Figure 3-11). MTMR2 is also expressed in other CNS cells such as neurons (Lee *et al.*, 2010) and astrocytes (this study). Despite of that, defects of the central nervous system have not been reported so far in CMT4B1, but CMT4B3 patients only (Alazami *et al.*, 2014; Romani *et al.*, 2016; Manole *et al.*, 2017). One explanation for that discrepancy could be a functional compensation of MTMR2 loss in OLs *in vivo*, for instance by MTMR1. Thus, Rab35 might also regulate MTMR complexes and mTORC1 activity in OLs.

Rab35 is reported to recruit the ARF6-GAP ACAP2 and thereby represses ARF6 activity and eventually OL differentiation (Miyamoto *et al.*, 2013). How ARF6 finally promotes the latter remains enigmatic. Alternatively, elevated mTORC1 activity could be the underlying cause. A gain in differentiation might even directly contribute to the observed *in vitro* hypermyelination in our cultures, though our setting did not allow us to analyze this in *Rab35* icKO cultures directly. Mono-cultures of Rab35-depleted OPCs displayed markedly reduced proliferation and increased cell death, and thus, were not sufficiently confluent for a comprehensive OL analysis upon early tamoxifen application (Figure 3-2a-c). The defects in proliferation might result from altered recycling and signaling of the main receptor for OPC proliferation, PDGFRα, as suggested from HEK cell experiments (Wheeler *et al.*, 2015). Interestingly, increased apoptosis of OPCs is also reported upon elevated mTORC1 activity in conditional *TSC1* knockout mice (Jiang *et al.*, 2016). However, this could also result from mTORC1-independent regulation by TSC1 (Figlia *et al.*, 2017). Interestingly, lower proliferation rates accompanied by increased apoptotic cell death have been observed for SC precursors depleted of MTMR2 in mono-cultures (Chojnowski *et al.*, 2007), though this effect was never reported upon co-culturing with neurons (Bolis *et al.*, 2009). Thus, our data could rather reflect the hypersensitivity of OPCs in mono-cultures, than predicting a great loss of Rab35-depleted OPCs *in vivo*.

Rab35 is presumed to mediate docking of MVBs to the plasma membrane and thus to promote the secretion of exosomes in oligodendrocytes (Hsu *et al.*, 2010). In the absence of the small GTPase, impaired exosome secretion is observed *in vitro*, accompanied by intracellular accumulation of PLP in LAMP-positive compartments. A function of Rab35 in the secretion of exosomes is also reported from non-myelinating cells (Novo *et al.*, 2018; Yang *et al.*, 2019). Intriguingly, the accumulation of MAG in LAMP-positive compartments is observed in cultured oligodendrocytes from *Fig4*$^{-/-}$ mice as well, which display reduced PI(3,5)P_2 levels (Mironova *et al*, 2016). Thus, defects in MVB fusion with the plasma membrane in the absence of Rab35 could be caused by dysregulateded PI(3)-phosphate conversion. However, the consequence of impaired exosome release on myelin formation in Rab35-depleted oligodendrocytes was not investigated so far (Hsu *et al.*, 2010). Recent publications indicate a crucial requirement of MAG- and PLP-release by LE/Lys in the formation of myelin sheaths (Simmons and Trajkovic, 2006; Winterstein *et al.*, 2008; Mironova *et al.*, 2016). Accordingly, PLP-containing MVBs located to non-compacted myelin regions, in paranodal loops and cytoplasmic channels, the presumed sites of myelin growth (Hsu *et al.*, 2010). The limited cell number in primary OL cultures did not allow us to

directly address this question by purification and thus, analysis of secreted exosomes. However, *Rab35* icKO oligodendrocytes form myelin sheets *in vitro*, even in excess, and without obvious intracellular accumulation of myelin proteins (Figure 3-3). Thus, how impaired exosome secretion in the absence of Rab35 can contribute to the observed gain of myelin formation *in vitro* (Miyamoto *et al.*, 2013; this study) remains elusive at this point.

In consequence, Rab35 is strongly implicated in myelin homeostasis of the CNS and our data might indicate that the regulation of PI(3)-phosphates and mTORC1 contributes to the observed effects upon Rab35 loss *in vitro*. However, *in vivo* analysis of CNS myelination in OL-specific *Rab35* knockout animals will reveal its physiological requirement. If myelin proteins are indeed accumulated intracellularly *in vivo*, could be investigated then by purification of the myelin exosomal fraction from these brains with subsequent analysis by mass spectrometry.

4.4 Rab35-dependent mechanisms which might contribute to the control of myelin homeostasis

Rapamycin treatment rescued myelination defects in the absence of Rab35 *ex vivo* and *in vitro*. However, impaired PNS myelin homeostasis *in vivo* is only partially ameliorated by mTORC1 inhibition. As already mentioned, this can be attributed to the treatment timing on the one hand. On the other, it could also indicate that other processes downstream of Rab35 and independent of mTORC1 contribute to PNS myelin homeostasis.

Rab35 is implicated in the regulation of the actin cytoskeleton via its effector protein fascin, the GEF DENND1C, as well as CDC42 and Rac1, in the formation of actin-rich protrusions during phagocytosis, filopodium and lamellipodium formation, as well as in neurite outgrowth (Shim *et al.*, 2010; Chevallier *et al.*, 2009). The regulation of the actin cytoskeleton is important in SC-mediated radial sorting of axons, and the axonal ensheathment by OLs and SCs (Bacon *et al.*, 2007; Benninger *et al.*, 2007; Nodari *et al.*, 2007; Chernousov *et al.* 2008). Despite, *Rab35* cKO^{SC} nerves did not display an obvious impairment or delay of axonal sorting and ensheathment. Alternatively, a loss of OCRL recruitment by Rab35 could contribute to aberrant myelination. PI(4,5)P_2 is the major PI in the plasma membrane (Deshmukh *et al.*, 1980) as well as in myelin layers, in which MBP binds to this lipid (Musse *et al.*, 2006). Interestingly, a myelination defect in the white matter was observed by MRI (magnetic resonance imaging) in some Lowe-Oculo-Cerebro-Renal syndrome patients, caused by mutations in OCRL (Carvalho-Neto *et al.*, 2009). This could implicate Rab35 in CNS myelination *in vivo* through regulation of OCRL as well.

In addition, the interaction between Rab35 and MTMR complexes could also regulate other mechanisms besides mTORC1 repression. Rab35 is involved in the recycling of different transmembrane receptors (Jean *et al.*, 2012; Xhabija *et al.*, 2011). In accordance, our screen for Rab35-associated proteins revealed a couple of receptors, including ErbB2 (Suppl-table 1). Interestingly, MTMR2 is involved in the recycling of AMPA receptors in spines (Lee *et al.*, 2010). Moreover, Schwann cell-specific knockout of VPS34, which causes severe hypomyelination *in vivo*, results in altered ErbB2/B3 recycling (Logan *et al.*, 2017). In addition, both, Rab35 and MTMR2 have been linked to the degradation of EGFR receptors (Allaire *et al.*, 2013; Cao *et al.*, 2008; Duan *et al.*, 2016; Zheng *et al.*, 2017; Ye *et al.*, 2018). ErbB2/B3 and EGFR (ErbB1) are closely related, internalized upon ligand binding and degraded in lysosomes. In contrast, we did not detect any gross changes in endomembrane organelles, including LE/Lys (Figure 3-16). However, loss of the PI(3)P- or PI(3,5)P_2-synthesizing enzymes, VPS34 or PIKfyve, but not of PI(3)-phosphatases have been reported to cause enlarged endosomal or lysosomal compartments (Bonangelino *et al.*, 2002; Ikonomov *et al.*, 2003; Dong *et al.*, 2010; Vaccari *et al.*, 2011; Carpentier *et al.*, 2013; Munson *et al.*, 2015; Jaber *et al.*, 2012; 2016). In agreement, altered endosomal or lysosomal morphology is not observed upon MTMR2 or -R13 depletion in Schwann cells or MEF cells (Ng *et al.*, 2013). A recent review proposes that ErbB receptor recycling could link the function of several CMT-associated proteins (Lee *et al.*, 2017). In contrast, neither ERK nor AKT activation downstream of ErbB receptors is altered in *MTMR2* KO or *Rab35* cKO^{SC} sciatic nerves (Bolino *et al.*, 2016; this study). Nevertheless, the potential involvement of Rab35 in ErbBR-recycling could be more directly addressed, for instance by the use of fluorescently labelled NRG1-III, or by analyzing the levels of phosphorylated, and thus activated receptors vs. total levels in *Rab35* cKO Schwann cells.

Finally, Rab35 might also function in exosome secretion in Schwann cells. Vesicular structures have been observed at cytoplasmic sites of the myelin sheath (Court *et al.* 2008; 2011a; Sotelo *et al.* 2013) and cytoplasmic paranodal loops are the presumed sites of membrane addition as well as the origin of focal hypermyelinaton (Berthold and Nilsson, 2002; Bolino *et al.*, 2004; Goebbels *et al.*, 2012). In a recent study the proteome of Schwann cell-derived exosomes has been analyzed. In contrast to OL-derived exosomes, myelin proteins were not identified (Wei *et al.*, 2019). However, cholesterol is released by exosome secretion as well, presumably for disposal (Canfran-Duque *et al.*, 2013). Thus, impaired cholesterol disposal together with mTORC1-mediated elevated cholesterol synthesis might lead to excessive and aberrant myelin growth. Notably, not only defective synthesis of

$PI(3,5)P_2$ but also elevated mTORC1 activity is linked to impaired exosome secretion in MEFs, HEK and HeLa cells (Zou *et al.*, 2018). In turn, rapamycin application or serum-starvation results in increased exosome release. Moreover, the loss of ARF6 causes hypomyelination of the PNS *in vivo*, and is accompanied by reduced mTORC1-, though also, MAPK/ERK- and PI3K/AKT- activation (Torii *et al.*, 2015). Notably, ARF6 has never been linked to $PI(3,5)P_2$ conversion, but was recently implicated in the regulation of mTORC1 activity at lysosomal sites by activating PLD (Knizhnik *et al.*, 2012). Furthermore, ARF6 is linked to MVB/exosome biogenesis by controlling the internalization of ILVs through its effector PLD2 (Ghossoub *et al.*, 2014). ARF6 acts also upstream of Rab35 by activating the Rab35-GAP TC1D10B (Chesneau *et al.*, 2012). Thus, the mutual regulation between Rab35 and ARF6 might function (mTORC1-dependent) in PNS myelination as well. ARF6 could link mTORC1 activation to exosome biogenesis, whereas Rab35 could couple mTORC1 inactivation via $PI(3,5)P_2$ dephosphorylation to exosome secretion. Exosomes are usually isolated from high-confluent cultures, and thus, the low yield of Schwann cells that are achieved from mouse nerves, limited the investigation of SC-derived exosomes from genetically modified mice so far. A recently published protocol circumvents these problems (Shojapour *et al.*, 2018). Here, exosomes are purified from a high yield of primary Schwann cells obtained through the degeneration of nerves from adult mice prior to SC isolation. This method could enable the analysis of SC-derived exosomes from *Rab35* cKO^{SC} mice.

4.5 The role of Rab35 in SV recycling

Rab35 is linked to the facilitation of synaptic vesicle recycling on an endosomal route in *D. melanogaster* (Uytterhoeven *et al.*, 2011). In the absence of its putative GAP Skywalker in fly NMJs, an increased abundance of endosomal compartments is reported to result from the upregulation of active Rab35. An accompanied elevation in SV protein degradation is presumed to lead to the observed increase in neurotransmitter release from these synapses. In contrast, in the absence of Rab35 we could not observe reduced formation of endosomal-like compartments in synapses of mammalian primary neurons (Figure S1i,j). In addition, SV endocytosis/ acidification of synaptotagmin1-pHluorin in these *Rab35* icKO neuronal cultures is unaffected (Figure S1f-h). Furthermore, surface and total protein pools of the SV proteins synaptotagmin1 and synaptophysin are not altered upon Rab35 depletion (Figure S1a-e). In parallel to our study, Waites and colleagues have investigated a potential function of Rab35 in the degradation of SV proteins in mammalian synapses (Sheehan *et al.*, 2016; Vaz-Silva *et al.*, 2018). In that study, elevated degradation of SV2 and VAMP2 upon neuronal activity or

overexpression of Rab35 has been observed. In turn, the depletion of Rab35 by shRNA-mediated knockdown led to decreased degradation (Sheehan *et al.*, 2016). The authors proposed a function of Rab35 in the endosomal sorting of distinct SV proteins for degradation into late endosomal MVBs. If and how degradation of SV proteins, of which only a subset is observed to depend on neuronal activity or Rab35 (Sheehan *et al.*, 2016), is achieved on the one hand, and impacts the recycling kinetics of SVs at mammalian synapses on the other, remains to be clarified. Our data show, that acute long-term depletion of Rab35 does not result in an overt defect in mammalian SV recycling *in vitro*. However, we cannot exclude a genetic compensation which is frequently observed in response to gene knockouts (El-Brolosy and Stainier, 2017). For instance, in *D. melanogaster*, Rab10 also controls $PI(4,5)P_2$ and ACAP-mediated ARF-6 regulation (Shi *et al.*, 2012). In addition, overlapping roles with Rab35 in the endosomal sorting of endocytosed cargo are displayed by Rab4, Rab5 and Rab11 (Pavlos *et al.*, 2010; Pavlos and Jahn, 2011).

Would altered SV recycling be expected due to the loss of lipid-regulated mTORC1 repression in the absence of Rab35? mTORC1 and $PI(3,5)P_2$-regulating enzymes are indeed implicated in synaptic functions, but so far, at postsynaptic compartments only. Presynaptic inactivity induces AMPA receptor-mediated mTORC1 activation at the postsynapse. This initiates presynaptic compensation by mTORC1-dependent translation of BDNF (brain-derived neurotrophic factor) (Henry *et al.*, 2018). MTMR2 is reported to function in the endocytic internalization of the AMPA receptor subunit GluA2 at postsynapses (Lee *et al.*, 2010). In addition, Vac14 or Fig4 depletion results in increased surface levels of GluA2 (Zhang *et al.*, 2012; McCartney *et al.*, 2014). Thus, a disturbance of synaptic plasticity might be an expectable outcome upon loss of Rab35. However, the application of inhibitors for AMPA and NMDA receptors in our system did not allow us to detect feedback loop-mediated effects from postsynaptic sites. In sum, we did not observe a direct effect of acute Rab35 depletion on SV recycling in primary neuronal cultures.

4.6 Future directions

This work unveils Rab35 as a novel regulator of myelin homeostasis in the PNS and a recruiter of MTMR lipid phosphatase complexes that dephosphorylate PI(3)P and PI(3,5)P_2 at late endosomal/ lysosomal membranes to suppress mTORC1 activity. This regulation might be required to tightly adapt the activity of the essential kinase complex to the availability of nutrients and axonal signals, and thus, contributes to Schwann cell survival and myelination adjustment to axonal parameters. These findings provide a deeper insight into a mechanism that might underlie common pathologies in demyelinating diseases but also raise new questions for future research.

Our data as well as recent studies implicate Rab35 in the control of oligodendrocytic myelin formation as well. If this regulation is also mediated by Rab35-dependent repression of mTORC1 activity should be further investigated. Furthermore, the sequential action of Rab35, PI(3)-phosphate regulation and mTORC1 activity could be implicated in controlling exosome secretion in OLs. Interestingly, PI(3)P and PI(3,5)P_2 synthesis at late endosomes/ MVBs is required for both, the fusion with lysosomes but also for exosome secretion (Cao *et al*., 2007; 2008; Mironova *et al*, 2016). How the fate of LE/Lys is determined to either of these endomembrane trafficking routes is still elusive. Nevertheless, how impaired secretion of major myelin proteins in the absence of Rab35 impacts myelin formation remains to be investigated and complicates a prediction of how loss of Rab35 will affect CNS myelination *in vivo*. According to our data, hypermyelination can be well expected.

Furthermore, despite of decades since the pathological features of focal hypermyelination have been first observed in demyelinating diseases (Madrid and Bradley 1975), the underlying molecular mechanisms that lead to their formation remain elusive. Similarly, how upregulated mTORC1 activity can induce these features is not resolved yet (Goebbels *et al*., 2012; Beirowski *et al*., 2017). Interestingly, tomacula and myelin outfoldings are also observed upon genetic defects in major myelin proteins (Sander *et al.*, 2000). As discussed, Rab35, PI(3)-phosphate lipid-conversion and mTORC1 might be linked at the level of cholesterol and myelin protein secretion as well. Thus, in addition to a transcriptional upregulation of myelin lipid synthesis by hyperactive mTORC1 in adult animals, impaired membrane addition, imbalanced myelin protein levels and/ or incorporation into nascent sheaths could account for the formation of aberrant myelin structures in *Rab35* cKO^{SC} animals. In accordance, the lack of myelin-residing proteins has been suggested to disrupt paranodal junctions and thereby contribute to focal hypermyelination (Guo *et al*.,

2014; Hu *et al*., 2016). Thus, the analysis of structural components within these regions might another conceivable approach in *Rab35* cKO^{SC} organotypic explants.

We could observe an accumulation of PI(3)P as well as increased mTORC1 activity in the absence of Rab35, in agreement with the reported activation of mTORC1 by PI(3)-phosphates in different cell types. Thus, Rab35-dependent repression of mTORC1 activity by recruiting MTMR lipid phosphatase complexes might be an ubiquitous mechanism. Our data reveal a crucial involvement of PI(3,5)P_2 in mTORC1 activation in Schwann cells. However, in other cell types mTORC1 activation might be dominated by PI(3)P, hydrolyzed by MTMR2 as well. Thus, why do MTMR2 and MTMR13 mutations almost exclusively affect Schwann cells? A possible explanation could be the association of active MTMR phosphatases with different pseudophosphatases in distinct tissues, such as MTMR5 and -R13 with MTMR2, which modulate their specificity towards PI(3)-phosphates. *Vice versa*, the loss or impairment of MTMR2 could be tissue-dependent compensated by another active MTMR phosphatase. Interestingly, overexpression of MTMR2 in myoblasts, which is usually expressed in these cells but presumably at low levels, can even rescue muscle defects in *MTM1* KO animals (Raess *et al.*, 2017). Our data reveal that pseudophosphatase complex partners of MTMR2 also associate with MTMR1. Thus, Rab35 can potentially control at least four different complexes. A cell type-specific redundancy of MTMR complexes could therefor account for varying sensitivities to the loss of distinct MTMR proteins. This might well explain the more severe focal hypermyelination in *Rab35* cKO^{SC} sciatic nerves compared to CMT4B-mouse models. Similarly, CMT4B2 results in a milder phenotype than CMT4B1 (Pareyson *et al.*, 2019), presumably due to the functional replacement of MTMR13 by MTMR5. However, if and in which context MTMR1 can substitute MTMR2 still needs to be investigated, *in vitro* and *in vivo*.

Finally, our findings implicate that mTORC1 activity might be dysregulated in CMT4B patients. Though this hypothesis remains to be confirmed, it is corroborated by the rescue effect of Niaspan: The downregulation of NRG-ErbBR and thus, AKT signaling in *MTMR2* KO nerve fibers ameliorates myelin outfoldings (Bolino *et al*., 2016). Nevertheless, Niaspan might also exert additional effects on several targets downstream of NRG-ErbBR. This could be circumvented by the potential use of Rapamycin and thus the direct tackling of mTORC1 activity in CMT4B patients.

5. Bibliography

Adlkofer K, Frei R, Neuberg DH-H, Zielasek J, Toyka KV, Suter U (1997) Heterozygous peripheral myelin protein 22-deficient mice are affected by a progressive demyelinating tomaculous neuropathy. *J Neurosci* 17:4662-4671

Aggarwal S, Yurlova L, Snaidero N, Reetz C, Frey S, Zimmermann J, Pähler G, Janshoff A, Friedrichs J, Müller DJ, Goebel C, Simons M (2011) A size barrier limits protein diffusion at the cell surface to generate lipid-rich myelin-membrane sheets. *Dev Cell* 21:445–456

Aggarwal S, Snaidero N, Pähler G, Frey S, Sánchez P, zweckstetter M, Janshoff A, Schneider A, Weil M-T, Schaap IAT, Görlich D, Simons M (2013) Myelin Membrane Assembly Is Driven by a Phase Transition of Myelin Basic Proteins Into a Cohesive Protein Meshwork. *PLOS Biology* 11(6):e1001577

Alazami AM, Alzahrani F, Bohlega S, Alkuraya FS (2014) SET binding factor 1 (SBF1) mutation causes Charcot-Marie-tooth disease type 4B3. *Neurology* 82:1665–1666

Allaire PD, Marat AL, Dall'Armi C, Di PG, McPherson PS, Ritter B (2010) The Connecdenn DENN domain: a GEF for Rab35 mediating cargo-specific exit from early endosomes. *Mol Cell* 37:370–382

Allaire PD, Seyed Sadr M, Chaineau M, Seyed Sadr E, Konefal S, Fotouhi M, Maret D, Ritter B, Del Maestro RF, McPherson PS (2013) Interplay between Rab35 and Arf6 controls cargo recycling to coordinate cell adhesion and migration. *J Cell Sci* 126(Pt3):722-731

Allen NJ, Barres BA (2009) Neuroscience: Glia - more than just brain glue. *Nature* 457:675-677

Alonso A, Sasin J, Bottini N, Friedberg I, Friedberg I, Osterman A, Godzik A, Hunter T, Dixon J, and Mustelin T (2004) Protein tyrosine phosphatases in the human genome. *Cell* 117(6):699-711

Anitei M, Ifrim M, Ewart MA, Cowan AE, Carson JH, Bansal R, Pfeiffer SE (2006) A role for Sec8 in oligodendrocyte morphological differentiation. *J Cell Sci* 119:807–818

Armada-Moreira A, Ribeiro FF, Sebastiao AM, Xapelli S (2015) Neuroinflammatory modulators of oligodendrogenesis. *Neuroimmunol Neuroinflamm* 2:263–273

Arthur-Farraj P, Wanek K, Hantke J, Davis CM, Jayakar A, Parkinson DB, Mirsky R, Jessen KR (2011) Mouse Schwann cells need both NRG1 and cyclic AMP to myelinate. *Glia* 59(5):720–733

Arthur-Farraj PJ, Latouche M, Wilton DK, Quintes S, Chabrol E, Banerjee A, Woodhoo A, Jenkins B, Rahman M, Turmaine M, Wicher GK, Mitter R, Greensmith L, Behrens A, Raivich G, Mirsky R, Jessen KR (2012) c-Jun reprograms Schwann cells of injured nerves to generate a repair cell essential for regeneration. *Neuron* 75:633-647

Asou H, Hamada K, Miyazaki T, Sakota T, Hayashi K, Takeda Y, Marret S, Delpech B, Itoh K, Uyemura K (1995) CNS myelinogenesis *in vitro*: time course and pattern of rat oligodendrocyte development. *J Neurosci Res* 40:519-534

Atluri PP, and Ryan TA (2006) The kinetics of synaptic vesicle reacidification at hippocampal nerve terminals. *J Neurosci* 26:2313-2320

Avni D, Biberman Y, Meyuhas O (1997) The 5' terminal oligopyrimidine tract confers translational control on TOP mRNAs in a cell type- and sequence context-dependent manner. *Nucleic Acids Res* 25:995-1001

Avruch J, Khokhlatchev A, Kyriakis JM, Luo Z, Tzivion G, Vavvas D and Zhang XF (2001) Ras activation of the Raf kinase: tyrosine kinase recruitment of the MAP kinase cascade. *Recent Prog Horm Res* 56(1):127–55

Azzedine H, Bolino A, Taïeb T, Birouk N, Di Duca M, Bouhouche A, Benamou S, Mrabet A, Hammadouche T, Chkili T, Gouider R, Ravazzolo R, Brice A, Laporte J, LeGuern E. (2003) Mutations in MTMR13, a new pseudophosphatase homologue of MTMR2 and Sbf1, in two families with an autosomal recessive demyelinating form of Charcot-Marie-Tooth disease associated with early-onset glaucoma. *Am J Hum Genet* 72(5):1141-53

Baba M, Hong SB, Sharma N, Warren MB, Nickerson ML, Iwamatsu A, Esposito D, Gillette WK, Hopkins III RF, Hartley JL, Furihata M, Oishi S, Zhen W, Burke Jr. TR, Linehan WM, Schmidt LS and Furihata M (2006) Folliculin encoded by the BHD gene interacts with a bindingprotein, FNIP1, and AMPK, and is involved in AMPK and mTOR signaling. *Proc Natl Acad Sci USA* 103:15552–15557

Bacon C, Lakics V, Machesky L, Rumsby M (2007) N-WASP regulates extension of filopodia and processes by oligodendrocyte progenitors, oligodendrocytes, and Schwann cells—Implications for axon ensheathment at myelination. *Glia* 55: 844–858

Bae E-J, Kim D-K, Kim C, Mante M, Adame A, Rockenstein E, Ulusoy A, Klinkenberg M, Jeong GR, Bae JR, Lee C, Lee H-J, Lee B-D, Di Monte DA, Masliah E and Lee S-J (2018) LRRK2 kinase regulates α-synuclein propagation via RAB35 phosphorylation. *Nat Commun* 9:3465

Baets J, Deconinck T, De Vriendt E, Zimoń M, Yperzeele L, Van Hoorenbeeck K, Peeters K, Spiegel R, Parman Y, Ceulemans B, Van Bogaert P, Pou-Serradell A, Bernert G, Dinopoulos A, Auer-Grumbach M, Sallinen SL, Fabrizi GM, Pauly F, Van den Bergh P, Bilir B, Battaloglu E, Madrid RE, Kabzińska D, Kochanski A, Topaloglu H, Miller G, Jordanova A, Timmerman V, De Jonghe P (2011) Genetic spectrum of hereditary neuropathies with onset in the first year of life. *Brain* 134:2664–76

Bago R, Malik N, Munson MJ, Prescott AR, Davies P, Sommer E, Shpiro N, Ward R, Cross D, Ganley IG and Alessi DR (2014) Characterization of VPS34-IN1, a selective inhibitor of Vps34, reveals that the phosphatidylinositol 3-phosphate-binding SGK3 protein kinase is a downstream target of class III phosphoinositide 3-kinase. *Biochem J* 463:413-427

Bakhti M, Winter C, Simons M (2010) Inhibition of myelin membrane sheath formation by oligodendrocyte-derived exosome-like vesicles. *J Biol Chem* 286:787–796

Bakhti M, Snaidero N, Schneider D, Aggarwal S, Möbius W, Janshoff A, Eckhardt M, Nave K-A and Simons M (2013) Loss of electrostatic cell-surface repulsion mediates myelin membrane adhesion and compaction in the central nervous system. *Proc Natl Acad Sci USA* 110:3143–3148

Bansal R., Stefansson K, Pfeiffer SE (1992). Proligodendroblast Antigen (POA), a Developmental Antigen Expressed by A007/O4-Positive Oligodendrocyte Progenitors Prior to the Appearance of Sulfatide and Galactocerebroside. *J Neuroch* 58(6):2221-2229

Bar-Peled L, Schweitzer LD, Zoncu R, Sabatini DM (2012) Ragulator is a GEF for the rag GTPases that signal amino acid levels to mTORC1. *Cell* 150(6):1196-208

Bar-Peled L, Chantranupong L, Cherniack AD, Chen WW, Ottina KA, Grabiner BC, Spear ED, Carter SL, Meyerson M, Sabatini DM (2013) A Tumor suppressor complex with GAP activity for the Rag GTPases that signal amino acid sufficiency to mTORC1. *Science* 340(6136):1100-6

Barateiro A, and Fernandes A (2014) Temporal oligodendrocyte lineage progression: *In vitro* models of proliferation, differentiation and myelination. *BBA-Mol Cell Res*

Barr F, Lambright DG (2010) Rab GEFs and GAPs. *Curr Opin Cell Biol* 22:461-70

Baumann N and Pham-Dinh D (2001) Biology of oligodendrocyte and myelin in the mammalian central nervous system. *Physiol rev* 81(2): 871-927

Beirowski B, Wong, KM, Babetto E and Milbrandt J (2017) mTORC1 promotes proliferation of immature Schwann cells and myelin growth of differentiated Schwann cells. *Proc. Natl Acad. Sci. USA* 114:E4261 – E4270

Belin S, Ornaghi F, Shackleford GG, Wang J, Scapin C, Lopez-Anido C, Silvestri N, Robertson N, Williamson C, Ishii A, Taveggia C, Svaren J, Bansal R, Schwab MH, Nave K-A, Fratta P, D'Antonio M, Poitelon Y, Feltri ML and Wrabetz L (2018) Neuregulin 1 type III improves peripheral nerve myelination in a mouse model of congenital hypomyelinating neuropathy. *Hum Mol Genet 28*(8):1260-1273

Benninger Y, Thurnherr T, Pereira JA, Krause S, Wu X, Chrostek-Grashoff A, Herzog D, Nave K-A, Franklin RJ, Meijer D, Brakebusch C, Suter U, Relvas JB (2007) Essential and distinct roles for cdc42 and rac1 in the regulation of Schwann cell biology during peripheral nervous system development. *J Cell Biol* 177:1051–1061

Bercury KK, Dai J, Sachs HH, Ahrendsen JT, Wood TL, Macklin WB (2014) Conditional ablation of raptor or rictor has differential impact on oligodendrocyte differentiation and CNS myelination. *J Neurosci.* 34(13):4466-80

Berger P, Bonneick S, Willi S, Wymann M, Suter U (2002) Loss of phosphatase activity in myotubularin-related protein 2 is associated with Charcot-Marie-Tooth disease type 4B1. *Hum Mol Genet* 11:1569–1579

Berger P, Schaffitzel C, Berger I, Ban N, Suter U (2003) Membrane association of myotubularin-related protein 2 is mediated by a pleckstrin homology-GRAM domain and a coiled-coil dimerization module. *Proc. Natl Acad. Sci. USA* 100(21):12177–12182

Berger P, Niemann A, Suter U (2006a) Schwann cells and the pathogenesis of inherited motor and sensory neuropathies (Charcot-Marie-Tooth disease). *Glia* 54:243–257

Berger P, Berger I, Schaffitzel C, Tersar K, Volkmer B, Suter U (2006b) Multi-level regulation of myotubularin-related protein-2 phosphatase activity by myotubularin-related protein-13/SET-binding factor-2. *Hum Mol Genet* 15(4):569–579

Berger P, Tersar K, Ballmer-Hofer K, Suter U (2011) The CMT4B disease-causing proteins MTMR2 and MTMR13/SBF2 regulate AKT signalling. *J Cell Mol Med* 15(2):307-15

Berghs S, Aggujaro D, Dirkx R Jr, Maksimova E, Stabach P, Hermel JM, Zhang JP, Philbrick W, Slepnev V, Ort T, Solimena M (2000). βIV spectrin, a new spectrin localized at axon initial segments and nodes of ranvier in the central and peripheral nervous system. *J Cell Biol* 151:985–1002

Berthold CH, Nilsson I, Rydmark M (1983) Axon diameter and myelin sheath thickness in nerve fibres of the ventral spinal root of the seventh lumbar nerve of the adult and developing cat. *J Anat* 136(Pt 3):483-508

Berthold CH and Nilsson RI (2002) De- and remyelination in spinal roots during normal perinatal development in the cat: a brief summary of structural observations and a conceptual hypothesis. *J Anat* 200:391-403

Bilanges B, Alliouachene S, Pearce W, Morelli D, Szabadkai G, Chung YL, chicanne G, Valet C, Hill JM, Voshol PJ, Collinson L, Peddie C, Ali K, Ghazaly E, Rajeeve V, Trichas G, Srinivas S, Chaussade C, Salamon RS, Backer JM, Scudamore CL, Whitehead MA, Keany EP, Murphy OL, Semple RK, Payrastre B, Tooze SA and Vanhaesebroeck B (2017) Vps34 PI 3-kinase inactivation enhances insulin sensitivity through reprogramming of mitochondrial metabolism. *Nat Commun* 8:1804

Bird TD (1998) Charcot-Marie-Tooth Neuropathy Type 4. *Seattle (WA): University of Washington, Seattle* 1993-2019

Birnboim HC and Doly J (1979) A rapid method for the purification of plasmid DNA. *Nucl Acids Res* 7:1513-1523

Bjartmar C, Yin X, Trapp BD (1999) Axonal pathology in myelin disorders. *J Neurocytol.* 28(4-5):383-95

Black JA, Kocsis JD, Waxman SG (1990) Ion channel organization of the myelinated fiber. *Trends Neurosci* 13:48-54

Blondeau F, Laporte J, Bodin S, Superti-Furga G, Payrastre B and Mandel JL (2000) Myotubularin, a phosphatase deficient in myotubular myopathy, acts on phosphatidylinositol 3-kinase and phosphatidylinositol 3-phosphate pathway. *Hum Mol Genet 9(15):2223-2229*

Blümer J, Rey J, Dehmelt L, Mazel T, Wu YW, Bastiaens P, Goody RS, Itzen A. (2013) RabGEFs are a major determinant for specific Rab membrane targeting. *J Cell Biol* 200:287–300

Bohlega S, Alazami AM, Cupler E, Al-Hindi H, Ibrahim E, Alkuraya FS (2011) A novel syndromic form of sensory-motor polyneuropathy is linked to chromosome 22q13.31-q13.33. *Clin Genet* 79:193–5

Bolino A, Marigo V, Ferrera F, Loader J, Romio L, Leoni A, Di Duca Marco, Cinti R, Cecchi C, Feltri ML, Wrabetz L, Ravazzolo R, Monaco AP (2002) Molecular characterization and expression analysis of Mtmr2, mouse homologue of MTMR2, the myotubularin-related 2 gene, mutated in CMT4B. *Gene* 283:17-26

Bolino A, Bolis A, Previtali SC, Dina G, Bussini S, Dati G, Amadio S, Del Carro U, Mruk DD, Feltri ML, Cheng CY, Quattrini A, Wrabetz L (2004) Disruption of Mtmr2 produces CMT4B1-like neuropathy with myelin outfolding and impaired spermatogenesis. *J Cell Biol* 167:711–721

Bolino A, Piguet F, Alberizzi V, Pellegatta M, Rivellini C, Guerrero-Valero M, Noseda R, Brombin C, Nonis A, D'Adamo P, Taveggia C and Previtali SC (2016) Niacin-mediated Tace activation ameliorates CMT neuropathies with focal hypermyelination. *EMBO Mol Med* 8(12):1438-1454

Bolis A, Coviello S, Bussini S, Dina G, Pardini C, Previtali SC, Malaguti M, Morana P, Del Carro U, Feltri ML, Quattrini A, Wrabetz L, Bolino A (2005) Loss of Mtmr2 phosphatase in Schwann cells but not in motor neurons causes Charcot-Marie-Tooth type 4B1 neuropathy with myelin outfoldings. *J Neurosci* 25:8567–8577

Bolis A, Zordan P, Coviello S and Bolino A (2007) Myotubularin-related (MTMR) phospholipid phosphatase proteins in the peripheral nervous system. *Mol Neurobiol* 35(3):308

Bolis A, Coviello S, Visigalli I, Taveggia C, Bachi A, Chishti AH, Hanada T, Quattrini A, Previtali SC, Biffi A, Bolino A (2009) Dlg1, Sec8, and Mtmr2 regulate membrane homeostasis in Schwann cell myelination. *J Neurosci* 29:8858–8870

Bonangelino CJ, Nau JJ, Duex JE, Brinkman M, Wurmser AE, Gary JD, Emr SD and Weisman LS (2002) Osmotic stress-induced increase of phosphatidylinositol 3,5-bisphosphate requires Vac14p, an activator of the lipid kinase Fab1p. *J Cell Biol* 156:1015-1028

Boussif O, Lezoualc'h F, Zanta MA, Mergny MD, Scherman D, Demeneix B, Behr JP (1995) A versatile vector for gene and oligonucleotide transfer into cells in culture and *in vivo*: polyethylenimine. *Proc Natl Acad Sci U S A* 92(16):7297-301

Bradford MM (1976) A rapid and sensitive method for the quantitation of microgram quantities of protein utilizing the principle of protein-dye binding. *Anal Biochem* 72:248-254

Bridges D, Ma JT, Park S, Inoki K, Weisman LS, Saltiel AR (2012) PI(3,5)P_2 plays a role in the activation and subcellular localization of mTORC1. *Mol Biol Cell* 23:2955–2962

Brinkmann, BG, Agarwal A, Sereda MW, Garratt AN, Müller T, Wende H, Nave K-A (2008) Neuregulin-1/ErbB signaling serves distinct functions in myelination of the peripheral and central nervous system. *Neuron* 59:581–595

Brockes JP, Fields KL, Raff MC (1979) Studies on cultured rat Schwann cells. I. Establishment of purified populations from cultures of peripheral nerve. *Brain Res* 165:105–118

Bujalka H, Koenning M, Jackson S, Perreau VM, Pope B, Hay CM,Mitew S, Hill AF, Lu QR, Wegner M, Srinivasan R, Svaren J, Willingham M, Barres BA, Emery B (2013) MYRF is a mem-brane-associated transcription factor that autoproteolytically cleaves todirectly activate myelin genes. *PLoS Biol* 11:e1001625

Buj-Bello A, Furling D, Tronchere H, Laporte J, Lerouge T, Butler-Browne GS, Mandel JL (2002) Muscle-specific alternative splicing of myotubularin-related 1 gene is impaired in DM1 muscle cells. *Hum Mol Genet* 11 2297–2307

Bunge M B, Williams AK and Wood PM (1982) Neuron-Schwann cell interaction in basal lamina formation. *Dev Biol* 92:449-460

Bunge RP, Bunge MB and Eldridge CF (1986) Linkage between axonal ensheathment and basal lamina production by Schwann cells. *Annu Rev Neurosc* 9:305-328

Bunge RP, Bunge MB and Bates M (1989) Movements of the Schwann cell nucleus implicate progression of the inner (axon-related) Schwann cell process during myelination. *J Cell Biol* 109:273-284

Burstein ES and Macara IG (1992) Interactions of the ras-like protein p25rab 3A with Mg2+ and guanine nucleotides. *Biochem J* 282(2):387-392

Byfield MP, Murray JT and Backer JM (2005) hVps34 is a nutrient-regulated lipid kinase required for activation of p70 S6 kinase. *J Biol Chem* 280:33076–33082

Cai Z, Sutton-Smith P, Swift J, Cash K, Finnie J, Turnley A, Thompson PD and Blumbergs PC (2002) Tomacula in MAG-deficient mice. *J PeripherNerv Sys7*(3):181-189

Caldwell KK, Lips DL, Bansal VS, Majerus PW (1992) Isolation and characterization of two 3-phosphatases that hydrolyze both phosphatidylinositol 3-phosphate and inositol 1,3-bisphosphate. *J Biol Chem* 266:18378–18386

Camargo N, Smit AB, Verheijen MH (2009) SREBPs: SREBP function in glia–neuron interactions. *FEBS J* 276: 628–636

Campeau PM, Kasperaviciute D, Lu JT, Burrage LC, Kim C, Hori M, Powell BR, Stewart F, Félix TM, van den Ende J, *et al*. (2014) The genetic basis of DOORS syndrome: an exome-sequencing study. *Lancet Neurol* 13(1):44-58

Canfran-Duque A, Pastor O, Quintana-Portillo R, Lerma M, de la Pena G, Martin-Hidalgo A, Fernández-Hernando C, Lasunción MA, Busto R (2013) Curcumin promotes exosomes/microvesicles secretion that attenuates lysosomal cholesterol traffic impairment. *Mol Nutr Food Re. 58*(4):687-697

Cao C, Laporte J, Backer J, Wandinger-Ness A, Stein M (2007) Myotubularin lipid phosphatase binds the hVPS15/hVPS34 lipid kinase complex on endosomes. *Traffic* 8:1052-1067

Cao C, Backer JM, Laporte J, Bedrick EJ, Wandinger-Ness A (2008) Sequential actions of myotubularin lipid phosphatases regulate endosomal PI(3)P and growth factor receptor trafficking. *Mol Biol Cell* 19(8):3334–3346

Cao Y, Wang Y, Saab WFA, Yang F, Pessin JE and Backer JM (2014) NRBF2 regulates macroautophagy as a component of Vps34 Complex I. *Biochem J* 461(2):315-322

Carpentier S, N'Kuli F, Grieco G, Van Der Smissen P, Janssens V, Emonard H, Bilanges B, Vanhaesebroeck B, Chevronnay HPG, Pierreux CE, Tyteca D, Courtoy PJ (2013) Class III phosphoinositide 3-kinase/VPS34 and dynamin are critical for apical endocytic recycling. *Traffic* 14(8):933-948

Carriere A, Romeo Y, Acosta-Jaquez HA, Moreau J, Bonneil E, Thibault P, Fingar DC, Roux PP (2010) ERK1/2 phosphorylate Raptor to promote Ras-dependent activation of mTOR complex 1 (mTORC1). *J Biol Chem* 286(1):567-77

Carson MJ, Behringer RR, Brinster RL, McMorris FA (1993) Insulin-like growth factor I increases brain growth and central nervous system myelination in transgenic mice. *Neuron* 10(4):729-40

Carson RP, Kelm ND, West KL, Does MD, Fu C, Weaver G, Ess KC (2015) Hypomyelination following deletion of Tsc2 in oligodendrocyte precursors. *Ann Clin Transl Neurol* 2:1041–1054

Carvalho-Neto Ad, Ono SE, Cardoso GdM, Santos ML, Schmitz F and Celidonio I (2009) Oculocerebrorenal syndrome of Lowe: magnetic resonance imaging findings in the first six years of life. *Arquivos de Neuro-Psiquiatria* 67(2a):305-307

Cauvin C, Rosendale M, Gupta-Rossi N, Rocancourt M, Larraufie P, Salomon R, Perrais D, Echard A (2016) Rab35 GTPase triggers switch-like recruitment of the lowe syndrome lipid phosphatase OCRL on newborn endosomes. *Curr Biol* 26:120–128

Cavanagh BL, Walker T, Norazit A, Meedeniya AC (2011) Thymidine analogues for tracking DNA synthesis. *Molecules* 16:7980–7993

Cebollero E, van der Vaart A, Zhao M, Rieter E, Klionsky DJ, Helms JB, Reggiori F (2012) Phosphatidylinositol-3-phosphate clearance plays a key role in autophagosome completion. *Curr Biol* 22:1545–1553

Chaineau M, Ioannou MS, McPherson PS (2013) Rab35: GEFs, GAPs and effectors. *Traffic* 14:1109-1117

Chang IA, Kim KJ and Namgung U (2018) α6 and β1 Integrin Heterodimer Mediates Schwann Cell Interactions with Axons and Facilitates Axonal Regeneration after Peripheral Nerve Injury. *Neuroscience 371:*49-59

Chantranupong L, Scaria SM, Saxton RA, Gygi M, Chen MS, Bermingham-McDonogh O, Danehy Jr FT, Nolan C, Scherer SS, Lucas J, David Gwynne & Marchionni MA (1994) Expression of multiple neuregulin transcripts in postnatal rat brains. *J Comp Neurol 349*(3):389-400

Chernousov MA, Yu WM, Chen ZL, Carey DJ, Strickland S (2008) Regulation of Schwann cell function by the extracellular matrix. *Glia* 56:1498–1507

Chesneau L, Dambournet D, Machicoane M, Kouranti I, Fukuda M, Goud B, Echard A (2012) An ARF6/Rab35 GTPase cascade for endocytic recycling and successful cytokinesis. *Curr Biol* 22:147–153

Chevallier J, Koop C, Srivastava A, Petrie RJ, Lamarche-Vane N, Presley JF (2009) Rab35 regulates neurite outgrowth and cell shape. *FEBS Lett* 583:1096–1101

Chiang GG, Abraham RT (2005) Phosphorylation of mammalian target of rapamycin (mTOR) at Ser-2448 is mediated by p70S6 kinase. *J Biol Chem* 280:25485–90

Chiu CC, Yeh TH, Lai SC, Weng YH, Huang YC, Cheng YC, Chen RS, Huang YZ, Hung J, Chen CC, Lin W-Y, Chang H-C, Chen Y-J, Chen C-L, Chen H-Y, Lin Y-W, Wu-Chou Y-H, Wang H-L and Lu Chin-Song (2016) Increased Rab35 expression is a potential biomarker and implicated in the pathogenesis of Parkinson's disease. *Oncotarget* 7:54215–27

Chiu SY, Ritchie JM (1984) On the physiological role of internodal potassium channels and the security of conduction in myelinated nerve fibres. *Proc R Soc Lond B Biol Sci 220(1221):415-22*

Chojnowski A, Ravisé N, Bachelin C, Depienne C, Ruberg M, Brugg B, Laporte J, Baron-Van Evercooren A, LeGuern E (2007) Silencing of the Charcot-Marie-Tooth associated MTMR2 gene decreases proliferation and enhances cell death in primary cultures of Schwann cells.*Neurobiol Dis.* 26(2):323-31

Chow E, Mottahedeh J, Prins M, Ridder W, Nusinowitz S and Bronstein JM (2005) Disrupted compaction of CNS myelin in an OSP/Claudin-11 and PLP/DM20 double knockout mouse. *Mol Cell Neurosci* 29:405–413

Chow CY, Zhang Y, Dowling JJ, Jin N, Adamska M, Shiga K, Szigeti K, Shy ME, Li J, Zhang X, Lupski JR, Weisman LS and Meisler MH (2007) Mutation of FIG4 causes neurodegeneration in the pale tremor mouse and patients with CMT4J. *Nature* 448:68–72

Chrast R, Saher G, Nave K-A, Verheijen MH (2011) Lipid metabolism in myelinating glial cells: lessons from human inherited disorders and mouse models. *J Lipid Res* 52(3):419-34

Clayton EL, Evans GJ, Cousin MA (2008) Bulk synaptic vesicle endocytosis is rapidly triggered during strong stimulation. *J Neurosci* 28(26):6627-32

Copp J, Manning G, Hunter T (2009) TORC-specific phosphorylation of mammalian target of rapamycin (mTOR): Phospho-Ser^{2481} is a marker for intact mTOR signaling complex 2. *Cancer Res.* 69:1821–1827

Cotter L, Ozcelik M, Jacob C, Pereira JA, Locher V, Baumann R, Relvas JB, Suter U, Tricaud N (2010) Dlg1-PTEN interaction regulates myelin thickness to prevent damaging peripheral nerve overmyelination. *Science* 328:1415–1418

Court FA, Sherman DL, Pratt T, Garry EM, Ribchester RR, Cottrell DF, Fleetwood-Walker SM, Brophy PJ (2004) Restricted growth of Schwann cells lacking Cajal bands slows conduction in myelinated nerves. *Nature* 431:191–195

Court FA, Hendriks WT, MacGillavry HD, Alvarez J, van Minnen J (2008) Schwann cell to axon transfer of ribosomes: Toward a novel understanding of the role of glia in the nervous system. *J Neurosci* 28:11024–11029

Court FA, Midha R, Cisterna BA, Grochmal J, Shakhbazau A, Hendriks WT, Van Minnen J (2011a) Morphological evidence for a transport of ribosomes from Schwann cells to regenerating axons. *Glia* 59:1529–1539

Court FA, Zambroni D, Pavoni E, Colombelli C, Baragli C, Figlia G, Sorokin L, Ching W, Salzer JL, Wrabetz L and Feltri ML (2011b) MMP2-9 cleavage of dystroglycan alters the size and molecular composition of Schwann cell domains. *J Neurosci* 31:12208–12217

Csibi, A, Lee, G, Yoon SO, Tong H, Ilter D, Elia I, Fendt S-M, Robert TM and Blenis J (2014) The mTORC1/S6K1 pathway regulates glutamine metabolism through the eIF4B-dependent control of c-Myc translation. *Curr Biol* 24(19):2274–2280

Dambournet D, Machicoane M, Chesneau L, Sachse M, Rocancourt M, El Marjou A, Formstecher E, Salomon R, Goud B and Echard A (2011) Rab35 GTPase and OCRL phosphatase remodel lipids and F-actin for successful cytokinesis. *Nat Cell Biol* 13:981-988

Danielian PS, Muccino D, Rowitch DH, Michael SK and McMahon AP (1998) Modification of gene activity in mouse embryos in utero by a tamoxifen-inducible form of Cre recombinase. *Curr Biol* 8:1323–1326

D'Antonio M, Musner N, Scapin C, Ungaro D, Del Carro U, Ron D, Feltri ML and Wrabetz L (2013) Resetting translational homeostasis restores myelination in Charcot–Marie–Tooth disease type 1B mice. *J. Exp. Med.* 210:821–838

Dateki M, Imamura O, Arai M, Shimizu H and Takishima K (2016) A novel strategy for selective gene delivery by using the inhibitory effect of blue light on jetPRIME-mediated transfection. *Biotechnol Bioeng* 113(7):1560-1567

Davey JR, Humphrey SJ, Junutula JR, Mishra AK, Lambright DG, James DE, Stockli J (2012) TBC1D13 Is A Rab35 Specific Gap That Plays An Important Role In GLUT4 Trafficking In Adipocytes. *Traffic* 13(10):1429-1441

Davis JQ, Lambert S, Bennett V (1996) Molecular composition of the node of Ranvier: Identification of ankyrin-binding cell adhesion molecules neurofascin (mucin+/third FNIII domain-) and NrCAM at nodal axon segments. *J Cell Biol* 135:1355–13567

Dawson MR, Levine JM and Reynolds R (2000) NG2-expressing cells in the central nervous system: Are they oligodendroglial progenitors. *J Neurosci Res* 61:471-479

Delague V, Jacquier A, Hamadouche T, Poitelon Y, Baudot C, Boccaccio I, Chouery E, Chaouch M, Kassouri N, Jabbour R, Grid D, Megarbane A, Haase G, Lévy N (2007) Mutations in FGD4 encoding the Rho GDP/GTP exchange factor FRABIN cause autosomal recessive Charcot-Marie-Tooth type 4H. *Am J Hum Genet* 81:1–16

De Leo MG, Staiano L, Vicinanza M, Luciani A, Carissimo A, Mutarelli M, Di Campli A, Polishchuk E, Di Tullio G, Morra V, Levtchenko E, Oltrabella F, Starborg T, Santoro M, Di Bernardo D, Devuyst O, Lowe M, Medina DL, Ballabio A, De Matteis MA (2016) Autophagosome-lysosome fusion triggers a lysosomal response mediated by TLR9 and controlled by OCRL. *Nat Cell Biol* 18(8):839-850

Demetriades C, Doumpas N and Teleman AA (2014) Regulation of TORC1 in response to amino acid starvation via lysosomal recruitment of TSC2. *Cell 156*(4):786-799

Deng, W, Wang, Y, Gu, L, Duan, B, Cui, J, Zhang, Y, Chen, Y, Sun, S, Dong, J, Du, J (2016) MICAL1 controls cell invasive phenotype via regulating oxidative stress in breast cancer cells. *BMC Cancer* 16*:*489

Deshmukh DS, Kuizon S, Bear WD and Brockeroff H (1980) Distribution of phosphoinositides among subfractions of rat brain myelin. *Lipids* 15:14–18

Devereaux K, Dall'Armi C, Alcazar-Roman A, Ogasawara Y, Zhou X, Wang F, Yamamoto A, De Camilli P and Di Paolo G (2013) Regulation of mammalian autophagy by class II and III PI 3-kinases through PI3P synthesis. *PloS one 8*(10):e76405

Di Paolo G and De Camilli P (2006) Phosphoinositides in cell regulation and membrane dynamics. *Nature* 443:651–657

Domenech-Estevez E, Baloui H, Meng X, Zhang Y, Deinhardt K, Dupree JL, Einheber S, Chrast R and Salzer JL (2016) Akt regulates axon wrapping andmyelin sheath thickness in the PNS. *J Neurosci* 36:4506–4521

Dong Z, Brennan A, Liu Y, Yarden Y, LefkowitzG, Mirsky R, Jessen KR (1995) Neu differentiation factor is a neuron-glia signal and regulates survival, proliferation, and maturation of rat Schwann cell precursors. *Neuron* 15:585–596

Dong XP, Shen D, Wang X, Dawson T, Li X, Zhang Q, Cheng X, Zhang Y, Weisman LS, Delling M and Xu H (2010) PI(3,5)P(2) controls membrane trafficking by direct activation of mucolipin Ca(2+) release channels in the endolysosome. *Nat Commun* 1:38

Dove SK, Cooke FT, Douglas MR, Sayers LG, Parker PJ and Michell RH (1997) Osmotic stress activatesphosphatidylinositol-3,5-bisphosphate synthesis. *Nature* 390:187–192

Duan B, Cui J, Sun S, Zheng J, Zhang Y, Ye B, Chen Y, Deng W, Du J, Zhu Y, Chen Y, Gu L (2016) EGF-stimulated activation of Rab35 regulates RUSC2-GIT2 complex formation to stabilize GIT2 during directional lung cancer cell migration. *Cancer Lett* 379:70-83

Düvel K, Yecies JL, Menon S, Raman P, Lipovsky AI, Souza AL, Triantafellow E, Ma Q, Gorski R, Cleaver S, Vander Heiden MG, MacKeigan JP, Finan PM, Clish CB, Murphy LO, Manning BD (2010) Activation of a metabolic gene regulatory network downstream of mTOR complex 1. *Mol Cell* 39:171–183

Ebner M, Sinkovics B, Szczygieł M, Ribeiro DW and Yudushkin I (2017) Localization of mTORC2 activity inside cells. *J Cell Biol* 216(2):343–353

Edgar JM McLaughlin M, Yool D, Zhang SC, Fowler JH, Montague P, Barrie JA, McCulloch M, Duncan ID, Barbern J, Nave K-A Griffiths IR (2004) Oligodendroglial modulation of fast axonal transport in a mouse model of hereditary spastic paraplegia. *J Cell Biol* 166:121–131

El-Abassi R, England JD, Carter GT (2014) Charcot-Marie-Tooth Disease: an overview of genotypes, phenotypes, and clinical management strategies. *PM R* 6(4):342–355

El-Brolosy MA, Stainier DYR (2017) Genetic compensation: A phenomenon in search of mechanisms. *PLoS Genet* 13(7):e1006780

Eldridge CF, Bunge MB, Bunge RP and Wood PM (1987) Differentiation of axon-related Schwann cells *in vitro*. I. Ascorbic acid regulates basal lamina assembly and myelin formation. *J Cell Biol* 105:1023-1034

Emery B, Dugas JC (2013) Purification of oligodendrocyte lineage cells from mouse cortices by immunopanning. *Cold Spring Harbor Protocols* 2013:854–868

Escher P, Lacazette E, Courtet M, Blindenbacher A, Landmann L, Bezakova G, Lloyd KC, Mueller U, Brenner HR (2005) Synapses form in skeletal muscles lacking neuregulin receptors. *Science* 308(5730):1920-3

Eshed Y, Feinberg K, Poliak S, Sabanay H, Sarig-Nadir O, Spiegel I, Bermingham JR Jr, Peles E (2005) Gliomedin mediates Schwann cell-axon interaction and the molecular assembly of the nodes of Ranvier. *Neuron* 47:215–229

Fabrizi GM, Taioli F, Cavallaro T, Rigatelli F, Simonati A, Mariani G, Perrone P and Rizzuto N (2000) Focally folded myelin in Charcot-Marie-Tooth neuropathy type 1B with Ser49Leu in the myelin protein zero. *Acta neuropathol 100*(3):299-304

Falace A, Filipello F, La Padula V, Vanni N, Madia F, De Pietri Tonelli D, de Falco FA, Striano P, Dagna Bricarelli F, Minetti C, Benfenati F, Fassio A, Zara F (2010) TBC1D24, an ARF6-interacting protein, is mutated in familial infantile myoclonic epilepsy. *Am J Hum Genet* 87(3):365-70

Falace A, Buhler E, Fadda M, Watrin F, Lippiello P, Pallesi-Pocachard E, Baldelli P, Benfenati F, Zara F, Represa A, Fassio A and Cardoso C (2014) TBC1D24 regulates neuronal migration and maturation through modulation of the ARF6-dependent pathway. *Proc Natl Acad Sci U S A* 111(6):2337-42

Falls DL (2003) Neuregulins: functions, forms, and signaling strategies. *Exp Cell Res* 284:14–30

Fang Y, Vilella-Bach M, Bachmann R, Flanigan A, Chen J (2001) Phosphatidic acid-mediated mitogenic activation of mTOR signaling. *Science* 294:1942–1945

Fang Y, Park IH, Wu AL, Du G, Huang P, Frohman MA, Walker SJ, Brown HA and Chen J (2003) PLD1 regulates mTOR signaling and mediates Cdc42 activation of S6K1. *Curr Biol 13*(23):2037-2044

Feltri ML, D'Antonio M, Previtali S, Fasolini M, Messing A, Wrabetz L (1999) P0-Cre transgenic mice for inactivation of adhesion molecules in Schwann cells. *Ann N Y Acad Sci* 883:116-123

Fernandez-Valle C, Gorman D, Gomez AM, Bunge MB (1997) Actin plays a role in both changes in cell shape and gene-expression associated with Schwann cell myelination. *J Neurosci* 17:241–250

Fields RD (2008) White matter in learning, cognition and psychiatric disorders. *Trends Neurosci* 31:361-370

Figlia G, Norrmen C, Pereira JA, Gerber D and Suter U (2017) Dual function of the PI3K-Akt-mTORC1 axis in myelination of the peripheral nervous system. *Elife* 6:e29241

Figlia G, Gerber D, and Suter U (2018) Myelination and mTOR. *Glia 66*(4):693-707

Filbin MT, Walsh FS, Trapp BD, Pizzey JA, Tennekoon GI (1990) Role of myelin P0 protein as a homophilic adhesion molecule. *Nature* 344:871–872

Fingar DC, Salama S, Tsou C, Harlow E, Blenis J (2002) Mammalian cell size is controlled by mTOR and its downstream targets S6K1 and 4EBP1/eIF4E. *Genes Dev* 16:1472–1487

Firestein R, Nagy PL, Daly M, Huie P, Conti M, Cleary ML (2002) Male infertility, impaired spermatogenesis, and azoospermia in mice deficient for the pseudophosphatase Sbf1. *J Clin Invest* 109:1165–1172

Flores AI, Narayanan SP, Morse EN, Shick HE, Yin X, Kidd G, Avila RL, Kirschner DA and Macklin WB (2008) Constitutively active Akt induces enhanced myelination in the CNS. *J Neurosci* 28(28):7174–7183

Flusser H, Halperin D, Kadir R, Shorer Z, Shelef I, Birk OS (2018) Novel SBF1 splice-site null mutation broadens the clinical spectrum of Charcot-Marie-Tooth type 4B3 disease. *Clin Genet* 94(5):473-9

Franklin NE, Taylor GS and Vacratsis PO (2011) Endosomal targeting of the phosphoinositide 3-phosphatase MTMR2 is regulated by an N-terminal phosphorylation site. *J Biol Chem* 286(18):15841-15853

Franklin NE, Bonham CA, Xhabija B and Vacratsis PO (2013) Differential phosphorylation of the phosphoinositide 3-phosphatase MTMR2 regulates its association with early endosomal subtypes. *J Cell Sci* 126(6):1333-1344

Fremont S, Hammich H, Bai J, Wioland H, Klinkert K, Rocancourt M, Kikuti C, Stroebel D, Romet-Lemonne G, Pylypenko O, Houdusse A and Echard A (2017) Oxidation of F-actin controls the terminal steps of cytokinesis. *Nat Commun* 8:14528

Fricker FR, Lago N, Balarajah S, Tsantoulas C, Tanna S, Zhu N, Fageiry SK, Jenkins M, Garratt AN, Birchmeier C, Bennett DL (2011) Axonally derived neuregulin-1 is required for remyelination and regeneration after nerve injury in adulthood. *J Neurosci* 31(9):3225-33

Friede RL, Beuche W (1985) Combined scatter diagrams of sheath thickness and fibre calibre in human sural nerves: changes with age and neuropathy. *J Neurol Neurosurg Psychiatry* 48(8):749-56

Frühbeis C, Fröhlich D, Kuo WP, Amphornrat J, Thilemann S, Saab AS, Kirchhoff F, Möbius W, Goebbels S, Nave K-A, Schneider A, Simons M, Klugmann M, Trotter J, Krämer-Albers E-M (2013) Neurotransmitter-triggered transfer of exosomes mediates oligodendrocyte-neuron communication. *PLoS Biol* 11:e1001604

Fruttiger M, Calver AR, Richardson WD (2000) Platelet-derivedgrowth factor is constitutively secreted from neuronal cellbodies but not from axons. *Curr Biol* 10:1283–6

Fuchs E, Haas AK, Spooner RA, Yoshimura S, Lord JM, Barr FA (2007) Specific Rab GTPase-activating proteins define the Shiga toxin and epidermal growth factor uptake pathways. *J Cell Biol* 177(6):1133-1143

Fumgalli S, Thomas G (2000) S6 phosphorylation and signal transduction. *Cold Spring Harbor Monograph Archive* 39:695-717

Fünfschilling U, Supplie LM, Mahad D, Boretius S, Saab AS, Edgar J, Brinkmann BG, Kassmann CM, Tzvetanova ID, Möbius W, Diaz F, Meijer D, Suter U, Hamprecht B, Sereda MW, Moraes CT, Frahm J, Goebbels S, Nave K-A (2012) Glycolytic oligodendrocytes maintain myelin and long-term axonal integrity. *Nature* 485(7399):517-21

Furusho M, Dupree JL, Nave K-A, Bansal R (2012) Fibroblast growth factor receptor signaling in oligodendrocytes regulates myelin sheath thickness. *J Neurosci* 32(19):6631-41

Furusho M, Ishii A and Bansal R (2017) Signaling by FGF receptor 2, not FGF receptor 1, regulates myelin thickness through activation of ERK1/2-MAPK, which promotes mTORC1 activity in an Akt-independent manner. *J Neurosci* 37:2931–2946

Gao Y, Balut CM, Bailey MA, Patino-Lopez G, Shaw S, Devor DC (2010) Recycling of the Ca2+-activated K+ channel, KCa2.3, is dependent upon RME-1, Rab35/EPI64C, and an N-terminal domain. *J Biol Chem* 285(23):17938-17953

Garbay B, Heape AM, Sargueil F, Cassagne C (2000) Myelin synthesis in the peripheral nervous system. *Prog Neurobiol* 61:267–304

Gayle S, Landrette S, Beeharry N, Conrad C, Hernandez M, Beckett P, Ferguson SM, Mandelkern T, Zheng M, Xu T, Rothberg J and Lichtenstein H (2017) Identification of apilimod as a first-in-class PIKfyve kinase inhibitor for treatment of B-cell non-Hodgkin lymphoma. *Blood* 129:1768-1778

Ghomashchi F, Zhang X, Liu L and Gelb MH (1995) Binding of prenylated and polybasic peptides to membranes: affinities and intervesicle exchange. *Biochemistry* 34:11910–11918

Ghossoub R, Lembo F, Rubio A, Gaillard CB, Bouchet J, Vitale N, Slavík J, Machala M, Zimmermann P (2014) Syntenin-ALIX exosome biogenesis and budding into multivesicular bodies are controlled by ARF6 and PLD2. *Nat Commun* 5:3477

Ghislain J, Charnay P (2006) Control of myelination in Schwann cells: a Krox20 cis-regulatory element integrates Oct6, Brn2 and Sox10 activities. *EMBO Rep* 7(1):52-8

Gibson EM, Geraghty AC, Monje M (2018) Bad wrap: Myelin and myelin plasticity in health and disease. *Dev Neurobiol* 78(2):123-135

Gillingham AK, Sinka R, Torres IL, Lilley KS and Munro S (2014) Toward a comprehensive map of the effectors of rab GTPases. *Dev Cell* 31(3):358-373

Gillooly DJ, Raiborg C, Stenmark H. (2003) Phosphatidylinositol 3-phosphate is found in microdomains of early endosomes. *Histochem Cell Biol* 120:445-453

Gingras, AC, Raught B & Sonenberg N (1999) eIF4 initiation factors: effectors of mRNA recruitment to ribosomes and regulators of translation. *Annu Rev Biochem* 68:913–963

Glenn TD, Talbot WS (2013a) Analysis of Gpr126 function defines distinct mechanisms controlling the initiation and maturation of myelin. *Development* 140:3167–3175

Goebbels S, Oltrogge JH, Kemper R, Heilmann I, Bormuth I,Wolfer S, Wichert SP, Möbius W, Liu X, Lappe-Siefke C, Rossner MJ, Groszer M, Suter U, Frahm J, Boretius S and Nave K-A (2010) Elevated phosphatidylinositol 3,4,5-trisphosphate in glia triggers cell-autonomous membrane wrappingand myelintion. *J Neurosci* 30:8953–8964

Goebbels S, Oltrogge JH, Wolfer S, Wieser GL, Nientiedt T, Pieper A, Ruhwedel T, Groszer M, Sereda M. and Nave K-A (2012) Genetic disruption of Pten in a novel mouse model of tomaculous neuropathy. *EMBO Mol Med* 4(6):486–499

Gomez-Sanchez JA, Carty L, Iruarrizaga-Lejarreta M,Palomo-Irigoyen M, Varela-Rey M, Griffith M, Hantke J,Macias-Camara N, Azkargorta M, Aurrekoetxea I, De JuanVG, Jefferies HB, Aspichueta P, Elortza F, Aransay AM, Martinez-Chantar ML, Baas F, Mato JM, Mirsky R,Woodhoo A and Jessen KR (2015) Schwann cell autophagy,myelinophagy, initiates myelin clearance from injured nerves. *J Cell Biol* 210:153–168

Goryunov D, Nightingale A, Bornfleth L, Leung C, Liem RK (2008) Multiple disease-linked myotubularin mutations cause NFL assembly defects in cultured cells and disrupt myotubularin dimerization. *J Neurochem* 104:1536–1552

Graham R and Karnovsky MJ (1966) The early stages of absorption of injected horseradish peroxidase in the proximal tubules of mouse kidney: ultrastructural cytochemistry by a new technique. *J Histochem Cytochem* 14:291-302

Graham FL, van der Eb AJ (1973) A new technique for the assay of infectivity of human adenovirus 5 DNA. *Virology*. 52:456–467

Gravel M, Peterson J, Yong VW, Kottis V, Trapp B and Braun PE (1996) Overexpression of 29,39-cyclic nucleotide 39-phosphodiesterase in transgenic mice alters oligodendrocyte development and produces aberrant myelination. *Mol Cell Neurosci* 7:453-466

Griffin JW, Thompson WJ (2008) Biology and pathology of nonmyelinating Schwann cells. *Glia* 56:1518-1531

Grosshans BL, Ortiz D, Novick P (2006) Rabs and their effectors: achieving specificity in membrane traffic. *Proc Natl Acad Sci U S A* 103(32):11821-7

Gu X, Orozco JM, Saxton RA, Condon KJ, Liu GY, Krawczyk PA, Scaria SM, Harper JW, Gygi SP and Sabatini DM (2017) SAMTOR is an S-adenosylmethionine sensor for the mTORC1 pathway. *Science* 358(6364):813–818

Guilbot A, Williams A, Ravise N, Verny C, Brice A, ShermanDL, Brophy PJ, LeGuern E, Delague V, Bareil C, MegarbaneA, Claustres M (2001) A mutation in periaxin is responsiblefor CMT4F, an autosomal recessive form of Charcot-Marie-Tooth disease. *Hum Mol Genet* 10:415–421

Gupta VA, Hnia K, Smith LL, Gundry SR, McIntire JE, Shimazu J, Bass JR, Talbot EA, Amoasii L, Goldman NE, Laporte J, Beggs AH (2013) Loss of Catalytically Inactive Lipid Phosphatase Myotubularin-Related Protein 12 Impairs Myotubularin Stability and Promotes Centronuclear Myopathy in Zebrafish. *PLoS Genet* 9(6):e1003583

Haley R, Wang Y, Zhou Z (2018) The small GTPase RAB-35 defines a third pathway that is required for the recognition and degradation of apoptotic cells. *PLoS Genet* 14(8):e1007558

Hammond GR, Schiavo G and Irvine RF (2009) Immunocytochemical techniques reveal multiple, distinct cellular pools of PtdIns4P and PtdIns(4,5)P_2. *Biochem J* 422:23–35

Hammond GR, Takasuga S, Sasaki T, Balla T (2015) The ML1Nx2 Phosphatidylinositol 3,5-Bisphosphate Probe Shows Poor Selectivity in Cells. *PLoS One* 10:e0139957

Han J M, Jeong SJ, Park MC, Kim G, Kwon NH, Kim HK, Ha S-H, Ryu S-H and Kim S (2012) Leucyl-tRNA synthetase is an intracellular leucine sensor for the mTORC1-signaling pathway. *Cell* 149(2):410-424

Han J, Zhang L, Guo H, Wysham WZ, Roque DR, Willson AK, Sheng X, Zhou C and Bae-Jump VL (2015a) Glucose promotes cell proliferation, glucose uptake and invasion in endometrial cancer cells via AMPK/mTOR/S6 and MAPK signaling. *Gynecologic oncology* 138(3):668–675

Han J, Li E, Chen L, Zhang Y, Wei F, Liu J, Deng H, Wang Y (2015b) The CREB coactivator CRTC2 controls hepatic lipid metabolism by regulating SREBP1. *Nature* 524(7564):243-6

Hanahan D (1983) Studies on transformation of Escherichia coli with plasmids. *J Mol Biol* 166(4):557-580

Hao F, Itoh T, Morita E, Shirahama-Noda K, Yoshimori T and Noda T (2016) The PtdIns3-phosphatase MTMR3 interacts with mTORC1 and suppresses its activity. *FEBS letters 590*(1):161-173

Harding AE and Thomas PK (1980) Autosomal recessive forms of hereditary motor and sensory neuropathy. *J Neurol Neurosurg Psychiatry* 43:669–678

Harrington LS, Findlay GM, Gray A, Tolkacheva T, Wigfield S, Rebholz H, Barnett J, Leslie NR, Cheng S, Shepherd PR, Gout I, Downes CP and Lamb RF (2004) The TSC1-2 tumor suppressor controls insulin-PI3K signaling via regulation of IRS proteins. *J Cell Biol* 166(2):213–223

Harris JJ, Attwell D (2012) The energetics of CNS white matter *J Neurosci* 32:356-371

Hasumi Y, Baba M, Ajima R, Hasumi H, Valera VA, Klein ME, Haines DC, Merino MJ, Hong SB, Yamaguchi TP, Schmidt LS, Linehan WM (2009) Homozygous loss of BHD causes early embryonic lethality and kidney tumor development with activation of mTORC1 and mTORC2. *Proc Natl Acad Sci U S A* 106:18722–18727

Hasumi Y, Baba M, Hasumi H, Huang Y, Lang M, Reindorf R, Oh HB, Sciarretta S, Nagashima K, Haines DC, Schneider MD, Adelstein RS, Schmidt LS, Sadoshima J, Marston Linehan W (2014) Folliculin (Flcn) inactivation leads to murine cardiac hypertrophy through mTORC1 deregulation. *Hum Mol Genet* 23(21):5706-19

Hayashi S and McMahon AP (2002) Efficient recombination in diverse tissues by a tamoxifen-inducible form of Cre: a tool for temporally regulated gene activation/inactivation in the mouse. *Dev Biol* 244:305–318

Heller BA, Ghidinelli M, Voelkl J, Einheber S, Smith R, Grund E, Morahan G, Chandler D, Kalaydjieva L, Giancotti F, King RH, Fejes-Toth AN, Fejes-Toth G, Feltri ML, Lang F, Salzer JL (2014) Functionally distinct PI 3-kinase pathways regulate myelination in the peripheral nervous system. *J Cell Biol* 204:1219–1236

Henry FE, Wang X, Serrano D, Perez AS, Carruthers CJL, Stuenkel EL and Sutton MA (2018) A unique homeostatic signaling pathway links synaptic inactivity to postsynaptic mTORC1. *J Neurosci 38*(9):2207-2225

Hildebrand C and Hahn R (1978) Relation between myelin sheath thickness and axon size in spinal cord white matter of some vertebrate species. *J Neurol Sci* 38:421–434

Hildebrand C, Remahl S, Persson H and Bjartmar C (1993) Myelinated Nerve Fibres in the Cns. *Prog Neurobiol* 40(3):319-84

Hirano R, Takashima H, Umehara F, Arimura H, Michizono K, Okamoto Y, Nakagawa M, Boerkoel CF, Lupski JR, Osame M, Arimura K (2004) SET binding factor 2 (SBF2) mutation causes CMT4B with juvenile onset glaucoma. *Neurology* 63:577–80

Hirsch DS, Shen Y, Dokmanovic M, Yu J, Mohan N, Elzarrad MK and Wu WJ (2014) Insulin activation of vacuolar protein sorting 34 mediates localized phosphatidylinositol 3-phosphate production at lamellipodia and activation of mTOR/S6K1. *Cell Signal* 26:1258–1268

Hnia K, Vaccari I, Bolino A, Laporte J (2012) Myotubularin phosphoinositide phosphatases: cellular functions and disease pathophysiology. *Trends Mol Med* 18:317–327

Holm S (1979) A simple sequentially rejective multiple test procedure. *Scan J Statistics* 6:65-70

Holz MK, Ballif BA, Gygi SP and Blenis J (2005) mTOR and S6K1 mediate assembly of the translation preinitiation complex through dynamic protein interchange and ordered phosphorylation events. *Cell* 123:569–580

Hong F, Larrea MD, Doughty C, Kwiatkowski DJ, Squillace R, and Slingerland JM (2008) mTOR-raptor binds and activates SGK1 to regulatep27 phosphorylation. *Mol Cell* 30:701–711

Hong Z, Pedersen NM, Wang L, Torgersen ML, Stenmark H and Raiborg C (2017) PtdIns3P controls mTORC1 signaling through lysosomal positioning. *J Cell Biol 216*(12):4217-4233

Hosokawa N, Hara T, Kaizuka T, Kishi C, Takamura A, Miura Y, Iemura S, Natsume T, Takehana K, Yamada N, Guan J-L, Oshiro N and Mizushima N (2009) Nutrient-dependent mTORC1 association with the ULK1-Atg13-FIP200 complex required for autophagy. *Mol Biol Cell* 20:1981–1991

Howe DG, McCarthy KD (2000) Retroviral inhibition of cAMP-dependent protein kinase inhibits myelination but not Schwann cell mitosis stimulated by interaction with neurons. *J Neurosci* 20:3513–3521

Hsu C, Morohashi Y, Yoshimura S, Manrique-Hoyos N, Jung S, Lauterbach MA, Bakhti M, Grønborg M, Möbius W, Rhee J, Barr FA, Simons M (2010) Regulation of exosome secretion by Rab35 and its GTPase-activating proteins TBC1D10A-C. *J Cell Biol* 189(2):223-32

Hsu PP, Kang SA, Rameseder J, Zhang Y, Ottina KA, Lim D, Peterson TR, Choi Y, Gray NS, Yaffe MB, Marto JA and Sabatini DM (2011) The mTOR-regulated phosphoproteome reveals a mechanism of mTORC1-mediated inhibition of growth factor signaling. *Science* 332:1317–1322

Hu QD, Ang BT, Karsak M, Hu WP, Cui XY, Duka T, Takeda Y, Chia W, Sankar N, Ng YK, Ling EA, Maciag T, Small D, Trifonova R, Kopan R, Okano H, Nakafuku M, Chiba S, Hirai H, Aster JC, Schachner M, Pallen CJ, Watanabe K, Xiao ZC (2003) F3/contactin acts as a functional ligand for Notch during oligodendrocyte maturation. *Cell* 115:163-175

Hu X, Hicks CW, He W, Wong P, Macklin WB, Trapp BD, Yan R (2006) Bace1 modulates myelination in the central and peripheral nervous system. *Nat Neurosci* 9:1520–1525

Hu JG, Wang YX, Wang HJ, Bao MS, Wang ZH, Ge X, Wang F-C, Zhou J-S and Lü HZ (2012) PDGF-AA mediates B104CM-induced oligodendrocyte precursor cell differentiation of embryonic neural stem cells through Erk, PI3K, and p38 signaling. *J Mol Neurosci* 46(3):644-653

Iida M, Koike H, Ando T, Sugiura M, Yamamoto M, Tanaka F and Sobue G (2012) A novel MPZ mutation in Charcot–Marie–Tooth disease type 1B with focally folded myelin and multiple entrapment neuropathies. *Neuromuscular Disord 22*(2):166-169

Ikonomov OC, Sbrissa D, Foti M, Carpentier JL and Shisheva A (2003) PIKfyve controls fluid phase endocytosis but not recycling/degradation of endocytosed receptors or sorting of procathepsin D by regulating multivesicular body morphogenesis. *Mol Biol Cell* 14:4581-4591

Ikonomov OC, Sbrissa D, Venkatareddy M, Tisdale E, Garg P and Shisheva A (2015) Class III PI 3-kinase is the main source of PtdIns3P substrate and membrane recruitment signal for PIKfyve constitutive function in podocyte endomembrane homeostasis. *Biochim Biophys Acta* 1853:1240-1250

Inoki K, Li Y, Zhu T, Wu J and Guan KL (2002) TSC2 is phosphorylated and inhibited by Akt and suppresses mTOR signalling. *Nat Cell Biol* 4:648–657

Isakoff SJ, Cardozo T, Andreev J, Li Z, Ferguson KM, Abagyan R, Lemmon MA, Aronheim A and Skolnik EY (1998) Identification and analysis of PH domain-containing targets of phosphatidylinositol 3-kinase using a novel *in vivo* assay in yeast. *EMBO J* 17:5374–5387

Ishii A, Furusho M, Bansal R (2013) Sustained activation of ERK1/2 MAPK in oligodendrocytes and schwann cells enhances myelin growth and stimulates oligodendrocyte progenitor expansion. *J Neurosci* 33:175–186

Jaber N, Dou Z, Chen J-S, Catanzaro J, Jiang Y-P, Ballou LM, Selinger E, Ouyang X, Lin RZ, Zhang J and Zong W-X (2012) Class III PI3K Vps34 plays an essential role in autophagy and in heart and liver function. *Proc. Natl Acad. Sci. USA* 109(6):2003-2008

Jaber N, Mohd-Naim N, Wang Z, DeLeon JL, Kim S, Zhong H, Sheshadri N, Dou Z, Edinger AL, Du G, Braga VM and Zong W-X (2016) Vps34 regulates Rab7 and late endocytic trafficking through recruitment of the GTPase-activating protein Armus. *J Cell Sci* 129(23):4424-4435

Jaegle M, Ghazvini M, Mandemakers W, Piirsoo M, Driegen S, Levavasseur F, Raghoenath S, Grosveld F and Meijer D (2003) ThePOU proteins Brn-2 and Oct-6 share important functions in Schwann cell development. *Genes Dev* 17:1380-1391

Jahn O, Tenzer S and Werner HB (2009) Myelin proteomics: molecular anatomy of an insulating sheath. *Mol Neurobiol* 40:55–72

Jang SW, Srinivasan R, Jones EA, Sun G, Keles S, Krueger C, Chang L-W, Nagarajan R, Svaren J (2010) Locus-wide identification of Egr2/Krox20 regulatory targets in myelin genes. *J Neuroch* 115:1409–1420

Jaworski A, Burden SJ (2006) Neuromuscular synapse formation in mice lacking motor neuron- and skeletal muscle-derived Neuregulin-1. *J Neurosci* 26(2):655-61

Jean S, Cox S, Schmidt EJ, Robinson FL and Kiger A (2012) Sbf/MTMR13 coordinates PI(3)P and Rab21 regulation in endocytic control of cellular remodeling. *Mol Biol Cell* 23(14):2723-40

Jean S, Cox S, Nassari S and Kiger AA (2015) Starvation-induced MTMR13 and RAB21 activity regulates VAMP8 to promote autophagosome-lysosome fusion. *EMBO Rep* 16(3):297-311

Jefferies HB, Reinhard C, Kozma SC and Thomas G (1994) Rapamycin selectively represses translation of the" polypyrimidine tract" mRNA family. *Proc. Natl Acad. Sci. USA* 91(10):4441-4445

Jeong GR, Jang EH, Bae JR, Jun S, Kang HC, Park CH, Shin JH, Yamamoto Y, Tanaka-Yamamoto K, Dawson VL, Dawson TM, Hur EM, Lee BD (2018) Dysregulated phosphorylation of Rab GTPases by LRRK2 induces neurodegeneration. *Mol Neurodegener* 13(1):8

Jessen KR, Mirsky R, Morgan L (1987) Myelinated, but not unmyelinated axons, reversibly down-regulate N-CAM in Schwann cells. *J Neurocytol* 16:681–688

Jessen K, Brennan A, Morgan L, Mirsky R, Kent A, Hashimoto Y and Gavrilovic J (1994) The Schwann cell precursor and its fate: a study of cell death and differentiation during gliogenesis in rat embryonic nerves. *Neuron* 12(3):509-527

Jessen KR, Mirsky R (1999) Why do Schwann cells survive in the absence of axons? *Ann NY Acad Sci* 883:109-115

Jessen KR and Mirsky R (2005) The origin and development of glial cells in peripheral nerves. *Nat. Rev Neurosci* 6:671–682

Jessen KR and Mirsky R (2019) The success and failure of the Schwann cell response to nerve injury. *Front Cell Neurosci* 13:33

Ji WT, Yang SR, Chen JY, Cheng YP, Lee YR, Chiang MK, Chen HR (2012) Arecoline downregulates levels of p21 and p27 through the reactive oxygen species/mTOR complex 1 pathway and may contribute to oral squamous cell carcinoma. *Cancer science* 103:1221–1229

Jiang M, Liu L, He X, Wang H, Lin W, Wang H, Yoon SO, Wood TL, and Lu QR (2016) Regulation of PERK-elF2α signalling by tuberous sclerosis complex-1 controls homeostasis and survival of myelinating oligodendrocytes. *Nat Commun* 7:12185

Jiang M, Rao R, Wang J, Wang J, Xu L, Wu LM, Chan JR, Wang H, Lu QR (2018) The TSC1-mTOR-PLK axis regulates the homeostatic switch from Schwann cell proliferation to myelination in a stage-specific manner. *Glia* 66:1947–59

Jin N, Chow CY, Liu L, Zolov SN, Bronson R, Davisson M, Petersen JL, Zhang Y, Park S, Duex JE, Goldowitz D, Meisler MH, Weisman LS (2008) VAC14 nucleates a protein complex essential for the acute interconversion of PI3P and PI(3,5)P(2) in yeast and mouse. *EMBO J* 27:3221–3234

Jin N, Mao K, Jin Y, Tevzadze G, Kauffman EJ, Park S, Bridges D, Loewith R, Saltiel AR, Klionsky DJ and Weisman LS (2014) Roles for PI(3,5)P2 in nutrient sensing through TORC1. *Mol Biol Cell* 25(7):1171-1185

Johansson O, Backman J (1983) Enhancement of immunoperoxidase staining using osmium tetroxide. *J Neurosci Methods* 7:185–193

Johansson M, Lehto M, Tanhuanpaeae K, Cover TL, Olkkonen VM (2005) The oxysterol-binding protein homologue ORP1L interacts with Rab7 and alters functional properties of late endocytic compartments. *Mol Biol Cell* 16:5480-5492

Johnstone RM (2005) Revisiting the road to the discovery of exosomes. *Blood Cells Mol Dis* 34(3):214-9

Julien LA, Carriere A, Moreau J and Roux PP (2010) mTORC1-activated S6K1 phosphorylates Rictor on threonine 1135 and regulates mTORC2 signaling. *Mol Biol Cell* 30(4):908-921

Jung CH, Jun CB, Ro SH, Kim YM, Otto NM, Cao J, Kundu M, Kim DH (2009) ULK-Atg13-FIP200 complexes mediate mTOR signaling to the autophagy machinery. *Mol Biol Cell* 20:1992–2003

Kabeya Y, Mizushima N, Ueno T, Yamamoto A, Kirisako T, Noda T, Kominami E, Ohsumi Y, Yoshimori T (2000) LC3, a mammalian homologue of yeast Apg8p, is localized in autophagosome membranes after processing. *EMBO J* 19:5720-8

Kaiser CL, Chapman BJ, Guidi JL, Terry CE, Mangiardi DA and Cotanche DA (2008) Comparison of activated caspase detection methods in the gentamicin-treated chick cochlea. *Hearing res 240*(1-2):1–11

Kalra H, Drummen GP, Mathivanan S (2016) Focus on extracellular vesicles: introducing the next small big thing. *Int J Mol Sci* 17:170

Kaminskyy V, Abdi A, Zhivotovsky B (2011) A quantitative assay for the monitoring of autophagosome accumulation in different phases of the cell cycle. *Autophagy* 7(1):83-90

Kao SC, Wu H, Xie J, Chang CP, Ranish JA, Graef IA, Crab-tree GR (2009) Calcineurin/NFAT signaling is required for neuregulin-regulated Schwann cell differentiation. *Science* 323: 651–654

Ke R, Liu L, Zhu Y, Li S, Xie X, Li F, Song Y, Yang L, Gao L, Li M (2016) Knockdown of AMPKα2 Promotes Pulmonary Arterial Smooth Muscle Cells Proliferation via mTOR/Skp2/p27(Kip1) Signaling Pathway. *Int J Mol Sci*.17(6):844

Ketel K, Krauss M, Nicot AS, Puchkov D, Wieffer M, Müller R, Subramanian D, Schultz C, Laporte J and Haucke V (2016) A phosphoinositide conversion mechanism for exit from endosomes. *Nature 529*(7586):408

Kidd GJ, Ohno N, Trapp BD (2013) Biology of Schwann cells. *Handb Clin Neurol* 115:55–79

Kim HA, DeClue JE, Ratner N (1997) cAMP-dependent protein kinase A is required for Schwann cell growth: Interactions between the cAMP and neuregulin/tyrosine kinase pathways. *J Neurosci Res* 49:236–247

Kim DH, Sarbassov DD, Ali SM, King JE, Latek RR, Erdjument-Bromage H, Tempst P, Sabatini DM (2002a) mTOR interacts with raptor to form a nutrient-sensitive complex that signals to the cell growth machinery. *Cell* 110:163–175

Kim SA, Taylor GS, Torgersen KM, Dixon JE (2002b) Myotubularin and MTMR2, phosphatidylinositol 3-phosphatases mutated in myotubular myopathy and type 4B Charcot-Marie-Tooth disease. *J Biol Chem* 277:4526–4531

Kim DH, Sarbassov DD, Ali SM, Latek RR, Guntur KV, Erdjument-Bromage H, Tempst P, Sabatini DM (2003a) GbetaL, a positive regulator of the rapamycin-sensitive pathway required for the nutrient-sensitive interaction between raptor and mTOR. *Mol Cell* 11:895–904

Kim SA, Vacratsis PO, Firestein R, Cleary ML, Dixon JE (2003b) Regulation of myotubularin-related (MTMR)2 phosphatidylinositol phosphatase by MTMR5, a catalytically inactive phosphatase. *Proc Natl Acad Sci USA* 100:4492–4497

Kim J, Kim YC, Fang C, Russell RC, Kim JH, Fan W, Liu R, Zhong Q and Guan KL (2013a) Differential regulation of distinct Vps34 complexes by AMPK in nutrient stress and autophagy. *Cell 152*(1-2):290-303

Kim SG, Buel GR, Blenis J (2013b) Nutrient regulation of the mTOR complex 1 signaling pathway. *Mol Cells* 35(6):463-73

Klinkert K, Rocancourt M, Houdusse A, Echard A (2016) Rab35 GTPase couples cell division with initiation of epithelial apico-basal polarity and lumen opening. *Nat Commun* 7:11166

Klöpper TH, Kienle N, Fasshauer D, Munro S (2012) Untangling the evolution of Rab G proteins: Implications of a comprehensive genomic analysis. *BMC Biol* 10:71

Knizhnik AV, Kovaleva OV, Komelkov AV, Trukhanova LS, Rybko VA, Zborovskaya IB and Tchevkina EM (2012) Arf6 promotes cell proliferation via the PLD-mTORC1 and p38MAPK pathways. *Mol Cell Biochem* 113:360-371

Kobayashi T, Vischer UM, Rosnoblet C, Lebrand C, Lindsay M, Parton RG, Kruithof EKO, Gruenberg J (2000) The tetraspanin CD63/lamp3 cycles between endocytic and secretory compartments in human endothelial cells. *Mol Biol Cell* 11:1829-1843

Kobayashi H, Etoh K, Fukuda M (2014a) Rab35 is translocated from Arf6-positive perinuclear recycling endosomes to neurite tips during neurite outgrowth. *Small GTPases 5*(3):e983874.

Kobayashi H, Etoh K, Ohbayashi N and Fukuda M (2014b) Rab35 promotes the recruitment of Rab8, Rab13 and Rab36 to recycling endosomes through MICAL-L1 during neurite outgrowth. *Biology open 3*(9):803-814

Kochański A, Drac H, Jędrzejowska H and Hausmanowa-Petrusewicz I (2003) Focally folded myelin in Charcot–Marie–Tooth type 1B disease is associated with Asn131Lys mutation in myelin protein zero gene. *Eur J Neurol 10*(5):547-549

Kordeli E, Davis J, Trapp B, Bennett V (1990) An isoform of ankyrin is localized at nodes of Ranvier in myelinated axons of central and peripheral nerves. *J Cell Biol* 110(4):1341-52

Kordeli E, Lambert S, Bennett V (1995) Ankyrin-G. A new ankyrin gene with neural-specific isoforms localized at the axonal initial segment and node of Ranvier. *J Biol Chem* 270:2352–2359

Korolchuk VI, Saiki S, Lichtenberg M, Siddiqi FH, Roberts EA, Imarisio S, Jahreiss L, Sarkar S, Futter M, Menzies FM, O'Kane CJ, Deretic V and Rubinsztein DC (2011) Lysosomal positioning coordinates cellular nutrient responses. *Nat Cell Biol* 13:453–460

Kouranti I, Sachse M, Arouche N, Goud B, Echard A (2006) Rab35 regulates an endocytic recycling pathway essential for the terminal steps of cytokinesis. *Curr Biol* 16:1719–1725

Krämer-Albers EM, Bretz N, Tenzer S, Winterstein C, Möbius W, Berger H, Nave K-A, Schild H and Trotter J (2007) Oligodendrocytes secrete exosomes containing major myelin and stress-protective proteins: Trophic support for axons? Proteomics *Clin Appl* 1446–1461

Lacher MD, Pincheira R, Zhu Z, Camoretti-Mercado B, Matli M, Warren RS and Castro AF (2010) Rheb activates AMPK and reduces p27Kip1 levels in Tsc2-null cells via mTORC1-independent mechanisms: Implications for cell proliferation and tumorigenesis. *Oncogene* 29:6543–6556

Laemmli UK (1970) Cleavage of structural proteins during theassembly of the head bacteriophage T4. *Nature* 227:680–685

Lange Y (1991) Disposition of intracellular cholesterol in human fibroblasts. *J Lipid Res.* 32(2):329-39

Lange S, Sylvester M, Schumann M, Freund C and Krause E (2010) Identification of phosphorylation-dependent interaction partners of the adapter protein ADAP using quantitative mass spectrometry: SILAC vs (18)O-labeling. *J Proteome Res* 9:4113-4122

La Marca R, Cerri F, Horiuchi K, Bachi A, Feltri ML, Wrabetz L, Blobel CP, Quattrini A, Salzer JL, Taveggia C (2011) TACE (ADAM17) inhibits Schwann cell myelination. *Nat Neurosci* 14:857–865

Laplante M and Sabatini DM (2012) mTOR signaling in growth control and disease. *Cell* 149:274-293

Laporte J, Hu LJ, Kretz C, Mandel JL, Kioschis P, Coy JF, Klauck SM, Poustka A and Dahl N (1996) A gene mutated in X–linked myotubular myopathy defines a new putative tyrosine phosphatase family conserved in yeast. *Nat Genet 13*(2):175

Laporte J, Guiraud-Chaumeil C, Vincent M-C, Mandel J-L, Tanner SM, Liechti-Gallati S, Wallgren-Pettersson C, Dahl N, Kress W, Bolhuis PA, Fardeau M, Samson F, Bertini E (1997) Mutations in the MTM1 Gene Implicated in X-Linked Myotubular Myopathy. *Hum Mol Genet* 6(9):1505–1511

Laporte J, Blondeau F, Buj-Bello A, Tentler D, Kretz C, Dahl N, Mandel JL (1998) Characterization of the myotubularin dual specificity phosphatase gene family from yeast to human. *Hum Mol Genet* 7:1703–1712

Laporte, J, Blondeau F, Gansmuller A, Lutz Y, Vonesch JL and Mandel JL (2002) The PtdIns3P phosphatase myotubularin is a cytoplasmic protein that also localizes to Rac1-inducible plasma membrane ruffles. *J Cell Sci 115*(15):3105-3117

Laporte J, Bedez F, Bolino A and Mandel JL (2003) Myotubularins, a large disease-associated family of cooperating catalytically active and inactive phosphoinositides phosphatases. *Hum Mol Genet* 12(suppl_2):R285-R292

Lappe-Siefke C Goebbels S, Gravel M, Nicksch E, Lee J, Braun PE, Griffiths IR and Nave K-A (2003) Disruption of Cnp1 uncouples oligodendroglial functions in axonal support and myelination. *Nat Genet* 33:366–374

Lassuthova P, Vill K, Erdem-Ozdamar S, Schröder JM, Topaloglu H, Horvath R, Müller-Felber W, Bansagi B, Schlotter-Weigel B, Gläser D, Neupauerová J, Sedláčková L, Staněk D, Mazanec R, Weis J, Seeman P, Senderek J (2018) Novel SBF2 mutations and clinical spectrum of Charcot-Marie-Tooth neuropathy type 4B2. *Clin Genet* 94:467–472

Le N, Nagarajan R, Wang JYT, Araki T, Schmidt RE and Milbrandt J (2005) Analysis of congenital hypomyelinating Egr2 Lo/Lo nerves identifies Sox2 as an inhibitor of Schwann cell differentiation and myelination. *Proc Natl Acad Sci USA* 102:2596–2601

Lebrun-Julien F, Bachmann L, Norrmen C, Trotzmuller M, Kofeler H, Ruegg MA, Hall MN and Suter U (2014) Balanced mTORC1 activity in oligodendrocytes is required for accurate CNS myelination. *J Neurosci* 34:8432–8448

Lee HW, Kim Y, Han K, Kim H, Kim E (2010) The phosphoinositide 3-phosphatase MTMR2 interacts with PSD-95 and maintains excitatory synapses by modulating endosomal traffic. *J Neurosci* 30(16):5508-18

Lee Y, Morrison BM, Li Y, Lengacher S, Farah MH, Hoffman PN, Liu Y, Tsingalia A, Jin L, Zhang PW, Pellerin L, Magistretti PJ, Rothstein JD (2012) Oligodendroglia metabolically support axons and contribute to neurodegeneration. *Nature* 487(7408):443-8

Lee SM, Chin LS, Li L (2017) Dysregulation of ErbB Receptor Trafficking and Signaling in Demyelinating Charcot-Marie-Tooth Disease. *Mol Neurobiol* 54(1):87-100

Lemke G, Chao M (1988) Axons regulate Schwann cell expression of the major myelin and NGF receptor genes. *Development* 102:499–504

Li S, Brown MS and Goldstein JL (2010) Bifurcation of insulin signaling pathway in rat liver: mTORC1 required for stimulation of lipogenesis, but not inhibition of gluconeogenesis. *Proc. Natl Acad. Sci. USA* 107(8):3441-3446

Li F, Yi L, Zhao L, Itzen A, Goody RS and Wu YW (2014) The role of the hypervariable C-terminal domain in Rab GTPases membrane targeting. *Proc. Natl Acad. Sci. USA* 111(7):2572-2577

Liu P, Gan W, Inuzuka H, Lazorchak AS, Gao D, Arojo O, Liu D, Wan L, Zhai B, Yu Y, Yuan M, Kim BM, Shaik S, Menon S, Gygi SP, Lee TH, Asara JM, Manning BD, Blenis J, Su B, Wei W (2013) Sin1 phosphorylation impairs mTORC2 complex integrity and inhibits downstream Akt signalling to suppress tumorigenesis. *Nat Cell Biol* 15(11):1340

Liu P, Gan W, Chin YR, Ogura K, Guo J, Zhang J, Wang B, Blenis J, Cantley LC, Toker A, Su B and Wei W (2015a) PtdIns(3,4,5)P3-Dependent Activation of the mTORC2 Kinase Complex. *Cancer discovery* 5(11):1194–1209

Liu Z, Jin Y-Q, Chen L, Wang Y, Yang X, Cheng J, Wu W, Qi Z, Shen Z (2015b) Specific Marker Expression and Cell State of Schwann Cells during Culture *in vitro*. *PLOS ONE* 10:e0123278

Logan AM, Mammel AE, Robinson DC, Chin AL, Condon AF and Robinson FL (2017) Schwann cell-specific deletion of the endosomal PI 3-kinase Vps34 leads to delayed radial sorting of axons, arrested myelination, and abnormal ErbB2-ErbB3 tyrosine kinase signaling. *Glia* 65:1452–1470

Lorenzo O, Urbé S, Clague MJ (2005) Analysis of phosphoinositide binding domain properties within the myotubularin-related protein MTMR3. *J Cell Sci* 118(Pt 9):2005–2012

Lorenzo O, Urbé S, Clague MJ (2006) Systematic analysis of myotubularins: heteromeric interactions, subcellular localisation and endosome related functions. *J Cell Sci* 119:2953-2959

Ludwin SK (1990) Oligodendrocyte survival in Wallerian degeneration. *Acta Neuropathol* 80:184-191

Ma L, Chen Z, Erdjument-Bromage H, Tempst P and Pandolfi PP (2005) Phosphorylation and functional inactivation of TSC2 by Erk implications for tuberous sclerosis and cancer pathogenesis. *Cell* 121:179–193

Maier O, Hoekstra D, Baron W (2008) Polarity development in oligodendrocytes: sorting and trafficking of myelin components. *J Mol Neurosci* 35:35–53

Majava V, Polverini E, Mazzini A, Nanekar R, Knoll W, Peters J, Natali F, Baumgärtel P, Kursula I, Kursula P (2010) Structural and functional characterization of human peripheral nervous system myelin protein P2. *PLoS ONE* 5:e10300

Manole A, Horga A, Gamez J, Raguer N, Salvado M, San Millan B, Navarro C, Pittmann A, Reilly MM and Houlden H (2017) SBF1 mutations associated with autosomal recessive axonal neuropathy with cranial nerve involvement. *neurogenetics* 18(1):63-67

Marat AL, Ioannou MS, McPherson PS (2012) Connecdenn 3/DENND1C binds actin linking Rab35 activation to the actin cytoskeleton. *Mol Biol Cell* 23:163–175

Marat AL and Haucke V (2016) Phosphatidylinositol 3-phosphates-at the interface between cell signalling and membrane traffic. *EMBO J* 35(6):561-79

Marat AL, Wallroth A, Lo WT, Muller R, Norata GD, Falasca M, Schultz C and Haucke V (2017) mTORC1 activity repression by late endosomal phosphatidylinositol 3,4-bisphosphate. *Science* 356:968-972

Martina JA, Chen Y, Gucek M, Puertollano R (2012) MTORC1 functions as a transcriptional regulator of autophagy by preventing nuclear transport of TFEB. *Autophagy* 8:903–914

Martini R, Mohajeri MH, Kasper S, Giese KP, Schachner M (1995) Mice doubly deficient in the genes for P0 and myelin basic protein show that both proteins contribute to the formation of the major dense line in peripheral nerve myelin. *J Neurosci* 15:4488–4495

Mathews ES, Mawdsley DJ, Walker M, Hines JH, Pozzoli M, Appel B (2014) Mutation of 3-hydroxy-3-methylglutaryl CoA synthase I reveals requirements for isoprenoid and cholesterol synthesis in oligodendrocyte migration arrest, axon wrapping, and myelin gene expression. *J Neurosci* 34:3402–3412

Mathews ES, Appel B (2016) Cholesterol Biosynthesis Supports Myelin Gene Expression and Axon Ensheathment through Modulation of P13K/Akt/mTor Signaling. *J Neurosci Off J Soc Neurosci* 36:7628–7639

Matthews MA (1968) An electron microscopic study of the relationship between axon diameter and the initiation of myelin production in the peripheral nervous system. *Anat Rec* 161:337–352

Maurel P, Einheber S, Galinska J, Thaker P, Lam I, Rubin MB, Scherer SS, Murakami Y, Gutmann DH, Salzer JL (2007) Nectin-like proteins mediate axon Schwann cell interactions along the internode and are essential for myelination. *J Cell Biol* 178:861–874

Mayinger P (2012) Phosphoinositides and vesicular membrane traffic. *Biochim Biophys Acta* 1821:1104–1113

McCartney AJ, Zhang Y, Weisman LS (2014) Phosphatidylinositol 3,5-bisphosphate: low abundance, high significance. *BioEssays* 36:52–64

McMorris FA (1984) Cyclic AMP induction of the myelin enzyme 2',3'- cyclic nucleotide 3'-phosphohydrolase (CNP) in rat oligodendrocytes. *J Neurochem* 41:506

McNiven MA (2005) Dynamin in disease. *Nat Genet* 37:215–216

Medina-Kauwe LK, Xie J, Hamm-Alvarez S (2005) Intracellular trafficking of nonviral vectors. *Gene Ther* 12:1734–1751

Meng J and Ferguson SM (2018) GATOR1-dependent recruitment of FLCN–FNIP to lysosomes coordinates Rag GTPase heterodimer nucleotide status in response to amino acids. *J Cell Biol* 217(8):2765-2776

Menon S, Dibble CC, Talbott G, Hoxhaj G, Valvezan AJ, Takahashi H,Cantley LC, Manning BD (2014) Spatial control of the TSC complex integrates insulin and nutrient regulation of mTORC1 at the lysosome. *Cell* 156(4):771–785

Meyer D, Yamaai T, Garratt A, Riethmacher-Sonnenberg E, Kane D, Theill LE and Birchmeier C (1997) Isoform-specific expression and function of neuregulin. *Development 124*(18):3575-3586

Meyuhas O (2000) Synthesis of the translational apparatus is regulated at the translational level. *Eur J Biochem/FEBS* 267:6321-30

Michailov GV, Sereda MW, Brinkmann BG, Fischer TM, Haug B, Birchmeier C, Role L, Lai C, Schwab MH, Nave K-A (2004) Axonal neuregulin-1 regulates myelin sheath thickness. *Science* 304:700–703

Miesenböck G, De Angelis DA and Rothman JE (1998) Visualizing secretion and synaptic transmission with pH-sensitive green fluorescent proteins. *Nature* 394:192-195

Mihaylova MM, Shaw RJ (2011) The AMPK signalling pathway coordinates cell growth, autophagy and metabolism. *Nat Cell Biol 13*(9):1016

Milburn MV, Tong L, deVos AM, Br€unger A, Yamaizumi Z, Nishimura S, Kim SH (1990) Molecular switch for signal transduction: structural differences between active and inactive forms of protooncogenic ras proteins. *Science* 247:939-45

Miller MW, Nowakowski RS (1988) Use of bromodeoxyuridine-immunohistochemistry to examine the proliferation, migration and time of origin of cells in the central nervous system. *Brain Res* 457:44–52

Minowa-Nozawa A, Nozawa T, Okamoto-Furuta K, Kohda H and Nakagawa I (2017) Rab35 GTPase recruits NDP52 to autophagy targets. *EMBO J 36*(18):2790–2807

Miron VE, Kuhlmann T and Antel JP (2011) Cells of the oligodendroglial lineage, myelination, and remyelination. *BBA-Mol Cell Res* 1812(2):184-193

Mironova YA, Lenk GM, Lin JP, Lee SJ, Twiss JL, Vaccari I, Bolino A, Havton LA, Min SH, Abrams CS, Shrager P,Meisler MH, Giger RJ (2016) PI(3,5)P2 biosynthesis regulates oligodendrocyte differentiation by intrinsic andextrinsic mechanisms. *eLife* 5:e13023

Miyamoto Y, Yamamori N, Torii T, Tanoue A, Yamauchi J (2014) Rab35, acting through ACAP2 switching off Arf6, negatively regulates oligodendrocyte differentiation and myelination. *Mol Biol Cell* 25(9):1532-42

Möbius W, Patzig J, Nave K-A, Werner HB (2008) Phylogeny of proteolipid proteins: divergence, constraints, and the evolution of novel functions in myelination and neuroprotection. *Neuron Glia Biol* 4:111–127

Mochizuki Y, Majerus PW (2003) Characterization of myotubularin-related protein 7 and its binding partner, myotubularin-related protein 9. *Proc Natl Acad Sci USA* 100(17):9768–9773

Mohan N, Shen Y, Dokmanovic M, Endo Y, Hirsch DS and Wu WJ (2016) VPS34 regulates TSC1/TSC2 heterodimer to mediate RheB and mTORC1/S6K1 activation and cellular transformation. *Oncotarget* 7:52239–52254

Monk KR, Naylor SG, Glenn TD, Mercurio S, Perlin JR, Dominguez C, Moens CB and Talbot WS (2009) AG protein–coupled receptor is essential for Schwann cells to initiate myelination. *Science* 325(5946):1402-1405

Morell P, Norton WT (1980) Myelin. *Sci Am* 242(5):88-119

Morgan L, Jessen KR, Mirsky R (1991) The effects of cAMP on differentiation of cultured Schwann cells: Progression from an early phenotype (04+) to a myelin phenotype (P0+, GFAP-, N-CAM-, NGF-receptor-) depends on growth inhibition. *J Cell Biol* 112:457–467

Morrissey TK, Levi AD, Nuijens A, Sliwkowski MX, Bunge RP (1995) Axon-induced mitogenesis of human Schwann cells involves heregulin and p185erbB2. *Proc Natl Acad Sci* USA 92:1431–1435

Munson MJ, Allen GF, Toth R, Campbell DG, Lucocq JM and Ganley IG (2015) mTOR activates the VPS34-UVRAG complex to regulate autolysosomal tubulation and cell survival. *EMBO J* 34(17):2272-2290

Murray JA and Blakemore WF (1980) The relationship between internodal length and fibre diameter in the spinal cord of the cat. *J Neurol Sci* 45:29-41

Musse AA, Boggs JM and Harauz G (2006) Deimination ofmembrane-bound myelin basic protein in multiple sclerosis exposesan immunodominant epitope. *Proc Natl Acad Sci U.S.A* 103:4422–4427

Nakhro K, Park JM, Hong YB, Park JH, Nam SH, Yoon BR, ... and Kim JY (2013) SET binding factor 1 (SBF1) mutation causes Charcot-Marie-Tooth disease type 4B3. *Neurology 81*(2):165-173

Naldini L, Blomer U, Gallay P, Ory D, Mulligan R, Gage FH, Verma IM, Trono D (1996) . *In vivo* gene delivery and stable transduction of nondividing cellswork by a lentiviral vector. *Science* 272:263–267

Nandagopal N and Roux PP (2015) Regulation of global and specific mRNA translation by the mTOR signaling pathway. *Translation* 3(1):e983402

Narayanan SP, Flores AI, Wang F and Macklin WB (2009) Akt signals through the mammalian target of rapamycin pathway to regulate CNS myelination. *J Neurosci* 29(21):6860–6870

Naughtin MJ, Sheffield DA, Rahman P, Hughes WE, Gurung R, Stow JL, Nandurkar HH, Dyson JM and Mitchell CA (2010) The myotubularin phosphatase MTMR4 regulates sorting from early endosomes. *J Cell Sci* 123:3071–3083

Nave K-A, Salzer JL (2006) Axonal regulation of myelination by neuregulin 1. *Curr Opin Neurobiol* 16*:*492–500

Nave K-A, Sereda MW, Ehrenreich H (2007) Mechanisms of disease: inherited demyelinating neuropathies—from basic to clinical research. *Nat Clin Pract Neurol* 3:453-64

Nave K-A (2010) Myelination and the trophic support of long axons. *Nat Rev Neurosci* 11:275–283

Nave K-A, Werner HB (2014) Myelination of the nervous system: mechanisms and functions. *Annu Rev Cell Dev Biol* 30:503-33

Neumann H, Medana IM, Bauer J and Lassmann H (2002) Cytotoxic T lymphocytes in autoimmune and degenerative CNS diseases. *Trends Neurosci* 25:313–319

Newbern J, Birchmeier C (2010) Nrg1/ErbB signaling networks in Schwann cell development and myelination. *Semin Cell Dev Biol* 21:922–928

Newbern JM, Li X, Shoemaker SE, Zhou J, Zhong J, Wu Y, Bonder D, Hollenback S, Coppola G, Geschwind DH,Landreth GE, Snider WD (2011) Specific functions for ERK/MAPK signaling during PNS development. *Neuron* 69:91–105

Ng AA, Logan AM, Schmidt EJ, Robinson FL (2013) The CMT4B disease-causing phosphatases Mtmr2 and Mtmr13 localize to the Schwann cell cytoplasm and endomembrane compartments, where they depend upon each other to achieve wild-type levels of protein expression. *Hum Mol Genet* 22(8):1493-506

Nishida E. and Gotoh Y. (1993) The MAP kinase cascade is essential for diverse signal transduction pathways. *Trends Biochem Sci* 18:128-131

Nobukuni T, Joaquin M, Roccio M, Dann SG, Kim SY, Gulati P, Byfield MP, Backer JM, Natt Francois, Johannes LB, Fried JT Zwartkruis and Zwartkruis FJ (2005) Amino acids mediate mTOR/raptor signaling through activation of class 3 phosphatidylinositol 3OH-kinase. *Proc. Natl Acad. Sci. USA* 102(40):14238-14243

Nodari A, Zambroni D, Quattrini A, Court FA, D'Urso A, Recchia A, Tybulewicz VL, Wrabetz L, Feltri ML (2007) Beta1 integrin activates Rac1 in Schwann cells to generate radial lamellae during axonal sorting and myelination. *J Cell Biol* 177:1063–1075

Nookala RK, Langemeyer L, Pacitto A, Ochoa-Montano B, Donaldson JC, Blaszczyk BK, Chirgadze DY, Barr FA, Bazan JF, Blundell TL (2012) Crystal structure of folliculin reveals a hid DENN function in genetically inherited renal cancer. *Open Biol* 2:120071

Norrmén C, **Suter U** (**2013)** Akt/mTOR signalling in myelination. *Biochem Soc Trans* 41:944–50

Norrmén C, Figlia G, Lebrun-Julien F, Pereira JA, Trötzmüller M, Köfeler HC, Rantanen *V*, Wessig C, van Deijk A-LF, Smit MAB, Verheijen HG, Rüegg MA, Hall MN, Suter U (2014) mTORC1 controls PNS myelination along the mTORC1-RXRγ-SREBP-lipid biosynthesis axis in Schwann cells. *Cell reports 9*(2):646-660

Norrmén C, Figlia G, Pfistner P, Pereira JA, Bachofner S and Suter U (2018) mTORC1 is transiently reactivated in injured nerves to promote c-Jun elevation and Schwann cell dedifferentiation. *J Neurosci 38*(20):4811-4828

Norton WT, Poduslo SE (1973) Myelination in rat brain: Changes in myelin composition during brain maturation. *J Neurochem* 21:759–773

Novo D, Heath N, Mitchell L, Caligiuri G, MacFarlane A, Reijmer D, Charlton L, Knight J, Calka M, McGhee E, Dorner E, Sumpton D, Mason S, Echard A, Klinkert K, Secklehner J, Kruiswijk, Vousden K, MacPherson IR, Blyth K, Bailey P, Yin H, Carlin LM, Morton J, Zanivan S and Norman JC (2018) Mutant p53s generate pro-invasive niches by influencing exosome podocalyxin levels. *Nat Commun 9*(1):5069

Ogata T, Iijima S, Hoshikawa S, Miura T, Yamamoto S, Oda H, Nakamura K, Tanaka SJ (2004) Opposing extracellular signal-regulated kinase and Akt pathways control Schwann cell myelination. *Neurosci* 24(30):6724-32

Panaretou C, Domin J, Cockcroft S, and Waterfield MD (1997) Characterization of p150, an adaptor protein for the human phosphatidylinositol (PtdIns) 3-kinase substrate presentation by phosphatidylinositol transfer protein to the p150·; PtdIns 3-kinase complex. *J Biol Chem* 272(4):2477-2485

Pareyson D, Saveri P, Pisciotta C (2017) New developments in Charcot-Marie-Tooth neuropathy and related diseases. *Curr Opin Neurol* 30:471-480

Pareyson D, Stojkovic T, Reilly MM, Leonard-Louis S, Laurà M, Blake J, Parman Y, Battaloglu E, Tazir M, Bellatache M, Bonello-Palot N, Lévy N, Sacconi S, Guimarães-Costa R[2], Attarian S, Latour P, Solé G, Megarbane A, Horvath R, Ricci G, Choi BO, Schenone A[19], Gemelli C, Geroldi A, Sabatelli M, Luigetti M, Santoro L, Manganelli F, Quattrone A, Valentino P, Murakami T, Scherer SS, Dankwa L, Shy ME, Bacon CJ, Herrmann DN, Zambon A, Tramacere I, Pisciotta C, Magri S, Previtali SC, Bolino A (2019) A multicenter retrospective study of charcot-marie-tooth disease type 4B (CMT4B) associated with mutations in myotubularin-related proteins (MTMRs). *Ann Neurol* 86(1):55-67

Parkinson DB, Dickinson S, Bhaskaran A, Kinsella MT, Brophy PJ, Sherman DL, Sharghi-Namini S, Duran Alonso MB, Mirsky R, Jessen KR (2003) Regulation of the myelin gene periaxin provides evidence for Krox-20-independent myelin-related signalling in Schwann cells. *Mol Cell Neurosci* 23:13–27

Parkinson DB, Bhaskaran A, Droggiti A, Dickinson S, D'AntonioM, Mirsky R, Jessen KR (2004) Krox-20 inhibits Jun-NH2-terminal kinase/c-Jun to control Schwann cell proliferation and death. *J Cell Biol* 164:385–394

Parkinson DB, Bhaskaran A, Arthur-Farraj P, Noon LA, Woodhoo A, Lloyd AC, Feltri ML, Wrabetz L, Behrens A, Mirsky R and Jessen KR (2008) c-Jun is a negative regulator of myelination. *J Cell Biol* 181: 625–637

Patino-Lopez G, Dong X, Ben-Aissa K, Bernot KM, Itoh T, Fukuda M, Kruhlak MJ, Samelson LE and Shaw S (2008) Rab35 and its GAP EPI64Cin T cells regulate receptor recycling and immunological synapse formation. *J Biol Chem* 283:18323–18330

Patzig J, Jahn O, Tenzer S, Wichert SP, de Monasterio-Schrader P, Rosfa S, Kuharev J, Yan K, Bormuth I, Bremer J, Aguzzi A, Orfaniotou F, Hesse D, Schwab MH, Möbius W, Nave K-A, Werner HB (2011) Quantitative and integrative proteome analysis of peripheral nerve myelin identifies novel myelin proteins and candidate neuropathy loci. *J Neurosci* 31*:*16369–16386

Patzig J, Kusch K, Fledrich R, Eichel MA, Lüders KA, Möbius W, Sereda MW, Nave K-A, Martini R. and Werner HB (2016) Proteolipid protein modulates preservation of peripheral axons and premature death when myelin protein zero is lacking. *Glia* 64*:*155–174

Pavlos NJ, Grønborg M, Riedel D, Chua JJ, Boyken J, Kloepper TH, Urlaub H, Rizzoli SO, Jahn R (2010) Quantitative analysis of synaptic vesicle Rabs uncovers distinct yet overlapping roles for Rab3a and Rab27b in Ca2+-triggered exocytosis. *J Neurosci* 30(40):13441-53

Pavlos NJ, Jahn R (2011) Distinct yet overlapping roles of Rab GTPases on synaptic vesicles. *Small GTPases* 2(2):77-81

Pear WS, Nolan GP, Scott ML, Baltimore D (1993) Production of high-titer helper-free retroviruses by transient transfection. *Proc. Natl. Acad. Sci. USA.* 90(18):8392–8396

Pellegrino RG, Spencer PS and Ritchie JM (1984) Sodium channels in the axolemma of unmyelinated axons: a new estimate *Brain Res*. 305, 357-360

Pereira-Leal JB, Seabra MC (2001) Evolution of the Rab familyof small GTP-binding proteins. *J Mol Biol* 313:889-901

Perez-Villegas EM, Olivier C, Spassky N, Poncet C, Cochard P, Zalc B, Thomas J-L and Martinez S (1999) Early specification of oligodendro-cytes in the chick embryonic brain. *Dev Biol* 216:98–113

Peters A, Palay SL, Webster Hd (1991) The fine structure of the nervous system. *Oxford University Press, New York.*

Peterson TR, Laplante M, Thoreen CC, Sancak Y, Kang SA, Kuehl WM, Gray NS, Sabatini DM. (2009) DEPTOR is an mTOR inhibitor frequently overexpressed in multiple myeloma cells and required for their survival. *Cell* 137:873–886

Peterson TR, Sengupta SS, Harris TE, Carmack AE, Kang SA, Balderas E, Guertin DA, Madden KL, Carpenter AE, Finck BN and Sabatini DM (2011) mTOR complex 1 regulates lipin 1 localization to control the SREBP pathway. *Cell* 146(3):408–420

Petersen SC, Luo R, Liebscher I, Giera S, Jeong SJ, Mogha A, Ghidinelli M, Feltri ML, Schöneberg T, Piao X, Monk KR (2015) The adhesion GPCR GPR126 has distinct, domain-dependent functions in Schwann cell development mediated by interaction with laminin-211. *Neuron* 85(4):755-69

Petit CS, Roczniak-Ferguson A and Ferguson SM (2013) Recruitment of folliculin to lysosomes supports the amino acid–dependent activation of Rag GTPases. *J Cell Biol 202*(7):1107-1122

Pfeffer S and Aivazian D (2004) Targeting Rab GTPases to distinct membrane compartments. *Nat Rev Mol Cell Bio 5*(11):886

Pfeiffer SE, Warrington AE, Bansal R (1993) The oligodendrocyte andits many cellular processes. *Trends Cell Biol* 3:191–197

Poliak S, Peles E (2003) The local differentiation of myelinated axons at nodes of Ranvier. *Nat Rev Neurosci* (12):968-80

Poncet C, Soula C, Trousse F, Kan P, Hirsinger E, Pourquié O, Duprat A-M and Cochard P (1996) Induction of oligodendrocyte progenitors in the trunk neural tube by ventralizing signals: effects of notochord and floor plate grafts, and of sonic hedgehog. *Mechanisms of development* 60(1):13-32

Porstmann T, Santos CR, Griffiths B, Cully M, Wu M, Leevers S, Griffiths JR, Chung Y-L and Schulze A (2008) SREBP activity is regulated by mTORC1 and contributes to Akt-dependent cell growth. *Cell metabolism* 8(3):224–236

Posor Y, Eichhorn-Gruenig M, Puchkov D, Schöneberg J, Ullrich A, Lampe A, Müller R, Zarbakhsh, Gulluni F, Hirsch E, Krauss M, Schultz C, Schmoranzer J, Noé F and Haucke V (2013) Spatiotemporal control of endocytosis by phosphatidylinositol-3, 4-bisphosphate. *Nature 499*(7457):233

Potthoff E, Guillaume-Gentil O, Ossola D, Polesel-Maris J, Leibundgut-Landmann S, Zambelli T, Vorholt JA (2012) Rapid and serial quantification of adhesion forces of yeast and Mammalian cells. *PLoS One* 7:e52712

Previtali SC, Zerega B, Sherman DL, Brophy PJ, Dina G, King RH., Salih MM, Feltri L, Quattrini A, Ravazzolo R and Wrabetz L (2003) Myotubularin-related 2 protein phosphatase and neurofilament light chain protein, both mutated in CMT neuropathies, interact in peripheral nerve. *Hum Mol Genet 12*(14):1713-1723

Previtali SC, Quattrini A and Bolino A (2007) Charcot–Marie–Tooth type 4B demyelinating neuropathy: deciphering the role of MTMR phosphatases. *Exp Rev Mol Med 9*(25):1-16

Pringle N, Collarini EJ, Mosley MJ, Heldin CH, Westermark B, Richardson WD (1989) PDGF A chain homodimersdrive proliferation of bipotential (O-2A) glial progenitor cellsin the developing rat optic nerve. *EMBO J* 8:1049–56

Pringle NP, Mudhar HS, Collarini EJ, Richardson WD (1992) PDGF receptors in the rat CNS: during late neurogenesis, PDGF alpha-receptor expression appears to be restricted to glial cells of the oligodendrocyte lineage. *Development* 115(2):535-51

Puertollano R (2014) mTOR and lysosome regulation. *F1000Prime Rep* 6:52

Purves D, Augustine GJ, Fitzpatrick D (2001) Increased Conduction Velocity as a Result of Myelination. *Neuroscience (2nd ed.). Sunderland (MA): Sinauer Associates*

Pusic KM, Pusic AD, Kraig RP (2016) Environmental Enrichment Stimulates Immune Cell Secretion of Exosomes that Promote CNS Myelination and May Regulate Inflammation. *Cell Mol Neurobiol* 36(3):313-325

Pylypenko O, Rak A, Durek T, Kushnir S, Dursina BE, Thomae NH, Constantinescu AT, Brunsveld L, Watzke A, Waldmann H, Goody RS, Alexandrov K (2006) Structure of doubly prenylated Ypt1:GDI complex and the mechanism of GDI-mediated Rab recycling. *EMBO J* 25:13- 23

Quattrone A, Gambardella A, Bono F, Aguglia U, Bolino A, Bruni AC, Montesi MP, Oliveri RL, Sabatelli M, Tamburrini O, Valentino P, Van Broeckhoven C, Zappia M (1996) Autosomal recessive hereditary motor and sen-sory neuropathy with focally folded myelinsheaths: clinical, electrophysiologic, and geneticaspects of a large family. *Neurology* 46:1318–1324

Raess MA, Cowling BS, Bertazzi DL, Kretz C, Rinaldi B, Xuereb JM, Kessler P, Romero NB, Payrastre B, Friant S and Laporte J (2017) Expression of the neuropathy-associated MTMR2 gene rescues MTM1-associated myopathy. *Hum Mol Genet 26*(19):3736-3748

Raff MC, Lillien L, Richardson WD, Burne JF, Noble M (1988) Platelet-derived growth factor from astrocytes drives the lock that times oligodendrocyte development in culture. *Nature* 333:562–5

Raiborg C, Schink KO and Stenmark H (2013) Class III phosphatidylinositol 3-kinase and its catalytic product PtdIns3P in regulation of endocytic membrane traffic. *FEBS J* 280:2730–2742

Raiborg C, EM Wenzel, Pedersen NM, Olsvik H, Schink KO, Schultz SW, Vietri M, Nisi V, Bucci C, Brech A, Johansen T and Stenmark H (2015) Repeated ER-endosome contacts promote endosome translocation and neurite outgrowth. *Nature* 520:234–238

Rameh LE, Tolias KF, Duckworth BC and Cantley LC (1997) A new pathway for synthesis of phosphatidylinositol 4,5-bisphosphate. *Nature* 390:192–196

Ranvier L (1871) Sur les éléments conjonctifs de la moelle épinière. *Compt Rend* 73:1168-1171

Rasband MN, Peles E, Trimmer JS, Levinson SR, Lux SE, Shrager P (1999a) Dependence of nodal sodium channel clustering on paranodal axoglial contact in the developing CNS. *J Neurosci* 19(17):7516-28

Rasband MN, Trimmer JS, Peles E, Levinson SR, Shrager P (1999b) K+ channel distribution and clustering in developing and hypomyelinated axons of the optic nerve. *J Neurocytol* 28(4-5):319-31

Raymond GV (2017) Leukodystrophy: basic and clinical. *Adv Neurobiol* 15:365–382

Readhead C, Popko B, Takahashi N, Shine HD, Saavedra RA, Sidman RL and Hood L (1987) Expression of a myelin basic protein gene in transgenic shiverer mice: correction of the dysmyelinating phenotype. *Cell* 48:703-712

Rebsamen M, Pochini L, Stasyk T, de Araújo ME, Galluccio M, Kandasamy RK, Snijder B, Fauster A, Rudashevskaya EL, Bruckner M, Scorzoni S, Przemyslaw AF, Huber KVM, Bigenzahn J, Heinz LX, Kraft C, Bennett KL, Indiveri C, Huber LA and Superti-Furga G (2015) SLC38A9 is a component of the lysosomal amino acid sensing machinery that controls mTORC1. *Nature* 519(7544):477–481

Reilly MM, Murphy SM, Laura M (2011) Charcot-Marie-Tooth disease. *J Peripher Nerv Syst* 16:1–14

Remahl S and Hildebrand C (1982) Changing relation between onset of myelination and axon diameter range in developing feline white matter. *J Neurol Sci* 54:33-45

Rinholm JE, Hamilton NB, Kessaris N, Richardson WD, Bergersen LH, Attwell D (2011) Regulation of oligodendrocyte development and myelination by glucose and lactate. *J Neurosci* 31:538-548

Rink J, Ghigo E, Kalaidzidis Y and Zerial M (2005) Rab conversion as a mechanism of progression from early to late endosomes. *Cell* 122:735-749

Ritchie JM (1982) On the relation between fibre diameter and conduction velocity in myelinated nerve fibres *Proc R Soc Lond B Biol Sci* 217:29-35

Robinson FL, Dixon JE (2006) Myotubularin phosphatases: policing 3-phosphoinositides. *Trends Cell Biol* 16:403–412

Robinson FL, Niesman IR, Beiswenger KK, Dixon JE (2008) Loss of the inactive myotubularin-related phosphatase Mtmr13 leads to a Charcot-Marie-Tooth 4B2-like peripheral neuropathy in mice. *Proc. Natl Acad. Sci. USA* 105(12):4916–4921

Robinson DC, Mammel AE, Logan AM, Larson AA, Schmidt EJ, Condon AF and Robinson FL (2018) An *in vitro* model of charcot-marie-tooth disease type 4B2 provides insight into the roles of MTMR13 and MTMR2 in schwann cell myelination. *ASN neuro 10*:1759091418803282

Romani M, Mehawej C, Mazza T, Megarbane A, Valente EM (2016) "Fork and bracket" syndrome expands the spectrum of SBF1-related sensory motor polyneuropathies. *Neurol Genet* 2(2):e61

Ronan B, Flamand O, Vescovi L, Dureuil C, Durand L, Fassy F, Bachelot M-F, Lamberton A, Mathieu M, Bertrand T, Marquette J-P, El-Ahmad Y, Filoche-Romme B, Schio L, Garcia-Echeverria C, Goulaouic H and Marquette JP (2014) A highly potent and selective Vps34 inhibitor alters vesicle trafficking and autophagy. *Nat Chem Biol* 10:1013-1019

Rosenbluth J (2009) Multiple functions of the paranodal junction of myelinated nerve fibers. *J Neurosci Res* 87(15):3250-8

Rosner M, Siegel N, Valli A, Fuchs C, Hengstschlager (2010) mTOR phosphorylated at s2448 binds to raptor and rictor. *Amino Acids* 38(1):223–228

Rossor AM, Polke JM, Houlden H, Reilly MM (2013) Clinical implications of genetic advances in Charcot-Marie-Tooth disease. *Nat Rev Neurol* 9:562–571

Roux KJ, Kim DI, Raida M, Burke B (2012) A promiscuous biotin ligase fusion protein identifies proximal and interacting proteins in mammalian cells. *J Cell Biol* 196:801–810

Rowitch DH (2004) Glial specification in the vertebrate neural tube. *Nat Rev Neurosci* 5(5):409-419

Roy S, Zhang B, Lee VM-Y and Trojanowski JQ (2005) Axonal transport defects: a common theme in neurodegenerative diseases. *Acta Neuropathol* 109:5–13

Rudnik-Schöneborn S, Bergmann C, Suter U, Zerres K, Timmermann V, Relvas JB and Senderek J (2007) Peripheral nerve demyelination caused by a mutant Rho GTPase guanine nucleotide exchange factor, frabin/FGD4. *Am J Hum Genet* 81:158–164

Rushton WAH (1951) A theory of the effects of fibre size in medullated nerve. *J Physiol* 115:101

Ruvinsky I, Sharon N, Lerer T, Cohen H, Stolovich-Rain M, Nir T, Dor Y, Zisman P and Meyuhas O (2005) Ribosomal protein S6 phosphorylation is a determinant of cell size and glucose homeostasis. *Genes & development 19*(18):2199-2211

Rychlik WJSW, Spencer WJ and Rhoads RE (1990) Optimization of the annealing temperature for DNA amplification *in vitro*. *Nucleic acids res*18(21):6409-6412

Sabatini DM, Erdjument-Bromage H, Lui M, Tempst P, Snyder SH (1994) RAFT1: a mammalian protein that binds to FKBP12 in a rapamycin-dependent fashion and is homologous to yeast TORs. *Cell* 78:35–43

Saher G, Quintes S, Möbius W, Wehr MC, Kraemer-Albers E-M, Brügger B, Nave K-A (2009) Cholesterol regulates the endoplasmic reticulum exit of the major membrane protein P0 required for peripheral myelin compaction. *J Neurosci* 29:6094–6104

Saher G, Simons M (2010) Cholesterol and myelin biogenesis. *Subcell Biochem* 51:489–508

Saiki RK, Gelfand DH, Stoffel S, Scharf SJ, Higuchi R, Horn GT, Mullis KB and Erlich HA (1988) Primer-directed enzymatic amplification of DNA with a thermostable DNA polymerase. *Science 239*(4839):487-491

Saito F, Moore SA, Barresi R, Henry MD, Messing A, Ross-Barta SE, Cohn RD, Williamson RA, Sluka KA, Sherman DL, Brophy PJ, Schmelzer JD, Low PA, Wrabetz L, Feltri ML, Campbell KP (2003) Unique role of dystroglycan in peripheral nerve myelination, nodal structure, and sodium channel stabilization. *Neuron* 38:747–758

Salzer JL (2015) Schwann cell myelination. *Cold Spring Harb Perspect Biol* 7(8):a020529

Sancak Y, Thoreen CC, Peterson TR, Lindquist RA, Kang SA, Spooner E, Carr SA, Sabatini DM (2007) PRAS40 is an insulin-regulated inhibitor of the mTORC1 protein kinase. *Mol Cell* 25:903–915

Sancak Y, Peterson TR, Shaul YD, Lindquist RA, Thoreen CC, Bar-Peled L, Sabatini DM (2008) The Rag GTPases bind raptor and mediate amino acid signaling to mTORC1. *Science* 320:1496–1501

Sancak Y, Bar-Peled L, Zoncu R, Markhard AL, Nada S, Sabatini DM (2010) Ragulator-Rag complex targets mTORC1 to the lysosomal surface and is necessary for its activation by amino acids. *Cell* 141(2):290-303

Sandbichler AM, Aschberger T and Pelster B (2013) A method to evaluate the efficiency of transfection reagents in an adherent zebrafish cell line. *Bio Res open access 2*(1):20-27

Sander S, Ouvrier RA, McLeod JG, Nicholson GA and Pollard JD (2000) Clinical syndromes associated with tomacula or myelin swellings in sural nerve biopsies. *J Neurol Neurosur Ps 68*(4):483-488

Sanger F and Coulson AR (1975) A rapid method for determining sequences in DNA by primed synthesis with DNA polymerase. *J Mol Biol* 94(3):441-448

Sankaranarayanan S, De Angelis D, Rothman JE, Ryan TA (2000) The use of pHluorins for optical measurements of presynaptic activity. *Biophys J* 79:2199–2208

Saporta MA (2014) Charcot-Marie-Tooth disease and other inherited neuropathies. *Continuum (Minneap Minn)* 20:1208–1225

Sarbassov DD, Ali SM, Kim DH, Guertin DA, Latek RR, Erdjument-Bromage H, Tempst P, Sabatini DM (2004) Rictor, a novel binding partner of mTOR, defines a rapamycin-insensitive and raptor-independent pathway that regulates the cytoskeleton. *Curr Biol* 14:1296–1302

Sarbassov DD, Guertin DA, Ali SM and Sabatini DM (2005) Phosphorylation and regulation of Akt/PKB by the rictor-mTOR complex. *Science* 307:1098–1101

Sasaki T, Kikuchi A, Araki S., Hata Y, Isomura M, Kuroda S and Takai Y (1990) Purification and characterization from bovine brain cytosol of a protein that inhibits the dissociation of GDP from and the subsequent binding of GTP to smg p25A, a ras p21-like GTP-binding protein. *J Biol Chem* 265(4):2333-2337

Sbrissa D, Ikonomov OC, Shisheva A (1999) PIKfyve, a mammalian ortholog of yeast Fab1p lipid kinase, synthesizes 5-phosphoinositides. Effect of insulin. *J Biol Chem*. 274:21589 – 21597

Sbrissa D, Ikonomov OC, Fu Z, Ijuin T, Gruenberg J, Takenawa T and Shisheva A (2007) Core protein machinery for mammalian phosphatidylinositol 3,5-bisphosphate synthesis and turnover that regulates the progression of endosomal transport: Novel Sac phosphatase joins the ArPIKfyve-PIKfyve complex. *J. Biol. Chem*. 282:23878–23891

Scapin C, Ferri C, Pettinato E, Zambroni D, Bianchi F, Del Carro U, Belin S, Caruso D, Mitro N, Pellegatta M, Taveggia C, Schwab MH, Nave K-A, Feltri ML, Wrabetz L and D'Antonio M (2018) Enhanced axonal neuregulin-1 type-III signaling ameliorates neurophysiology and hypomyelination in a Charcot–Marie–Tooth type 1B mouse model. *Hum Mol Genet 28*(6):992-1006

Schaletzky J, Dove SK, Short B, Lorenzo O, Clague MJ, Barr FA (2003) Phosphatidylinositol-5-phosphate activation and conserved substrate specificity of the myotubularin phosphatidylinositol 3-phosphatases. *Curr Biol* 13:504–509

Scherer SS, Xu YT, Roling D, Wrabetz L, Feltri ML, Kamholz J (1994). Expression of growth-associated protein-43 kD in Schwann cells is regulated by axon-Schwann cell interactions and cAMP. *J Neurosci Res* 38:575–589

Schneider A, Younis RH, Gutkind JS (2008) Hypoxia-induced energy stress inhibits the mTOR pathway by activating an AMPK/REDD1 signaling axis in head and neck squamous cell carcinoma. *Neoplasia* 10:1295–1302

Schröder B, Wrocklage C, Pan C, Jäger R, Kösters B, Schäfer H, Elsässer H-P, Mann M and Hasilik A (2007) Integral and associated lysosomal membrane proteins. *Traffic 8*(12):1676-1686

Sehgal SN, Baker H, Vézina C (1975) Rapamycin (AY-22,989), a new antifungal antibiotic. II. Fermentation, isolation and characterization. *J Antibiot* 28:727–732

Senderek J, Bergmann C, Weber S, Ketelsen UP, Schorle H, Rudnik-Schoneborn S, Buttner R, Buchheim E, Zerres K (2003) Mutation of the SBF2 gene, encoding a novel member of the myotubularin family, in Charcot-Marie-Tooth neuropathy type 4B2/11p15. *Hum Mol Genet* 12:349–356

Settembre C. Di Malta C, Polito VA, Arencibia MG, Vetrini F, Erdin S, Erdin SU, Huynh T, Medina D, Colella P, Sardiello M, Rubinsztein DC and Ballabio A (2011) TFEB links autophagy to lysosomal biogenesis. *Science 332*(6036):1429-1433

Shapiro L, Doyle JP, Hensley P, Colman DR, Hendrickson WA (1996) Crystal structure of the extracellular domain from P0, the major structural protein of peripheral nerve myelin. *Neuron* 17:435–449

Sheean ME, McShane E, Cheret C, Walcher J, Muller T, Wulf-Goldenberg A, Hoelper S, Garratt AN, Kruger M, Rajewsky K, Meijer D, Birchmeier W, Lewin GR, Selbach M and Birchmeier C (2014) Activation of MAPK overrides the termination of myelin growth and replaces Nrg1/ErbB3 signals during Schwann cell development and myelination. *Genes Dev* 28: 290–303

Sheehan P, Zhu M, Beskow A, Vollmer C, Waites CL (2016) Activity-Dependent Degradation of Synaptic Vesicle Proteins Requires Rab35 and the ESCRT Pathway. *J Neurosci* 36(33):8668-86

Shen P, Wyant K., Wang TGA, Harper JW, Gygi SP and Sabatini DM (2016) The CASTOR Proteins Are Arginine Sensors for the mTORC1 Pathway. *Cell* 165(1):153–164

Shenoy S, Shekhar P, Heinrich F, Daou MC, Gericke A, Ross AH and Lösche M (2012) Membrane association of the PTEN tumor suppressor: molecular details of the protein-membrane complex from SPR binding studies and neutron reflection. *PLoS ONE* 7:e32591

Sherman D and Brophy P (2005) Mechanisms of axon ensheathment and myelin growth. *Nature Rev Neurosci* 6:683–690

Sherman DL, Wu LM, Grove M, Gillespie CS, Brophy PJ (2012a) Drp2 and periaxin form Cajal bands with dystroglycan but have distinct roles in Schwann cell growth. *J Neurosci* 32:9419–9428

Sherman DL, Krols M, Wu LM, Grove M, Nave K-A, Gangloff YG, Brophy PJ (2012b) Arrest of myelination and reduced axon growth when Schwann cells lack mTOR. *J Neurosci*. 32(5):1817-25

Shi A, Liu O, Koenig S, Banerjee R, Chen CC, Eimer S, Grant BD (2012) RAB-10-GTPase-mediated regulation of endosomal phosphatidylinositol-4,5-bisphosphate. *Proc Natl Acad Sci U S A* 109(35):E2306-15

Shim J, Lee SM, Lee MS, Yoon J, Kweon HS, Kim YJ (2010) Rab35 mediates transport of Cdc42 and Rac1 to the plasma membrane during phagocytosis. *Mol Cell Biol* 30:1421–1433

Shojapour M, Mosayebi G, Hajihossein R, Noorbakhsh F, Mokarizadeh A, Ghahremani MH (2018) A Simplified Protocol for the Purification of Schwann Cells and Exosome Isolation from C57BL/6 Mice. *Rep Biochem Mol Biol* 7(1):9-15

Shy ME (2006) Peripheral neuropathies caused by mutations in the myelin protein zero. *J Neurol Sci* 242:55 – 66

Simons M, Trajkovic K (2006) Neuron-glia communication in the control of oligodendrocyte function and myelin biogenesis. *J Cell Sci* 119:4381–4389

Simpson AH, **Gillingwater TH**, **Anderson H**, **Cottrell D**, **Sherman DL, Ribchester RR and Brophy PJ (2013)** Effect of limb lengthening on internodal length and conduction velocity of peripheral nerve. *J. Neurosci* 33:4536–39

Skre H (1974) Genetic and clinical aspects of Charcot–Marie–Tooth's disease. *Clin Genet* 6:98–118

Smirnov NV (1944) Approximate distribution laws for random variables, constructed from empirical data. *Uspekhi Mat. Nauk* 10:179–206

Smolders I, Smets I, Maier O, vandeVen M, Steels P, Ameloot M (2010) Simvastatin interferes with process outgrowth and branching of oligodendrocytes. *J Neurosci Res* 88:3361–3375

Snaidero N, Möbius W, Czopka T, Hekking LH, Mathisen C, Verkleij D, Goebbels S, Edgar J, Merkler D, Lyons DA, Nave K-A and Simons M (2014) Myelin membrane wrapping of CNS axons by PI (3, 4, 5) P3-dependent polarized growth at the inner tongue. *Cell 156*(1-2):277-290

Sotelo JR, Canclini L, Kun A, Sotelo-Silveira JR, Xu L, Wallrabe H, Calliari A, Rosso G, Cal K, Mercer JA (2013) Myosin-Va-dependent cell-to-cell transfer of RNA from Schwann cells to axons. *PLoS ONE* 8:e61905

Spiegel I, Adamsky K, Eshed Y, Milo R, Sabanay H, Sarig-Nadir O, Horresh I, Scherer SS, Rasband MN, Peles E (2007) A central role for Necl4 (SynCAM4) in Schwann cell–axon interaction and myelination. *Nat Neurosci* 10:861–869

Stallcup WB, Beasley L (1987) Bipotential glial precursor cells of the optic nerve express the NG2 proteoglycan. *J Neurosci* 7:2737–2744

Steger M, Tonelli F, Ito G, Davies P, Trost M, Vetter M, Wachter S, Lorentzen E, Duddy G, Wilson S, Baptista MAS, Fiske BK, Fell MJ, Morrow JA, Reith AD, Alessi DR, Mann M (2016) Phosphoproteomics reveals that Parkinson's disease kinase LRRK2 regulates a subset of Rab GTPases. *Elife* 5:e12813

Steger M, Diez F, Dhekne HS, Lis P, Nirujogi RS, Karayel O, Tonelli F, Martinez TN, Lorentzen E, Pfeffer SR, Alessi DR, Mann M (2017) Systematic proteomic analysis of LRRK2-mediated Rab GTPase phosphorylation establishes a connection to ciliogenesis. *Elife* 6:e31012

Stendel C, Roos A, Deconinck T, Pereira J, Castagner F, Niemann A, Kirschner J, Korinthenberg, R, Ketelsen UP, Battaloglu E, Parman Y, Nicholson G, Ouvrier R, Seeger J, De Jonghe P, Weis J, Krüttgen A,

Stephens L, Anderson K, Stokoe D, Erdjument-Bromage H, Painter GF, Holmes AB, Gaffney PRJ, Reese CB, McCormick F, Tempst P, Coadwell J, Hawkins PT (1998) Protein kinase B kinases that mediate phosphatidylinositol 3, 4, 5-trisphosphate-dependent activation of protein kinase B. *Science 279*(5351):710-714

Sternberg N and Hamilton D (1981) Bacteriophage P1 site-specific recombination. I. Recombination betweenloxPsites. *J Mol Biol*150:467–486

Stoffel W, Hillen H, Giersiefen H (1984) Structure and molecular arrangement of proteolipid protein of central nervous system myelin. *Proc Natl Acad Sci USA* 81:5012–5016

Studier FW, Moffatt BA (1986) Use of bacteriophage T7 RNA polymerase to direct selective high-level expression of cloned genes. *J Mol Biol* 189:113-130

Suter U (2007) Phosphoinositides and Charcot-Marie-tooth disease: new keys to old questions. *Cell Mol Life Sci* 64:3261–3265

Taguchi-Atarashi N, Hamasaki M, Matsunaga K, Omori H, Ktistakis NT, Yoshimori T, Noda T (2010) Modulation of local PtdIns 3 P levels by the PI phosphatase MTMR 3 regulates constitutive autophagy. *Traffic* 11:468–478

Tatebe H, Shiozaki K. (2017) Evolutionary Conservation of the Components in the TOR Signaling Pathways. *Biomolecules* 7(4):77

Taveggia C, Zanazzi G, Petrylak A, Yano H, Rosenbluth J, Einheber S, Xu X, Esper RM, Loeb JA, Shrager P, Chao MV, Falls DL, Role L, Salzer JL (2005) Neuregulin-1 type III determines the ensheathment fate of axons. *Neuron* 47:681–694

Taveggia C and Bolino A (2018) DRG Neuron/Schwann Cells Myelinating Cocultures. *Methods Mol Biol* 1791:115-129

Taylor GS, Maehama T, Dixon JE (2000) Myotubularin, a protein tyrosine phosphatase mutated in myotubular myopathy, dephosphorylates the lipid second messenger, phosphatidylinositol 3-phosphate. *Proc. Natl Acad. Sci. USA* 97(16):8910–8915

Taylor PM (2013) Role of amino acid transporters in amino acid sensing. *The American journal of clinical nutrition 99*(1):223S-230S

Tegel H, Tourle S, Ottonson J, Persson A (2010) Increased levels of recombinant human proteins with the *Escherichia coli* strain Rosetta(DE3) *Protein Expr Purif* 69:159–167

Tersar K, Boentert M, Berger P, Bonneick S, Wessig C, Toyka KV, Young P and Suter U (2007) Mtmr13/Sbf2-deficient mice: an animal model for CMT4B2. *Hum Mol Genet 16*(24):2991-3001

Timsit S, Martinez S, Allinquant B, Peyron F, Puelles L and Zalc B (1995) Oligodendrocytes originate in a restricted zone of the embryonic ventral neural tube defined by DM-20 mRNA expression. *J Neurosci* 15(2):1012-1024

Tiosano D, Baris HN, Chen A, Hitzert MM, Schueler M, Gulluni F, Wiesener A, Bergua A, Mory A, Copeland B, Gleeson JG, Rump P, van Meer H, Sival DA, Haucke V, Kriwinsky J, Knaup KX, Reis A, Hauer NN, Hirsch E, Roepman R, Pfundt R, Thiel CT, Wiesener MS, Aslanyan MG, Buchner DA (2019) Mutations in PIK3C2A cause syndromic short stature, skeletal abnormalities, and cataracts associated with ciliary dysfunction. *PLoS Genet* 15(4):e1008088

Topilko P, Schneider-Manoury S, Levi G, Baron-Van EvercoorenA, Chennoufi ABY, Seitanidou T, Babinet C, Charnay P (1994) Krox-20 controls myelination in the peripheral nervous system. *Nature* 371:796–799

Torii T, Miyamoto Y, Yamamoto M, Ohbuchi K, Tsumura H, Kawahara K, Tanoue A, Sakagami H, Yamauchi J (2015) Arf6 mediates Schwann cell differentiation and myelination. *Biochem Biophys Res Commun* 465:450-457

Tosch V, Rohde HM, Tronchere H, Zanoteli E, Monroy N, Kretz C, Dondaine N, Payrastre B, Mandel JL and Laporte J (2006) A novel PtdIns3P and PtdIns(3,5)P2 phosphatase with an inactivating variant in centronuclear myopathy. *Hum Mol Genet* 15:3098–3106

Touchot N, Chardin P, Tavitian A (1987) Four additional members of the ras gene superfamily isolated by an oligonucleotide strategy: Molecular cloning of YPT-related cDNAs from a rat brain library. *Proc Natl Acad Sci USA* 84:8210-4

Toyama BH, Savas JN, Park SK, Harris MS, Ingolia NT, Yates JR 3rd., Hetzer MW (2013) Identification of long-lived proteins reveals exceptional stability of essential cellular structures. *Cell* 154:971–982

Trajkovic K, Dhaunchak AS, Goncalves JT, Wenzel D, Schneider A, Bunt G, Nave K-A, Simons M (2006) Neuron to glia signaling triggers myelin membrane exocytosis from endosomal storage sites. *J. Cell Biol* 172:937–948

Trapp BD, Andrews SB, Wong A, O'Connell M, Griffin JW (1989) Co-localization of the myelin-associated glycoprotein and the microfilament components, F-actin and spectrin, in Schwann cells of myelinated nerve fibres. *J Neurocytol* 18:47–60

Tronchère H, Laporte J, Pendaries C, Chaussade C, Liaubet L, Pirola L, Mandel J-L and Payrastre B (2004) Production of phosphatidylinositol 5-phosphate by the phosphoinositide 3-phosphatase myotubularin in mammalian cells. *J Biol Chem 279*(8):7304-7312

Truett GE, Heeger P, Mynatt RL, Truett AA, Walker JA and Warman ML (2000) Preparation of PCR-quality mouse genomic DNA with hot sodium hydroxide and tris (HotSHOT). *Biotechniques 29*(1):52-54

Tsujita K, Itoh T, Ijuin T, Yamamoto A, Shisheva A, Laporte J, Portis F, Rusconi S, Payrastre B, Laporte J, Van Obberghen E (2004) Myotubularin regulates the function of the late endosome through the gram domain-phosphatidylinositol 3,5–bisphosphate interaction. *J Biol Chem* 279*:*13817–13824

Tsun ZY, Bar-Peled L, Chantranupong L, Zoncu R, Wang T, Kim C, Spooner E, Sabatini DM (2013) The folliculin tumor suppressor is a GAP for the RagC/D GTPases that signal amino acid levels to mTORC1. *Mol Cell* 52(4):495-505

Tyler WA, Gangoli N, Gokina P, Kim HA, Covey M, Levison SW, Wood TL (2009) Activation of the mammalian target of rapamycin (mTOR) is essential for oligodendrocyte differentiation. *J Neurosci* 29(19):6367-78

Tyler WA, Jain MR, Cifelli SE, Li Q, Ku L, Feng Y, Li H, Wood TL (2011) Proteomic identification of novel targets regulated by the mammalian target of rapamycin pathway during oligodendrocyte differentiation. *Glia*. 59(11):1754-69

Uschkureit T, Sporkel O, Stracke J, Bussow H, Stoffel W (2000) Early onset of axonal degeneration in double (plp-/-mag-/-) and hypomyelinosis in triple (plp-/-mbp-/-mag-/-) mutant mice. *J Neurosci* 20(14):5225-33

Uytterhoeven V, Kuenen S, Kasprowicz J, Miskiewicz K, Verstreken P (2011) Loss of skywalker reveals synaptic endosomes as sorting stations for synaptic vesicle proteins. *Cell* 145:117-132

Vaccari I, Dina G, Tronchère H, Kaufman E, Chicanne G, Cerri F, Wrabetz L, Payrastre B, Quattrini A, Weisman LS, Meisler MH, Bolino A (2011) Genetic interaction between MTMR2 and FIG4 phospholipid phosphatases involved in Charcot-Marie-Tooth neuropathies. *PLoS Genet* 7(10):e1002319

Velichkova M, Juan J, Kadandale P Jean S, Ribeiro I, Raman V, Stefan C and Kiger AA (2010) Drosophila Mtm and class II PI3K coregulate a PI(3)P pool with cortical and endolysosomal functions. *J Cell Biol* 190(3):407–425

Velumian AA, Samoilova M, Fehlings MG (2011) Visualization of cytoplasmic diffusion within living myelin sheaths of CNS white matter axons using microinjection of the fluorescent dye Lucifer Yellow. *Neuroimage.* 56(1):27-34

Vergne I, Roberts E, Elmaoued RA, Tosch V, Delgado MA, Proikas-Cezanne T, Laporte J, Deretic V (2009) Control of autophagy initiation by phosphoinositide 3 -phosphatase Jumpy. *EMBO J* 28:2244–2258

Verity AN, Campagnoni AT (1988) Regional expression of myelin protein genes in the developing mouse brain: in situ hybridization studies. *J Neurosci Res* 21(2-4):238-48

Villarroel-Campos D, Henriquez DR, Bodaleo FJ, Oguchi ME, Bronfman FC, Fukuda M and Gonzalez-Billault C (2016) Rab35 functions in axon elongation are regulated by P53-related protein kinase in a mechanism that involves Rab35 protein degradation and the microtubule-associated protein 1B. *J Neurosci* 36(27):7298-7313

Virchow R (1854) Ueber das ausgebreitete Vorkommen einer dem Nervenmark analogen Substanz in den thierischen Geweben. *Virchows Arch Eur J Pathol* 6:562–572

Volinia S, Dhand R, Vanhaesebroeck B, MacDougall LK, Stein R, Zvelebil MJ, Domin J, Panaretou C and Waterfield MD (1995) A human phosphatidylinositol 3-kinase complex related to the yeast Vps34p-Vps15p protein sorting system. *EMBO J* 14(14):3339-3348

Voyvodic JT (1989) Target size regulates calibre and myelination of sympathetic axons. *Nature* 342:430–433

Wahl SE, McLane LE, Bercury KK, Macklin WB, Wood TL (2014) Mammalian target of rapamycin promotes oligodendrocyte differentiation, initiation and extent of CNS myelination. *J Neurosci* 34(13):4453-65

Wake H, Lee PR, Fields RD (2011) Control of local protein synthesis and initial events in myelination by action potentials. *Science* 333:1647–1651

Walseng E, Bakke O, and Roche PA (2008). Major histocompatibility complex class II-peptide complexes internalize using a clathrin-and dynamin-independent endocytosis pathway. *J Biol Chem 283*(21):14717-14727

Wang Z and Storm DR (2006) Extraction of DNA from mouse tails. *BioTechniques* 41(4):410-412

Wang H, Tewari A, Einheber S, Salzer JL, Melendez-Vasquez CV (2008) Myosin II has distinct functions in PNS and CNS myelin sheath formation. *J Cell Biol* 182:1171–1184

Wang S, Tsun ZY, Wolfson RL, Shen K, Wyant GA, Plovanich ME, Yuan ED, Jones TD, Chantranupong L, Comb W, Wang T, Bar-Peled L, Zoncu R, Straub C, Kim C, Park J, Sabatini BL and Sabatini DM (2015) Metabolism. Lysosomal amino acid transporter SLC38A9 signals arginine sufficiency to mTORC1. *Science* 347(6218):188–194

Warner LE, Mancias P, Butler IJ, McDonald CM, Keppen L, Koob KG, Lupski JR (1998) Mutations in the early growth response 2 (EGR2) gene are associated with hereditary myelinopathies. *Nat Genet* 18:382-384

Waxman SG and Bennett MV (1972) Relative conduction velocities of small myelinated and non-myelinated fibres in the central nervous system. *Nat. New Biol* 238:217-219

Waxman SG (1980) Determinants of conduction velocity in myelinated nerve fibers. *Muscle Nerve* 3:141–150

Waxman SG (1997) Axon-glia interactions: building a smart nerve fiber. *Curr Biol* 7:R406–R410

Waxman SG (2006) Ions, energy and axonal injury: towards a molecular neurology of multiple sclerosis. *Trends Mol. Med.* 12:192–195

Webster HD, Martin R, O'Connell MF (1973) The relationships between interphase Schwann cells and axons before myelination: A quantitative electron microscopic study. *Dev Biol* 32(2):401–416

Wegner M (2008) A matter of identity: Transcriptional con-trol in oligodendrocytes. *J Mol Neurosci* 35:3–12

Wei Z, Fan B, Ding H, Liu Y, Tang H, Pan D, Shi J, Zheng P, Shi H, Wu H, Li A, Feng S (2019) Proteomics analysis of Schwann cell-derived exosomes: a novel therapeutic strategy for central nervous system injury. *Mol Cell Biochem* 457(1-2):51-59

Werner H., Nave K. (2005) Glial Cells and Myelination. In: Encyclopedic Reference of Genomics and Proteomics in Molecular Medicine. Springer, Berlin, Heidelberg

Wheeler DB, Zoncu R, Root DE, Sabatini DM, Sawyers CL (2015) Identification of an oncogenic RAB protein. *Science* 350:211-217

Wienisch M and Klingauf J (2006) Vesicular proteins exocytosed and subsequently retrieved by compensatory endocytosis are nonidentical. *Nat Neurosci 9*(8):1019

Wilkins A, Majed H, Layfield R, Compston A and Chandran S (2003) Oligodendrocytes promote neuronal survival and axonal length by distinct intracellular mechanisms: a novel role for oligodendrocyte-derived glial cell line-derived neurotrophic factor. *J Neurosci* 23:4967–4974

Willem M, Garratt AN, Novak B, Citron M, Kaufmann S, Rittger A, DeStrooper B, Saftig P, Birchmeier C, Haass C (2006) Control of peripheral nerve myelination by the b-secretase BACE1. *Science* 314: 664–666

Winterstein C, Trotter J, Krämer-Albers EM (2008) Distinct endocytic recycling of myelin proteins promotes oligodendroglial membrane remodeling. *J Cell Sci* 121:834–842

Wittinghofer A, Vetter IR (2011) Structure-function relationships of the G domain, a canonical switch motif. *Annu Rev Biochem* 80:943-71 PMID:21675921

Wolfson RL, Chantranupong L, Saxton RA, Shen K, Scaria SM, Cantor JR and Sabatini DM (2015). Sestrin2 is a leucine sensor for the mTORC1 pathway. *Science* 351(6268):43–48

Wolfson RL, Chantranupong L, Wyant GA, Gu X, Orozco JM, Shen K, Condon KJ, Petri S, Kedir J, Scaria SM, Abu-Remaileh M, Frankel WN and Sabatini DM (2017) KICSTOR recruits GATOR1 to the lysosome and is necessary for nutrients to regulate mTORC1. *Nature* 543(7645):438–442

Wrabetz L, Feltri ML, Quattrini A, Imperiale D, Previtali S, D'Antonio M, Martini R, Yin X, Trapp BD, Zhou L, Chiu S-Y, Messing A (2000) P0 glycoprotein overexpression causes congenital hypomyelination of peripheral nerves. *J Cell Biol 148*(5):1021-1034

Wu Y-W, Tan K-T, Waldmann H, Goody RS, Alexandrov K (2007) Interaction analysis of prenylated Rab GTPase with Rab escort protein and GDP dissociation inhibitor explains the need for both regulators. *Proc Natl Acad Sci USA* 104:12294-9

Wu X, Bradley, MJ, Cai Y, Kümmel D, Enrique M, Barr FA and Reinisch KM (2011) Insights regarding guanine nucleotide exchange from the structure of a DENN-domain protein complexed with its Rab GTPase substrate. *Proc. Natl Acad. Sci. USA 108*(46):18672-18677

Wu Y, Cheng S, Zhao H, Zou W, Yoshina S, Mitani S, Zhang H, Wang X (2014) PI3P phosphatase activity is required for autophagosome maturation and autolysosome formation. *EMBO Rep*. 15(9):973-81

Wullschleger S, Loewith R and Hall MN (2006) TOR signaling in growth and metabolism. *Cell* 124:471–484

Wurm FM (2004) Production of recombinant protein therapeutics in cultivated mammalian cells. *Nat Biotechnol* 22:1393–1398

Xhabija B, Taylor GS, Fujibayashi A, Sekiguchi K, Vacratsis PO (2011) Receptor mediated endocytosis 8 is a novel PI(3)P binding protein regulated by myotubularin-related 2. *FEBS Lett* 585(12):1722–1728

Xia W, Bringmann P, McClary J, Jones PP, Manzana W, Zhu Y, Wang S, Liu Y, Harvey S, Madlansacay MR, McLean K, Rosser MP, MacRobbie J, Olsen CL, Cobb RR (2006) High levels of protein expression using different mammalian CMV promoters in several cell lines. *Protein Expr Purif* 45:115–124

Xu L, Salloum D, Medlin PS, Saqcena M, Yellen P, Perrella B and Foster DA (2011) Phospholipase D mediates nutrient input to mammalian target of rapamycin complex 1 (mTORC1). *J Biol Chem* 286(29):25477-25486

Yang Q, Inoki K, Ikenoue T, Guan KL (2006) Identification of Sin1 as an essential TORC2 component required for complex formation and kinase activity. *Genes Dev* 20:2820–2832

Yang L, Peng X, Li Y, Zhang X, Ma Y, Wu C, Fan Q, Wei S, Li H and Liu J (2019) Long non-coding RNA HOTAIR promotes exosome secretion by regulating RAB35 and SNAP23 in hepatocellular carcinoma. *Molecular cancer* 18(1):78

Ye B, Duan B, Deng W, Wang Y, Chen Y, Cui J, Sun S, Zhang Y, Du J, Gu L, Lin L, Tang Y (2018) EGF Stimulates Rab35 Activation and Gastric Cancer Cell Migration by Regulating DENND1A-Grb2 Complex Formation. *Front Pharmacol* 9:1343

Yin X, Peterson J, Gravel M, Braun PE and Trapp BD (1997) CNP overexpression induces aberrant oligodendrocyte membranes and inhibits MBP accumulation and myelin compaction. *J. Neurosci. Res.* 50:238-247

Yoon C, Korade Z, Carter BD (2008) Protein kinase A-induced phosphorylation of the p65 subunit of nuclear factor- j B promotes Schwann cell differentiation into a myelinating phenotype. *J Neurosci* 28:3738–3746

Yoon MS, Du G, Backer JM, Frohman MA and Chen J (2011) Class III PI-3-kinase activates phospholipase D in an amino acid–sensing mTORC1 pathway. *J Cell Biol 195*(3):435-447

Yoon MS, Son K, Arauz E, Han JM, Kim S and Chen J (2016) Leucyl-tRNA synthetase activates Vps34 in amino acid-sensing mTORC1 signaling. *Cell reports 16*(6):1510-1517

Yoshimura S, Gerondopoulos A, Linford A, Rigden DJ and Barr FA (2010) Family-wide characterization of the DENN domain Rab GDP-GTP exchange factors. *J Cell Biol* 191(2):367-81

Young JZ (1938) The Functioning of the Giant Nerve Fibres of the Squid. *J Exp Biol* 15(2):170–185

Young KM, Psachoulia K, Tripathi RB, Dunn SJ, Cossell L, Attwell D, Tohyama K and Richardson WD (2013) Oligodendrocyte dynamics in thehealthy adult CNS: evidence for myelin remodeling. *Neuron* 77:873–885

Yuan HX, Russell RC and Guan KL (2013) Regulation of PIK3C3/VPS34 complexes by MTOR in nutrient stress-induced autophagy. *Autophagy* 9:1983–1995

Zalc B, Goujet D, Colman D (2008) The origin of the myelination program in vertebrates. *Curr Biol* 18:R511–R512

Zalc B (2016) The acquisition of myelin: An evolutionary perspective. *Brain Res.* 1641:4–10

Zanoteli E, Laporte J, Rocha JC, Kretz C, Oliveira AS, Mandel JL, Perez AB, Gabbai AA, Buj-Bello A (2005) Deletion of both MTM1 and MTMR1 genes in a boy with myotubular myopathy. *Am J Med Genet A 134*(3):338-340

Zarich N, Oliva JL, Martínez N, Jorge R, Ballester A, Gutiérrez-Eisman S, Garcia-Vargas S and Rojas JM (2006) Grb2 is a negative modulator of the intrinsic Ras-GEF activity of hSos1. *Mol Biol Cell 17*(8):3591-3597

Zeng LH, Rensing NR, Zhang B, Gutmann DH, Gambello MJ, Wong M (2011) Tsc2 gene inactivation causes a more severe epilepsy phenotype than Tsc1 inactivation in a mouse model of tuberous sclerosis complex. *Hum Mol Genet* 20(3):445-54

Zerial M, McBride HM (2001) Rab proteins as membrane organizers. *Nat Rev Mol Cell Biol* 2(2):107-117

Zhang J, Schulze KL, Hiesinger PR, Suyama K, Wang S, Fish M, Acar M, Hoskins RA, Bellen HJ, Scott MP (2007) Thirty-one flavors of Drosophila rab proteins. *Genetics* 176(2):1307-22

Zhang J, Fonovic M, Suyama K, Bogyo M, Scott MP (2009) Rab35 controls actin bundling by recruiting fascin as an effector protein. *Science* 325:1250–1254

Zhang Y, McCartney AJ, Zolov SN, Ferguson CJ, Meisler MH, Sutton MA, Weisman LS (2012) Modulation of synaptic function by VAC14, a protein that regulates the phosphoinositides PI(3,5)P_2 and PI(5)P. *EMBO J*. 31(16):3442-56

Zhao J, Zhai B, Gygi SP and Goldberg AL (2015) mTOR inhibition activates overall protein degradation by the ubiquitin proteasome system as well as by autophagy. *Proc. Natl Acad. Sci. USA* 112(52):15790-15797

Zheng J, Duan B, Sun S, Cui J, Du J, Zhang Y (2017) Folliculin Interacts with Rab35 to Regulate EGF-Induced EGFR Degradation. *Front Pharmacol* 8:688

Zhou J, Tan SH, Nicolas V, Bauvy C, Yang ND, Zhang J, Xue Y, Codogno P, Shen HM (2013) Activation of lysosomal function in the course of autophagy via mTORC1 suppression and autophagosome-lysosome fusion. *Cell Res* 23:508–23

Zhu AX, Zhao Y, Flier JS. (1994) Molecular cloning of two small GTP-binding proteins from human skeletal muscle. *Biochem Biophys Res Commun* 205*:*1875–1882

Zolov SN, Bridges D, Zhang Y, Lee WW, Riehle E, Verma R, Lenk GM, Converso-Baran K, Weide T, Albin RL, Saltiel AR, Meisler MH, Russell MW, Weisman LS (2012) *In vivo*, Pikfyve generates PI(3,5)P2, which serves as both a signaling lipid and the major precursor for PI5P. *Proc Natl Acad Sci U S A*. 109(43):17472-7

Zoncu R, Bar-Peled L, Efeyan A, Wang S, Sancak Y, Sabatini DM (2011) mTORC1 senses lysosomal amino acids through an inside-out mechanism that requires the vacuolar H(+)-ATPase. *Science*. 334(6056):678-83

Zorick TS, Syroid DE, Brown A, Gridley T, Lemke G (1999) Krox-20 controls SCIP expression, cell cycle exit and susceptibility to apoptosis in developing myelinating Schwann cells. *Development* 126:1397–1406

Zou J, Chang SC, Marjanovic J, Majerus PW (2009) MTMR9 increases MTMR6 enzyme activity, stability, and role in apoptosis. *J. Biol. Chem.* 284(4):2064–2071

Zou J, Zhou L, Du XX, Ji Y, Xu J, Tian J, Jiang W, Zou Y, Yu S, Gan L, Luo M, Yang Q, Cui Y, Yang W, Xia X, Chen M, Zhao X, Shen Y, Chen PY, Worley PF, Xiao B. (2010) Rheb1 is required for mTORC1 and myelination in postnatal brain development. *Dev Cell* 20(1):97-108

Zou, J., Zhang, C., Marjanovic, J., Kisseleva, M. V., Majerus, P. W., and Wilson, M. P. (2012) Myotubularin-related protein (MTMR) 9 determines the enzymatic activity, substrate specificity, and role in autophagy of MTMR8. *Proc Natl Acad Sci USA* 109:9539–9544

Zou Y, Jiang W, Wang J, Li Z, Zhang J, Bu J, Zou J, Zhou L, Yu S, Cui Y, Yang W, Luo L, Lu QR, Liu Y, Chen M, Worley PF, Xiao B (2014) Oligodendrocyte precursor cell-intrinsic effect of Rheb1 controls differentiation and mediates mTORC1-dependent myelination in brain. *J Neurosci* 34(47):15764-78

Zou W, Lai M, Zhang Y, Zheng L, Xing Z, Li T, Zou Z, Song Q, Zhao X, Xia L, Yang J, Liu A, Zhang H, Cui ZK, Jiang Y, Bai X (2018) Exosome Release Is Regulated by mTORC1. *Adv Sci (Weinh)* 6(3):1801313

Zuchner S, Noureddine M, Kennerson M, Verhoeven K, Claeys K, De Jonghe P, Merory J, Oliveira SA, Speer MC, Stenger JE, Walizada G, Zhu D, Pericak-Vance MA, Nicholson G, Timmermann V and Vance JM (2005) Mutations in the pleckstrin homology domain of dynamin 2 cause dominant intermediate Charcot-Marie-Tooth disease. *Nat Genet* 37:289–294

6 Appendix

6.1 List of Abbreviations

Ø	diameter
4E-BP1	eIF 4E-binding protein 1
α (y-α-x)	"anti": antibody, raised in species y and targets protein x
aa	amino acid
ACAP2	Arf-GAP with coiled-coil, ANK repeat and PH domain-containing protein 2
ADAM17	A disintegrin and metalloproteinase domain 17
AKT	Ak strain transforming 1
AKT(CA)	constitutively active AKT ("DD" - T308D and S473D)
AMP	adenosine monophosphate
AMPA(R)	α-amino-3-hydroxy-5-methyl-4-isoxazolepropionic acid (receptor)
AMPK	AMP-activated protein kinase
AP	action potential
APS	ammoniumpersulfat
APV	DL-2-Amino-5-phosphonopentanoic acid
Ara-C	cytosine β-D-arabinofuranoside
ARF-6	ADP-ribosylation factor 6
ATG	autophagy related
ATP	adenosine triphosphate
BACE	β-site of APP cleaving enzyme
BDNF	brain-derived neurotrophic factor
bioAMP	biotinoyl-5'-AMP
BioID	proximity-dependent biotin identification
BirA(*)	protein biotin ligase from *E. coli* (promiscuous mutant)
BLB	biopsy lysis buffer
bp	base pair
BrdU	bromodeoxyuridine
BSA	bovine serum albumin
BSL1	*Griffonia (Bandeiraea) Simplicifolia* lectin 1
CA	constitutively active
CADM	cell adhesion molecule
CAG	CMV early enhancer element
CAM	cell adhesion molecules
cAMP	cyclic adenosine monophosphate
CC	coiled-coil
CCP	clathrin-coated pit
CCV	clathrin-coated vesicle
Cdc42	cell division cycle 42
CdK	cycline dependent kinase
C. elegans	*Caenorhabditis elegans*
ch	chicken
c-Jun	leucine-zipper zinc-finger transcription factor
cKO^{SC}	Schwann cell-specific conditional knockout
CMT	Charcot-Marie-Tooth
CMV	cytomegalovirus
CNPase	2′,3′-cyclic nucleotide 3′-phosphodiesterase
CNS	central nervous system
CNTF	ciliary neurotrophic factor
CNQX	6-cyano-7-nitroquinoxaline-2,3-dione
Cre	Cre recombinase

***Cre*^{ER}**	Chimera of Cre recombinase and LBD-ER^{TM}
CRTC2	cAMP response element-binding protein (CREB) regulated transcription coactivator2
Ctrl	control
Da	dalton [g/mol]
DAB	3,3′-diaminobenzidine tetrahydrochloride
DAPI	4',6-Diamidino-2-phenylindol
DENN	differentially expressed in neoplastic versus normal cells
DEPTOR	DEP domain containing mTOR-interacting protein
Dhh	Desert hedge hoc
DIV	day(s) *in vitro*
dk	donkey
Dlg-1	discs large homolog 1
D. melanogaster	*Drosophila melanogaster*
DMEM	Dulbecco's modified Eagle medium
DMSO	dimethyl sulfoxide
DNA	deoxyribonucleic acid
DNase	deoxyribonuclease
dNTP	2´-desoxynucleoside-5´-triphosphates
D-PBS (+/- Ca^{2+}/Mg^{2+})	Dulbecco's Phosphate-Buffered Saline (with/ without calcium and magnesium ions)
DPSS	diode pumped solid state
DRG	Dorsal root ganglion
DSM	DMEM-Sato based growth medium
E(number)	embryonic day number x
EBSS	Earle's balanced salt solution
ECL	enhanced chemiluminescence
E. coli	*Escherichia coli*
EDTA	ethylene diamine tetraacetic acid
EEA1	early endosomal antigen 1
EF	endotoxin-free
eGFP	enhanced green fluorescent protein
eGFP-2xFYVE (Hrs)	eGFP-tagged tandem version of the PI(3)P binding FYVE domain of Hrs
EGFR	epidermal growth factor receptor
EGTA	ethylene glycol-bis(ß-aminoethyl ether)-N,N,N'N'-tetraacetic acid
eIF	eukaryotic translation initiation factor
ELV	endosomal-like vacuole
ERK	extracellular signal–regulated kinase
ESCRT	endosomal sorting complexes required for transport
F_0	initial fluorescence intensity
F-actin	filamenteous actin
FastAP	alkaline phosphatase
FBS	fetal bovine serum
FGF2	fibroblast growth factor 2
Fig. (Sx)	figure (supplementary figure number x)
FKBP12	FK506 binding protein 12 kDa
FL	full-length
Fl	„floxed" = loxP sites inserted
F_{max}	Peak fluorescence intensity
fw	forward
FYVE	Fab1, YOTB, Vac1, EEA1
GalC	galactocerebroside

GAP	GTPase-activating protein
GC	guanine-cytosine
GDI	Rab-GDP dissociation inhibitor
GDNF	glial cell line-derived neurotrophic factor
GDP	guanosine nucleotide diphosphate
GEF	guanine nucleotide exchange factor
GFP	green fluorescent protein
GLUT4	glucose transporter 4
gp	guinea pig
GRAM	glycosyltransferase, Rab-like GTPase activator and myotubularin
Grb	growth factor receptor bound protein
GST	glutathione sepharose tag
gt	goat
GTP (yS)	guanosine triphosphate (non-hydrolyzable)
GTPase	GTP hydrolase
h	hour(s)
HBS	HEPES buffered saline
HBSS	Hanks' balanced salt solution
HCl	hydrochloride
HEK	human embryonic kidney cells strain 293T
HEPES	4-(2-hydroxyethyl) piperazine-1-ethanesulfonic acid
HNPP	Hereditary Neuropathy with liability to pressure palsies
HOS	high-ovomucoid solution
HRP	horseradish peroxidase
HS	horse serum
HSC70	heat shock cognate 70
hu	human
ICC	immunocytochemistry
icKO	tamoxifen-inducible conditional knockout
Ig	immunoglobulin
IGF1	insulin-like growth factor 1
IHC	immunohistochemistry
ILV	intraluminal vesicle
INPP4B	Inositol polyphosphate-4-phosphatase type II
IPTG	isopropyl β-D-1-thiogalactopyranosid
JNK	c-Jun N-terminal kinase
KD	knockdown
kDa	kilodalton
KI	knock in
KO	knockout
K_v	voltage-gated potassium channels
L-15	Leibovitz's L-15 medium
LAGeSo	Landesamt für Gesundheit und Soziales
LAMP(-1/2)	lysosomal-associated membrane protein 1
LB(-agar/-medium)	lysogeny broth
LBD-ER™	ligand binding domain of estrogen receptor (tamoxifen-responsive)
LC3	microtubule-associated protein 1 light chain 3
LC3-I	cytosolic LC3
LC3-II	phosphatidylethanolamine-conjugated LC3 at autophagosomal membranes
LC-MS/MS	liquid chromatography - tandem mass spectrometry
LE/Lys	late endosomal/ lysosomal compartment
LFQ	label-free quantification

LKB1	liver kinase B1
LOS	low-ovomucoid solution
MAG	myelin-associated glycoprotein
MAPK	mitogen-activated protein kinase
MBP	myelin basic protein
mCCM	mammalian cell culturing medium
MEF	mouse embryonic fibroblast
MEK	MAPK/ERK kinase
MEK(CA)	Constitutively active MEK (S218D; S222D)
MEM	minimum essential medium
MICAL1	molecules interacting with casL 1
min	minute(s)
MOG	myelin oligodendrocyte glycoprotein
MOI	multiplicity of infection
ms	mouse
MS	mass spectrometry
mRNA	messenger RNA
mSin1	mammalian stress-activated protein kinase-interacting protein 1
MTM(R)	myotubularin-related lipid phosphatase
mTOR	mechanistic target of rapamycin
mTORC	mTOR complex
MVB	multi vesicular body
myc	myelocytomatose
NA	numerical aperture
NaOH	sodium hydroxide
Na_v	voltage-gated sodium channel
NBA	neurobasal medium A
N-CAM	nerve CAM
NCV	nerve conduction velocity
NDP52	nuclear dot protein 52 kDa
NDS	normal donkey serum
NFAT	nuclear factor of activated T cells
NF-L/M	Neurofilament- low/ medium molecular weight
NG2	neural glial antigen 2
NGS	normal goat serum
NMDA(R)	N-methyl-D-aspartate (receptor)
NMJ	neuromuscular junction
norm.	normalized
Notch	neurogenic locus notch homolog protein
NRG1(-III)	neuregulin1 (type III)
n.s.	not significant
NT-3	neurotrophin-3
OCRL	oculocerebrorenal syndrome of Lowe
OL(s)	oligodendrocyte(s)
OPC(s)	oligodendrocyte precursor cell(s)
p-(S/T/Y x)y	phosphorylated protein y (at Serine/Threonine/ Tyrosine number x)
P0	myelin protein 0
P(number)	postnatal day number x
PA	phosphatic acid
PBS	phosphate buffered saline
PBS-T	PBS with 0.05 % (v/v) TWEEN-20
PC	phosphatidylcholine

PCR	polymerase chain reaction
PDGF	platelet-derived growth factor
PDGFR	platelet-derived growth factor receptor
PDK1	3-phosphoinositide-dependent kinase 1
PDL	poly-D-lysine hydrobromide
PDZ	PSD-95/Dlg-1/ZO1
PFA	paraformaldehyde
PH	pleckstrin homology
pH	potential hydrogen
pHluorin	pH-sensitive GFP variant
PI	phoshatidylinositol
PI(3)P	phosphatidylinositol-3-phosphate
PI(4)P	phosphatidylinositol-4-phosphate
PI(5)P	phosphatidylinositol-5-phosphate
PI(3,4)P_2	phosphatidylinositol-3,4-bisphosphate
PI(3,5)P_2	phosphatidylinositol-3,5-bisphosphate
PI(4,5)P_2	phosphatidylinositol-4,5-bisphosphate
PI(3,4,5)P_3	phosphatidylinositol-3,4,5-trisphosphate
PI3K/(C2)	phosphatidylinositol 3-kinase class I/ class II
PI5P 4K	type II PI(5)P 4-hydroxy kinases
PiB	PIPES-based buffer
PIC	mammalian protease inhibitor cocktail
PIKfyve	PI(3)-phosphate 5-kinase type III, FYVE finger-containing
PIPES	piperazine-N,N'-bis-2-ethanesulfonic acid
PLC	phospholipase C
PLD	Phoshpolipase D
PLL	poly-L-lysine hydrobromide
PLP	proteolipid protein
PM	plasma membrane
PMP	peripheral myelin protein
PMSF	phenylmethylsulfonyl fluoride
PNS	peripheral nervous system
POI	protein of interest
POU	Pit-Oct-Unc
PRAS40	proline-rich Akt substrate of 40 kDa
P/S	penicillin/ streptomycin
PTEN	dual protein and lipid phosphatase and tensin homolog on chromosome 10
PTP(i)	phosphotyrosine phosphatase (inactive)
Rab	Ras-related in brain
***Rab35*$^{Fl/+}$**	mice with heterozygously „floxed“ Rab35 gene/ one allele with loxP site insertion
***Rab35*$^{Fl/Fl}$**	mice with homozygously „floxed“ Rab35 gene/ both alleles with loxP site insertion
Rab35^GTPys/GDP	nucleotide-loaded Rab35 (with GTPys or GDP)
Rac1	Ras-related C3 botulinum toxin substrate 1
Rag	Ras-related GTPases
Rapa	Rapamycin
Raptor	regulatory-associated protein of mTOR
Ras	rat sarcoma
rb	rabbit
REDD1	regulated in DNA damage and development 1
rev	reverse
Rheb	Ras homolog enriched in brain
Rho	Ras homolog gene family

Rictor	Raptor-independent companion of mTOR
RNA	ribonucleic acid
RNase	ribonuclease
ROI	region of interest
rpm	rounds per minute
RT	room temperature
RTK	receptor tyrosine kinase
S6	40s ribosomal protein S6
S6K	p70 S6 Kinase 1
Sbf	SET-binding factor
SC(s)	Schwann cell(s)
scr	scrambled (non-targeting [negative control] si/shRNA)
SD	standard deviation
SDS(-PAGE)	sodiumdodecylsulfate (- polyacrylamide gel electrophoresis)
SEM	standard error of the mean
SF	surface
shRNA	small hairpin RNA
siRNA	small interfering RNA
SLI(s)	Schmidt-Lantermann-incisure(s)
SN	sciatic nerve (*N. sciaticus*)
Sox	SRY (sex determining region Y)-box
SREBP	sterol regulatory element-binding protein
Suppl.	supplementary
SV(s)	synaptic vesicle(s)
SV2	synaptic vesicle protein 2
Syph	synaptophysin
Syt1	synaptotagmin1
Syt1-pH	chimera of synaptotagmin1 and pHluorin
τ	endocytic time constant
T3	thyroid hormone triiodothyronine
table Sx	supplementary table number x
TACE	tumor necrosis factor (TNFα) converting enzyme
TAE	TRIS-acetate-EDTA
TBC	Tre2/Bub2/Cdc16
TBE	TRIS-borate-EDTA
TBS	TRIS-buffered saline
TE	TRIS-EDTA
TEMED	N,N,N',N'-Tetramethylethylenediamin
TES	N-tris(hydroxymethyl)methyl-2-aminoethane sulfonic acid
TFEB	transcription factor EB
TfR	transferrin receptor
TGFβ	transforming growth factor ß
TLB	tail lysis buffer
TMX	tamoxifen ((Z)-4-hydroxytamoxifen)
TNB	tail neutralization buffer
TRIS	Tris-(hydroxymethyl)-aminomethan
TSC	tuberous sclerosis complex
TWEEN	polyethyleneglycolsorbitanmonolaurate
ULK1/Atg13/FIP200	unc-51-like kinase 1/mammalian autophagy-related gene 13/focal adhesion kinase family-interacting protein of 200kDa
UV	ultraviolet
Vac	vacuole-related protein

VAMP	vesicle associated membrane protein
Veh	vehicle
VPS	vacuolar protein sorting
VSV-G	vesicular stomatits virus G protein
v/v	volume per volume
WT	wild type
w/v	weight per volume
x g	multiplicity of acceleration of gravity
XLCNM	X-linked centronuclear myopathy
YT	yeast extract tryptone

6.2 Supplement

6.2.1 Mass spectrometry results of the Rab35-BioID

Table S1: Proteins, selectively enriched in Rab35-BioID samples. bold – linked to Rab35 by literature

Gene	Protein
ABCC1	Multidrug resistance-associated protein 1
ABCC5	Multidrug resistance-associated protein 5
ADCY9	Adenylate cyclase type 9
AGPAT9	Glycerol-3-phosphate acyltransferase 3
AKT2	RAC-beta serine/threonine-protein kinase
ALCAM	CD166 antigen
ANKS6	Ankyrin repeat and SAM domain-containing protein 6
ATP6AP2	Renin receptor
ATP7A	Copper-transporting ATPase 1
ATP7B	Copper-transporting ATPase 2;WND/140 kDa
BASP1	Brain acid soluble protein 1
CAMLG	Calcium signal-modulating cyclophilin ligand
CCDC8	**Coiled-coil domain-containing protein 8**
CDC42EP1	Cdc42 effector protein 1
CDC42EP4	Cdc42 effector protein 4
CHM	**Rab proteins geranylgeranyltransferase component A 1**
CHMP6	Charged multivesicular body protein 6
COL1A1	Collagen alpha-1(I) chain
CXADR	Coxsackievirus and adenovirus receptor
DAG1	Dystroglycan; Alpha-dystroglycan; Beta-dystroglycan
DENND5B	**DENN domain-containing protein 5B**
DENR	Density-regulated protein
DHRS7	Dehydrogenase/reductase SDR family member 7
DOCK8	Dedicator of cytokinesis protein 8
DOCK9	Dedicator of cytokinesis protein 9
DSC3	Desmocollin-3
EFNB1	Ephrin-B1
EFNB3	Ephrin-B3
EGFR	Epidermal growth factor receptor
EPHA2	Ephrin type-A receptor 2
EPHA7	Ephrin type-A receptor 7
ERBB2	Receptor tyrosine-protein kinase erbB-2
EWSR1	RNA-binding protein EWS
FAM171B	Protein FAM171B
FAM207A	Protein FAM207A
FLOT2	Flotillin-2
FLRT3	Leucine-rich repeat transmembrane protein FLRT3
FLVCR1	Feline leukemia virus subgroup C receptor-related protein 1
GTF2B	Transcription initiation factor IIB

GULP1	PTB domain-containing engulfment adapter protein 1
HM13	Minor histocompatibility antigen H13
HMGCR	3-hydroxy-3-methylglutaryl-coenzyme A reductase
HMOX2	Heme oxygenase 2
IFNGR1	Interferon gamma receptor 1
IGF1R	Insulin-like growth factor 1 receptor
IGHA1; IGHA2	Ig alpha-1 chain C region;Ig alpha-2 chain C region
IGSF3	Immunoglobulin superfamily member 3
INSR	**Insulin receptor**
ITGA6	**Integrin alpha-6**
ITGB1	**Integrin beta-1**
JAM3	Junctional adhesion molecule C
KIAA0319L	Dyslexia-associated protein KIAA0319-like protein
KIAA0355	Uncharacterized protein KIAA0355
KIRREL	Kin of IRRE-like protein 1
KLRG2	Killer cell lectin-like receptor subfamily G member 2
LNPEP	Leucyl-cystinyl aminopeptidase, pregnancy serum form
LPHN2	Latrophilin-2
LRP2	Low-density lipoprotein receptor-related protein 2
MARCKSL1	MARCKS-related protein
MCAM	Cell surface glycoprotein MUC18
MINA	Bifunctional lysine-specific demethylase and histidyl-hydroxylase MINA
MINK1	Misshapen-like kinase 1
MPP6	MAGUK p55 subfamily member 6
MPZL1	Myelin protein zero-like protein 1
MYBBP1A	Myb-binding protein 1A
NCAM1	Neural cell adhesion molecule 1
NDC1	Nucleoporin NDC1
NDRG3	Protein NDRG3
NF2	Merlin
NUCB1	Nucleobindin-1
OCLN	Occludin
PALM	Paralemmin-1
PCDH19	Protocadherin-19
PCDH9	Protocadherin-9
PHF6	PHD finger protein 6
PHLDB2	Pleckstrin homology-like domain family B member 2
PIK3R2	Phosphatidylinositol 3-kinase regulatory subunit beta
PIP5K1C	Phosphatidylinositol 4-phosphate 5-kinase type-1 gamma
PLXNA1	Plexin-A1
PREB	Prolactin regulatory element-binding protein
PTK7	Inactive tyrosine-protein kinase 7
PTPLAD1	Very-long-chain (3R)-3-hydroxyacyl-[acyl-carrier protein] dehydratase 3
PTPRJ	**Receptor-type tyrosine-protein phosphatase eta**

PVRL3	Poliovirus receptor-related protein 3
RAB23	Ras-related protein Rab-23
RALBP1	RalA-binding protein 1
RCC1	Regulator of chromosome condensation
RELL1	RELT-like protein 1
ROBO1	Roundabout homolog 1
ROR2	Tyrosine-protein kinase transmembrane receptor ROR2
RPL18	60S ribosomal protein L18
RPS19	40S ribosomal protein S19
RRAGC; RRAGD	Ras-related GTP-binding protein C; Ras-related GTP-binding protein D
SAFB; SAFB2	Scaffold attachment factor B1; Scaffold attachment factor B2
SBF2	**Myotubularin-related protein 13**
SCAMP1	Secretory carrier-associated membrane protein 1
SEMA4C	Semaphorin-4C
SEMA6A	Semaphorin-6A
SH3GL3	Endophilin-A3
SLC12A7	Solute carrier family 12 member 7
SLC19A1	Folate transporter 1
SLC1A3	Excitatory amino acid transporter 1
SLC20A1	Sodium-dependent phosphate transporter 1
SLC20A2	Sodium-dependent phosphate transporter 2
SLC25A22; SLC25A18	Mitochondrial glutamate carrier 1+ 2
SLC27A4	Long-chain fatty acid transport protein 4
SLC29A1	Equilibrative nucleoside transporter 1
SLC30A1	Zinc transporter 1
SLC38A1	Sodium-coupled neutral amino acid transporter 1
SLC38A2	Sodium-coupled neutral amino acid transporter 2
SLC39A10	Zinc transporter ZIP10
SLC39A14	Zinc transporter ZIP14
SLC39A6	Zinc transporter ZIP6
SLC4A2	Anion exchange protein 2
SLC6A8	Sodium- and chloride-dependent creatine transporter 1
SLC7A2	Low affinity cationic amino acid transporter 2
SLC7A5	Large neutral amino acids transporter small subunit 1
SLC9A3R2	Na(+)/H(+) exchange regulatory cofactor NHE-RF2
SNAP47	Synaptosomal-associated protein 47
SNX30	Sorting nexin-30
SPTLC1	Serine palmitoyltransferase 1
SRC	Proto-oncogene tyrosine-protein kinase Src
SSR1	Translocon-associated protein subunit alpha
STBD1	Starch-binding domain-containing protein 1
STEAP3	Metalloreductase STEAP3
STIM2	Stromal interaction molecule 2
STK11IP	Serine/threonine-protein kinase 11-interacting protein
STX18	Syntaxin-18

STX3	Syntaxin-3
STX4	Syntaxin-4
STX7	Syntaxin-7
SUSD5	Sushi domain-containing protein 5
SYTL4	Synaptotagmin-like protein 4
TADA3	Transcriptional adapter 3
TAPT1	Transmembrane anterior posterior transformation protein 1 homolog
TBC1D13	**TBC1 domain family member 13**
TC2N	Tandem C2 domains nuclear protein
TLDC1	TLD domain-containing protein 1
TMEM2	Transmembrane protein 2
TMX1	Thioredoxin-related transmembrane protein 1
TRUB1	Probable tRNA pseudouridine synthase 1
TULP3	Tubby-related protein 3
UBXN6	UBX domain-containing protein 6
UNC5B	Netrin receptor UNC5B
UNC5C	Netrin receptor UNC5C
VANGL1	Vang-like protein 1
VAT1	Synaptic vesicle membrane protein VAT-1 homolog
ZDHHC5	Palmitoyltransferase ZDHHC5

Table S2: Proteins, more than fivefold enriched (LFQ-intensity BirA*Rab35/BirA*) in Rab35-BioID samples in n = 2 independent experiments. Enrichment: mean ± SD; bold -– linked to Rab35 by literature

Rank	Gene	Protein	Fold enrichment
1	RAB35	Ras-related protein Rab-35	745.72 ± 347.31
2	**TFRC**	**Transferrin receptor protein 1**	**45.86 ± 48.09**
3	SLC3A2	4F2 cell-surface antigen heavy chain	44.72 ± 35.72
4	LSR	Lipolysis-stimulated lipoprotein receptor	36.04 ± 11.34
5	SLC12A2	Solute carrier family 12 member 2	36.00 ± 5.00
6	STX12	Syntaxin-12	35.95 ± 38.94
7	CACHD1	VWFA and cache domain-containing protein 1	34.44 ± 39.70
8	**SBF1**	**Myotubularin-related protein 5**	**28.92 ± 1.45**
9	**CHML**	**Rab proteins geranylgeranyltransferase component A 2**	**23.35 ± 16.53**
10	SLC1A5	Neutral amino acid transporter B(0)	22.19 ± 5.44
11	CNNM3	Metal transporter CNNM3	21.10 ± 18.18
12	ATP2B1	Plasma membrane calcium-transporting ATPase 1	13.35 ± 4.94
13	UACA	Uveal autoantigen with coiled-coil domains and ankyrin repeats	10.90 ± 6.91
14	IGF2R	Cation-independent mannose-6-phosphate receptor	8.17 ± 1.84
15	SLC4A7	Sodium bicarbonate cotransporter 3	7.01 ± 1.09
16	MARCKS	Myristoylated alanine-rich C-kinase substrate	6.65 ± 0.02
17	VAMP2; VAMP3	Vesicle-associated membrane protein 2	6.53 ± 2.11

6.2.2 SV recycling in *Rab35* icKO primary neuronal cultures

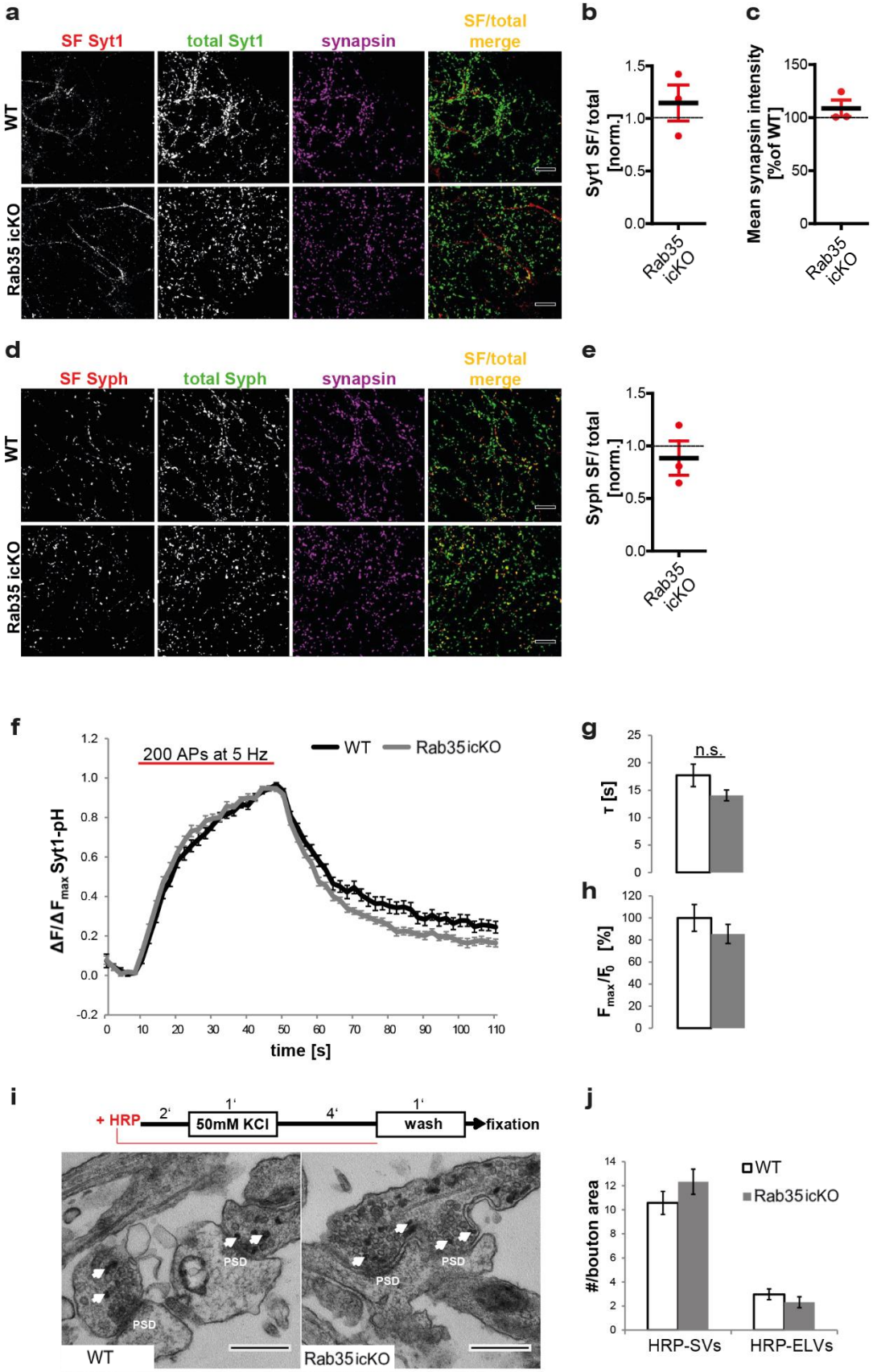

Figure S1: No major alterations in the synaptic vesicle recycling of *Rab35* icKO primary neuronal cultures. Primary cultures of hippocampal neurons were prepared from tamoxifen-inducible *Rab35* icKO (*Rab35*$^{Fl/Fl}$ x Cre^{ER}) and WT (*Rab35*$^{Fl/Fl}$) animals and cultured in the presence of 0.4 µM tamoxifen until DIV14. **(a-e)** Surface levels of two major transmembrane synaptic vesicle (SV) proteins are not altered. Cells were fixed and immunolabelled for the plasma membrane-residing surface (SF) pool of SV proteins, under non-permeabilizing conditions using antibodies targeting their luminal domain. Total protein levels were revealed by subsequent immunolabelling with an antibody recognizing the corresponding cytoplasmic domain under permeabilizing conditions. Immunostaining for synapsin was performed to mark synaptic areas. No significant changes were observed for any protein pool in *Rab35* icKO compared to WT synapses. (a) Representative confocal images of synaptotagmin1 (Syt1) surface (SF; red) and total levels (green). Synapses are depicted by synapsin (magenta); Scale bars: 10 µm. (b) Quantification of surface over total Syt1 mean intensities in synapsin-positive areas, in *Rab35* icKO normalized to WT cells (=1); (mean ± SEM; n = 3 independent experiments; one sample two-tailed student's t-test with a theoretical mean of 1; p = 0.3899). (c) Quantification of synapsin mean intensities in *Rab35* icKO normalized to WT cells (100 %), reveals no change upon loss of Rab35; (mean ± SEM; n = 3 independent experiments; one sample two-tailed student's t-test with a theoretical mean of 100; p = 0.4781). (d) Representative confocal images of synaptophysin (Syph) surface (SF; red), total levels (green) and synapsin (magenta). Scale bars: 10 µm. (e) Quantification of surface over total synaptophysin mean intensities in synapsin-positive areas, in *Rab35* icKO normalized to WT cells (= 1); (mean ± SEM; n = 3 independent experiments; one sample two-tailed student's t-test with a theoretical mean of 1; p = 0.5515). **(f-h)** Synaptic vesicle recycling of synaptotagmin1-pHluorin is unaltered in *Rab35* icKO neurons. Primary hippocampal cultures were transfected at DIV7 with a plasmid encoding for synaptotagmin1-pHluorin (Syt1-pH) under control of a synapsin-promoter. Live-cell imaging according to a pHluorin-based assay (Miesenböck *et al.*, 1998) was performed at DIV14. Neuronal activity in the cultures was elicited by electrical field stimulation with 200 action potentials (AP) at 5 Hz and SV recycling kinetics were analyzed from n = 5 independent experiments. (f) Relative fluorescence intensity course ($\Delta F/\Delta F_{max}$) of Syt1-pH over time of *Rab35* WT and icKO cells, used to calculate the endocytic decay. (g) Quantification of the endocytic decay, depicted by the decay time constant (τ), revealed no significant change of endocytic uptake/ re-acidification in *Rab35* icKO neurons; (two-tailed paired student's t-test; p = 0.1079). (h) Quantification of the relative peak fluorescence intensity upon stimulation (F_{max}/F_0) depicted normalized to WT cells (mean = 100 %). The amplitude of peak fluorescence is unaltered in *Rab35* icKO neurons; (two-tailed paired student's t-test; p = 0.4240). **(i, j)** Rab35 depletion does not alter the number of endocytical-derived synaptic or endosome-like vesicles in synapses. Primary neuronal cultures were chemically stimulated with 80 mM potassium chloride for 1 min in the presence of horse-radish peroxidase (HRP) in order to label newly endocytosed vesicles. Cells were fixed 5 min post-stimulation. HRP was visualized by 3,3'-diaminobenzidine (DAB)-mediated chromogenic detection and the number of HRP-positive synaptic vesicles (SVs) and endosome-like vesicles (ELVs) in presynapses was ultrastructurally analysed by electron microscopy (EM), performed by Dr. Dmytro Puchkov (FMP, Berlin). (i) Representative ultrastructural images of *Rab35* WT and icKO synapses. Arrows indicate HRP-containing organelles in presynapses. PSD – postsynaptic density; Scale bar: 300 µm. (j) Quantification of the number of HRP-containing SVs and ELVs in *Rab35* WT and KO presynapses reveals no major difference in n = 1 experiment.

6.3 List of tables and figures

6.3.1 List of tables

6.3.2 List of figures

6.4 Publications

Sawade L, Grandi F, Mignanelli M, Patiño-López G, Klinkert K, Langa Vives F, Di Guardo R, Echard A, Bolino A, Haucke V (2019) Rab35-regulated lipid turnover by myotubularins represses mTORC1 activity and controls myelin growth. *Nature communications* under review

Kononenko NL, Puchkov D, Classen GA, Walter AM, Pechstein A, Sawade L, Kaempf N, Trimbuch T, Lorenz D, Rosenmund C, Maritzen T, Haucke V (2014) Clathrin/AP-2 mediate synaptic vesicle reformation from endosome-like vacuoles but are not essential for membrane retrieval at central synapses. *Neuron* 82(5):981-8.

Klemke F, Beyer G, Sawade L, Saitov A, Korte T, Maldener I, Lockau W, Nürnberg DJ, Volkmer T (2014) All1371 is a polyphosphate-dependent glucokinase in Anabaena sp. PCC 7120. *Microbiology* 160(Pt 12):2807-19